Soft Sensor Modelling for the inline characterisation of Polylactide (PLA) in a twin screw extrusion process

Konrad Mulrennan

Supervisors: Dr. Marion McAfee, Dr. Leo Creedon, Dr. John Donovan

A thesis presented for the degree of

Doctor of Philosophy

Submitted to the Institute of Technology, Sligo, August 2018

Abstract

The development of a soft sensor technology to predict material properties of polylactide (PLA), extruded from a twin screw extrusion process, has been examined in this study. PLA is a bioresorbable (or biodegradable depending on the application) polymer used in the production of medical devices, pharmaceuticals, food and waste packaging. Industries processing PLA face challenges in melt processing of PLA due to its poor thermal stability which is influenced by processing temperatures and process induced mechanical shearing.

The characterisation of processed products currently takes place offline in laboratory environments. Scrap rates of a PLA medical grade product can be high as there is no current inline method to identify whether or not these were within specification during production. This study investigates using inline process data to make predictions of material properties, which are currently assessed offline. The properties examined are the yield stress, molecular weight and mass change of PLA.

A slit die has been designed to house a number of transducers, which record the data required for the soft sensors. The transducers measure pressure, temperature and near-infrared (NIR) spectral data. Using a slit die design also allows an estimate of the material's shear viscosity to be made. This estimate was of interest in assessing whether the relationship between shear viscosity and the polymer's molecular weight, (i.e. a change in molecular weight will result in a change in shear viscosity), could be useful for modelling the end properties.

In-process degradation of the material will have significant impact on the final properties of the PLA product as well as its degradation behaviour. The relationships between the inline and end properties of the material are complex and non-linear and cannot realistically be derived from first principles. Machine learning algorithms pose a potential solution due to their ability to identify relationships between input and output data sets and their ability to continue to auto adapt and update over time with further observations.

An initial set of experiments were designed over a range of processing condi-

tions. The extruded samples underwent an accelerated degradation procedure. This allowed for nondegraded samples and also samples at various stages of degradation to be tested for material properties. The data collected from the initial experiments was used to train Principal Component Analysis Random Forest (PCA-RF) soft sensor models. A second set of experiments was then carried out to capture data to validate the soft sensors. The yield stress soft sensor has been successfully developed for samples, which have not been degraded, and has generalised well using the validation data set, returning a root mean squared error (RMSE) of 1.24 MPa. This soft sensor has great potential for application within industry. The molecular weight and mass change soft sensor models have not had the same success and the rationale for this is discussed in detail.

Publications

Konrad Mulrennan, John Donovan, Leo Creedon, Ian Rogers, John G. Lyons and Marion McAfee, 'A Soft Sensor for Prediction of Mechanical Properties of extruded PLA sheet using an Instrumented Slit Die and Machine Learning Algorithms', *Polymer Testing, vol.69, 462-469, 2018*

Konrad Mulrennan, Fraser Buchanan, Mark Billham, Thomas Smyth, John Donovan, Leo Creedon and Marion McAfee, 'Degradation profiles of Polylactide - A comparative study of machine learning soft sensors used for inline prediction', *33rd Polymer Processing Society conference in Cancun, Mexico, 2017*

Konrad Mulrennan, Fraser Buchanan, Mark Billham, John Donovan, Leo Creedon and Marion McAfee, 'Using machine learning as a Quality Assurance tool for a polymer extrusion process', *34th International Manufacturing Conference in Sligo, Ireland, 2017*

Konrad Mulrennan, Fraser Buchanan, Mark Billham, John Donovan, Leo Creedon and Marion McAfee, 'Developing a soft sensor Random Forest model for the inline product characterization of Polylactide (PLA) in a twin screw melt extrusion process', *ANTEC conference in Anaheim, USA, 2017*

Dedication

To my wife Giedre, I love you.

Declaration

I, Konrad Mulrennan, declare that this thesis, titled 'Soft Sensor Modelling for the inline characterisation of Polylactide (PLA) in a twin screw extrusion process', and the work presented in it are my own. I confirm that this work was carried out by me for the degree of Doctor of Philosophy under the supervision of Dr. Marion McAfee, Dr. Leo Creedon and Dr. John Donovan. Where I have discussed the published work of others, it is always clearly attributed.

Signed: _____ (Candidate)

Signed: _____ (Supervisor)

Signed: _____ (Supervisor)

Signed: _____ (Supervisor)

Date: _____

Acknowledgements

My first thank you is extended to my research supervisors, Marion McAfee, Leo Creedon and John Donovan. I would like to express a deep gratitude to you all for your investment in me and the guidance provided throughout this project. Each of you has made a lasting impression on me and your enthusiasm for research is inspiring. Hopefully, we'll sustain our friendships and have more success together for many years into the future.

A sincere thanks to all of the staff from the Polymer Processing Research Centre at Queen's University Belfast. A special mention has to go to Fraser Buchanan, Mark Billham, Bronagh Millar, Mark McCourt and Paula Douglas who provided me with access to equipment, training, expert knowledge and are just really friendly and nice people to have worked with.

Thanks to everyone from the Applied Polymer Technology Gateway in Athlone Institute of Technology. Every one of you made me feel welcome and provided me with a platform to complete this research. Particular thanks is extended to Sean Lyons, Michael Nugent, Ian Rogers, Alan Mannion, Paddy Doran, Andrew Healy and Shane Halligan.

I am indebted to the lecturing, technical and administrative staff within Institute of Technology Sligo who have help progress this research at various

stages. Thanks to Aidan Murtagh, Ross McMorrow, Ray Tobin, Aengus Sheerin, Gerry Maguire, John Kavanagh, JohnJoe McGloin, James Kelly, Mary Connolly, Áine Fox, Margaret Mulrooney, Lorraine Archer, Frankie Doherty, Sarah Hehir, Thomas Smyth, Fiona Fox, Mary McLoughlin, Ursula Cox, Veronica Cawley, Madeline Finan, Declan Flavin, John Bartlett, Sean Mullery, Domenico Carbone, Linzi Ryan, Alan Hernon and David Tormey.

I gratefully acknowledge the funding received towards my PhD from the Institute of Technology Sligo and the EU FP7 "Research for the Benefit of SMEs" programme.

A word of thanks has to go to Erhard Giese for sharing his brilliant technical knowledge to support the project when hardware wasn't working. Thanks to Michael Swanton for taking my call and providing the information which I could not source in the literature.

I was in with a fantastic group of people throughout this who always kept our research office in good spirits. We shared struggles, joys, arguments, cynicism, optimism and some curious views of the world. All in all, each provided me with a resource of support at one time or another and I will forever hold them all in the highest regard. The glue that signifies our bond, **none of us know anything about Matlab**. Thanks to William Wilson, Fergal Gallagher, Kieran Hughes, Malgorzata Wieteska, Glenn Gordon, Darren Reape, Michael Cafferty, Saritha Unnikrishnan, Gerard McGranaghan, Caroline Mullan, David Collery, Brian Golden and Morgan Smyth.

I need to mention the contributions Darren Whitaker gave to me throughout this project. Thank you Daz for your friendship and insight at various times. Thanks to Don and Martine Donoghue for their friendship for the duration.

Thank you mum and dad for all of your support, this wasn't possible without you. Thanks to Ethan, Claire and Laura.

I don't think Giedre will ever know how much she has contributed to me or this research project but I must finish by thanking her from the bottom of my heart. Your support, friendship and love have guided me through it all, thank you.

Contents

List of Figures

List of Tables

Symbols & Abbreviations

$\%\Delta M$	Percentage mass change
ΔP	Pressure drop in the slit die
ΔP_{asd}	Pressure drop between adaptor and slit die
$\dot{\gamma}$	Shear rate
$\dot{\gamma}_a$	Apparent shear rate
$\dot{m}$	Average mass flow rate
η	Shear viscosity
$\hat{\eta}$	Shear viscosity estimate
μ	Mean
σ	Standard deviation
σ^2	Variance
σ_y	Yield stress
τ	Shear stress

τ_w	Wall shear stress
ADC	Analog to digital
Da	Dalton
DAQ	Data acquisition
DE	Differential evolution
DSC	Differential scanning calorimetry
FRA	Fast recursive algorithm
FSO	Full scale output
GC	Gas chromatography
GPC	Gel permeation chromatography
H	Slit die height
$HDPE$	High density polyethylene
$HIPS$	High-impact polystyrene
$HPLC$	High-performance liquid chromatography
IR	Infra-red
$IRTP$	Infra-red temperature prediction
IS	Impact strength
ISO	International organisation for standardisation

L_s	Slit length
L_t	Length between the pressure transducers in the slit die
$LDPE$	Low density polyethylene
M_0	The initial mass
M_1	Mass recorded at time
M_n	Number average molecular weight
M_w	Weight average molecular weight
mPE	Metalocene-catalysed polyethylene
MSE	Mean squared error
$MTPP$	Melt temperature profile prediction
NaK	Sodium-potassium
$NFIR$	Non-linear finite impulse response
NIR	Near-infrared
$NMSE$	Normalised mean squared error
NPE	Normalised prediction error
OOB	Out-of-bag
$P1$	Dynisco NaK filled pressure transducer
$P2$	FOS Messetechnik fibre optic pressure transducer

$P3$	FOS Messetechnik fibre optic pressure transducer
PBS	Phosphate buffer saline solution
PCA	Principal component analysis
$PCA-RF$	Principal Component Analysis Random Forest
PCs	Principal components
PET	Polyethylene terephthalate
PLA	Polylactide
PLS	Partial least squares
PP	Polypropylene
PS	Polystyrene
PSD	Power spectral density
Q	Volumetric flow rate
QA	Quality Assurance
RBF	Radial basis function
RF	Random Forest
$RMSE$	Root mean squared error
RSS	Residual sum of squares
SEC	Size exclusion chromatography

slm	Standard litre per minute
$T1$	Type K thermocouple
$T2$	Type K thermocouple
T_g	Glass transition temperature
$TP1$	Type J thermocouple
$TP2$	Type K thermocouple
$TP3$	Type K thermocouple
$UV - Vis$	Ultraviolet-Visible
W	Slit die width
$wt\%$	Weight percentage

Chapter 1

Introduction

Polylactide (PLA) is a polymer derived from renewable resources such as corn starch, and when disposed of correctly, degrades and become harmless to the ecosystem making it an attractive alternative to petroleum based polymers. There are many applications for PLA ranging from packaging (biodegradable) to medical devices (bioresorbable). In the medical device industry PLA is used to create implants such as fixation screws, tissue scaffolds and sutures. These devices offer support and ideally degrade at the same rate as the body heals, which eliminates the need for a second operation to remove the device.

PLA is a high cost commodity due to the high production costs from polymerisation through to processing, especially for medical grades. Typical costs of a medical grade PLA can be in the region of thousands of euro per kilogram. PLA is of particular interest for medical applications as a number of FDA approved products already exist. However, the industry faces issues regarding processing these polymers and their Quality Assurance once processed. Identification and control of suitable processing conditions is extremely challenging

usually relying on trial and error. This leads to material and machine specific solutions to processing problems that occur for manufacturers. Although it can be processed on typical extrusion machinery, its poor thermal stability means it has a narrow processing window, which varies from batch to batch (Fambri and Migliaresi, 2010). The characterisation of the processed product is lengthy and expensive to determine important properties including the molecular weight, monomer content and degradation behaviour. This characterisation is usually completed using techniques such as Gel Permeation Chromatography (GPC), Gas Chromatography (GC) and various mechanical tests. This can result in high scrap rates if products fall out of specification. Furthermore, if a new batch of raw material resin is used, variations in the characteristics of the new batch may need a process of trial and error to find the best working conditions again. As a result of all of this, the development of new products is lengthy and expensive.

1.1 Aims and Objectives

The aim of this project is to develop soft sensors which can indicate changes in key end product PLA material properties, which are currently assessed offline, in real time using available system data. The ability to predict these properties from processing data would prove a significant advancement in the development of PLA products.

The specific objectives are to:

- Search for correlations between the real time processing data and the end properties of PLA.

- Investigate if soft sensors can be developed to predict physio-chemical changes such as molecular weight changes to the material from the available in-process data.
- Investigate if soft sensors can be developed to predict post processing mechanical properties from the available in-process data.
- Investigate if soft sensors can be developed to predict the degradation profile of the extruded samples from the available in-process data.

The focus of this project is to develop predictive models which will correlate available data from an extrusion process to key material properties of the end product. This work aims to eliminate many of the issues faced by manufacturers in developing products by increasing the speed to production while eliminating high scrap rates associated with the development of the products created from these biopolymers.

1.1.1 Potential Impact

The potential impact of this research can be broken down into various stages and groups. Initially this research will have a specific impact on the Irish and international medical device market. Manufacturers will potentially be enabled to accurately and consistently attain specified properties of PLA medical devices. This will be achieved by using data collected inline, in real time, to predict the characteristics of the processed material. Data collection from industrial processes and industrial trials of the developed soft sensors will be required before implementing the predictive monitoring system.

The optimisation of the extrusion processes can also be attained through this research by:

- Achieving specified end properties of materials.
- Controlling and predicting degradation behaviour and rates.
- Reducing scrap rates.
- Reducing lead times.
- Reducing the time and cost of process development.

By optimising processes and reducing waste, manufacturers will be able to minimise energy costs making the processes more energy efficient. This leads to an improved environmental impact by reducing their CO_2 footprint. This research has the potential to provide indigenous and international medical device manufacturers a competitive edge by reducing the cost of processing these polymers due to the above mentioned benefits. A reduction in the cost of manufacture of these medical devices can lead to reduced costs for patients in the long term. This will result in the patients who are most in need of these medical devices having access to them. Additionally, these soft sensors will allow for faster development and commercialisation of new products, which was previously cost prohibitive due to manufacturing related expenses.

Furthermore, the research discussed herein will also impact on the academic community who are involved in researching polymer processing, polymer science, soft sensors, data science and machine learning.

1.1.2 The scope of this project

This project aims to contribute to the advanced monitoring of PLA twin screw extrusion processing. The main focus in this work is the development of soft sensor models. These soft sensors will enable a reduced time between processing and laboratory assessment of the extruded materials. By building reliable soft sensors for this purpose, manufacturers can state with a degree of confidence, whether a product will be within its desired specifications during processing. Laboratory assessment will still be required as these soft sensor models will need to be updated over time to adapt to process, material and environmental changes. However, it is hoped that this measure will be reduced and only be necessary for validating the soft sensor predictions. There is an extensive literature of the material, process monitoring technologies and modelling approaches relevant to the desired outcome. The work contained here relates to a packaging grade PLA, Ingeo™ Biopolymer 2003D and was obtained from NatureWorks LLC. This is a cost effective material for completing the extensive processing trials and laboratory work required to achieve the aims of the project. It should be noted that the processing experiments carried out herein relate to a single twin screw extruder. It is hoped that with further investment and research, any methodology used to create and validate tools can be further extended to other grades of PLA.

1.2 Polylactide (PLA)

Polylactide (PLA) is a biodegradable polymer which has come under increasing focus in the past five decades. Its originally published use was in the development

of medical devices such as sutures, fixation screws and other surgical implants (Kulkarni et al., 1967; Cutright and Hunsuck, 1971; Cutright, Hunsuck, and Beasley, 1971). PLA is produced commercially by ring opening polymerisation and has taken on a greater research interest due to an increased production and availability of raw material resin (Vink et al., 2004; Groot and Borén, 2010; Vink and Davies, 2015). Some of the factors which affect the end performance of processed PLA are controlled at the polymerisation stage and include monomer selection, initiator selection and the polymerisation process conditions (Garlotta, 2002). These factors have an influence on the properties of the raw material resin which is produced. The molecular weight, melt temperature, glass transition temperature, crystallinity and the presence of residual monomer of PLA are all determined at the polymerisation process (Garlotta, 2002; Auras, Harte, and Selke, 2004). All these characteristics can also be influenced by further processing.

The current research interests for this multi-functional material are across a multitude of industries including medical devices, food and waste packaging (Garlotta, 2002; Auras, Harte, and Selke, 2004; Jamshidian et al., 2010). Research has been carried out extensively on the synthesis, processing and product development of PLA (Auras et al., 2010; Castro-Aguirre et al., 2016). PLA has mechanical properties similar to petroleum based polyesters (Liu and Zhang, 2011) (Table 1.1). It has satisfactory gas barrier properties for use with food products and when compared to conventional food packaging polymers, it is between polyethylene terephthalate (PET) and polystyrene (PS) as an oxygen barrier (Auras et al., 2003). PLA has received FDA approval for numerous medical device products. Perhaps its most attractive feature is that PLA degrades,

which is unlike most petroleum based polymeric materials used for comparable applications.

Table 1.1: Comparison of mechanical properties of PLA to selected petroleum based polymers, adapted from Liu and Zhang (2011).

	PLA	**PET**	**PS**	**HIPS**	**PP**
T_g (°C)	53	54	45	23	31
Tensile strength (MPa)	3.4	2.8	2.9	2.1	0.9
Elongation at break (%)	6	130	7	45	120
Notched Izod IS (J/m)	13	59	27	123	27
PET: polyethylene terephthalate; PS: polystyrene; HIPS: high-impact polystyrene; PP: polypropylene; T_g: glass transition temperature; IS: impact strength.					

PLA has various degradation mechanisms, which are determined by the material properties and the method, which catalyses the degradation process including thermal, hydrolytic, enzymatic and biodegradation processes (Table 1.2 adapted from Tsuji (2010)). When PLA degrades it is converted into H_2O and CO_2 making it an attractive option for packaging and medical applications.

Table 1.2: Summary of PLA degradation factors and degradation monitoring methods, adapted from Tsuji (2010).

Material Factors	**Media-Related Factors**	**Material-Based Indexes**
Molecular weight	Temperature	Mass change
Crystallinity	pH	Molecular weight
Composites	Enzymes	Mechanical properties
Material morphology	Microbes	Thermal properties
Material shape and dimensions	Stress or strain	Material morphology
Porosity and pore size		

In the case of thermal degradation of PLA, many studies have found that at high temperatures complex reactions occur (Kopinke et al., 1996; Kopinke and

Mackenzie, 1997; Tsuji et al., 2003). A number of reaction mechanisms which cause degradation are proposed in the literature, these include inter- and intra-molecular ester exchange; random chain scissation; hydrolysis; and unzipping depolymerisation (Kopinke et al., 1996; Garlotta, 2002; Signori, Coltelli, and Bronco, 2009; Carrasco et al., 2010; Nishida, 2010). These reactions are promoted at higher processing temperatures, however additional factors are also responsible for variation in degradation rate (Wachsen, Platkowski, and Reichert, 1997; Hyon, Jamshidi, and Ikada, 1998; Ohkita and Lee, 2006; Paakinaho et al., 2009; Speranza, De Meo, and Pantani, 2014), the presence of moisture (Wang et al., 2008; Signori, Coltelli, and Bronco, 2009) and the concentration of residual and hydrolysed monomers and oligomers (Hyon, Jamshidi, and Ikada, 1998; Auras, Harte, and Selke, 2004; Ellä, Nikkola, and Kellomäki, 2010; Paakinaho et al., 2011).

Paakinaho et al. (2009) found that the starting molecular weight of three different batches of a medical grade PLA had a large bearing on the thermal degradation rate during processing. Post extrusion, the screws were removed from the barrel and samples were taken from various screw pitches along its length. The molecular weights of these samples were then determined by size exclusion chromatography (SEC) (See Figure 1.1).

Wang et al. (2008) found a reduction in the molecular weight of extrudate, which had increased moisture content during processing compared to extrudate which had undergone a drying regime prior to processing. The authors suggest that in addition to thermal degradation there is increased hydrolytic degradation occurring due to the raised moisture levels.

Hyon, Jamshidi, and Ikada (1998), Paakinaho et al. (2011), and Ellä, Nikkola,

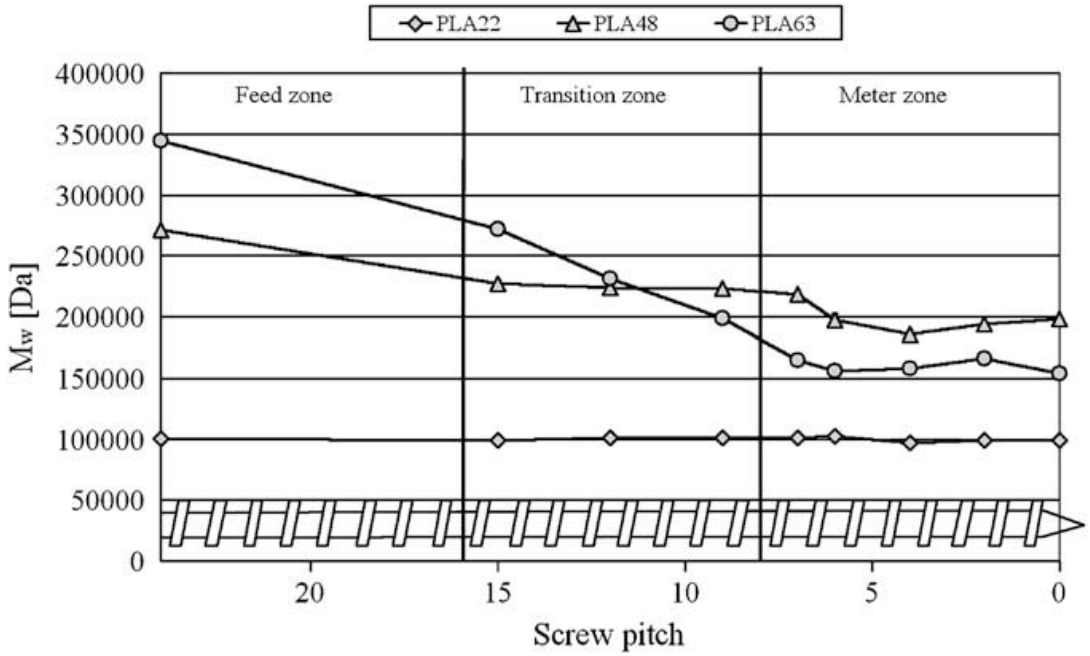

Figure 1.1: The rate of thermal degradation influenced by different starting molecular weights of PLA (Paakinaho et al., 2009).

and Kellomäki (2010) all investigated the effect of lactide monomer on the degradation profiles of PLA. Hyon, Jamshidi, and Ikada (1998) examined samples with varying weight percentage (wt%) of monomer in an *in vitro* degradation test at 37 °C in a Phosphate Buffer Saline (PBS) solution. The samples were kept in solution for 8 weeks and were assessed for % weight change and loss of tensile properties at various time points. There were clear indicators that increased monomer content accelerates the degradation rate (Hyon, Jamshidi, and Ikada, 1998).

Paakinaho et al. (2011) produced various extrusion batches creating mixed quantities of monomer in each batch. The lactide monomer content was assessed with a gas chromatograph (GC). The monomer content of the raw material was <0.02 wt% and this was varied by adding *L*-lactide as 4 wt% to the

raw material resin prior to processing. Monomer content increased with increasing temperatures during processing causing greater thermal degradation. The results from this study clearly indicate an increased rate of degradation with increased monomer content which agrees with the findings of Hyon, Jamshidi, and Ikada (1998). The samples which contained lactide wt% ≥ 3 % showed identical degradation profiles suggesting this may be a critical level of monomer in the extrudate to accelerate degradation post extrusion (Paakinaho et al., 2011).

The work of Ellä, Nikkola, and Kellomäki (2010) was in agreement with both Hyon, Jamshidi, and Ikada (1998) and Paakinaho et al. (2011). This study induced monomer by thermally degrading the polymer in-process. Again, lactide monomer content was assessed with a gas chromatograph (GC). By increasing processing temperatures and increasing the residence time of the material in the barrel, thermal degradation in excess of normal levels was achieved for the same starting material under the investigated conditions. This resulted in increased monomer content of extruded fibres and a reduction in molecular weight (see Figure 1.2). The higher the monomer content the faster the fibres degraded in a phosphate buffer saline (PBS) solution held at 37 °C for 9 weeks (Ellä, Nikkola, and Kellomäki, 2010).

Hydrolysis is the breaking of chemical bonds caused by a reaction to moisture (see Figure 1.3). Hydrolytic degradation and the control of hydrolytic degradation during processing and for post-processed PLA products is a significant area of interest (Hyon, Jamshidi, and Ikada, 1998; Hakkarainen, 2000; Garlotta, 2002; Tsuji et al., 2003; Auras, Harte, and Selke, 2004; Wang et al., 2008; Carrasco et al., 2010; Speranza, De Meo, and Pantani, 2014). To limit the possibility of hydrolysis occurring during processing, the raw material resin

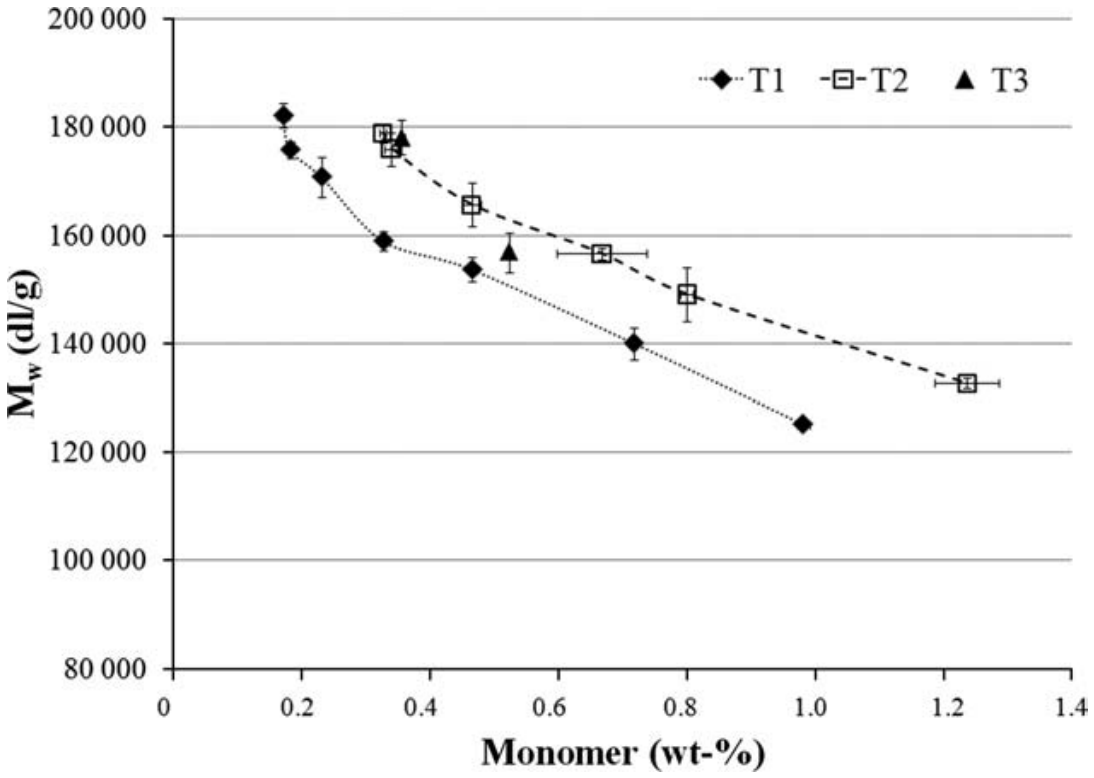

Figure 1.2: The correlation between molecular weight reduction and increased monomer content tested in Ellä, Nikkola, and Kellomäki (2010). Each individual data point represents a combination of residence time and temperature profile.

typically undergoes a drying regime to remove any residual moisture (Weiler and Gogolewski, 1996; Wang et al., 2008; Gu et al., 2009; Yuzay, Auras, and Selke, 2010; Nekhamanurak, Patanathabutr, and Hongsriphan, 2012; Sabzi et al., 2013; Speranza, De Meo, and Pantani, 2014).

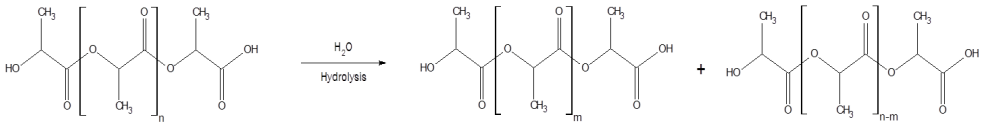

Figure 1.3: Hydrolysis of PLA.

A recent study has modelled the viscosity of dried versus undried PLA pel-

lets. A reduction in viscosity is viewed as an indicator that there is a reduction in molecular weight. By modelling the complex viscosity of dried versus undried PLA, the thermal degradation can be separated from the overall degradation, which is also impacted by hydrolysis (Speranza, De Meo, and Pantani, 2014). The results from this study highlight that there are lower complex viscosities for the undried PLA pellets over time at comparable processing temperatures to the dried PLA pellets. These lower complex viscosities could indicate that there is a further reduction in molecular weight over time for the undried samples in comparison to the dried samples when processed in the temperature range 180 °C - 220 °C. This is an indicator that the undried samples undergo further hydrolytic degradation due to the moisture retained in the samples.

1.2.1 Application and Degradation of packaging grade PLA

For PLA's use for packaging applications, there are two competing functions outside of the desired mechanical and barrier properties.

(A) The product must be fit for purpose for the duration of its shelf life.

(B) The product must be degradable once it has served its purpose.

As such, PLA is currently used for short shelf life, single use food packaging and utensil products (Garlotta, 2002; Auras, Harte, and Selke, 2004; Jamshidian et al., 2010). Typically a PLA packaging product is designed to undergo degradation in industrial composting facilities once it has performed its function. Another advantage it also holds over competing products is that food

waste can be disposed of along with the PLA product and undergo the same composting. Extensive research has been carried out to validate the degradation of PLA in compost with varying results (Hakkarainen, 2000; Ohkita and Lee, 2006; Sikorska et al., 2008; Karamanlioglu and Robson, 2013). The International Organisation for Standardisation (ISO) has published guidelines for manufacturers to test whether their products meet the required composting standard (ISO 14855-1 2012).

Ohkita and Lee (2006) investigated the enzymatic degradation of PLA and PLA/corn starch (CS) composites buried in soil. Samples of PLA and the PLA/CS composite were placed in an enzyme rich Proteinase K solution and also within a control solution, which did not contain the Proteinase K for comparison. The results for the enzymatic degradation tests showed near linear complete % weight loss for all of the samples in 10 days. The PLA samples had little indication of degradation when buried in soil. The composites had an improved degradation in the soil when compared to PLA. The composites degradation rate also increased with a greater loading of corn starch.

Studies by Hakkarainen (2000) and Karamanlioglu and Robson (2013) both investigated how PLA degraded in compost micro-organism and abiotic conditions. Both works agreed that the samples had a greater level of degradation caused by the compost micro-organisms when compared to samples degraded in abiotic mediums. Karamanlioglu and Robson (2013) also found that their samples, which were buried in micro-organism rich and sterile compost and soil, showed no change to tensile properties after one year at constant temperatures of 25 °C. Samples buried in soil at 37 °C also showed no significant change to tensile properties while the samples buried in micro-organism rich compost at

37 °C began to show signs of degradation after 8 months. The authors suggest that this could indicate that PLA may be a possible pollutant in the future if waste accumulates in the environment as it needs specific conditions for enzymatic biodegradation and hydrolysis to be optimised. This seems to agree with the findings of Ohkita and Lee (2006) who also found little degradation of pure PLA over an extended time period when buried in soil.

1.2.2 Application and Degradation of medical grade PLA

Extensive research has been carried out in the development of PLA for use in medical devices (Kulkarni et al., 1967; Cutright and Hunsuck, 1971; Cutright, Hunsuck, and Beasley, 1971; Barber et al., 2000; Middleton and Tipton, 2000; Nuutinen, Clerc, and Törmälä, 2003; Weir et al., 2004a; Weir et al., 2004b; Maurus and Kaeding, 2004; Renouf-Glauser et al., 2005; Nair and Laurencin, 2007; Brown and Farrar, 2008; Paakinaho et al., 2009; Ellä, Nikkola, and Kellomäki, 2010; Ellä et al., 2011; Bergström and Hayman, 2016; Ramot et al., 2016; Leroy et al., 2017).

Kulkarni et al. (1967) had the first publication investigating the use of PLA as a surgical implant. It was discovered through *in vivo* experiments with guinea pigs and rats that PLA film and powder implants were non-toxic and non-inflammatory to surrounding tissue. The implants degraded very slowly but the degraded by-products were completely metabolised. This work introduced the possibility of a PLA bioresorbable surgical implant.

The United States Army followed this work up with tests developing bioresorbable sutures (Cutright and Hunsuck, 1971; Cutright, Hunsuck, and Beasley,

1971). An *in vivo* study on 40 rats found that the PLA sutures degrade gradually and that there was some mild inflammatory reaction after 42 days. In some cases there were still PLA strands remaining after 70 days (Cutright and Hunsuck, 1971). A separate *in vivo* study was completed involving five rhesus monkeys. This work involved implanting each of the specimens with PLA sutures for osseous fixation to treat fracture. Each of the treatments showed progressive healing and eliminated the need for a second operation to remove the implant (Cutright, Hunsuck, and Beasley, 1971).

There are a number of advantages and considerations which have to be made when using a bioresorbable PLA implant (adapted from Middleton and Tipton (2000), Garlotta (2002), Nair and Laurencin (2007), and Brown and Farrar (2008):

- The material can be processed on existing polymer processing equipment.
  - PLA has a narrow processing window due to its poor thermal stability.
- PLA undergoes hydrolytic degradation when implanted into the body which removes the need for a second operation to remove the implant.
  - The rate of hydrolytic degradation needs to be controlled, predictable and consistent.
- An implant must provide mechanical support for a desired time frame while transferring the load gradually, at a controlled rate, to recovering bone and soft tissue during the regeneration process.
- The device must be non-inflammatory to the surrounding tissue.

- An implant can be used to release bioactive agents to promote healing.
  - The rate of release will need to be controlled and consistent.

The ideal implant will retain mechanical properties while tissue is healing and rapidly degrade and leave no trace once it has fulfilled its purpose of assisted healing (Brown and Farrar, 2008). One issue which faces PLA is that it has been reported to take up to 4 years to degrade when implanted in the body (Barber et al., 2000).

Modelling the *in vivo* degradation behaviour of PLA *in vitro* is of great interest and has had success (Weir et al., 2004a). Running *in vivo* and *in vitro* tests simultaneously, the research group suggested that under controlled conditions PLA degrades at the same rate *in vivo* as it does *in vitro* (Weir et al., 2004a). The *in vivo* tests were carried out in 12 Sprague Dawley rats. The *in vitro* tests were carried out in a phosphate buffer saline (PBS) solution at 37 °C. The duration of this study was 44 weeks. The samples from each were assessed under mechanical properties, % mass change and molecular weight amongst other characterisations. There was high correlation between the results of the *in vivo* and *in vitro* characterisations. Weir et al. (2004a) presents linear models for the number average molecular weight (M_n) using time points as the predictor variable for the models. The number average molecular weight is the total weight of polymer divided by the total number of molecules. The authors found that the models had a good fit up until 44 weeks under degradation conditions at 37 °C *in-vivo* and *in-vitro* (Weir et al., 2004a).

Expanding on this work, Weir et al. (2004b) developed an accelerated degradation test which modelled the rate at which PLA would degrade *in vivo*. Sam-

ples were kept in a PBS solution at temperatures of 50 °C and 70 °C. After 23 days at 70 °C there was a decrease of 95 % of the molecular weight compared to an 82 % decrease in molecular weight after 44 weeks at 37 °C. An un-catalysed linear regression degradation model and an auto-catalysed linear regression degradation model were both applied to molecular weight over time data, collected at 37 °C, 50 °C and 70 °C. The auto-catalysed linear model at 37 °C and 50 °C had a better fit than at 70 °C while the un-catalysed linear model at 70 °C had a better fit than at lower temperatures. Relative to the rate of molecular weight loss at 37 °C, at 50 °C the molecular weight loss was four times greater and at 70 °C it was forty times greater.

Weir et al. (2004b) observed relationships between the % mass change, the melt temperature, the glass transition temperature (T_g) and the rate of loss of molecular weight at 37 °C, 50 °C and 70 °C. These observations indicate that testing at elevated temperatures may be a suitable accelerated test method to predict PLA's degradation behaviour. Although these results show great promise, Weir et al. (2004b) have expressed concerns about testing at a temperature (70 °C) above the T_g of PLA and using the data to predict the degradation behaviour of PLA at 37 °C. These concerns are caused by only testing at one temperature above PLA's T_g. Weir et al. (2004b) have suggested that a range of temperatures above and below the T_g of PLA need to be examined to fully understand the implications of testing above PLA's T_g.

1.3 Summary

Due to the complex degradation mechanisms and variations in starting material properties there are many considerations for process engineers to evaluate before the optimal processing conditions for PLA can be achieved. Further issues are presented due to the inability to directly monitor key indicators such as changes to molecular weight or changes to the viscosity in-process. Throughout the literature, molecular weight changes are viewed as a key indicator of the rate of degradation. Predicting the degradation behaviour of PLA is of great interest. The difficulty with quantifying any changes to the molecular weight of PLA is that these changes are assessed offline. Currently there are no reported methods or technologies which allow for molecular weight to be monitored inline during the melt extrusion process.

Chapter 2

State of the art of extrusion monitoring technologies

2.1 Introduction

This chapter reviews the current state of the art in monitoring polymer extrusion processes. The monitoring of a typical industrial polymer extrusion process relies on temperature, pressure and screw speed measurement which has not changed from the early days of extrusion processing (Maddock, 1959; Maddock, 1964; Rauwendaal, 2014). Accurate monitoring of these process variables is also considered a vital requirement for troubleshooting any issues that may arise in-process (Noreiga and Rauwendaal, 2010; Rauwendaal, 2014).

Polymer morphology refers to the underlying molecular structure of the material. Polymers undergo morphology changes during processing, which cannot be directly detected by conventional transducers. These changes to the molecular structure of the material as well as variation in processing conditions such

as melt temperature and melt pressure determine the quality of the extruded product. The quality of the extruded product is defined as having material characteristics that are within the specifications determined by a manufacturer or consumer. Various techniques to quantify these morphological changes have been reviewed with a focus on inline spectroscopy (Alig, Steinhoff, and Lellinger, 2010; Saerens et al., 2014).

Shear viscosity is the viscosity of a polymer melt measured under shear stress. The shear viscosity of the melt can also be a key indicator as to the molecular changes which the material is undergoing in extrusion and thus can be related to changes in the material's end properties (Shaw, 2012). Viscosity measurements of the melted polymer cannot be directly quantified without disturbing the melt. Various techniques to monitor this dynamic material property have been developed, including the use of a piezoelectric sensor (Rezazadeh et al., 2010), a dielectric sensor (Abu-Zahra, 2004) and also vibration sensors (Riesch et al., 2009; Song, Fang, and Zhao, 2013) as well as the use of side stream rheometers (Dealy and Rey, 1996; McAfee and McNally, 2006). The development of soft sensor models to predict melt viscosity changes in-process have also been investigated successfully (Chen, Chao, and Chiu, 2003; Abu-Zahra, 2004; McAfee and McNally, 2006; McAfee and Thompson, 2007a; Son, 2007; Liu et al., 2012b).

2.2 Pressure/Temperature

Pressure and temperature are the two essential measurements on any extrusion system. Both measurements are a means of gathering vital information about

the performance of the system and also determine the safety of the process in its working environment (Maddock, 1964; Rauwendaal, 2014).

2.2.1 Pressure

Accurate pressure measurement is an absolute requirement within extrusion as a means of ensuring that the process is safe (Noreiga and Rauwendaal, 2010; Rauwendaal, 2014). Apart than safety considerations, variations in pressure are directly related to the morphological and molecular changes materials undergo in-process (Maddock, 1959; Maddock, 1964; Rauwendaal, 2014). Inline pressure measurements have have been used extensively throughout the literature as an indicator of extruded polymer quality (Lane et al., 2003; Chen, Gao, and Chen, 2004; McAfee and McNally, 2006; McAfee and Thompson, 2007a; McAfee and Thompson, 2007b; Liu et al., 2012a; Liu et al., 2012c; Deng et al., 2013; Mulrennan et al., 2017a; Mulrennan et al., 2018). Throughout the literature, desirable extrudate has material characteristics that are within the specifications determined by a manufacturer or consumer.

The most common pressure transducers in extrusion are based on strain gauges (Rauwendaal, 2014). These transducers have two diaphragms, one in contact with the melt and the other a distance away and the space between the two diaphragms is filled with a fluid. This fluid is usually mercury – chosen for its high density - but in the case of the extrusion of medical products and food packaging production the most common alternative is sodium-potassium (NaK) (Rauwendaal, 2014). When the diaphragm, which is in contact with the melt, is deformed by the molten polymer being pushed through the extruder, it moves

the thermally isolated diaphragm which is typically connected to a Wheatstone bridge. A Wheatstone bridge measures the variation in a circuit's resistance caused by the deformation of the diaphragm and the output voltage signal from the bridge circuit is then converted into a pressure reading.

FOS Messtechnik GmbH have developed a fibre optic pressure transducer, which withstands high temperatures (up to 600 °C) and has a very rugged construction due to a thicker diaphragm than fluid filled pressure transducers. The diaphragm, in contact with the melt, does not have to displace any fluid, which creates the force that performs the mechanical action for fluid filled transducers to work. A mirror is fitted to the back of the diaphragm and a light is transmitted upon the mirror's surface. As the diaphragm undergoes deformation, the position of the mirror alters and the reflected light signal, which is collected by a signal conditioning receiver, is transformed into a pressure reading. Systems which incorporate these transducers can have extremely fast response times as the slowest communication is between the signal conditioning unit and the data acquisition system. The signal conditioning unit receives the data at the speed of light (Giese, 1988; Rauwendaal, 2014).

2.2.2 Melt Temperature

Thermocouples

Thermocouples are used for a variety of purposes within extrusion to control heating zone temperatures and monitor the temperature of the melt. In this section it is the role of thermocouples in monitoring melt temperature which will be investigated. Thermocouple locations within the process set up determine

the accuracy of their measurement in relation to the melt temperature (Shen, Malloy, and Pacini, 1992; Sabota, Lawson, and Huizinga, 1995; Brown, Kelly, and Coates, 2004; Kelly et al., 2008).

Thermocouples which are embedded in the extruder barrel wall or in an extruder die are heavily influenced by the heated metal of the barrel or die which surrounds the transducer. These do not give clear indications of the polymer melt temperature as it flows through the extruder and die, but they are adequate for control of the barrel and die temperatures (Shen, Malloy, and Pacini, 1992; Rauwendaal, 2014). Flush mounted thermocouples are non-intrusive into the melt but are again heavily influenced by the barrel or die wall temperature (Shen, Malloy, and Pacini, 1992; Abeykoon et al., 2012).

Extended thermocouples protrude into the melt and give a point measurement of the melt temperature at the location of their junction. These thermocouples are also influenced by shear heating effects as a result of the heated polymer flowing against and passing over the extended part of the transducer. This results in an inaccurate measurement reading for the melt temperature (Shen, Malloy, and Pacini, 1992; Rauwendaal, 2014). If used in the barrel, these transducers require alterations to the extrusion screw to have slots cut out to accommodate the protruding transducer. This in turn has a knock on effect on the flow patterns and temperature distribution of the polymer melt (Rauwendaal, 2014). Additionally using thermocouples which extend into the melt may cause disruption to the flow of the material which can result in non-uniform extrudate (Shen, Malloy, and Pacini, 1992).

Traversing thermocouples have been used as a means of determining the melt profile of the cross section of the flowing polymer in the extruder. This

is achieved by taking point measurements as the thermocouple moves across the extruder channel (Shen, Malloy, and Pacini, 1992; Sabota, Lawson, and Huizinga, 1995; Rauwendaal, 2014). The issues faced by traversing thermocouples are similar to those faced by extended thermocouples. They alter the flow of the melt and suffer from errors caused by shear heating and thermal conduction along the length of the transducer (Rauwendaal, 2014).

A research team from the University of Bradford have utilised a method of capturing the entire melt temperature profile. A thermocouple mesh was employed to capture the temperature data while the polymer flows in the extruder (Brown, Kelly, and Coates, 2004). The thermocouple mesh was made up of thin criss-crossing thermocouple wires, placed at the entrance to the extruder die, which have multiple junctions.

The mesh has been used to examine the melt profile of polymers in various studies (Brown, Kelly, and Coates, 2004; Kelly et al., 2008; Abeykoon et al., 2011; Abeykoon et al., 2014a; Vera-Sorroche et al., 2012; Vera-Sorroche et al., 2013; Vera-Sorroche et al., 2014). A number of issues arose when using the device in situ. These included the disturbance of the polymer flow (Brown, Kelly, and Coates, 2004; Kelly et al., 2008) and also the fragility of the thermocouple wires. The fragility of the mesh is caused by prolonged use in high temperature conditions as well as undergoing shear heating effects in the extruder (Brown, Kelly, and Coates, 2004). Due to these issues it is not a viable option for industrial use but has become a very useful tool in research.

In an early study using five and seven junction thermocouple meshes with polyethylene in a single screw extruder, a relationship between screw speed and the melt temperature profile was proven (Brown, Kelly, and Coates, 2004).

Higher screw speeds resulted in a maximum temperature in the centre of the flow with lower temperatures closer to the barrel walls. The better resolution of the seven junction thermocouple mesh identified complex melt temperature profiles containing shoulder regions (Brown, Kelly, and Coates, 2004). These are evident in Figure 2.1.

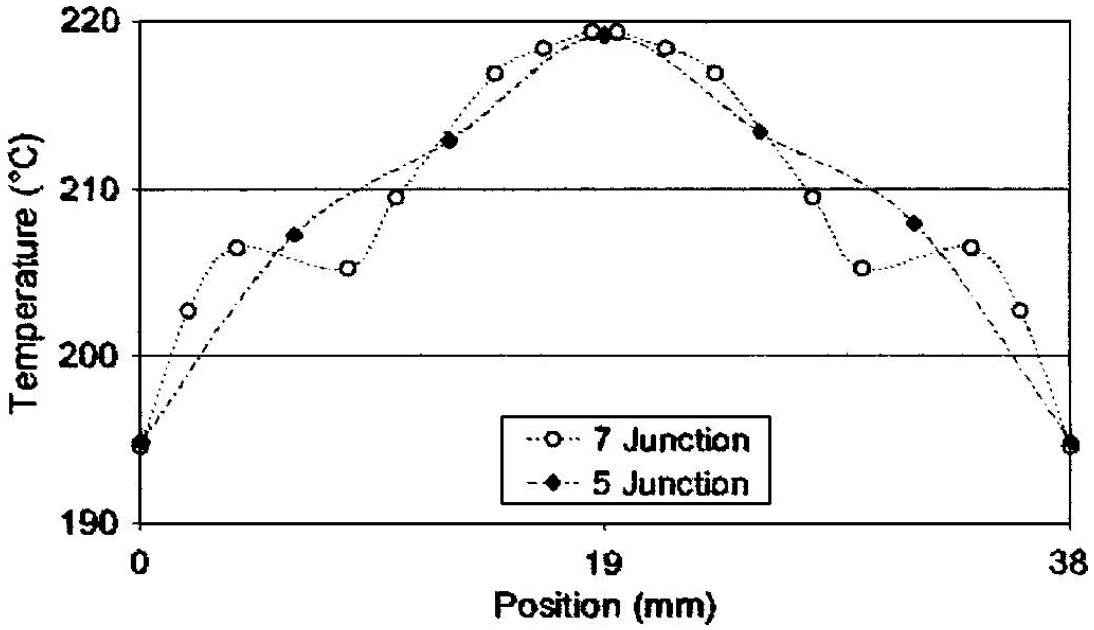

Figure 2.1: The resolution of thermocouple meshes with varying numbers of junctions reported in Brown, Kelly, and Coates (2004).

Further investigations discovered variations in the melt temperature profiles of different materials processed under the same conditions in a single screw extruder. This may be partly explained by the different thermal and rheological characteristics of each material (Kelly et al., 2008). In the same study, the effects of screw speed and throughput on the melt temperature profile of low density polyethylene (LDPE) in a twin screw extruder were investigated. At the lower screw speed and lower throughput investigated, it was discovered that neither had an impact on the temperature profile with comparably flat profiles for each

throughput examined. Results showed that increased screw speed resulted in a maximum temperature at the centre point of each screw and this becomes more pronounced with increased throughput (Kelly et al., 2008).

The results of these trials have helped develop an understanding of the complex melt temperature profile of materials in an extruder. These profiles are non-uniform and influenced by a material's thermal and rheological characteristics, screw speed and throughput (Brown, Kelly, and Coates, 2004; Kelly et al., 2008).

Infra-Red (IR) Transducers

Infra-Red (IR) transducers are commercially available measurement devices which offer a non-intrusive alternative for the collection of temperature data in the extrusion process (Rauwendaal, 2014). However, there are no off the shelf options currently available from the product catalogues of the leading retailers in extrusion transducer and sensor technology.

Typically these transducers measure the bulk temperature of the material as it passes through the extruder with a measurement depth of up to 5mm and very high response speeds of about 10 milliseconds (Rauwendaal, 2014). The depth up to which IR transducers can successfully measure depend on the volume of material in front of the transducer and the emissivity of the polymer (Maier, 1996).

A previous study has shown the success of IR temperature measurement of PET micro-fibres as they exit an extruder die. In the production of micro-fibres, control of the cooling rate is essential to create product which is within specification as the cooling rate has direct implications on the rate of crystallisation.

A pyrometer was developed to monitor the temperature of the micro-fibres as they exited the extrusion die onto the cooling rollers to determine the optimum parameters for the extrusion of these PET micro-fibres (Bendada and Lamontagne, 2004).

Recently an IR transducer, which fits in a standard instrumentation mounting tapping for most extruders, has been successfully used to estimate the melt temperature profiles of polymer flows in the extruder. The transducer is a Dynisco MTX 922 and it was placed in both the die adapter and barrel of the extruder during these trials. The data collected from the IR transducer was correlated to thermocouple mesh measurements, which were gathered under the same conditions (Vera-Sorroche et al., 2012; Vera-Sorroche et al., 2013; Vera-Sorroche et al., 2014; Abeykoon et al., 2014b). When the IR transducer was placed in the barrel rather than the die, the collected data was more comparable with the data collected by the thermocouple mesh. This is argued to be due to the limited penetration depth available to the transducer in the die (Vera-Sorroche et al., 2012). Further work into the use of this IR transducer resulted in its use to optimise the extrusion process as a non-intrusive monitoring tool to determine the bulk melt temperature of polymer melts (Vera-Sorroche et al., 2013; Vera-Sorroche et al., 2014). The results showed that the IR transducer bulk melt temperature measurements were similar to those collected from the thermocouple mesh; the thermocouple mesh disturbs the flow of the material in the extruder (Vera-Sorroche et al., 2013; Vera-Sorroche et al., 2014).

These results offer significant opportunity in an industrial application for a non-intrusive monitoring tool which can be used to optimise the melting performance of an extrusion process. As pointed out though, there are no off the shelf

IR transducers available which will fit an extruder. A personal communication with Dynisco's Director of Sales for Europe, Michael Swanton, on 13th November 2014 regarding the transducer detailed in the previous paragraph returned the following information. The Dynisco MTX 922 has not been in production since 2002 and the reason production concluded was due to the poor uptake from industry for the product.

Fluorescence

Ultraviolet-Visible (UV-Vis) spectroscopy of polymers, doped with a fluorescent dye, has been investigated to determine the temperature profile and temperature gradients of polymer resins flowing in the melt state in the extruder (Migler and Bur, 1998; Bur, Vangel, and Roth, 2001; Bur et al., 2004). These dyes, which are temperature sensitive, are added to the polymer before extrusion. The dyes are excited by UV radiation and the reaction to this energy is quantified as a temperature using UV-Vis spectroscopy (Migler and Bur, 1998).

Fluorescence temperatures have been collected using UV-Vis spectroscopy and are compared to thermocouple temperature readings from the same trials (Bur, Vangel, and Roth, 2001). This set of trials was carried out under varying screw speeds in a single screw extruder. As the thermocouple is flush mounted in the barrel wall, the temperature data collected is heavily influenced by the temperature of the surroundings. The fluorescence temperature data is more representative of the bulk material temperature (Bur, Vangel, and Roth, 2001). The study has found that an increase in screw speed has little effect on the thermocouple readings. This is in conflict with an increase of nearly 20 °C in the bulk temperature measurement of the material which is detected using

the fluorescent dye with UV-Vis spectroscopy. It is reasonable to accept these findings as previously discussed work with the thermocouple mesh has found increased bulk temperature measurements with increased screw speed in single screw extrusion (Kelly et al., 2008).

2.3 Soft Sensors

Soft sensors are inferential models which make use of inline, easy to gather, process measurements such as pressure or temperature, and make an estimation of hard to measure quantitative variables. These variables may be hard to measure due to a lack of inline measurement technology being available, a high cost associated with the required measurement technology or they may require laboratory assessment which results in long delays (Gonzalez, 1999; Fortuna et al., 2007). Soft sensor models are an appealing option as the models make use of multivariate data which is already being collected to predict the measurements of the hard to measure variables. They can work instead of and also alongside hardware sensors to provide real time information, which in turn, results in more robust monitoring and control systems.

There have been a number of review papers and books which discuss the development and adaption of soft sensors within industry (Gonzalez, 1999; Dote and Ovaska, 2001; Bishop, 2006; Fortuna et al., 2007; Kadlec, Gabrys, and Strandt, 2009; Kadlec, Grbić, and Gabrys, 2011; Mandenius and Gustavsson, 2015). All of these indicate that the use of data driven soft sensors has increased significantly in the last two decades.

The soft sensors developed for polymer extrusion processing in the literature

are focused on inferring the conditions of the polymer melt (i.e. temperature profile, viscosity or physico-chemical changes), and using the information for advanced monitoring or control of the process (Coates et al., 2003; Li, Campanella, and Hardacre, 2004; McAfee and McNally, 2006; McAfee and Thompson, 2007a; Barnes et al., 2007; Abeykoon et al., 2011; Abeykoon, 2014; Whitaker et al., 2015; Whitaker et al., 2018). Another focus of soft sensors has been for fault detection, which highlights when deviations from normal operating conditions have occurred (Liu et al., 2012a). When these abnormal changes occur the quality of the extrudate is depreciated (McKay et al., 1996; Wagner, Montague, and Tham, 1997; Lane et al., 2003; Chen, Gao, and Chen, 2004; McAfee and Thompson, 2007a; Deng et al., 2013; Abeykoon, 2014).

2.3.1 Dynamic Soft Sensors

Temperature

Abeykoon (2014) generated a soft sensor model for the melt temperature profile of a high density polyethylene (HDPE) in a single screw extruder. In previous works (Brown, Kelly, and Coates, 2004; Kelly et al., 2008), a team from the University of Bradford investigated the use of a thermocouple mesh to monitor the melt temperature profile of polymer melts (See section 2.2.2 for more details). The authors used screw speed, the radial positions of the thermocouple mesh wires in the die as well as the temperatures from the barrel, adaptor and die zones as the model inputs. The two soft sensors were designed; a melt temperature profile prediction (MTPP) soft sensor and an IR temperature prediction (IRTP) soft sensor which used a temperature feedback from an IR sensor. Both soft

sensors are nonlinear polynomial models that use a fast recursive algorithm (FRA). The FRA constructs a model using only the most significant terms and parameters. The MTPP soft sensor was a 15 term second order model with a normalised prediction error (NPE) of 1.22 % (Abeykoon, 2014). The IRTP soft sensor was a 6 term second order model with a NPE of 0.25 % (Abeykoon, 2014).

Viscosity

The shear viscosity of a polymer is quantified as the ratio of shear stress to shear rate of a polymer melt. The ratio of the two properties is dependant on the polymer's rheological properties. These rheological properties determine how difficult polymers can be to process and also give an indication as to what can be expected of their characteristics following processing. High molecular weight polymers tend towards having superior mechanical properties over low molecular weight alternatives. In contrast high molecular weight polymers are more difficult to process as a higher molecular weight results in higher viscosity. Higher viscosity polymers require increased temperatures and higher shear rates to reach a homogeneous melt state. As a result, polymer's rheological properties are strongly temperature sensitive (Shaw, 2012). A homogeneous melt is difficult to achieve in typical extrusion processes, as proven by the complex melt temperature profiles discovered in previously discussed studies (Brown, Kelly, and Coates, 2004; Kelly et al., 2008; Vera-Sorroche et al., 2012; Vera-Sorroche et al., 2013; Vera-Sorroche et al., 2014).

Successfully monitoring a material's viscosity in-process has difficulties as the material's rheological response in an extruder depends on screw geometry,

screw speed, melt temperature and material properties (Vera-Sorroche et al., 2014).

Online side stream rheometers use a gear pump to draw a stream of molten polymer from the barrel and continuously feed it through a capillary or slit channel. The material may flow through the capillary or slit channel into the atmosphere or it may be routed back into the extruder barrel using a second gear pump. The viscosity is calculated by measuring the pressure drop between two or more points along the length of the measuring channel or by measuring the drop between pressure measurement points at the barrel exit point and a pressure measurement point in the capillary or slit before the material is released into the atmosphere.

The equations for this method have been well documented (Dealy, 1982; Dealy and Wissbrun, 1990; Dealy and Broadhead, 1993; Chen, Chao, and Chiu, 2003; Li, Campanella, and Hardacre, 2004; McAfee and McNally, 2006; Son, 2007; Liu et al., 2012c). This viscosity calculation (Equation 2.1) is dependent on knowledge of the material throughput and calculating the apparent shear rate of the material in the capillary or slit flow channel.

A number of counterproductive issues, which negate the use of a side stream rheometer, have been adapted from Dealy and Broadhead (1993), Dealy and Rey (1996), and McAfee and McNally (2006). These include:

- Time lag in measurement.
  - The material needs to be pumped from the main stream in the barrel through the capillary or slit measuring channel.
- The material needs to be kept at melt temperature which can be difficult

to control.

- All material released to the atmosphere is wasted.
- The material in the capillary or slit may not be representative of the bulk material, which is in the barrel, and in some cases can be very different.
- Changes to processing conditions in an extruder will not be identified by the side stream rheometer as shear rates are influenced by the gear pump and transfer channel.

The apparent shear viscosity of a material is given by Equation 2.1, which is a ratio of shear stress to shear rate. In the case of the measurement technique that has been outlined, the shear stress measurement is defined as the shear stress at the wall of the measurement channel. The wall shear stress can be calculated from the pressure drop and the geometric constants of the measurement channel. Typically the symbol used to represent the wall shear stress in this application is τ_w. The shear rate is an apparent shear rate as it cannot be measured directly. The symbol used for apparent shear rate is $\dot{\gamma}_a$.

$$\eta = \frac{\tau}{\dot{\gamma}} \tag{2.1}$$

η = shear viscosity

τ = shear stress

$\dot{\gamma}$ = shear rate

For non-Newtonian fluids such as polymers, the Rabinowitsch correction factor is applied when there is knowledge of a material's shear thinning index (also known as the power law index). Shear thinning is the reduction of viscosity

under increasing shear stress and is commonly referred to as pseudoplastic behaviour. The Rabinowitsch correction adjusts the apparent shear rate and is used due to the pseudoplastic behaviour of a polymer melt. The shear thinning index is usually obtained from offline laboratory rheometers which test materials at various shear rates under different temperatures. The shear thinning index is taken from the shear rate/viscosity curves which result from the temperatures examined in the rheometer and can only be applied to the equations when the operating conditions in the extruder are the same as the shear rate and temperature investigated offline. It can describe the viscosity of a material in the processing range of shear rates and temperatures in an extruder.

Numerous studies have been carried out using various inline slit die rheometers to monitor the viscosity of a selection of non-Newtonian polymeric fluids (Rauwendaal and Fernandez, 1985; Vergnes, Della Valle, and Tayeb, 1993; Li, Campanella, and Hardacre, 2004; McAfee and McNally, 2006; Son, 2007; Aho and Syrjälä, 2011; Deng et al., 2014). The major advantage of using a slit die rheometer is its ability to monitor rheological changes to a material continuously while in-process.

The shear viscosity estimates using a slit die have been found to be lower than offline laboratory tests using parallel plate and capillary rheometers (Rauwendaal and Fernandez, 1985; McAfee and McNally, 2006; Aho and Syrjälä, 2011). It has been suggested that these results are caused by a material's shear history, which has a bearing on the viscosity of the polymer, as it passes through the rheometer. In the slit die used as part of an extrusion line, the polymer can undergo shear effects from the screw and barrel wall prior to entrance to the die (Rauwendaal and Fernandez, 1985). In comparison, when a polymer is

examined in laboratory based instruments, shearing is negligible prior to the beginning of any test (Rauwendaal and Fernandez, 1985).

A wide range of width (W) to height (H) ratios in rectangular slit dies were examined to determine an accurate shear stress (τ) and shear rate ($\dot{\gamma}$) relationship from the flow data available (Son, 2007). Widths in the range of 3 to 10 mm and heights in the range of 1 to 3 mm were investigated. This study also examined the optimal $\frac{W}{H}$ ratios for viscosity (η) calculations in slit dies (Son, 2007). Son (2007) found that as the ratio $\frac{W}{H}$ increased, the % error decreased. For example, the ratio $\frac{W}{H} = 10$ had a 10 % error and the ratio $\frac{W}{H} = 20$ had a 5 % error respectively in calculating τ and $\dot{\gamma}$ (Son, 2007). The authors' in this instance suggests that slit dies with $\frac{W}{H}$ ratio ≥ 20 would be suitable for use in practice (Son, 2007). Typically though $\frac{W}{H} \geq 10$ is accepted as a reasonable aspect ratio for use to calculate η, τ and $\dot{\gamma}$ in a rectangular slit die (Dealy, 1982; Aho and Syrjälä, 2011).

Aho and Syrjälä (2011) measured the shear viscosity of different grades of polypropylene and polystyrene using a slit die with three variable heights in an injection moulding process. The results were very comparable to the offline rheological assessment of the materials (Aho and Syrjälä, 2011). The viscosity curves in this study (Aho and Syrjälä, 2011), were generally lower than the offline capillary rheometer curves as reported elsewhere (Rauwendaal and Fernandez, 1985; McAfee and McNally, 2006).

Chiu, Yiu, and Pong (1997) used a stress sensor and shear rate sensor in a capillary channel after the screw and before the die in an extruder. The results from the capillary die are questionable. The stress sensor consisted of a strain gauge attached to a hollow beam and recorded the stress applied to the end of

the beam as the flowing LDPE passes it. Assumptions are made that the material is homogeneous under each processing condition to validate the equations used. The flow rate in the capillary is measured and used to calculate the shear rate. For the Rabinowitsch correction, the experimental results do not explain how the shear thinning index values (n) were derived for all of the temperatures investigated in the extruder. Offline rheometry was performed at a single temperature (160 °C), although there were three temperatures under investigation in the extruder 150 °C, 160 °C and 170 °C. For the single temperature that there was offline rheology data to compare to, the estimated viscosities are consistently much lower, for similar shear rates, using the capillary rheometer (Chiu, Yiu, and Pong, 1997). This result is opposing the results of other studies which reported the inline process viscosity to be lower than the offline capillary viscosity results (Rauwendaal and Fernandez, 1985; McAfee and McNally, 2006; Aho and Syrjälä, 2011).

A torque sensor used at the tip of an extruder screw in a single screw extruder was used to correlate torque measurements to viscosity (Revesz and Hubeny, 1977). The shear stress at this point of measurement for the torque sensor was not controlled nor could it be mathematically quantified. The authors have used the shear stress from the wall of the barrel in their equations for torque measurement (Revesz and Hubeny, 1977), but this is not representative of the shear stress at the screw tip. The authors state that these torque measurements correlate to the material's apparent viscosity but provide no evidence to back these claims up calling this method into question.

A study has been carried out comparing a side stream capillary die, an inline slit die and an offline capillary rheometer by McAfee and McNally (2006). The

results show promise for the effectiveness of using the inline slit die as a real time tool to monitor the absolute viscosity of a low density polyethylene (LDPE) and a metalocene-catalysed polyethylene (mPE) in extrusion. It was found, through investigation, that the throughput of the polyethylene had a linear relationship with screw speed when processing temperatures were kept constant (McAfee and McNally, 2006). It should be noted that the linear relationship between the mass throughput and screw speed in this body of work may not extend to other materials or other single screw extruders. The viscosity estimates from the slit die showed high correspondence with offline rheological tests carried out in a Rosand dual capillary rheometer (McAfee and McNally, 2006). The material in the capillary rheometer was made fluid by heating and then forced through a capillary die to resemble conditions that are experienced in extrusion processing. Measurements are carried out at a constant temperature and the shear stress (τ) can be calculated from the pressure drop through the capillary and the geometric constants of radius and length of the capillary. The shear rate ($\dot{\gamma}$) can be calculated from the volumetric flow rate and the capillary radius. The offline rheology tests were carried out over a number of temperatures and shear rates representative of the actual processing conditions in which testing was carried out in the extruder (McAfee and McNally, 2006).

Expanding on this work, the authors developed grey box soft sensor models using a Genetic Algorithm approach to model the viscosity in the slit die and also model the pressure reading of the first transducer in the slit die (closest to the slit die entrance) (McAfee and Thompson, 2007a; McAfee and Thompson, 2007b). A grey box model combines physical knowledge of a system with the input/output data of the system (Kroll, 2007). An open loop viscosity model

was used to estimate the shear viscosity of LDPE from system inputs. A feedback model used predictions from the open loop viscosity model, along with an error measurement between predictions from a pressure model and actual pressure measurements, to adjust the viscosity prediction in real time (McAfee and Thompson, 2007a). The viscosity model had a percentage root mean squared error (RMSE) of 0.95 % and the pressure model 2.2 % (McAfee and Thompson, 2007a). In addition to the previously discussed work, the authors completed another study that investigated two different grades of LDPE (PE1 and PE2) using the same model (McAfee and Thompson, 2007b). The percentage RMSE values for the viscosity model for PE1 was 1.03 % and the value for PE2 was 0.68 % (McAfee and Thompson, 2007b). This work highlights that by updating the same model with the new material properties, the model performance does not deteriorate while processing on the same equipment (McAfee and Thompson, 2007b).

Liu et al. (2012c) created a dynamic grey-box non-linear finite impulse response (NFIR) model for the real time prediction of the shear viscosity of a number of polymers in a single screw extrusion process. Initially a viscosity model and a barrel pressure model were both created from first principles before using a Genetic Algorithm approach. The residuals of the predicted and observed barrel pressure were used to adjust the viscosity model for real time predictions. A percentage RMSE was used to evaluate the model's performance for six different polymers, which included different grades of LDPE, HDPE and a single grade of polypropylene (PP), two different dies, a capillary and a slit, and two different single screw extruders. The percentage RMSE was in the range of 0.96 % to 2.05 % for all combinations of material, die and extruders

(Liu et al., 2012c). The results of this study indicate that the dynamic grey-box NFIR model is robust to process and material changes in an extrusion process.

Deng et al. (2013) developed a viscosity soft sensor based on a radial basis function (RBF) neural network model. The study was carried out on a single screw extruder using two grades of LDPE. The non-linear model parameters of the RBF neural networks were optimised using the differential evolution (DE) algorithm. The final RBF neural network model is selected by a two-stage selection algorithm. The melt pressure, melt temperature and armature current of the screw driving motor were selected as model inputs. The model predictions proved to be robust to the change in material (i.e. the grade of LDPE) and the percentage RMSE on the test data was 9.35 % (Deng et al., 2013). The authors make the argument that this is an acceptable generalisation error as the model was trained over a large number of operating conditions.

2.3.2 Static Soft Sensors

Mechanical Properties

A study by Fischer et al. (2011) used inline ultrasonic and near-infrared (NIR) spectroscopic measurements to infer the mechanical properties of PP nanocomposites processed in a twin screw extruder. The ultrasonic and NIR measurements were fed into chemometric PLS-1 models to make inline predictions of the impact strength of the extruded product. PLS-1 is a variant of the partial least squares regression model whereby the '1' indicates that there is a single response column i.e. the impact strength of PP. The model using ultrasonic measurements as inputs, had an R^2 value of 0.942 while the model using the

NIR measurements had an R^2 value of 0.999 (Fischer et al., 2011).

A number of recent studies have investigated the development of soft sensors for the inline characterisation of PLA by predicting the flexural strength at break at various time points during a PLA product's degradation cycle (Mulrennan et al., 2017a; Mulrennan et al., 2017b). The authors have used an estimated shear viscosity using a slit die (based on the methods described in Li, Campanella, and Hardacre, 2004; McAfee and McNally, 2006; McAfee and Thompson, 2007b), the readings from two pressure transducers and the pressure drop between the transducers as model inputs. The soft sensor models were developed using a Random Forest approach. The models had a percentage RMSE which is in the range of 0.9 % to 3.2 % for all of the flexural strength models at each of the investigated time points during degradation (Mulrennan et al., 2017a; Mulrennan et al., 2017b).

In a follow on study, Mulrennan et al. (2018) developed methods to predict the yield stress of PLA using inline data captured in a slit die. Data captured as a shear viscosity estimate, two pressure readings and the pressure drop between two transducers in the slit die were used to model the yield stress of the extruded PLA sheet. The authors have reported a RMSE error of 0.249 MPa for a Principal Component Analysis Random Forest (PCA-RF) soft sensor model.

Degradation

Molecular weight, which is viewed as a key indicator of degradation during processing and of material performance post processing (Wang et al., 2008; Paakinaho et al., 2009; Ellä, Nikkola, and Kellomäki, 2010), has been monitored and controlled during polymerisation using near-infrared (NIR) spectroscopy.

A number of studies have quantified monomer content, which is another indicator of the level of degradation occurred during processing (Ellä, Nikkola, and Kellomäki, 2010; Paakinaho et al., 2011), and molecular weight inline during the polymerisation process (Cherfi, Fevotte, and Novat, 2002; Fontoura and Santos, 2003; Othman et al., 2004; Nogueira, Borges, and Pinto, 2005; Silva, Chicoma, and Giudici, 2011). Molecular weight has been monitored and controlled during polymerisation by chemometric methods which use the wavenumbers of the NIR spectra as the input variables (Cherfi, Fevotte, and Novat, 2002; Fontoura and Santos, 2003; Othman et al., 2004; Nogueira, Borges, and Pinto, 2005). Similar approaches have been taken to monitor monomer content of the produced polymer during this process (Othman et al., 2004; Silva, Chicoma, and Giudici, 2011).

Whitaker et al. (2015) have used NIR spectroscopic measurements to make inline predictions of molecular weight (Mw) and monomer content of extruded Polylactide in a twin screw fibre extrusion process. The Mw and monomer content of the extruded samples werre assessed offline by GPC and GC-MS. A chemometric modelling approach was employed by the authors. Principal component analysis (PCA) was performed on the NIR spectra and the first three principal components were passed as inputs to a Partial Least Squares (PLS) regression model. A multivariate statistical process control chart plotting Hotelling's T^2 statistic was used to indicate whether the specification of the products was going outside of the set limits during processing (Whitaker et al., 2015).

NIR spectral data has also been used to predict the degree of thermal degradation incurred during the processing of Polyhydroxyalkanoate (PHA)

(Montano-Herrera et al., 2014). PHA is a biopolymer with low thermal stability meaning temperature has a huge impact on its material characteristics. The NIR data was collected inline during an extrusion process and was used along with multivariate data analysis to model material characteristic changes caused by thermal degradation. Principal component analysis (PCA) was used to assess trends in the thermal degradation of the different batches of PHA that were investigated in this study. The NIR spectra was used to build a PLS regression model, which detected the formation of co-oligomers which are viewed as an indicator of the level of thermal degradation which is occurring in-process (Montano-Herrera et al., 2014).

Muroga, Hikima, and Ohshima (2018) have recently used NIR hyperspectral imaging along with PLS regression to model the effects of hydrolysis on compression moulded PLA samples. Samples were moulded under a number of processing conditions which varied temperature and hold times to affect the rate of hydrolysis and the annealing rate was also controlled and varied. The samples' flexural properties and degree of crystallinity were assessed. The authors found correlations between each of these properties and the recorded NIR spectra (Muroga, Hikima, and Ohshima, 2018).

Ultraviolet-Visible (UV-Vis) spectroscopy has previously been used to determine the magnitude of thermal degradation caused to PLA during processing in a twin screw extruder (Wang et al., 2008). PLA has poor thermal stability which can cause changes to material properties in-process due to high processing temperatures and shear heating of the material in an extruder. Light in the UV-Vis range was transmitted through the polymer melt, and the absorption of the UV-Vis spectra was correlated to the number average molecular weight re-

duction, which is an indicator of thermal degradation (Wang et al., 2008). Wang et al. (2008) have used a linear model to predict the number average molecular weight of PLA from the inline UV-Vis spectral data. The authors used a specific wavelength in the UV-Vis spectral region as the model predictor. The change in amplitude of the wavelength 310 nm was used to predict the changes in molecular weight using a linear model for dried PLA (Wang et al., 2008). However, the model did not have good results for PLA samples containing moisture (Wang et al., 2008). The authors report that there is no variation in the absorbed UV-Vis spectra between dried PLA samples and samples which contain moisture but report significant variation in the level of degradation between dry and moist PLA processed under the same conditions (Wang et al., 2008). This indicates that the method is not robust enough for industrial application as processing would need to be done under highly controlled conditions due to the hygroscopic nature of PLA.

Wang et al. (2008) also proposed that a relationship exists between the *in vitro* mass loss of extruded samples and inline UV-Vis absorption spectra of PLA melt in a twin screw extruder. The authors' performed accelerated degradation on the extruded PLA samples at 60 °C and discovered that higher mass loss is related to higher UV-Vis absorption bands in the melt (Wang et al., 2008). The authors' did not extend this to prediction of mass loss from the UV-Vis absorption spectra. However, if validated, their results indicate the possibility of developing a soft sensor technology using these UV-Vis spectra to make predictions for the mass loss of PLA at various stages of degradation over time.

2.4 Research Proposal

Mechanical properties are key performance metrics when evaluating processed PLA (Ghosh et al., 2007; Paakinaho et al., 2009; Ellä, Nikkola, and Kellomäki, 2010; Mulrennan et al., 2018). Yield stress (σ_y) is viewed as a critical mechanical characteristic when assessing PLA samples (Auras et al., 2003; Weir et al., 2004c; Signori, Coltelli, and Bronco, 2009; Mulrennan et al., 2017a; Mulrennan et al., 2017b; Mulrennan et al., 2018). Currently there are no inline monitoring technologies which can quantify whether a PLA sample's yield stress will be within specification post processing.

During extrusion, PLA undergoes process induced degradation which has a significant effect on its final properties. The mechanical properties of an extruded PLA product are influenced by a number of factors including temperature (Barbieri et al., 2013) and molecular weight (Paakinaho et al., 2009). PLA is particularly susceptible to thermal degradation (Wang et al., 2008; Ellä, Nikkola, and Kellomäki, 2010; Al-Itry, Lamnawar, and Maazouz, 2012; Barbieri et al., 2013) meaning it has a very narrow processing window. A key indicator of thermal degradation is a reduction in molecular weight (Tsuji et al., 2003; Wang et al., 2008; Paakinaho et al., 2009; Al-Itry, Lamnawar, and Maazouz, 2012).

The molecular weight of PLA during degradation is a key metric when evaluating whether processed PLA is suitable for an application. Medical devices that are manufactured from PLA need to have controlled, predictable and repeatable degradation profiles (Farrar, 2008; Brown and Farrar, 2008). There have been many investigations measuring and modelling the degradation profile

of PLA used for medical applications (Weir et al., 2004a; Weir et al., 2004b; Weir et al., 2004c; Tsuji et al., 2008; Wang et al., 2008; Paakinaho et al., 2009; Paakinaho et al., 2011; Ellä et al., 2011; Barbieri et al., 2013; Navarro-Baena et al., 2016; Leroy et al., 2017).

Other grades of PLA, used for differing packaging applications, need controlled conditions to degrade fully. A number of studies have investigated varying degradation conditions using molecular weight to assess the degradation profile of the material (Hyon, Jamshidi, and Ikada, 1998; Ohkita and Lee, 2006; Sikorska et al., 2008; Karamanlioglu and Robson, 2013; Gorrasi and Pantani, 2013; Mulrennan et al., 2017c). All of these studies have focused on a wide range of grades as well as different processing and preparatory conditions of PLA.

In-process degradation of PLA will have significant impact on the final properties of any product as well as its degradation behaviour. Arguably, the degradation is best assessed by analysis of the molecular weight and/or degradation products present. Degradation products are monomer, dimer, trimer and longer length oligomers. The molecular weight of PLA is viewed as the key indicator of the level of thermal degradation incurred during processing (Wang et al., 2008) and also of product performance post processing (Paakinaho et al., 2009; Ellä, Nikkola, and Kellomäki, 2010; Bergmann et al., 2013). Unfortunately it is not possible to analyse molecular weight in real time on the production line.

PLA has complex degradation mechanisms which are influenced by product properties and processing conditions (Tsuji et al., 2003; Tsuji, 2010). However, it is known that thermal degradation will alter the viscosity of the PLA melt and this in turn will impact melt pressures and temperatures in the process. These relationships are complex and non-linear and have not been derived from first

principles. Near-infrared (NIR) spectroscopy has found application during the polymerisation process to quantify molecular weight inline during the process (Cherfi, Fevotte, and Novat, 2002; Fontoura and Santos, 2003; Othman et al., 2004; Nogueira, Borges, and Pinto, 2005). Using the NIR spectra to model the molecular weight has been achieved using chemometric methods.

In addition, a number of studies have also investigated the mass change profile of PLA during degradation (Hyon, Jamshidi, and Ikada, 1998; Ohkita and Lee, 2006; Sikorska et al., 2008; Wang et al., 2008; Karamanlioglu and Robson, 2013; Gorrasi and Pantani, 2013; Navarro-Baena et al., 2016; Mulrennan et al., 2017b). Mass loss at late stage degradation determines the biological response for medical implants to a great extent (Farrar, 2008). A body's new tissue cannot replace an implant until mass loss occurs (Farrar, 2008).

The method applied in this thesis aims to link the relationships between thermal degradation, molecular weight and a polymer's mechanical properties by using an instrumented slit die. There are a number of studies which have highlighted the use of a slit die to monitor or estimate shear viscosity (η) during extrusion (Rauwendaal and Fernandez, 1985; McAfee and McNally, 2006; Deng et al., 2014). This approach was taken to investigate whether the shear viscosity estimate would make a good predictor of PLA material characteristic properties by exploiting the relationship between shear viscosity and the polymer's molecular weight (i.e. a change in molecular weight will result in a change in shear viscosity). In addition, the NIR spectral data will also be used for the models as NIR spectroscopy has found application in extrusion (Whitaker et al., 2015) and during the polymerisation process to quantify molecular weight (Cherfi, Fevotte, and Novat, 2002; Fontoura and Santos, 2003; Othman et al., 2004; Nogueira,

Borges, and Pinto, 2005).

This work aims to minimise the time between production and receiving feedback about the extruded material's quality. This real time feedback will allow manufacturers to state, with a degree of confidence, whether a product will be within specification during processing. All of the aforementioned relationships are complex and non-linear and subject to many unknown material properties, hence are difficult to derive from first principles. The shear viscosity of a polymer will not only change due to variations in the molecular weight but also due to varying temperatures and shear rates which it undergoes during extrusion. Machine learning is proposed as a solution to modelling these relationships due to methodologies which are adaptable to non-linear systems.

Chapter 3

Machine Learning

3.1 Overview

This work proposes an approach which utilises machine learning algorithms. Machine learning poses a potential solution to modelling the complex and non-linear relationships between process data and material characteristics due to the ability to identify patterns in complex data sets and then map input features to desired outputs. These algorithms can also continue to adapt and update over time with further observations and potentially improve performance. The programming of learning algorithms on computers constitutes the science of machine learning (Michalski, Carbonell, and Mitchell, 1983; Mitchell, 1997; Kubat, 2015). All of the soft sensor approaches previously described from the literature fall under the heading of machine learning. This means that a set of models are programmed to learn about a system logically.

This is achieved by 3 methods (Raschka and Vahid, 2017):

- Supervised learning.

- Unsupervised learning.
- Reinforcement learning.

In the context of the work carried out herein, the focus has been on supervised and unsupervised learning algorithms. Both of these approaches are discussed in further detail in Sections 3.3 and 3.4. An essential precursor to any machine learning is robust and repeatable data science.

The algorithms discussed in the following sections have been used in this thesis. Principal component analysis has been used extensively to reduce large numbers of features while retaining most of the information in a data set (Jolliffe, 2002). The Random Forest algorithm has had success in modelling static responses for regression analysis (Breiman, 2001; Segal, 2004; Biau, 2012).

Prior to choosing the Random Forest model a number of approaches were investigated. The most comparable result to the chosen algorithm was presented in Mulrennan et al. (2017c). This work details the results of soft sensor models created using Bagging, Random Forest and Neural Network algorithms (Mulrennan et al., 2017c). The data set that was used in Mulrennan et al. (2017c) is different to those discussed later in this thesis. The features used to train the models were two pressure transducers, the pressure drop between those transducers and a shear viscosity estimate. A summary of the experimental conditions and the models is presented in Appendix A.

The major difference in each of the approaches was the time required to train the models. The Neural Network models took up to ≈144 times longer to train when compared to the Random Forest or Bagging models, i.e. ≈12 to 24 hours versus ≈5 to 10 minutes. The models were compared to each other using

a normalised root mean squared error (NRMSE) between the model predictions and the response vector. Normalisation of the vector of predictions and the vector of observations for the response results in a mean equal to zero and a standard deviation equal to one for each vector. Figure 3.1 presents the NRMSE for the three learning algorithms at five time points during a degradation cycle for PLA samples. The models predict the molecular weight of the PLA samples at each time point. The Bagging models and Random Forest models perform better than the Neural Networks as can be viewed in Figure 3.1. It was decided to continue with the Random Forest methodology as it allowed for considerably faster training and testing of models.

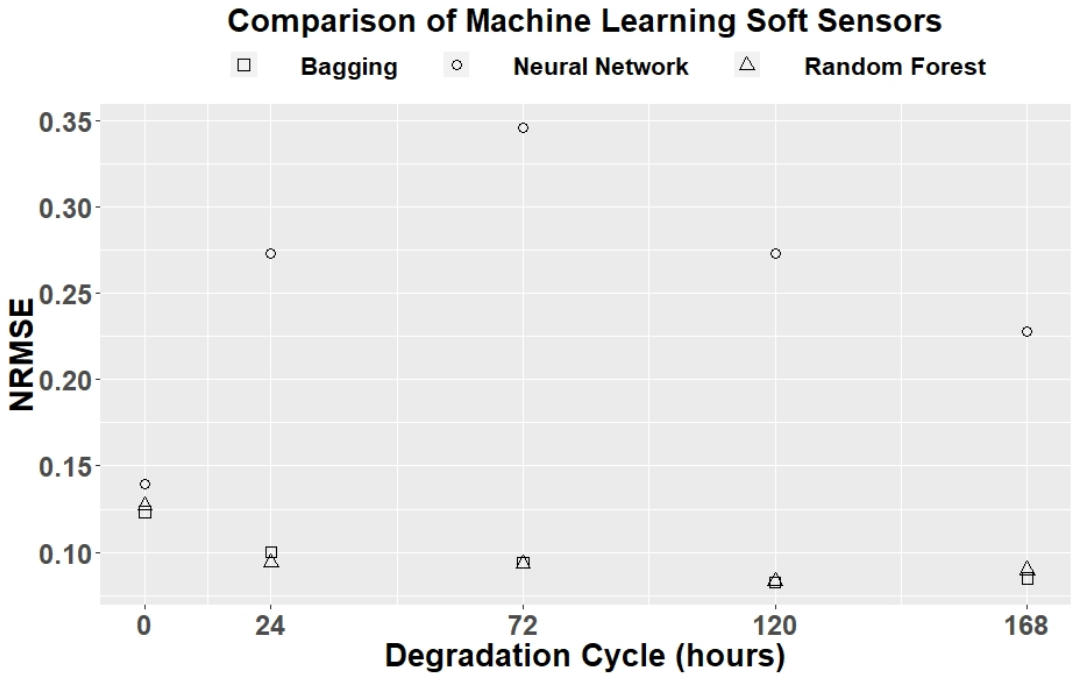

Figure 3.1: This figure compares the results of machine learning models using a NRMSE. The lowest NRMSE value indicates the best performance. This figure was originally printed in Mulrennan et al. (2017c).

3.2 Data Science

Data science has a number of methodological steps which precede the information which is presented to the end viewer.

These include (Peng and Matsui, 2017):

1. Stating and refining the question.
2. Getting and cleaning data.
3. Exploratory data analysis.
4. Feature selection.
5. Modelling the data.
6. Interpreting the results.
7. Communicating the results.

Replication of the scientific method and results is of significant interest in the research community following on from the findings of the Open Science Collaboration (OSC, 2015). This contribution discovered that over two-thirds of 100 replicated studies completed by 270 scientists failed to recreate the results of original published journal articles. For further references see the Open Science Collaboration website which contains all of their test data and results.

Data science provides a robust framework for the treatment and interpretation of data as well as providing a platform which enables replication of experiments. All stages of the data science processes should undergo meticulous documentation (Peng, 2016; Wickham and Grolemund, 2016). This allows for

fellow researchers, scientists and engineers to reproduce the results produced in any original work. There are a number of software packages e.g. Wickham (2017), Xie (2017), and Allaire et al. (2017) under constant development and an increase in publications (Peng and Matsui, 2017; Peng, 2016; Wickham and Grolemund, 2016) that enable better understanding of data and more rigorous scientific findings.

3.3 Unsupervised Learning Algorithms

Unsupervised learning draws inference from data structures which do not contain a labelled response feature. It can perform two functions in machine learning. Unsupervised learning can find the underlying structure of the data or it can perform feature reduction (Raschka and Vahid, 2017). Both functions are useful for exploratory data analysis and preprocessing of data prior to a supervised learning approach. Using cluster analysis techniques, the data structure can be explored to find hidden structure or patterns. These techniques can group data into clusters without any prior information relating to the clusters. The clusters identify data points which share some similarity and the data points are usually grouped together by a distance metric. The clusters can return important information in relation to the links between features.

Feature or variable reduction helps reduce a model's complexity by reducing the number of input features used to train the model. This may be possible if there are a number of features which have a high correlation with each other or if a feature just does not map well to a response. By removing features from the model the noisy data within those features is also removed. There are

a number of feature reduction techniques, most notably principal component analysis (PCA).

3.3.1 Principal Component Analysis

The primary objective of principal component analysis (PCA) is to reduce the dimensionality of data sets which contain a number of features with highly correlated data (Jolliffe, 2002). In essence a number of features which contain correlated data may be redundant. This means that the information from one feature x_i may also be retained in other features with which it is highly correlated. PCA transforms the data set into a new data set in which the new features, the principal components, are linear combinations of the original features. A linear combination of n features is an expression $k_1x_1 + k_2x_2.... + k_nx_n$ where k_i is a constant. The newly formed principal component 1 (PC1) will contain the greatest variance of the original data set, and each subsequent PC will contain less variance than the previous. The total variance of all the PCs combined will equal that of the original data set. In addition all of the PCs will have little or no correlation. The objective is to find a number of PCs, which is less than the total number of features in the original data set, and retain most of the variance of the original data set within them.

The transformation of data sets is achieved using linear algebra. The original data set should be normalised (μ=0, σ=1) as the transformation will maximise the variance in the newly generated PCs. Normalisation returns the features on the same scale. PCA utilises eigendecomposition to generate the PCs. The eigenvalues and eigenvectors of the original data set are calculated. The largest

eigenvalue represents PC1 and the eigenvector associated with that eigenvalue represents the loadings for PC1. The PCs are ordered from the highest eigenvalue to the lowest.

3.4 Supervised Learning Algorithms

The aim of supervised learning is to train a model using labelled data to make predictions from previously unseen data. Supervised refers to a set of samples of known labelled input features/predictors and output feature/s (Raschka and Vahid, 2017). Supervised learning provides feedback as the model predictions can be measured against the actual response. An aim of supervised learning is to create a model which will make good predictions for previously unseen data. If the developer does not have two data sets, one for training and one for testing/validation, then a single data set can be split into a training set and a testing set.

3.4.1 Decision Trees

A decision tree model uses a number of if-then-else statements for input features to make logical decisions which partition data (Breiman et al., 1984). Regression trees are a type of decision tree using a recursive binary splitting algorithm to subdivide the initial training data set contained in the root node into subsequent internal nodes and terminal or leaf nodes. Regression analysis is predictive modelling techniques, which are used to produce a quantitative measure to determine the strength of relationships between a response and the features used to predict the response. The regression tree model searches every

input feature and every value of the input features to find the combination of features and values, which partitions the data set into two subsequent nodes B_1 and B_2, minimising the combined residual sum of squares RSS as in Equation 3.1.

$$RSS = \sum_{y_i \in B_1} (y_i - \bar{y}_{B_1})^2 + \sum_{y_i \in B_2} (y_i - \bar{y}_{B_2})^2 \tag{3.1}$$

Here $\bar{y}_{B_1}$ and $\bar{y}_{B_2}$ are the mean observed response values within the internal nodes B_1 and B_2. This process is repeated at each node until the splits reach a certain criterion such as a minimum number of observations (n_{min}) in the terminal nodes. To obtain a prediction, the same if-then-else statements are followed for a new sample until a terminal node is reached. The prediction for a regression tree is the mean of the observations in that terminal node.

In Figures 3.2 and 3.3 an example of a regression decision tree is presented. The tree is presented at two different depths from the root node. This tree is built using the data in this study. The root node has a depth equal to zero in this example and the leaf nodes have a depth equal to one (Figure 3.2) and two (Figure 3.3). These images are generated from the R packages rpart, rpart.plot, rattle and Cairo (Therneau, Atkinson, and Ripley, 2015; Milborrow, 2017; Williams, 2017; Urbanek and Horner, 2015).

In Figures 3.2 and 3.3, the root node, in all instances, contains all of the data in the data set. This is represented by the percentage in the figure which is 100 % for the root node. All of the nodes contain an n value which represents the total number of observed values in the node of interest. This n value is also represented as a percentage in each of the nodes. In Figure 3.2, the n value

presented in the leaf node labelled 2 is 9850. This is 32 % of the original data set. If all the nodes are summed at each level of node depth, their percentages will equal 100 %. The number in the top centre of each node represents the mean value of the observed values, of the characteristic being predicted, within that node. In the example displayed in Figures 3.2 and 3.3, the characteristic of interest is the yield stress. For example, in the root node this value is 33 MPa (the units are not displayed in the image). Each node contains this same information.

When new data is fed into the model and follows the if-then-else rules defined by the recursive binary splitting algorithm, the mean of the observations in the terminal nodes is used as the model prediction. The features used to predict yield stress in the example are shear viscosity ($pa.s$) and pressure ($pdsd$ and $P3$). The first split that is determined in Figures 3.2 and 3.3 is made on the input feature $pa.s$ and a value of 408. This value is chosen after the algorithm has searched through all features and values of observations to determine that the feature $pa.s$ at the value 408 splits the data set and minimises the RSS in the two subsequent data partitions. All observations with $pa.s$ measurements less than 408 go down the left branch of the tree. All those observations with $pa.s$ measurements greater than or equal to 408 go down the right branch. This 'if-then-else' is repeated at each node, with different split conditions, until a stopping criteria is reached. The if-then-else rule for using Figure 3.2 as a model is:

$$\text{if } pa.s < 408 \text{ then Prediction} = 27 \text{ MPa}$$
$$\text{else Prediction} = 36 \text{ MPa}$$

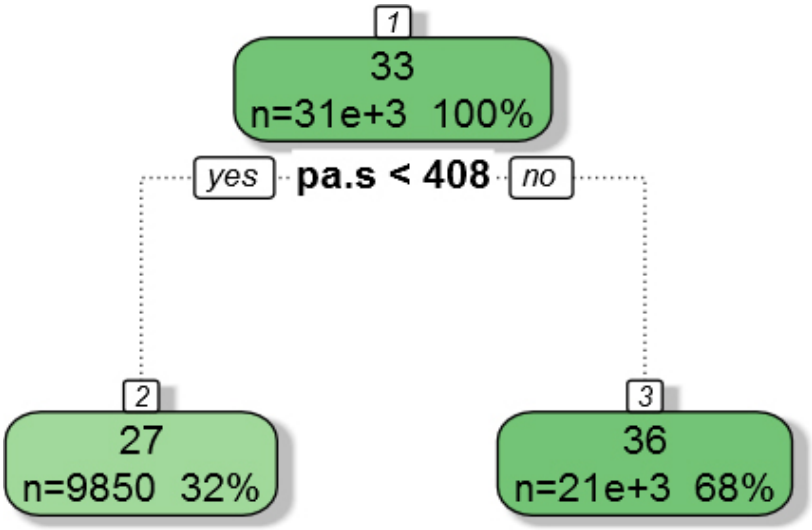

Figure 3.2: A regression decision tree with depth 1.

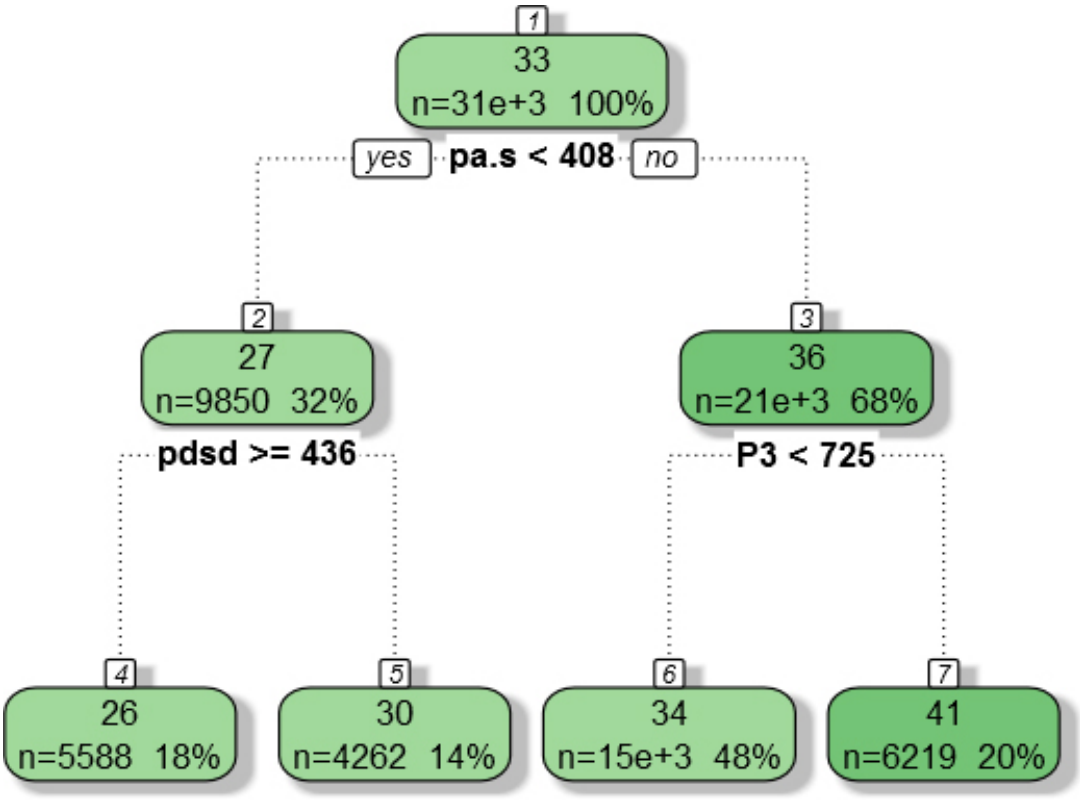

Figure 3.3: A regression decision tree with depth 2.

A tree is considered fully grown (unpruned) when the data continues to be split until each leaf node contains more than or equal to a predetermined number of observations allowed (n_{min}). A node will not be split further if it results in either of the two possible new nodes having less than the predetermined number of observations. In the case of regression, this value is typically five observations, which is an accepted heuristic. A fully grown tree also models the noise in the data. The resulting tree will overfit the training data. This means that the tree model will not make good predictions on any new data sets. Decision trees can be pruned to prevent overfitting. The stopping criteria can also be changed to stop splitting earlier but if splitting is stopped too early then the tree model error will not generalise. Another approach to overcome the overfitting problem caused by fully grown trees is to create an ensemble of trees in a random forest model (Breiman, 2001). The Random Forest error measurement follows the law of large numbers (Breiman, 2001), which states that given enough trials (trees) the observed error will converge to match the predicted error. Decision trees are the building blocks for the modelling approaches of Bagging and Random Forests which are discussed in the following sections.

3.4.2 Bagging

The Bagging approach utilises an ensemble of decision trees to make a prediction from the model. The data for each tree in the Bagging model is generated by creating a bootstrapped data set from the original training data set. A bootstrap data set is a random sample of the original data set taken with replacement. This means that data observations from the original data set can be used multiple

times within each newly created bootstrap sample set. The tree model is used to create a fully grown tree using each bootstrapped data set. The prediction for the Bagging model, using regression trees, is the aggregation (mean) of the predictions from each individual tree. The term Bagging comes from this method of bootstrap aggregation (Breiman, 1996a).

Out-Of-Bag Error

Approximately 37 % of observations from the original training data set are omitted from newly generated bootstrap sample sets. This remaining 37 % of data is then used to create out-of-bag (OOB) error measurements on the training data set. The 37 % is predetermined by the Bagging algorithm (Breiman, 1996a). Each of the observations that are left out of the tree construction are used to make predictions. These can be considered as an internal test set, used to create an accurate estimate of the generalisation error rate of the bagged features. This removes the need for cross-validation and requires little additional computing. The OOB error measurements have been shown to be as accurate as using a test set of equivalent size to the training set (Breiman, 1996b). In regression the model performance metric most commonly used is the root mean squared error (RMSE) given in Equation 3.2. This is computed using the OOB predictions y_{OOB}.

$$RMSE = \sqrt{\frac{\sum_{i=1}^{n}(y_i - y_{OOBi})^2}{n}} \tag{3.2}$$

As more of the randomised regression trees are grown and added to an ensemble, the OOB error measurement reaches a plateau. This error measurement

is usually a reasonable indicator of the prediction error in a test data set. The prediction error from the test data set is also referred to as the generalisation error. This is the error which is expected when the model is applied to any new data sets.

3.4.3 Random Forest

The Random Forest model is an extension of Bagging (Breiman, 2001). The introduction of a tuning parameter m, commonly referred to as m_{try} in the literature (and also in the software packages in R), allows the Random Forest model to control the number of input features to choose from when splitting the data at any node. This tuning parameter is what differentiates the Random Forest model from a Bagging model. m is a number which controls the size of the subset of input features to be chosen at random at each split point in every decision tree in the Random Forest. At each split point in a tree, a random subset of size m of all available input features is created. The model then searches for the best feature and split value from within that subset. The tuning parameter m adds additional randomness to the model along with the generation of the bootstrapped trees.

Trees that are grown fully have a low bias as the recursive splitting algorithm minimises the error at each split. The same trees will have a high variance as all of the noise is also modelled in the unpruned trees. Variance reduction is achieved by averaging the prediction of each tree in the Random Forest model. If there is a strong feature, then a common characteristic of the trees will be to choose that feature for the split in the bootstrapped trees. This results in

highly correlated trees. If m equals the total number of input features, then the Random Forest model is a Bagging model. By selecting an m value which is less than the total number of input features, only a subset of input features are considered at each split. This is known as decorrelation of the trees and results in a variance reduction of the model. This is achieved as averaging a number of uncorrelated features results in greater variance reduction than averaging a number of positively correlated features. The following steps summarise the algorithm.

1. Choose the total number of trees to grow in the Random Forest T.
2. Choose a value for $m \leq$ the number of input features.
3. For $t = 1$ to T:
    a Generate a bootstrap data set from the training data.
    b Grow a Random Forest regression tree R_t to the bootstrapped data, by recursively repeating the following steps for each terminal node of the tree, until the stopping criteria is reached. In this study the minimum node size, $n_{min} = 5$, was used as the stopping criteria.
        i Select m input features at random as candidates for splitting.
        ii Pick the best feature/split-point among the m which minimises the RSS in Equation 3.1.
        iii Partition the node into two internal nodes or terminal nodes in the case of the final split.
4. Output the ensemble of trees $\{R_1, R_2, ..., R_T\}$.

Breiman (2001) states that the Random Forest approach is robust to overfitting but it should be noted that there have been instances which have shown the model to overfit (Segal, 2004). To make a prediction from the Random Forest for regression, the average of the predictions of each tree in the model is determined.

3.5 Model Selection

Machine learning comes under point 5 in the data science list. After the data has undergone treatment and initial exploratory analysis the models can be built. There are no modelling solutions which suit all data types and to find the best fit for the data a number of steps are taken and considerations made. Best initial practice is to fit the data using a number of approaches and assess each against the other. By assessing the performance of each model, the best can be chosen for a given application (Hastie, Tibshirani, and Friedman, 2009).

3.5.1 Prediction Error

Three types of prediction error occur when testing a predictive model for regression on unseen test data. These apply to a mean squared error (MSE) (Equation 3.3) which measures the average squared distance between a predicted value (y_p) and an observed value (y_o).

$$MSE = \frac{\sum(y_o - y_p)^2}{n} \tag{3.3}$$

The three error types are:

- The irreducible error.
- Bias.
- Variance.

Irreducible error is the term applied to the variance in the unseen test data (Hastie, Tibshirani, and Friedman, 2009). This error cannot be reduced. Bias and variance are both error terms which can be minimised by an algorithm to attain the best model performance possible (Hastie, Tibshirani, and Friedman, 2009; James et al., 2013; Matloff, 2017). High bias and high variance error terms can prevent models from generalising well beyond the data which they are trained on (Raschka and Vahid, 2017; Matloff, 2017).

The bias error term is the expected value of the difference between the average of the predictions and the actual value of the response. High bias results from the over simplification of a system's model e.g. using linear regression to model non-linear relationships. An over simplified model will not have enough features to map to the desired response, resulting in underfitting. Ignoring or missing important features, which contain information related to a response, will result in a higher bias term. Including more features with information related to the response will reduce the bias term but also increase model complexity.

The variance error term is the variance of the predictions from a model. As a model's complexity increases so does its variance term. High variance means that small changes to the data can result in large variation in the predictions of the response. This is caused by having too many features, many of which are

redundant, or modelling the random noise in the training data which results in model overfitting. There are approaches to minimise the risk of both of these problems. Intelligent feature selection and testing with different size splits of training, test and validation data sets can result in variance reduction.

Beyond the techniques already expressed, there are number of bias and variance reduction techniques applied for specific models. Examples of these have been discussed in previous sections.

3.5.2 Tuning Parameters

The tuning parameters for a given model vary the model's complexity. The aim of the tuning parameter is to minimise the model error. For example, a Random Forest is a class of model, the final model is the class of model tuned with the tuning parameters. Each Random Forest, trained on a data set, can be a vastly different model with different tuning parameter values. The values chosen for tuning parameters can come from heuristic knowledge of a machine learning algorithm, the system that is being modelled or trial and error.

3.5.3 Feature Selection

Feature selection involves choosing the features, i.e. input variables, which are relevant to predicting the response (Blum and Langley, 1997). It should be noted that in some cases an increased number of features may improve the accuracy of the model response. Feature selection typically means choosing a reduced number of features, which will predict the response, without losing much of the accuracy of using all features. This can often improve model performance

by removing noise which would otherwise be modelled. Feature selection may also be required to reduce large data sets, to remove noise from data sets or to prevent overfitting of the model during training. Reducing the number of features used to model a system will in turn reduce the model's complexity as well as reducing the computational cost of training the model.

Feature selection is achieved through, but not limited to, the following approaches (adapted from (Guyon and Elisseeff, 2003)):

- Inherent knowledge of the system.
  - Features can be removed as not all may be required to model the response.
- Feature importance algorithms.
  - These rank features in order of importance and the least important features can often be discarded.
- Statistical analysis techniques to detect features which are outliers or contain a lot of noisy data.

Random Forest - Feature Importance Scores

The Random Forest algorithm evaluates the importance of the features by permuting each feature individually when building the model and assessing how each will affect the overall model error. Features are ranked from top based on those which had the greatest influence on the RMSE value. This proves beneficial when working with large data sets as this characteristic of the algorithm

can identify features which have a little or no influence on the model error and can therefore be discarded.

3.6 Summary

This chapter has outlined the machine learning approaches that have been used to develop the soft sensors. An introduction to the principals of data science was provided as well as a review of the literature for the proposed methods. The fundamental algorithms are principal component analysis and the random forest algorithm. A description has also been provided for the various models and tuning parameters which make up the random forest algorithm.

Chapter 4

Extrusion Processing - Hardware and Experiments

4.1 Introduction

This section details the hardware used during twin screw extrusion processing. This includes the processing equipment and the data acquisition (DAQ) system components. The available data variables that can be monitored from the experimental trials on the extrusion process investigated in this research, are shown in the first column of Table 4.1. The objective is to utilise the data gathered from these sources to build models to predict the changing final properties of the material in process (outlined in the second and third columns). The aim is to use these models and advance their in-process prediction capabilities of these end material properties. Manufacturers view these material characteristics as important. The degradation rate in Table 4.1 can be defined as either the rate of change of mass or the rate of change of molecular weight over time.

Table 4.1: The inline process data and the properties of interest to predict.

Process Monitoring	**Material Structure**	**End Properties**
Pressure Temperature Viscosity estimate NIR spectra	Molecular weight	Mechanical properties Degradation rate

4.2 Extrusion

There is a large variety of designs for polymer extruders. A simplified breakdown of an extruder's operating principles is provided here and Figure 4.1 can be used as a reference. Typical components are the feed hopper, the screw (or screws for twin or multi-screw extruders), the barrel and the die. It should be noted that there are extensive differences in the design of twin screw extruders making it difficult to provide general comments on operating principles (Rauwendaal, 2014). Typical applications for twin screw extrusion include profile extrusion and compounding (Rauwendaal, 2014). Material is fed into an extruder barrel from a feed hopper typically flowing by gravity. The dry material is then conveyed through the barrel by the flights of the extruder screw/s as they rotate. The conveying action is determined by screw types and configurations. The polymer becomes molten absorbing heat via the barrel heaters. In addition, there is a mechanical shear heating of the polymer caused by friction of the polymer against the screw/s and the barrel wall as it moves through the extruder. Ideally, a homogeneous molten polymer will be pushed through a die at the end of the extruder adopting the shape of the flow channel. Rauwendaal (2014) provides a great resource on the process operation and mechanisms of polymer extrusion.

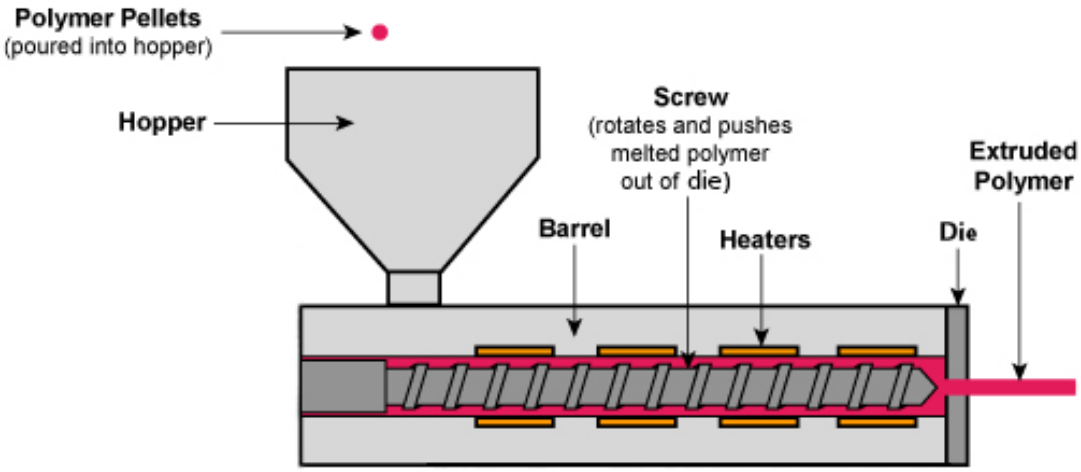

Figure 4.1: An example of an extruder and extrusion process. This image was originally posted online by The University of Akron (2019) and has been edited for presentation here.

4.3 Twin Screw Extruder

The experimental work in this study was carried out on a Prism twin screw extruder. The extruder had 16 mm diameter co-rotating screws in a length to diameter ratio of 25:1. An adaptor and slit die were attached to the end of the extruder and both were instrumented (see Section 4.3.3). A Thermo-Prism TSE Systems calender roll off unit was used to haul the extruded PLA from the die as sheet. See Figure 4.2.

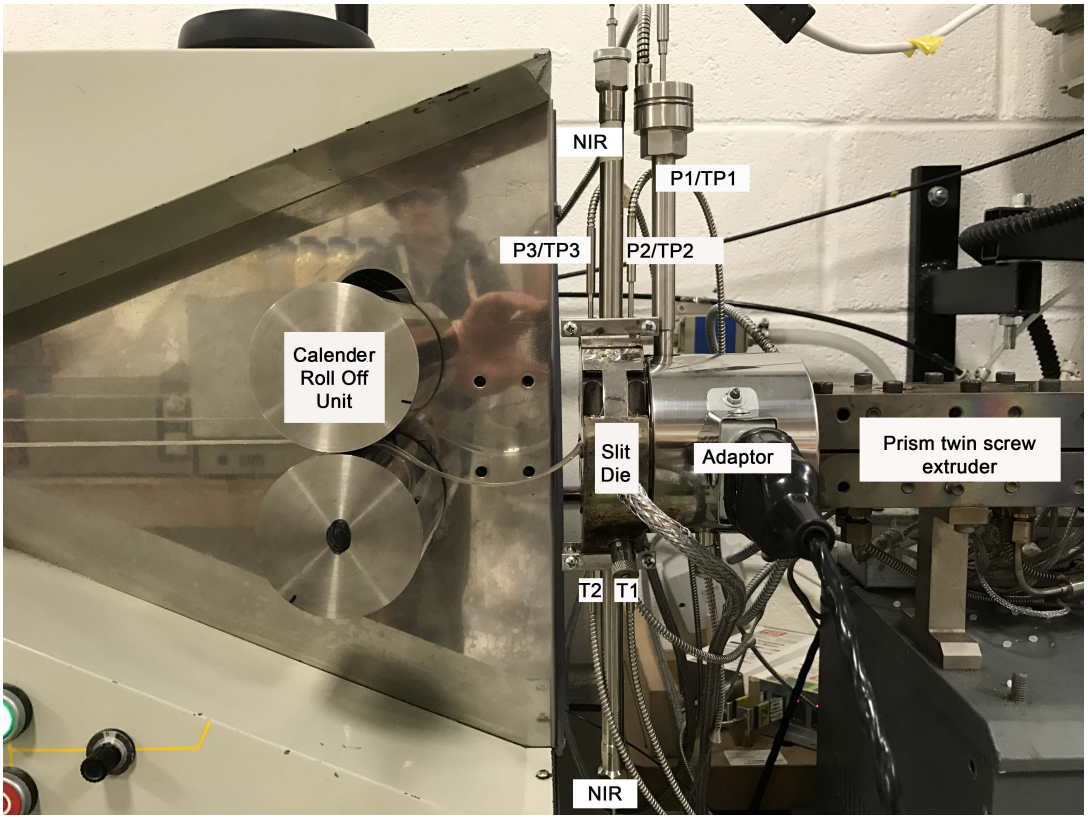

Figure 4.2: The extruder, adaptor, slit die and calender roll off unit.

The screw speed was controlled by a hand held digital control unit. The actual screw speed had to be measured using a tachometer at a number of control units settings. The black dots in Figure 4.3 represent the manual measurements of the screw speed at each of the control unit's settings. The dial settings begin at 4.5 on the control unit increasing in steps of 0.5 up until 22. The red line represents the linear model, which has been used to approximate the screw speeds used for this study. Each screw speed used is represented by the blue dots; these are ≈56 RPM and ≈83 RPM. The approximations used by this model are supported by results from power spectrum analysis (Section 6.5) performed on pressure measurements recorded during the extrusion process.

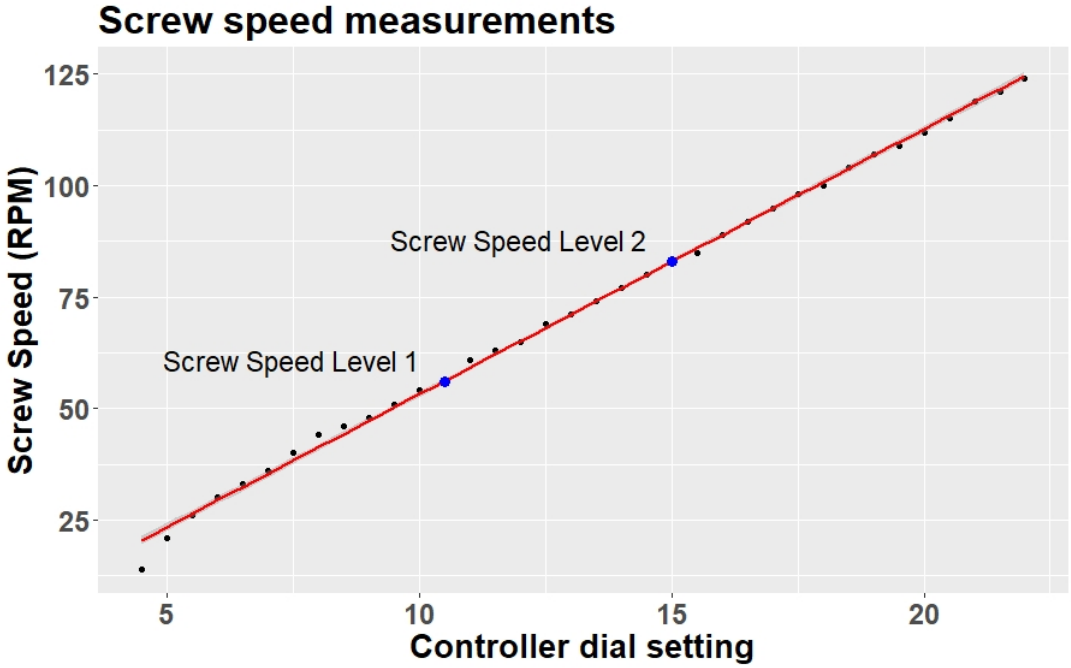

Figure 4.3: The screw speed plotted against the dial settings used to control the motor driving the screws.

4.3.1 Volumetric Feeder

A Colorette volumetric feeder was used and controlled with a rotary dial. Prior to the processing experiments, a number of trials were carried out using an analytical balance to measure the feed rate at different settings of the dial. The rotary dial was set and the PLA resin mass was measured every 30 seconds with an analytical balance. This test was repeated at three settings of the rotary dial, in triplicate, to measure the feed rate at those settings and also to test for repeatability. It was discovered that there was a linear relationship between the settings of the rotary dial on the volumetric feeder and the amount of material which was dispensed. This allowed for a linear model to be built, using the mean of the triplicate values recorded for each of the controller dial settings, to

approximate the feed rate (Figure 4.4).

Table 4.2: Feed rate triplicate measurements and the variance between measurements.

Measurement	Controller Dial Setting		
	1	1.5	2
1 (g/30 s)	5.48	10.19	15.58
2 (g/30 s)	6.56	10.59	15.45
3 (g/30 s)	5.95	10.7	14.83
Mean	**5.99**	**10.49**	**15.29**
Variance	**0.29**	**0.07**	**0.16**

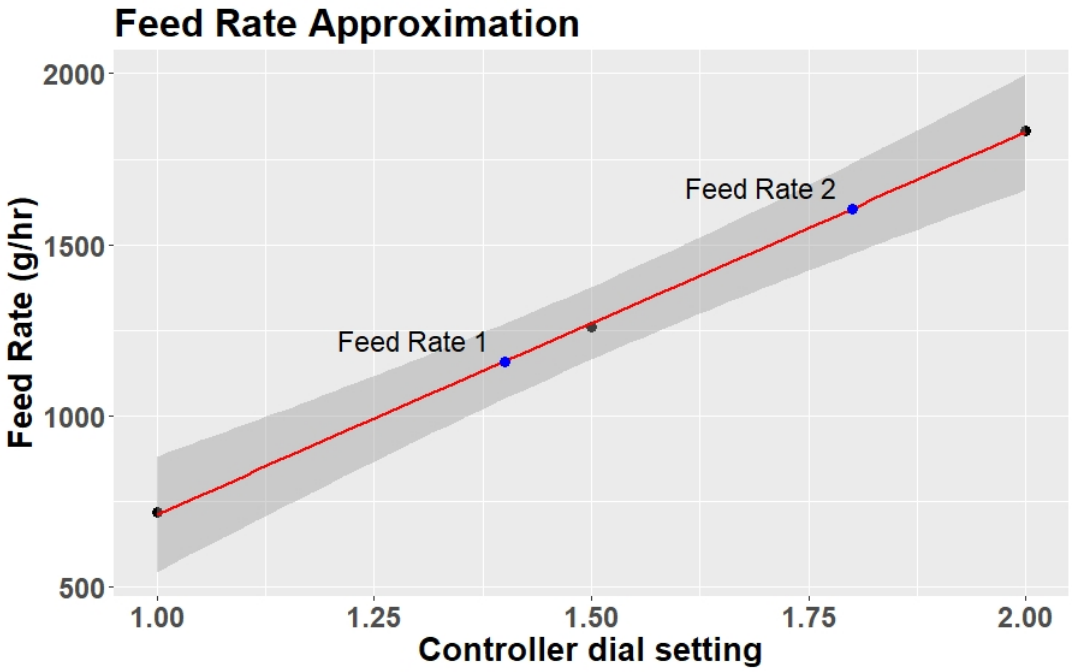

Figure 4.4: The feed rate plotted against the dial settings used to control the motor driving the screws in the feeder; the greyed region in the plot represents the 95 % confidence intervals.

4.3.2 Slit Die

The instrumented slit die (Figure 4.5) is a key element of this research as it enables collection of data from four sensors and two NIR transducers in contact with the melt. The slit die had dimensions of 34 mm slit length (L_s), 1 mm slit height (H) and 20 mm slit width (W).

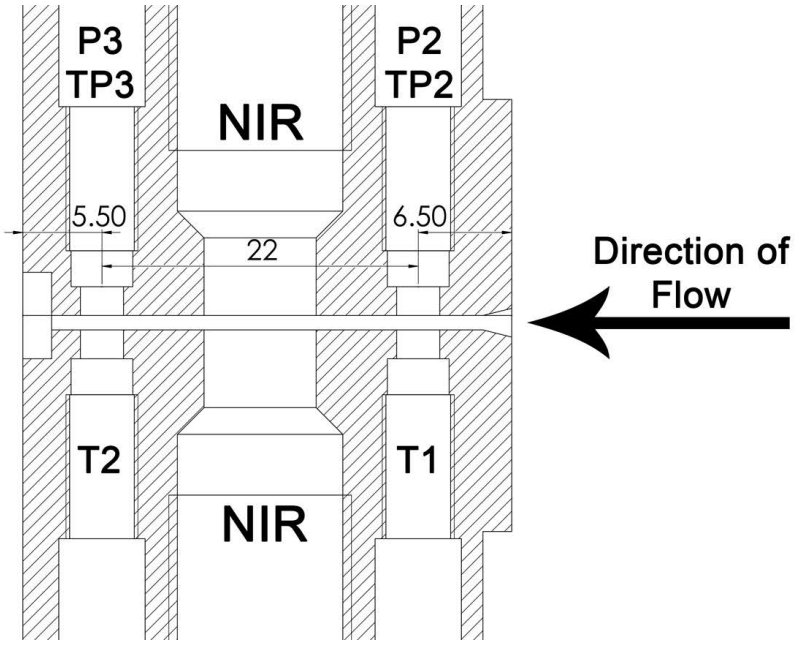

Figure 4.5: The slit die (measurements are in mm).

For each experimental condition, the throughput (mass flow rate) was measured once the system reached a steady state, which could take up to ≈30 minutes in the most extreme case when changing between operating conditions. The time at which the throughput measurements were taken was recorded so that these measurements could be matched to the data being captured by the data acquisition system. The average mass flow rate ($\dot{m}$ with units g/hr) was measured manually by measuring the average mass of the extruded sheet over

six 30 second periods for each experimental condition.

The material's density (ρ with units kg/m^3), which was taken from the material data sheet, is then required to calculate the average volumetric flow rate (Q with units m^3/s) in Equation 4.1. As the melt temperature increases during processing, the density of the material will decrease. The material's density at varying temperatures has not been investigated. Therefore, the value taken from the material data sheet has been used for all calculations. This is a source of error for the true value of shear viscosity of the material during processing. This does not prevent the estimated value being used as a reference or as a predictive input value in a model.

The 34 mm length of the slit means that the estimated additional average residence times (t_R) for the system in steady state were limited to a range of ≈3.2-5.4 seconds. The average residence time is presented in Equation 4.2 as the volume of the slit channel divided by the volumetric flow rate of the material (Q).

$$Q = \frac{\dot{m}}{3600 * 1000 * \rho} \tag{4.1}$$

$$t_R = \frac{L_s HW}{Q} \tag{4.2}$$

There are a number of studies which have highlighted the use of a slit die to measure shear viscosity (η) (Rauwendaal and Fernandez, 1985; McAfee and McNally, 2006; Deng et al., 2014) in extrusion processing. The value of shear viscosity can be estimated from the pressure drop (ΔP) between the two pressure transducers in the slit die, the volumetric flow rate, the slit die geometric

constants - width, height and the length between the transducers (L_t) and the Rabinowitsch correction factor. The apparent shear viscosity of a polymer (η) is given by the ratio of shear stress (τ) to shear rate ($\dot{\gamma}$) in Equation 4.3. The wall shear stress can be calculated from the pressure drop (ΔP) and the geometric constants (H and L_t) of the flow channel in Equation 4.4. The apparent shear rate is calculated from the volumetric flow rate and the geometric constants (W and H) of the flow channel in Equation 4.5.

$$\eta = \frac{\tau}{\dot{\gamma}} \tag{4.3}$$

$$\tau = \frac{H\Delta P}{2L_t} \tag{4.4}$$

$$\dot{\gamma} = \frac{6Q}{WH^2} \tag{4.5}$$

This shear viscosity calculation (Equation 4.3) holds true for cases where fully developed flow has been achieved in the slit die. In a study by Drexler and Han (1973), a streak photography method relating to shear stress in the slit die was applied to polymer melts. The polymer was processed in a single screw extruder which had a gear pump connected to pump the melt through a slit die. These results indicated that a fully developed flow was achieved at an entrance length of 2 to 3 times the slit height (or capillary diameter). This result should be taken with caution when considering the findings from Han and Charles (1970) which found that shear stress alone may not be sufficient for predicting a fully developed flow in the die. Han and Charles (1970) found that

in some cases the ratio of entrance length to diameter could be as large as 20:1 for a fully developed flow to occur in a capillary die. The entrance length of the melt in the slit die in this work is 6.5 mm i.e. an L/D ratio of 6.5:1 (see Figure 4.5).

The Rabinowitsch correction factor is applied when knowledge of the material's shear thinning index (n) is available (Equation 4.6). The Rabinowitsch correction factor has not been used when estimating shear viscosity in this study due to degradation occurring to the PLA during offline rheological testing. The results from the offline rheology were too variable to determine the shear thinning index with confidence (see Appendix C). Work described in Nguyen, McNally, and Clarke (2014) also describes a viscosity soft sensor based on a slit die which only uses the ΔP and Q variables which appeared to be applied successfully in a control scheme to modulate viscosity changes in the extrusion of recycled polymer. A shear viscosity estimate ($\hat{\eta}$) which was used as a feature variable for the soft sensor models described in this research is shown in Equation 4.7 i.e. the combination of Equations 4.4 and 4.5.

$$\eta = \left(\frac{\Delta P W H^3}{12 L_t Q}\right)\left(\frac{3n}{2n+1}\right) \tag{4.6}$$

$$\hat{\eta} = \frac{\Delta P W H^3}{12 L_t Q} \tag{4.7}$$

4.3.3 Sensors

A Dynisco TPT412-3M-6/18-C16 NaK filled pressure transducer ($P1$) with an embedded Type J thermocouple ($TP1$) was used in the adaptor. The Dynisco

pressure transducer had a full scale output of 20.7 MPa with a repeatability of measurement rated at ±0.1 % of the full scale output. The combined error is ±0.25 % of the full scale output.

Two miniature fibre-optic pressure transducers ($P2$ and $P3$) were placed at the slit die channel entrance and exit. These transducers have a 3 mm diameter diaphragm in contact with the melt. Each transducer had a range of 0-25 MPa with a repeatability of measurement rated at ±0.2 % of the full scale output. The transducers each had an embedded Type K thermocouple ($TP2$ and $TP3$). Two miniature probe housings were especially developed to each contain a flush mounted Type K thermocouple ($T1$ and $T2$). Thermocouples which are embedded in an extruder die are heavily influenced by the heated metal of the die which surrounds the transducer. These do not give clear indications of the polymer melt temperature as it flows through the die (Shen, Malloy, and Pacini, 1992; Brown, Kelly, and Coates, 2004; Rauwendaal, 2014). It was anticipated that $T1$ and $T2$ would give a better measurement of the melt temperature of the material in the slit die in comparison to $TP2$ and $TP3$. The dimensions of the housings matched those of the miniature pressure transducers. The miniature fibre optic pressure transducers and the miniature thermocouples were manufactured by FOS Messetechnik Gmbh.

All pressure and temperature signals are transmitted through signal conditioners to an analog to digital (ADC) unit which transmits the individual output signals via USB. All of this hardware was supplied by FOS Messtechnik Gmbh. The pressure and temperature data was collected using a LabVIEW VI created and supplied by FOS Messtechnik Gmbh. This system was updated to capture additional data from the Dynisco transducer used in the adaptor zone.

4.3.4 Near-infrared (NIR) Spectroscopy

A spectroscopy system, provided by FOS Messtechnik Gmbh, consisted of two fibre-optic probes, the probe housings and an LR1 compact USB spectrometer manufactured by Aseq-Instruments. Data acquisition was carried out through a LabVIEW interface developed by FOS Messtechnik Gmbh. The spectrometer operated in the near-infrared region in transmission mode and had both probes attached in the central tappings of the slit die. NIR spectra are measured in the 4000-7500 cm^{-1} wavenumber range and the spectrometer has a resolution of 4 cm^{-1}. A laptop, supplied by FOS Messtechnik Gmbh, captures NIR spectra at user specified time points using Interspectrum software. The samples were typically collected every 30 seconds.

4.4 Processing Experiments

The processing experiments were carried out over two days. The first set of experiments were conducted on 02/03/2017. These are referred to as the 'initial experiments' and allowed for sufficient data to be collected to develop the soft sensor models. The second set of experiments, known as the 'validation experiments' were conducted on 06/02/2018 and were used to validate the soft sensor models.

4.4.1 Initial Experiments

Twelve different sets of processing conditions (treatments) were investigated using different combinations of feed rate, screw speed and the temperature profile

of the barrel, adaptor and slit die. An experimental design approach was employed to utilise the benefits of randomisation and replication. In most statistical modelling methodology it is usually required that the observations are independent and identically distributed (i.i.d) random variables and this is achieved through the randomisation of the experimental runs. This randomisation also averages out any unknown systematic bias which may distort any results. Replication is an independent random repetition of all experimental process variable combinations and is used to increase the precision or reduce the variability of an experiment. Replication also provides a platform to estimate the experimental error by identifying variability between and within experimental runs.

There were three controllable input process variables (factors): temperature profile, screw speed and feed rate. The high and low levels for these factors were based on the published literature (Gao et al., 2000; Brown, Kelly, and Coates, 2004; Kelly et al., 2008; Wang et al., 2008; Ellä, Nikkola, and Kellomäki, 2010; Robin et al., 2011; Paakinaho et al., 2011) and Differential Scanning Calorimetry (DSC) results (these are presented in Appendix B) as to which processing conditions were likely to have an impact on the final product characteristics. To limit the number of experimental runs required, the temperature profile was chosen as a factor rather than each individual temperature zone. The temperature profile included four barrel zones, the adaptor zone and the die zone. Although best efforts were taken to completely randomise the processing runs, the time required for temperature profiles to reach steady state between factor levels limited the options available. The final experimental design randomised the order of the temperature profiles and then randomised the treatments within the temperature profiles. The chosen levels for each factor are highlighted in

Tables 4.3, 4.4 and 4.5. In total there were 24 experiments which included two replicates for each treatment. Table 4.6 outlines each of the treatments and replicates.

Prior to all processing experiments, the PLA was dried for four hours at 65 °C. This was done to remove any residual moisture contained within the raw material resin. This was in line with the drying procedures for all of the material characterisation tests.

Table 4.3: Factor levels for the feed rate.

Factor Level	Feed Rate (g/hr)
Low	1160
High	1600

Table 4.4: Factor levels for the screw speed.

Factor Level	Screw Speed (RPM)
Low	56
High	83

Table 4.5: Factor levels for the temperature profile.

Factor Level	Temperature Profile (°C)					
	Zone 1	Zone 2	Zone 3	Zone 4	Adaptor	Die
Low	130	190	200	200	200	200
Mid	130	190	200	205	210	210
High	130	190	200	210	220	220

Table 4.6: Processing runs and each treatment.

Processing Run No.	Treatment	Screw Speed Level	Feed Rate Level	Temperature Profile Level
1	1	Low	Low	Mid
2	2	High	Low	Mid
3	2	High	Low	Mid
4	3	Low	High	Mid
5	4	High	High	Mid
6	1	Low	Low	Mid
7	3	Low	High	Mid
8	4	High	High	Mid
9	5	High	High	High
10	6	Low	High	High
11	7	Low	Low	High
12	8	High	Low	High
13	7	Low	Low	High
14	6	Low	High	High
15	5	High	High	High
16	8	High	Low	High
17	9	High	Low	Low
18	10	Low	High	Low
19	9	High	Low	Low

Continue on the next page

20	10	Low	High	Low
21	11	High	High	Low
22	11	High	High	Low
23	12	Low	Low	Low
24	12	Low	Low	Low

4.4.2 Validation Experiments

The extruder was refurbished, with new barrel heating cartridges, in the time between the initial experiments and the validation experiments. Although some of the validation experiments had barrel zone temperatures set at the same levels as the initial experiments, the temperature in these zones did not reach the same levels as the initial experiments.

The factor levels for the temperature profile for the validation experiments are presented in Table 4.7. It had been planned to run a *Low-Mid* temperature profile for the validation experiments. With the difficulties caused by the barrel temperatures, three profiles were run as close to the original temperature profiles as possible, while a fourth temperature profile was also run. None of the runs were replicated in this set of experiments.

There were six processing runs in total and four of these were set to the same treatment combinations as the initial experiments. Although those four were set to the same levels these temperatures were not reached as has been pointed out. Two of the validation experiments' processing runs used the *Low-Mid* temperature profile.

Table 4.7: Factor levels for the temperature profile.

Factor Level	Temperature Profile (°C)					
	Zone 1	Zone 2	Zone 3	Zone 4	Adaptor	Die
Low	130	180	200	200	200	200
Low-Mid	130	180	200	200	205	205
Mid	130	180	200	200	205	210
High	130	180	200	200	210	220

Table 4.8: Processing runs and each treatment.

Processing Run No.	Treatment	Screw Speed Level	Feed Rate Level	Temperature Profile Level
25	10	Low	High	Low
26	8	High	Low	High
27	14	Low	High	Low-Mid
28	3	Low	High	Mid
29	13	Low	Low	Low-Mid
30	9	High	Low	Low

4.5 Summary

The processing hardware and design of experiments have been detailed in this chapter. The slit die, which is the vital component for capturing process data, has been described and a description of the estimated shear viscosity equations

has also been provided. The issues relating to the refurbishment of the extruder between the initial and validation experiments have been highlighted. Post the initial and validation experiments, the material properties of the extruded sheet had to be characterised and quantified. These properties are the model responses for the soft sensors.

Chapter 5

Material - Preparation and Characterisation

5.1 Introduction

The PLA grade used in this study was Ingeo™ Biopolymer 2003D and was obtained from NatureWorks LLC. This is a general purpose extrusion grade suitable for sheet production and can be processed on conventional extrusion equipment. This chapter discusses the characterisation of PLA material properties, and the methodologies applied, for the extruded samples from each processing run.

5.2 Sample Preparation

Post extrusion, samples had to be cut from the extruded sheets. To ensure accurate and consistent sample dimensions a cutting die was designed and man-

ufactured for use with a Ray-Ran pneumatic operated test sample cutting press. The press generates on average a cutting force of up to 50 kN and was operated at 0.7 MPa. The cut samples were 40 mm x 10 mm x 1 mm. In total 450 samples were cut for characterisation, i.e. three samples for each of the thirty processing runs at five time points for degradation testing (the degradation procedure is detailed in Section 5.4). All samples were then coded to ensure that no errors occurred with the data collection during the characterisation testing. See Table 5.1 for a detailed explanation of the sample coding.

Table 5.1: Sample codes for accelerated degradation testing and characterisation testing.

1-30	This number represents the experimental run when the sample was processed in the extruder
A,B,C,D,E	A = 0 hours under accelerated degradation conditions B = 24 hours under accelerated degradation conditions C = 72 hours under accelerated degradation conditions D = 120 hours under accelerated degradation conditions E = 168 hours under accelerated degradation conditions
1-3	This number represents which of the triplicates it is from the sample batch
Example code 22B1	This is a sample which was processed during run 22 out of 30 It has undergone accelerated degradation conditions for 24 hours It is the first of the triplicates from the sample batch 22B

5.3 Yield Stress Characterisation

In total 90 samples were cut for yield stress characterisation and none of these underwent degradation testing. This gave a set of triplicates for each of the 30 processing runs. A tensile test for each sample was carried out on a Zwick Roell z0.5 table top testing machine. The testing apparatus with a sample loaded is shown in Figure 5.1. This machine has a load cell of 0.5 kN and the measurement error was recorded as ± 1 % at the last calibration prior to testing. The tests were carried out in triplicate at a speed of 5 mm/min and each sample was assessed for its yield stress (σ_y), measured in MPa. The yield point on the stress-strain curve indicates the limit of elastic behaviour of a sample and the stress at which this occurs is referred to as the yield stress.

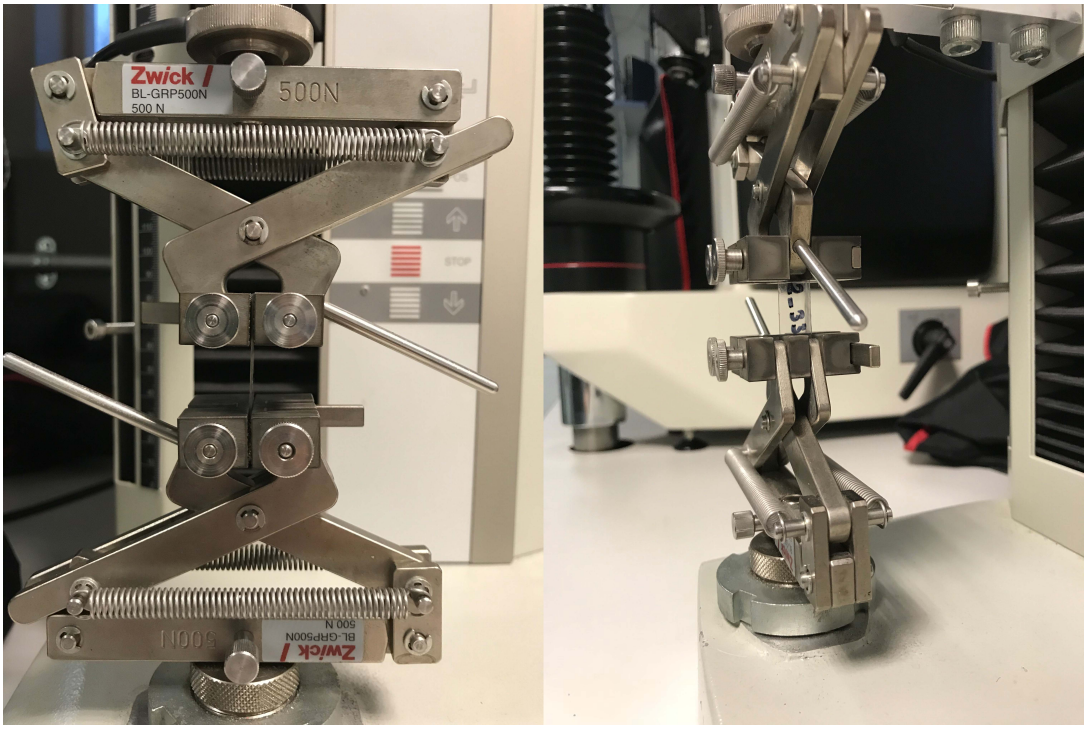

Figure 5.1: The front and side views of the Zwick Roell z0.5 tensile tester with a sample loaded.

5.4 Accelerated Degradation Procedure

Accelerated degradation testing was completed in accordance with the International Organisation for Standardisation (ISO) 15814:1999. Phosphate buffer saline (PBS) solution was prepared by dissolving a single PBS tablet in 200 ml of deionised water. 360 snap top vials were each filled with 20 ml of this PBS solution. A single sample was placed in each vial. The ratio of the test solution in millilitres to the mass of the test sample in grams was greater than 30:1 for each case.

These vials were then placed in an air flow oven at 70 °C. Samples were removed from the oven after 24 hours, 72 hours, 120 hours and 168 hours. The samples are estimated to degrade at $\approx$ 27 times their normal rate under these accelerated conditions (Weir et al., 2004b). 168 hours under accelerated conditions is estimated to be the equivalent of 6 months *in vivo*. Upon removal from the oven, samples were rinsed with deionised water to remove as much PBS solution as possible and patted dry with a paper towel. These samples were then put into an air flow oven at 30 °C for 48 hours with 500 grams of desiccant to remove all residual moisture. After 48 hours the samples' dry masses were recorded.

Figure 5.2 highlights how samples were immersed in the PBS solution and held within the glass vials. The sample codes are clearly identifiable in Figure 5.2. Figures 5.3, 5.4, 5.5 and 5.6 show the samples after removal from the oven and PBS solution after 24 hours, 72 hours, 120 hours and 168 hours respectively. It is evident in Figures 5.5 and 5.6 that the samples became much more fragile at later time points and small boxes were made to contain each sample as they

began to fragment. In the case of the samples at 168 hours, i.e. Figure 5.6, nearly all samples fell apart after removal from the oven.

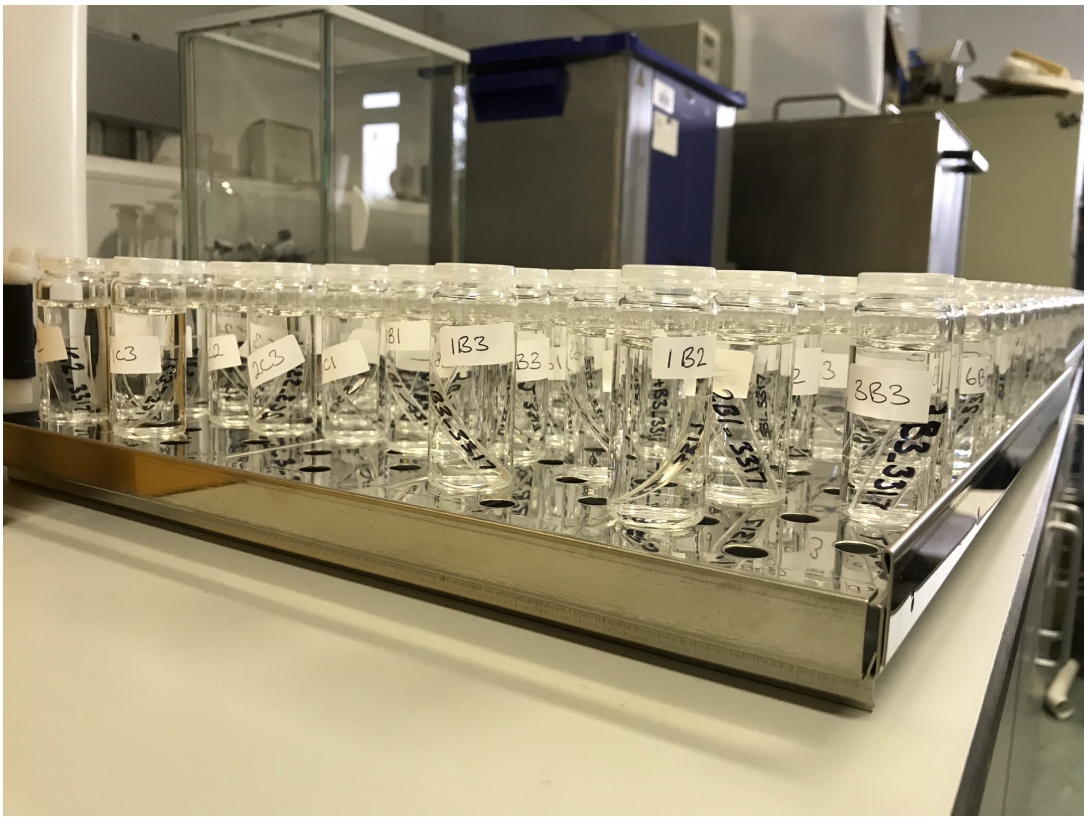

Figure 5.2: The samples are contained within 22 ml snap top glass vials with 20 ml of PBS, each with a label to identify the sample.

Figure 5.3: Samples removed from the oven after 24 hours.

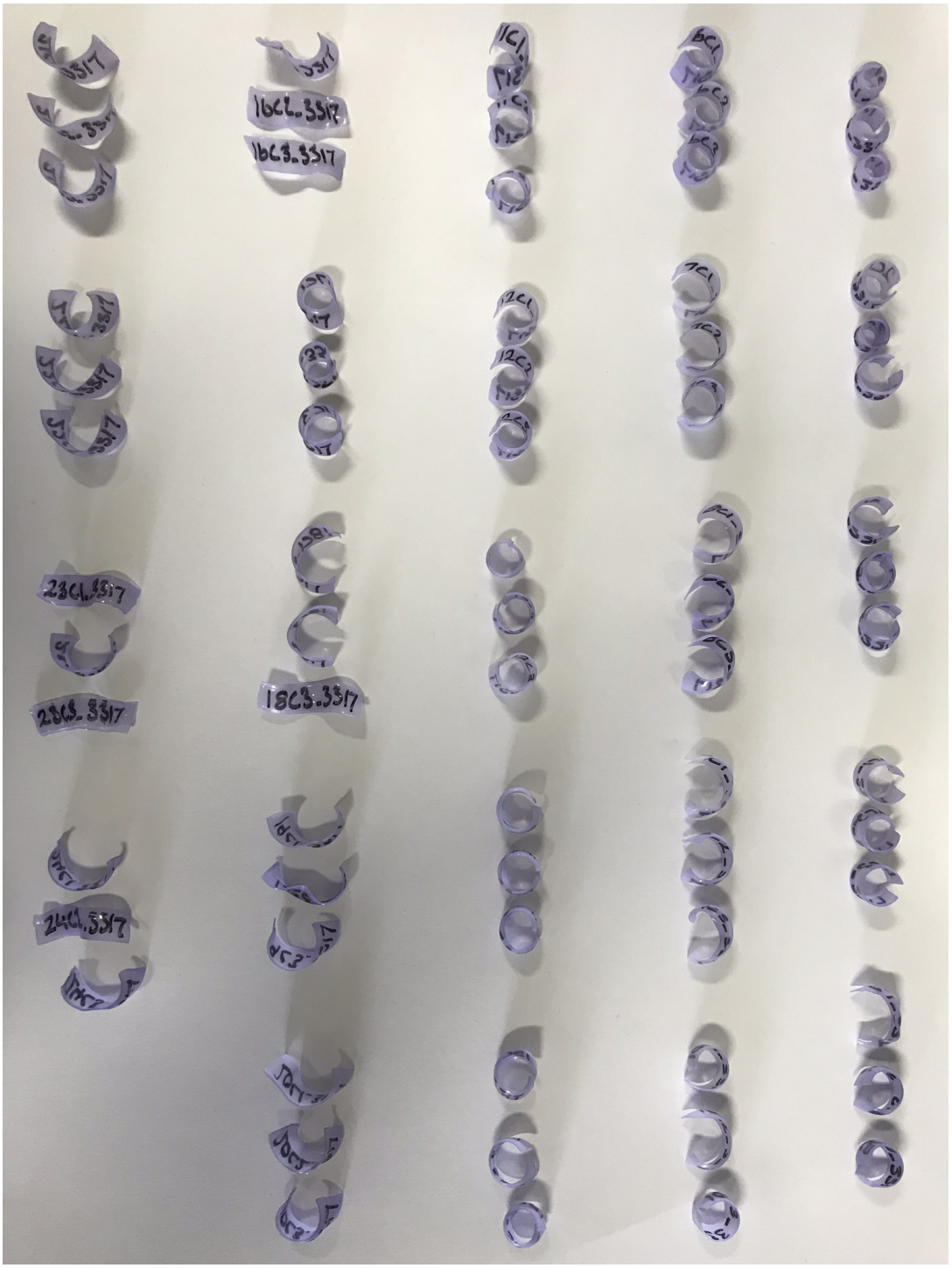

Figure 5.4: Samples removed from the oven after 72 hours.

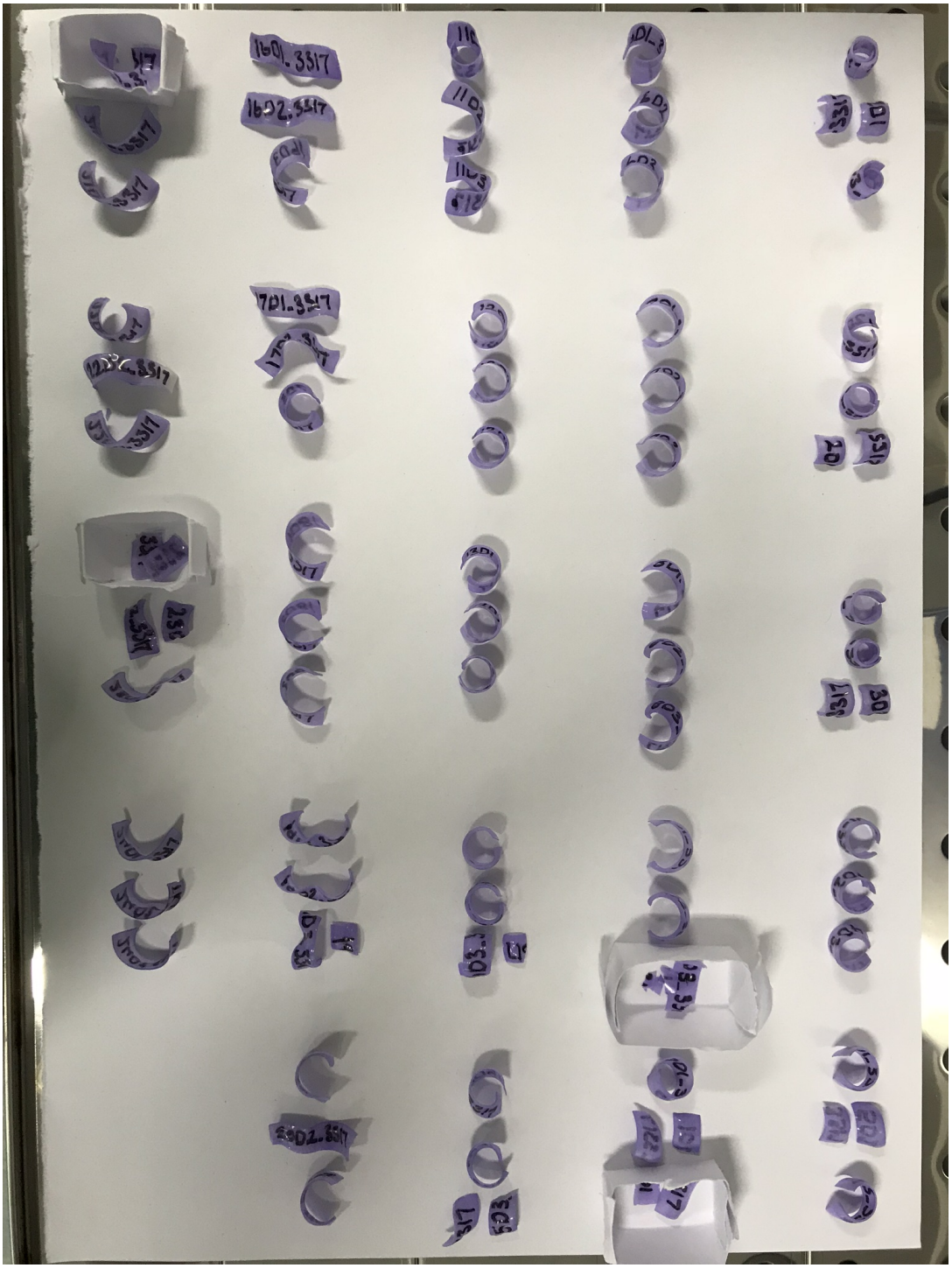

Figure 5.5: Samples removed from the oven after 120 hours.

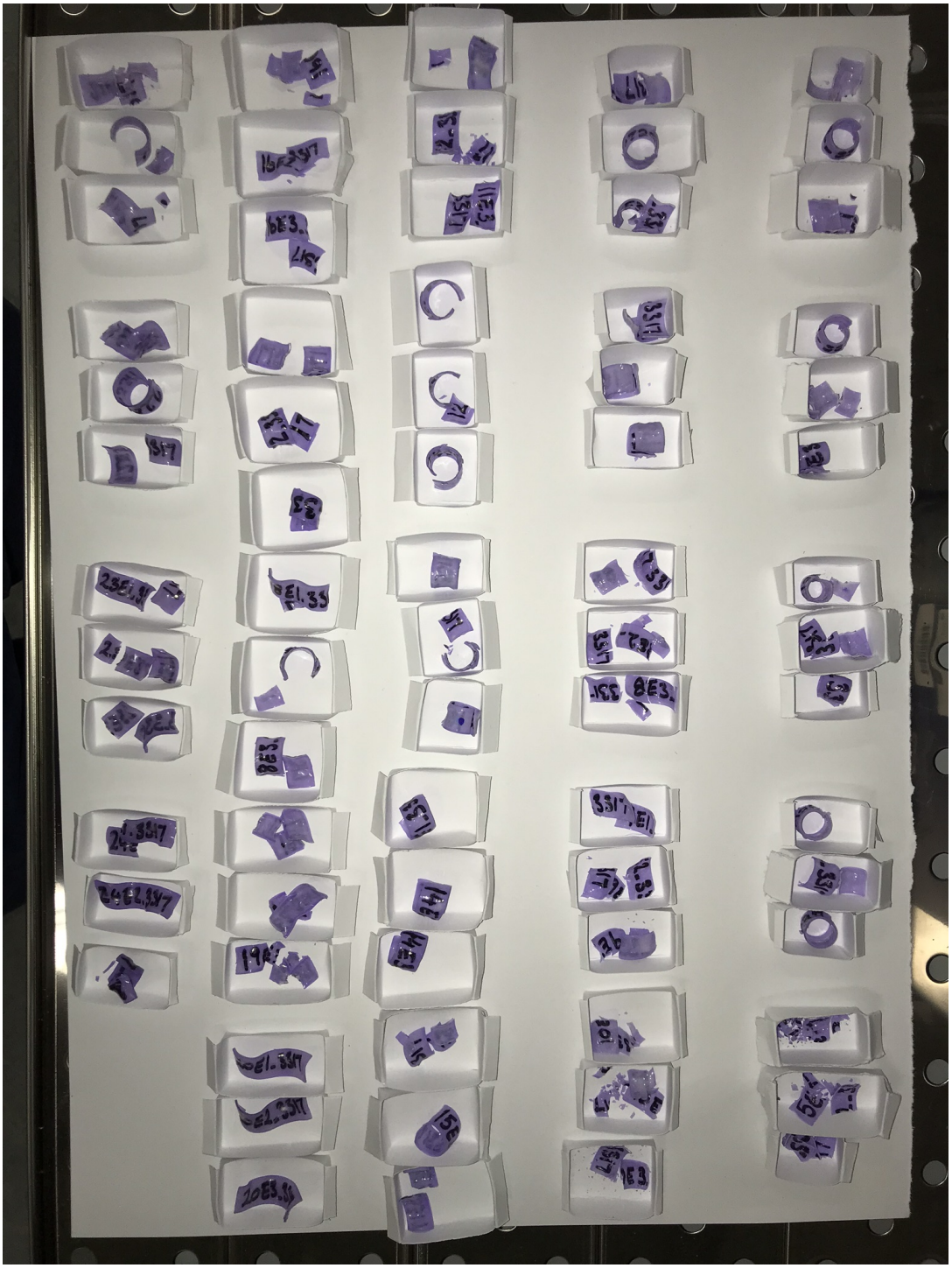

Figure 5.6: Samples removed from the oven after 168 hours.

5.5 Mass Change Characterisation

The initial mass was recorded for all samples using an analytical gravimetric balance (resolution of 0.1 mg) prior to the commencement of characterisation tests. In total there were 360 samples used for the accelerated degradation procedure. Upon completion of the accelerated degradation procedure, samples were removed from the oven, rinsed with deionised water to remove as much phosphate buffer saline solution as possible and patted dry with a paper towel. These samples were then put into an air flow oven at 30 °C for 48 hours with 500 grams of desiccant to remove all residual moisture. After 48 hours the samples' dry masses were recorded. The percentage (%) mass change (%ΔM)was calculated using the initial mass recordings and the mass of the dried samples recorded post accelerated degradation testing in Equation 5.1. M_1 is the mass recorded at time, i.e. the degradation time point, and M_0 is the initial mass of the sample. The mean mass change of triplicates for each processing run at each time point of the accelerated degradation procedure are presented in Figure 7.1.

$$\%\Delta M = \frac{M_1 - M_0}{M_0} \times 100 \tag{5.1}$$

5.6 Molecular Weight Characterisation

Once samples had undergone accelerated degradation conditions and had their dry mass recorded, each sample was stored in a freezer at -40 °C to prevent further degradation. Samples were removed from the freezer when required for testing and had mass of 5 mg recorded on an analytical gravimetric balance

(resolution of 0.1mg). Samples were dissolved in 2 mL of high-performance liquid chromatography (HPLC) grade chloroform in GC vials, which had a screw cap. These vials were left overnight. The following day each sample solution was filtered through a membrane filter with a pore size of 0.45 μm.

5.6.1 Gel Permeation Chromotography (GPC)

Gel Permeation Chromotography (GPC) analysis of the PLA samples molecular weight was carried out by high-performance liquid chromatography (HPLC). Samples prepared in chloroform had a concentration of 2.5 mg/mL and were injected at a flow rate of 0.8 mL/min. The mobile phase was chloroform. The columns used were an Agilent ResiPore Guard precolumn 50 x 7.5 mm and an Agilent ResiPore 300 x 7.5 mm. The column was kept at a temperature of 30 °C. The HPLC system is a Thermo-Scientific Dionex Ultimate 3000 and the detector (Varian 385-LC) is an evaporative light-scattering detector. The detector had an evaporator temperature of 50 °C, a nebuliser temperature of 50 °C and a carrier flow rate of 1.4 slm (standard litre per minute). The light source intensity was 10 %. The system was calibrated using polystyrene standards 2000, 10000, 30000, 70000, 150000 and 300000 Daltons. The injection volume of the samples was 10 μL. Each extrusion processing condition had a single sample tested at each time point during the accelerated degradation cycle.

5.6.2 Calculating Molecular Weight from Retention Times

The molecular weight of the standard set is known and the retention time is recorded for each standard. The retention time refers to the amount of time

which has passed from the sample being injected into the system until a peak is recorded. The samples' molecular weight is assessed by measuring the retention time of each sample and fitting it to the standards curve. The standards curve is fit with a third order polynomial model. The analysis of the chromatograms indicates a clear shift in the retention time of the peaks of samples which were processed under the same conditions at each time point of the accelerated degradation cycle. The shift in peak retention time indicates that the molecular weight is reducing during the degradation cycle. All of the samples at 0, 24 and 72 hours had a single peak. A shoulder region develops for some of the samples at 120 hours of the degradation cycle. The other samples at this time point have two peaks. All of the samples at 168 hours have two peaks. This indicates that the samples were beginning to break down into lower molecular weight components at these times. For all of the samples which have two peaks, an average molecular weight value has been used for modelling purposes.

5.7 Summary

The methodologies applied to characterise the extruded samples have been discussed in this chapter. The results from each of the techniques, i.e. yield stress, mass change and molecular weight measurements, are to be used as the response features when developing the soft sensor models. The obtained inline process data will be used to train models to predict these material properties.

Chapter 6

Preliminary Data Analysis and Preprocessing

6.1 Introduction

This chapter discusses the data obtained from the sensors in the adaptor and slit die and how that data was preprocessed prior to modelling. The data acquired from the sensors was used to develop the soft sensor models. Data was obtained from a NaK filled pressure transducer with an embedded thermocouple, two miniature fibre optic pressure transducers with embedded thermocouples, two thermocouples in contact with the polymer melt and two near-infrared (NIR) probes (one transmitter, one receiver). The pressure difference between the transducer in the adaptor and the transducer at the entrance of the slit die ($\Delta P_{asd} = P1 - P2$) and the pressure drop between the transducers in the slit die ($\Delta P = P2 - P3$) were also used as input features to the soft sensor model discussed in Chapters 7 and 8.

6.2 Thermocouples

It was discovered during processing that the two type K thermocouples ($T1$ and $T2$), which were in contact with the melt, returned a number of temperature values equal to zero. Through closer inspection and discussion with the manufacturer, this was believed to be caused by the thermocouple wire making contact with its housing, due to system vibrations, and creating a short circuit. To treat this, all of the zero values were replaced with the preceding non-zero value. Figures 6.1 and 6.3 present the raw temperature data from the initial experiments and validation experiments as captured. Figures 6.2 and 6.4 present the temperature data after it had been treated. The temperature data captured by each thermocouple for each of the processing experiments is presented in Appendix E.

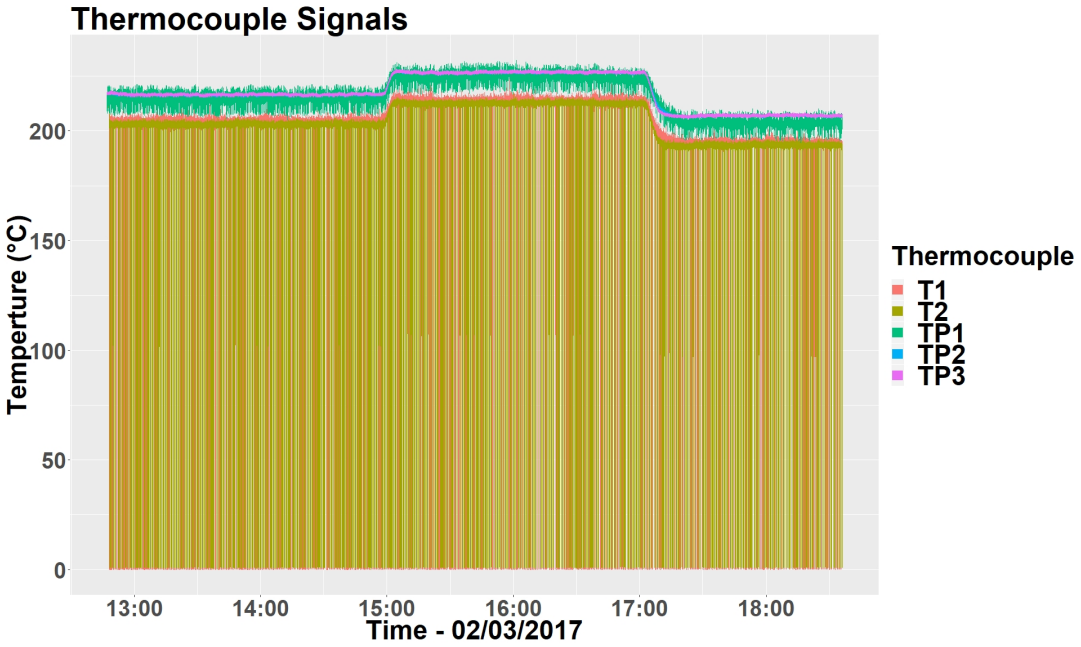

Figure 6.1: The thermocouple signals from the initial experiments where the short circuits had been identified.

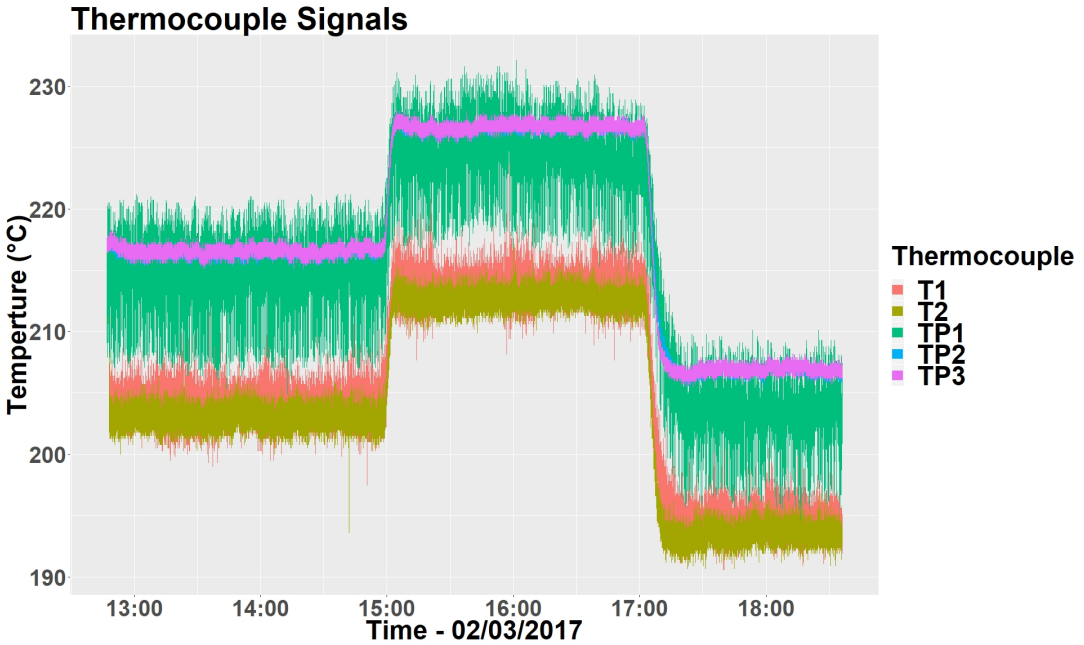

Figure 6.2: The thermocouple signals from the initial experiments after the data was treated.

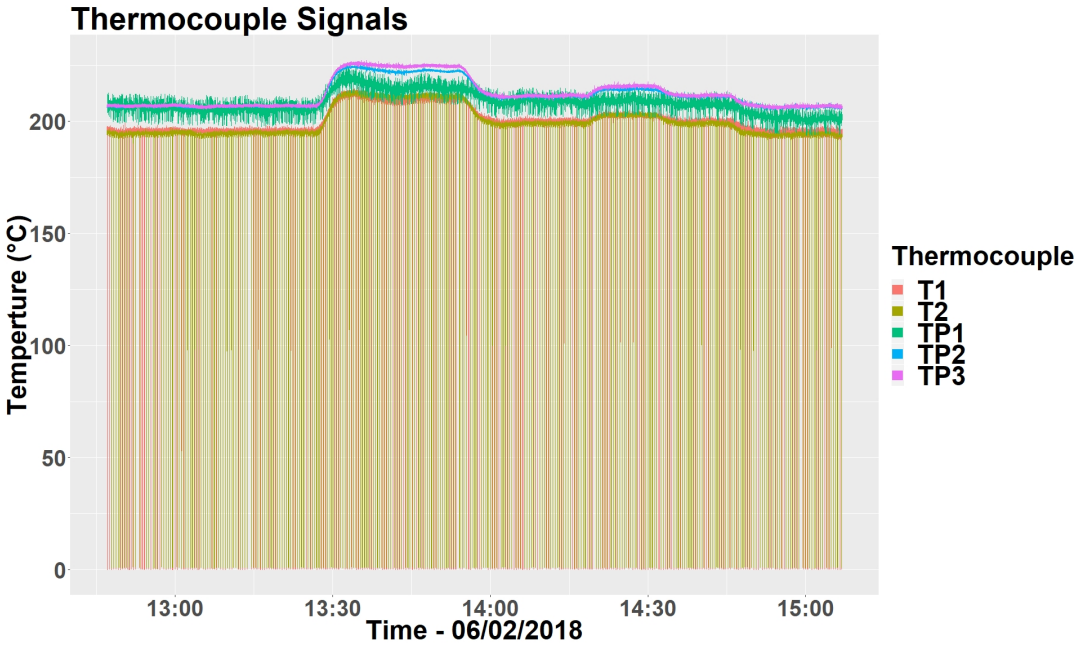

Figure 6.3: The thermocouple signals from the validation experiments where the short circuits had been identified.

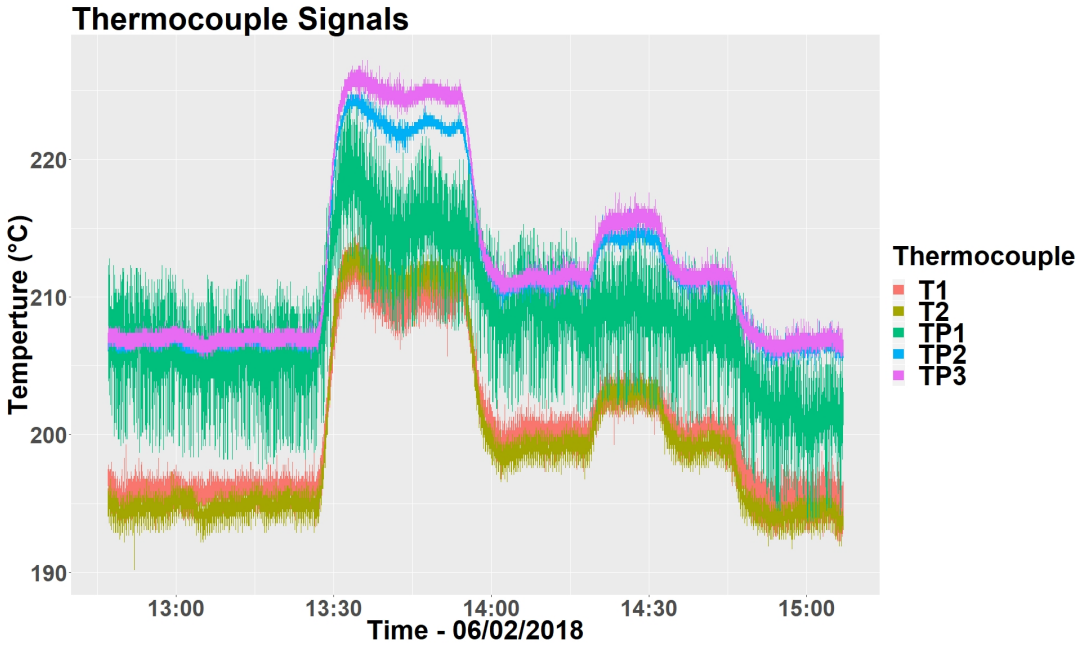

Figure 6.4: The thermocouple signals from the validation experiments after the data was treated.

6.3 Sampling Rate

The sampling rate of the data acquisition system used to collect pressure and temperature data was set at 10 Hz at the beginning of the initial experimental work and also at the beginning of the validation experiments. Further investigation post the initial experimental phase of work discovered a deterioration of the sampling rate over time to ≈5 Hz. This deterioration of sampling rate was also observed post the validation experiments to ≈7 Hz. The sampling rates for the experiments carried out on both days for each processing run can be viewed in Figures 6.5 and 6.6.

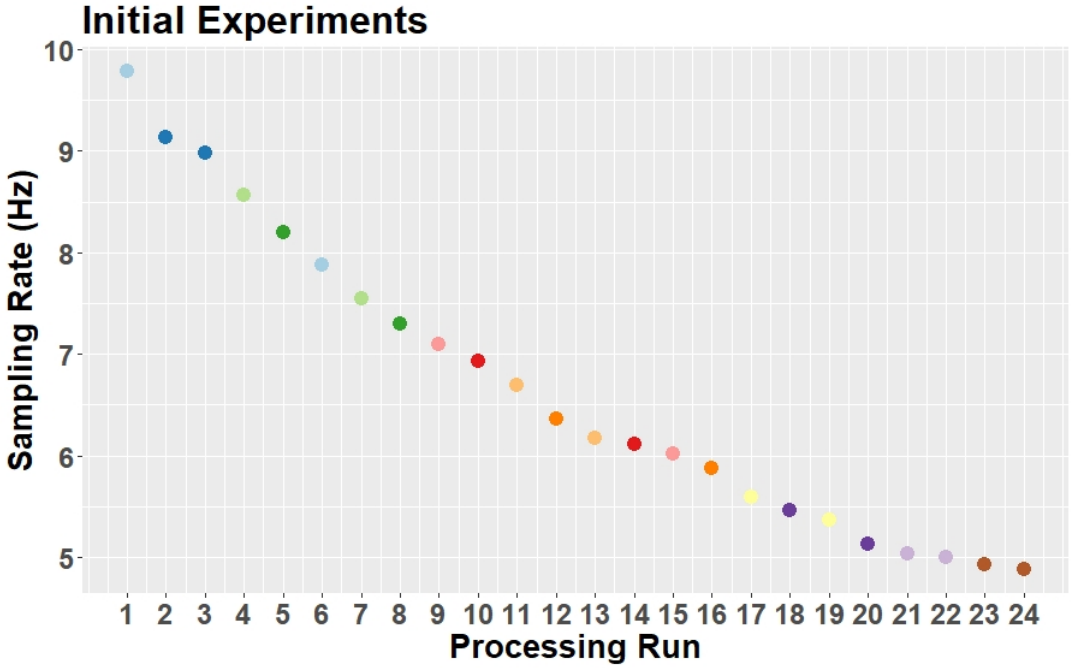

Figure 6.5: Sampling rates plotted for the initial experiments.

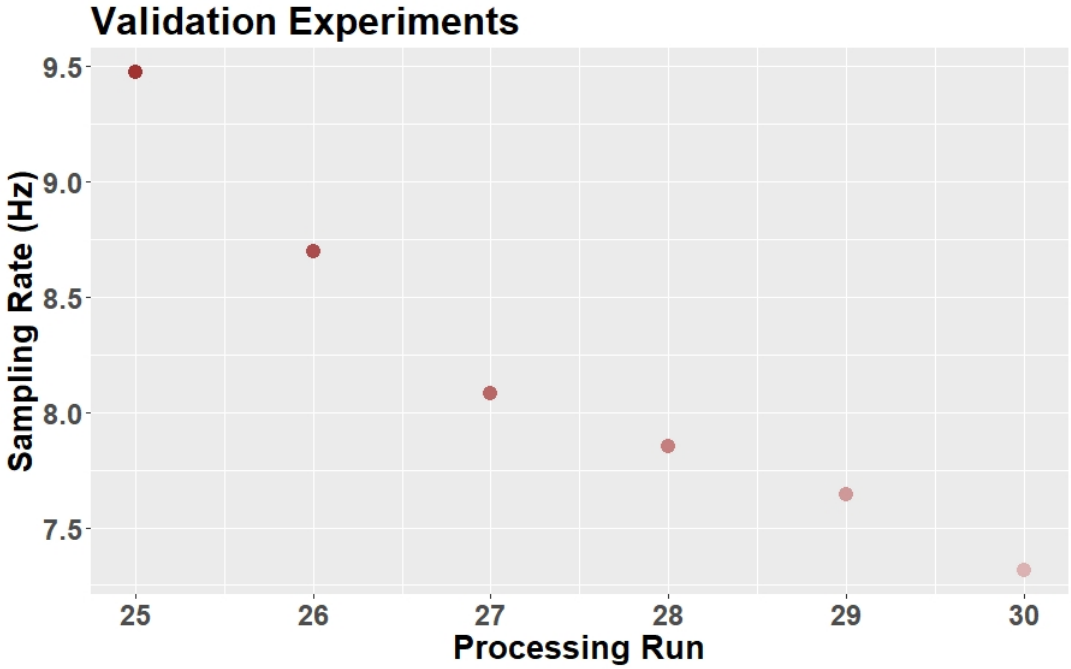

Figure 6.6: Sampling rates plotted for the validation experiments.

6.4 Pressure Sensors

The pressure sensors had been specified for a previous project. The measurements from each sensor have been examined for measurement uncertainty. This was carried out to investigate whether any of the processing runs had conditions which resulted in measurements so close to zero that they are less than the measurement uncertainty.

The measurement uncertainty of a transducer's measurement reflects the doubt surrounding the result of any measurement (Bell, 1999). The uncertainty is expressed as a $\pm$ value on the manufacturers calibration certificate. The uncertainty of a measurement is usually evaluated from statistical analysis of a series of measurements and can be characterised by an experimental standard deviation or multiples of standard deviation (Bell, 1999). The information regarding the type of measurement test carried out by the transducer manufacturers and the statistical analysis completed for the transducers is not available. All that is available is the reported measurement uncertainty of the transducers. Transducer $P1$ has a reported measurement uncertainty of ± 0.25 % or ± 51.75 kPa. Transducers $P2$ and $P3$ have a reported measurement uncertainty of ± 0.2 % or ± 50 kPa.

The results of the analysis of each transducer are presented in Table 6.1. Transducer $P3$ has returned readings that are less than 50 kPa on a number of occasions. Tables 6.2, 6.3 and 6.4 present a statistical analysis of transducer $P3$ for each processing run. The max, min, mean, standard deviation (SD) and variance values for all obtained measurements from $P3$ are presented. It is evident from this analysis that processing run 26 contains the observations

which are less than 50 kPa. The measurements obtained by $P3$ for processing run 26 are presented in Figure 6.7. As Figure 6.7 shows, most (or all) of the variation in the pressure readings may be explained by measurement error of the pressure transducer.

Other processing runs, which have noticeably low pressure measurements, include runs 9 through to 13. All processing runs which have had measurements of low pressures were processed under the high temperature profile. The same statistical analysis for the other two pressure transducers ($P1$ and $P2$), and the pressure drop measurements between $P1$ and $P2$ as well as $P2$ and $P3$ are presented in tables in Appendix D.

Table 6.1: Pressure sensor measurement errors; % Max = maximum measurement presented as a percentage of the full scale output (FSO); % Min = minimum measurement presented as a percentage of the FSO; % MU = $\pm$ the percentage measurement uncertainty of the transducer; MU (kPa) = the measurement uncertainty presented in the measurement units.

	% Max	% Min	% MU	MU (kPa)
P1	19.7	4.6	0.25	51.7
P2	13	1.1	0.2	50
P3	3.2	0.14	0.2	50

Table 6.2: Measurement statistics for pressure transducer P3 for processing runs 1-10.

Processing Run	**1**	**2**	**3**	**4**	**5**	**6**	**7**	**8**	**9**	**10**
Max (kPa)	220	245	233	245	270	233	295	295	178	178
Min (kPa)	160	153	160	173	203	160	215	220	105	105
Mean (kPa)	194	205	198	214	238	200	250	261	144	145
SD (kPa)	10	15	14	10	12	12	14	12	14	12
Variance (kPa^2)	103	233	191	95	147	136	206	155	188	141

Table 6.3: Measurement statistics for pressure transducer P3 for processing runs 11-20.

Processing Run	**11**	**12**	**13**	**14**	**15**	**16**	**17**	**18**	**19**	**20**
Max (kPa)	140	165	178	258	265	258	760	778	735	795
Min (kPa)	85	98	110	190	210	203	690	723	665	735
Mean (kPa)	113	131	148	229	237	233	725	752	706	767
SD (kPa)	9	11	13	10	11	10	12	9	12	11
Variance (kPa^2)	89	122	157	107	113	101	142	81	147	113

Table 6.4: Measurement statistics for pressure transducer P3 for processing runs 21-30.

Processing Run	**21**	**22**	**23**	**24**	**25**	**26**	**27**	**28**	**29**	**30**
Max (kPa)	808	808	773	765	400	**115**	408	233	375	425
Min (kPa)	735	740	698	703	338	**35**	358	185	315	350
Mean (kPa)	772	780	741	734	373	**76**	381	209	341	394
SD (kPa)	11	12	11	11	10	**15**	10	9	11	15
Variance (kPa^2)	125	146	124	113	91	**229**	105	77	113	212

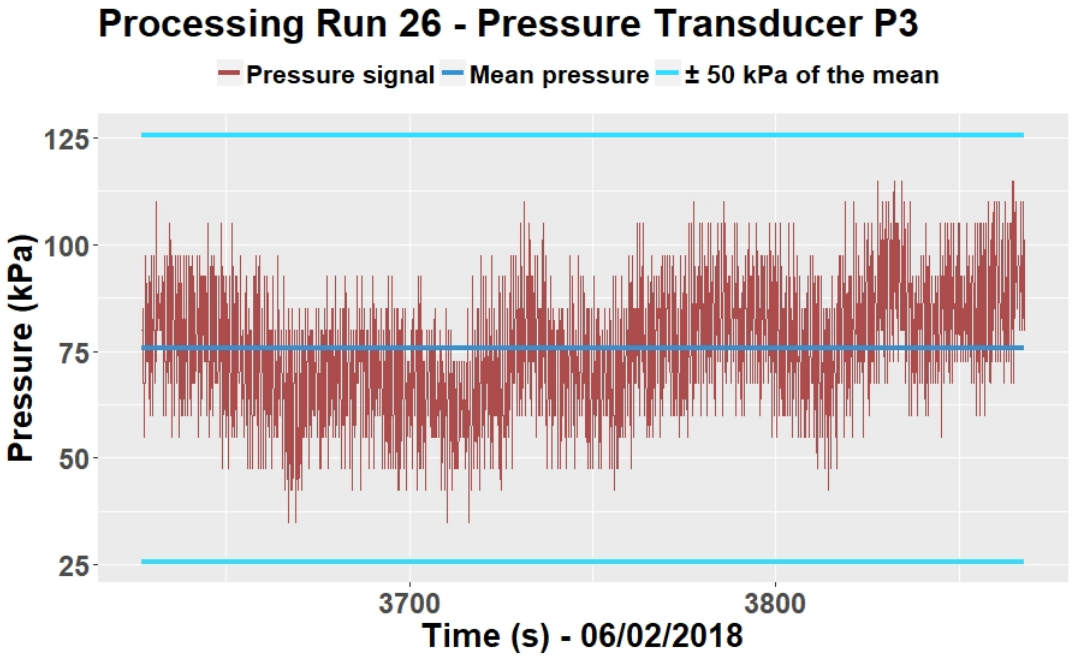

Figure 6.7: The measurements from transducer P3 from processing run 26.

Inspection of further plots of raw pressure signals for each processing condition gave a visual indication of the periodic nature of these signals. An example of some of these raw signals is presented in Figure 6.8. The pressure transducer measurements from $P1$ are presented in each of these figures. Each transducer

has near identical measurement profiles for each processing run and it is not necessary to view all of the transducers' measurements due to this. The plots for every processing run, for transducer $P1$, are presented in Appendix D, only a subset of runs are presented here.

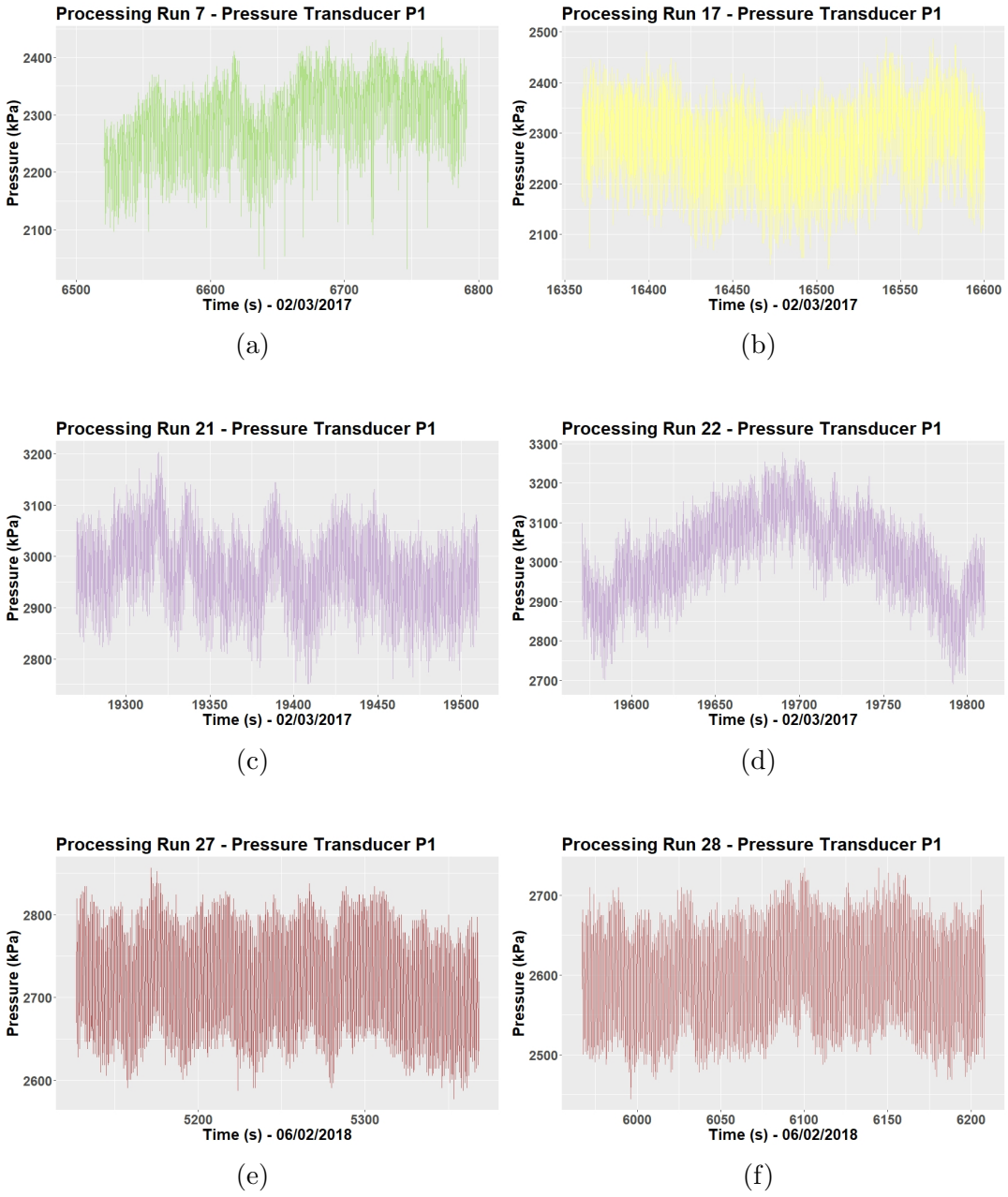

Figure 6.8: The pressure signals from the *P1* transducer for selected processing runs.

6.5 Power Spectral Density Analysis

By performing a power spectral density (PSD) analysis on the pressure signals presented in Figure 6.8, the inherent frequencies in the data were found (Stoica and Moses, 2005). The PSD is a function which characterises the signal in the frequency domain. The PSD of a signal presents the signal's power as a function of frequency. The frequencies at which power was most concentrated represent the periodicity of the screw rotations at a processing condition. In Section 4.3, the screw speed was discussed and offline measurements for the two speeds used in the initial and validation experiments were ≈56 RPM and ≈83 RPM. In the frequency domain these are ≈0.93 Hz and ≈1.38 Hz. These are clearly the dominant frequencies with the greatest power in Figure 6.9 (all processing runs are presented in Appendix D). The other frequencies with the most concentrated power are multiples of that screw rotation frequency. These frequencies, in the power spectral density plots, match the RPM of the screws at those processing settings when measured using a tachometer. Figure 6.9 highlights the power spectral density plots for the same processing runs shown in Figure 6.8. The PSD analysis was performed using the 'psd' package (Barbour and Parker, 2014) in R.

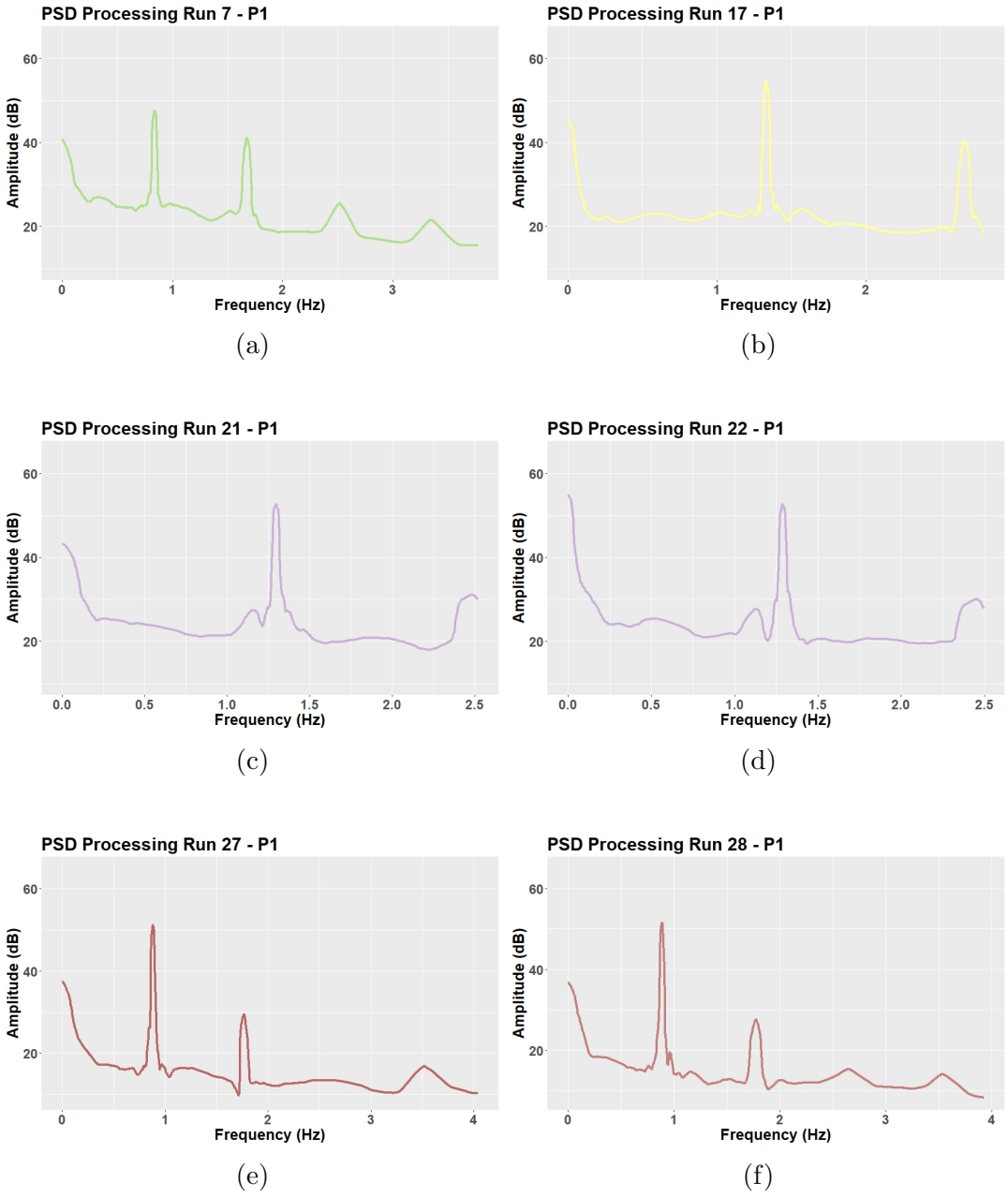

Figure 6.9: The power spectral density plots for selected processing runs using measurements taken from pressure transducer P1.

The apparent high power at low frequencies, close to 0 Hz, is known as the $\frac{1}{f}$ noise or pink noise (Smith, 2003). This noise phenomena appears in a number of natural and man made systems and lacks a generally accepted mathematical explanation (Ward and Greenwood, 2007). The baseline in each of the plots is the white noise element of the data (Smith, 2003). The plots indicate that the variation in the sampling rate is not critical to the performance of the models. All of the processing runs have had enough data acquired to capture the underlying structure of the data at low frequencies. The soft sensor, which has been developed, still performs exceptionally well and has indicated a robustness against varying sampling rates without any additional treatment of the raw data. Figure 6.10 displays the harmonics of the screw rotation frequency for each processing condition.

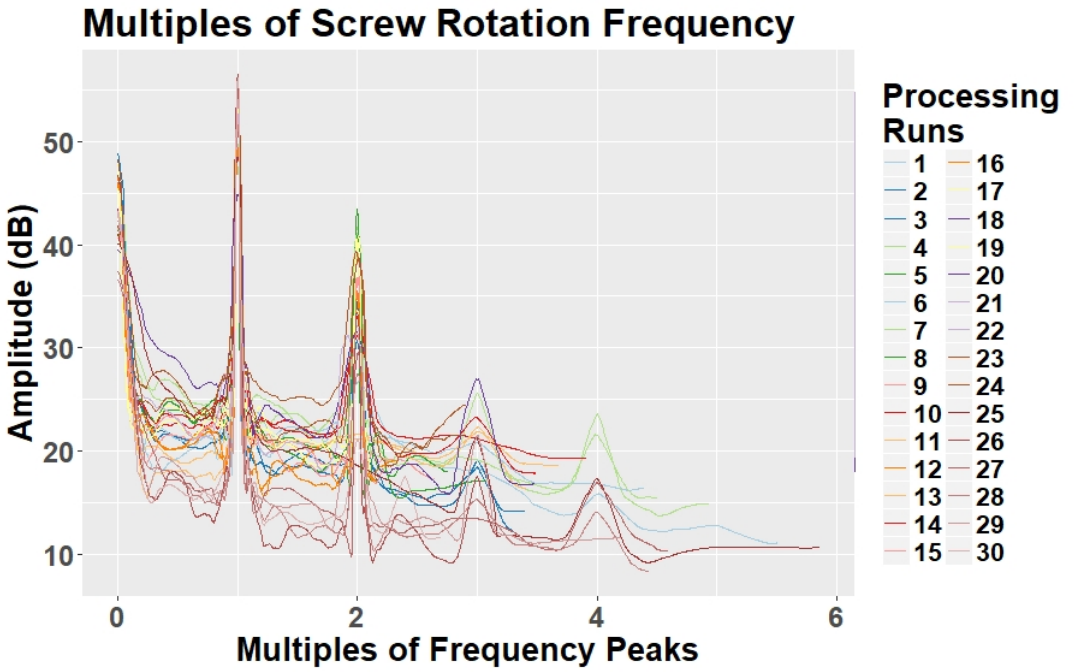

Figure 6.10: The sampling rate of the DAQ system deteriorated over time but it is shown above that the frequencies in the data are still captured for each processing run regardless of the sampling rate.

6.6 Near-Infrared Data

Near-infrared (NIR) spectral data is suitable for multivariate statistical approaches as it has broad absorption bands. Measuring at many different wavelengths results in inherently multivariate data. In essence, each absorption band or wavenumber is an input feature/variable. NIR spectra are dominated by overlapping overtone bands and combination bands (Workman and Weyer, 2007). Chemometrics is the use of mathematical and statistical methods to discern chemical information about a material or system through analysing chemical data (Massart et al., 2003) and has found very useful application with spectral data (see Section 2.3).

NIR spectral data was recorded, using a transmittance probe and receiver probe in the slit die, over the range 4000-7500 cm^{-1} and a subset of the wavenumbers was analysed for each of the processing runs. Wavenumbers, which are expected to have suitable characteristics for predictions, have been found in the region 6100-6700 cm^{-1}. According to Workman and Weyer (2007), this region relates to the first C-H stretching overtones. See Figures 6.11 and 6.12 for the raw NIR spectra of the initial and validation experiments. As the sampling rate of the NIR system is significantly different to the DAQ system used to capture the pressure and temperature data, a zero-order hold was applied to the NIR data. This filled in missing values in the time between each of the recorded NIR spectra so the data could be used along with the pressure and temperature data. The protocol for preprocessing of the data, so that the spectra are consistent and variances due to instrumental drift are accounted for, consists of:

- Convert spectra from transmittance to absorbance (Figures 6.13 and 6.14).
- Create a subset for the wavenumber range (Figures 6.15 and 6.16).
- Perform multiplicative scatter correction (MSC) (Figures 6.17 and 6.18).
- Perform baseline correction.
- Interpolate onto the same wavenumber axis (Figures 6.19 and 6.20).

These pretreatments are well known and described in a number of textbooks and other studies, not limited to Massart et al. (2003), Saerens et al. (2012), McLauchlin, Ghita, and Gahkani (2014), and Montano-Herrera et al. (2014). The steps are achieved through the R packages 'hyperSpec' (Beleites and Sergo, 2017) and 'pls' (Mevik, Wehrens, and Liland, 2016).

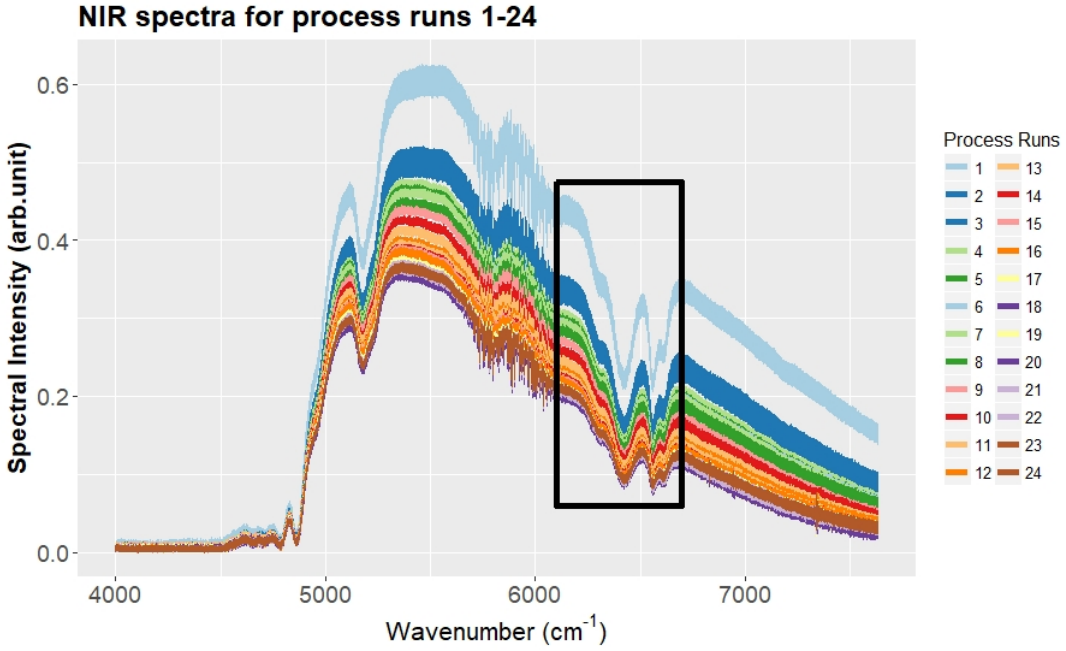

Figure 6.11: NIR spectra for runs 1-24; the wavenumber subset is in the box.

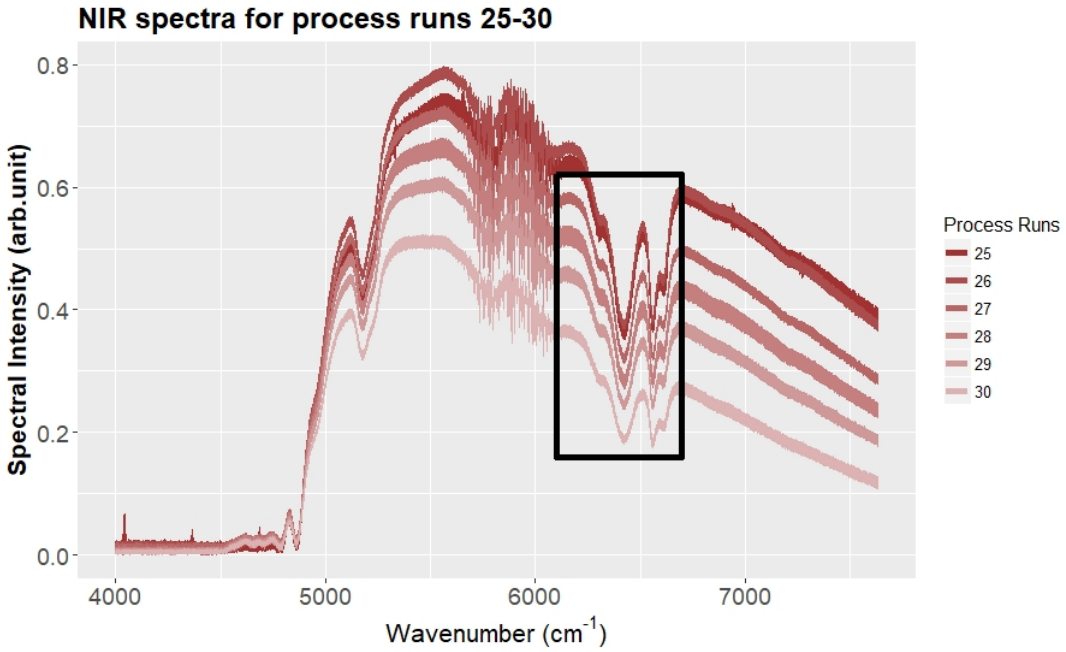

Figure 6.12: NIR spectra for runs 25-30; the wavenumber subset is in the box.

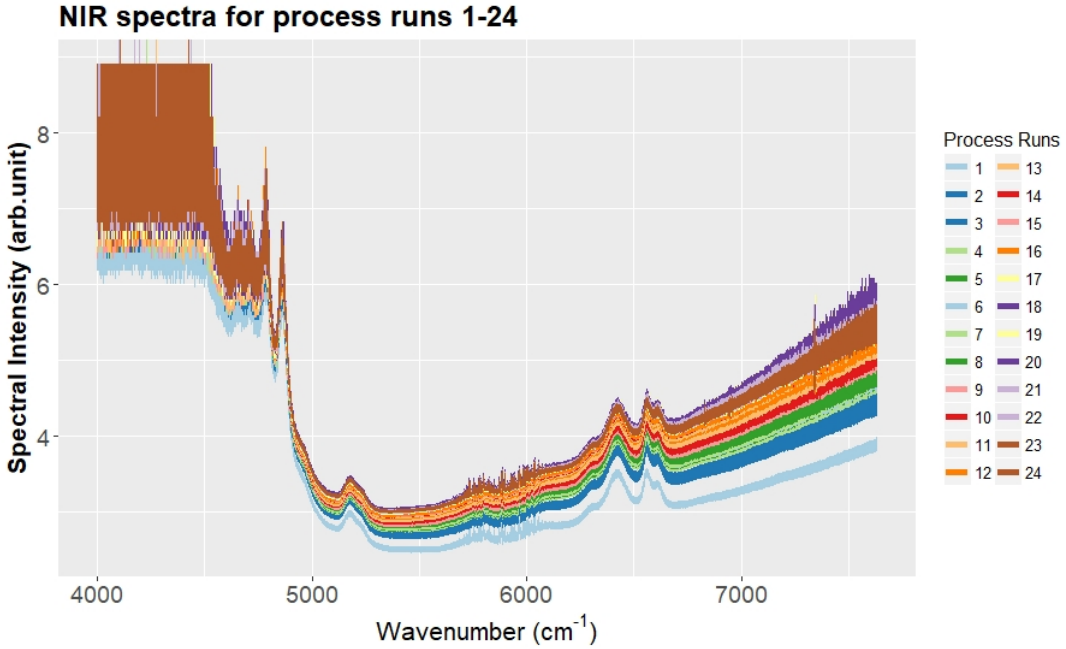

Figure 6.13: NIR absorbance spectra for processing runs 1-24.

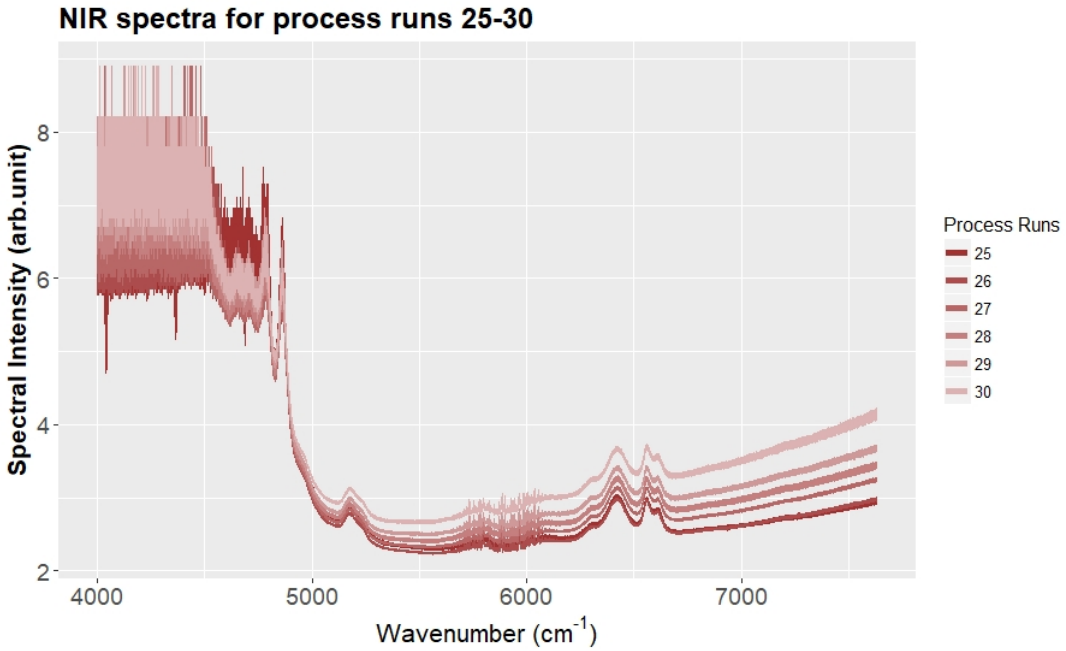

Figure 6.14: NIR absorbance spectra for processing runs 25-30.

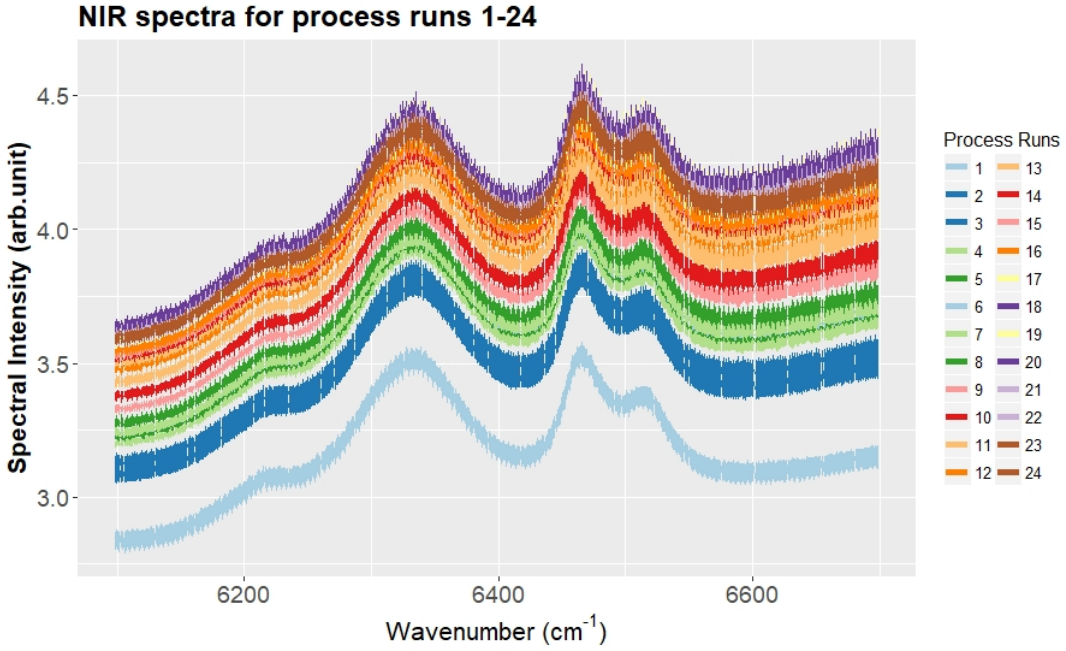

Figure 6.15: The subset of NIR spectra of interest for processing runs 1-24.

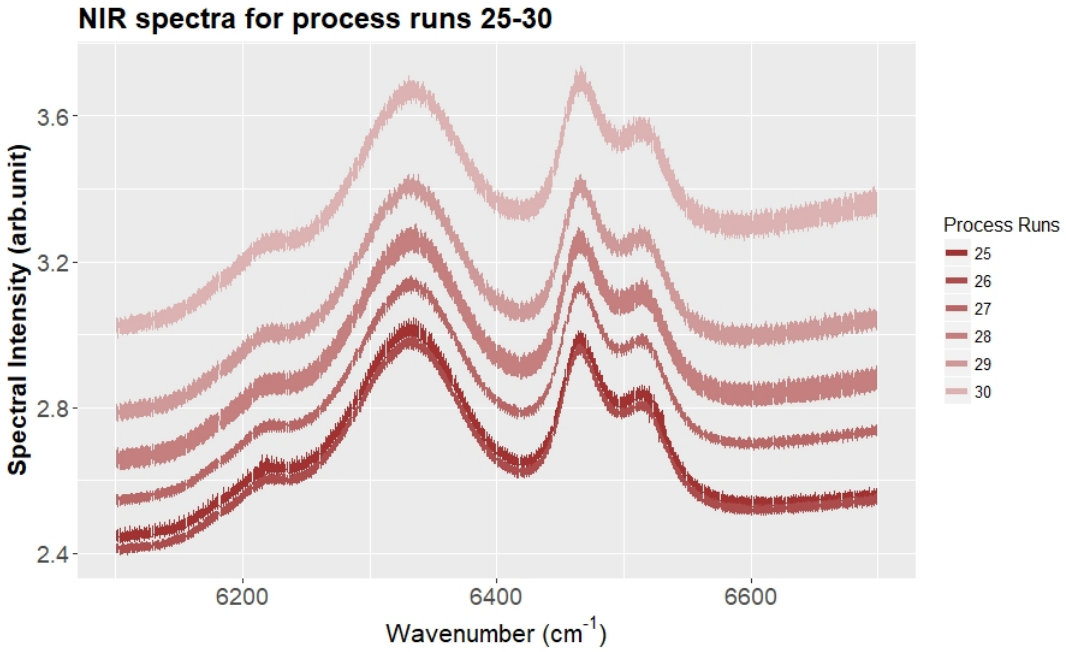

Figure 6.16: The subset of NIR spectra of interest for processing runs 25-30.

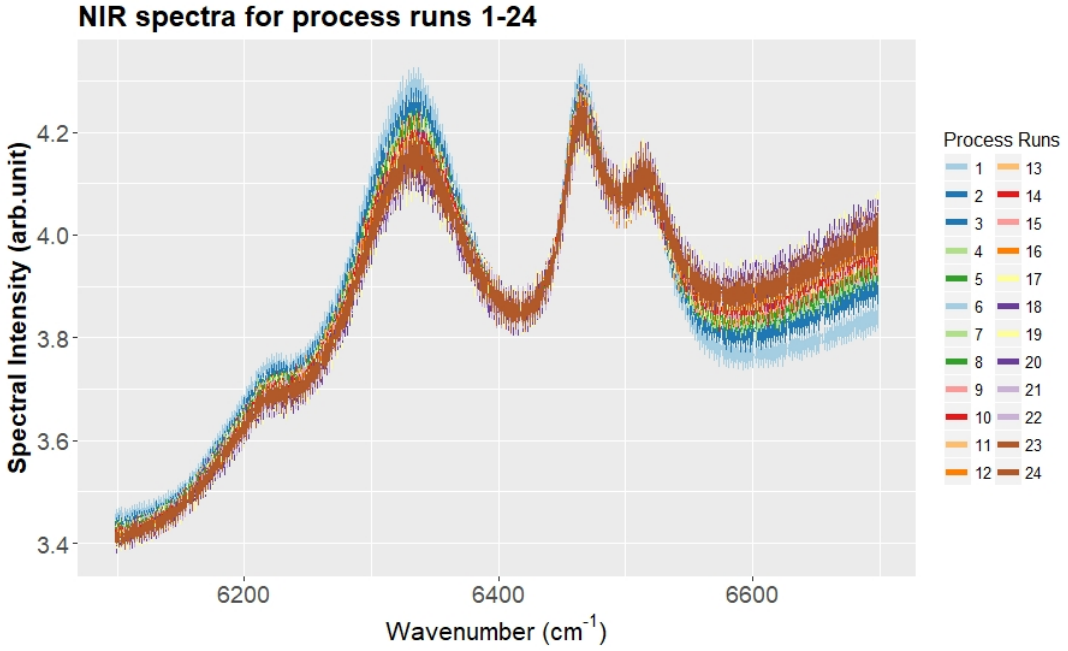

Figure 6.17: MSC performed on NIR spectra for processing runs 1-24.

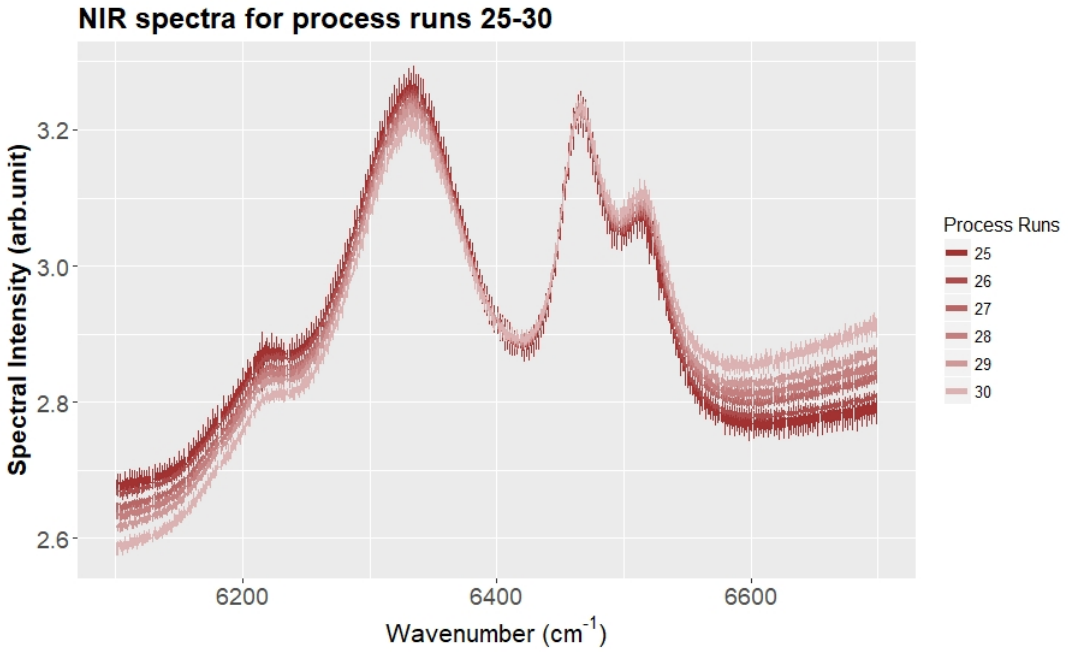

Figure 6.18: MSC performed on NIR spectra for processing runs 25-30.

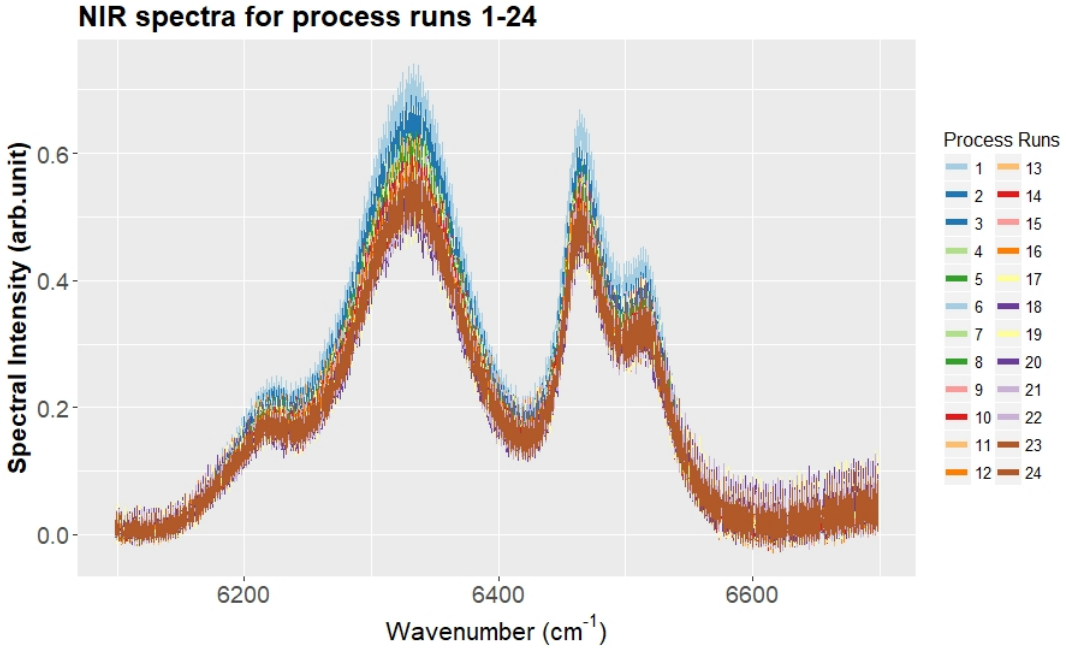

Figure 6.19: Baseline corrections applied to NIR spectra for runs 1-24.

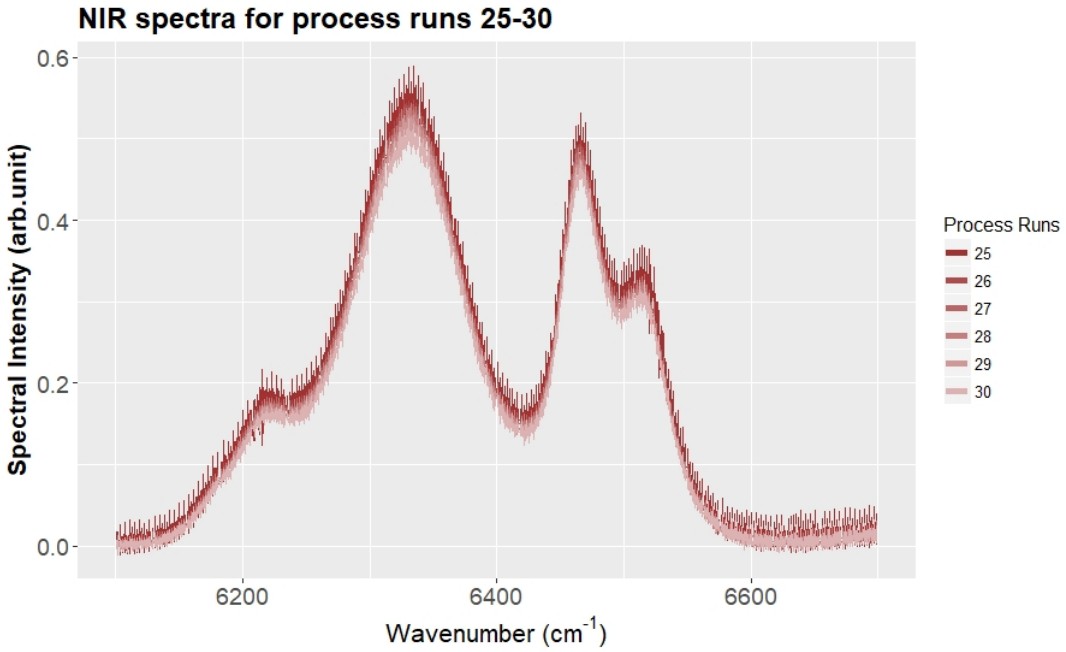

Figure 6.20: Baseline corrections applied to NIR spectra for runs 25-30.

6.7 Extruder Data

Temperature data from the extruder barrel zones was captured on a local DAQ system. This data could not be exported during processing and there was no control of the sampling rate. Upon further investigation it was discovered that samples were logged every ≈22 seconds. This data was used in the early stages of model training and it was discovered that it did not improve model performance. The difficulties in converting the data to a useable format; the fact that it could not be transferred to any of the developed models in real time without significant effort; and also the fact that this data did not improve model performance meant the decision was taken not to include it in the developed models.

6.8 Data Preparation

The data recorded during extrusion processing was preprocessed. Preprocessing the data involved applying a number of steps to the raw data before it was fit for modelling. These included:

- Data captured from initial experimental work (March 2017)
  - Labelling the data.
  - Applying a -5.5 bar offset to $P1$ due to drift once processing temperatures were reached. The transducer could not be zeroed at temperature and so the adjustment had to be applied when the data was exported.
  - It was discovered during processing that the system recording $P3$ was out by a factor of 10 due to human error during setup.

- All pressure data was converted from bar to kPa.
- Temperature recordings from $T1$ and $T2$ were treated for values of 0 by replacing with the preceding non-zero value.
- The times at which the throughput measurements were recorded were input manually to match the DAQ system clock.
- These times were then used to identify the rows in the raw data set which matched to the processing experiments so that a subset of the initial data set could be generated. This meant that the initial data set was divided into subsets for each processing run per the times recorded for the throughput measurements plus 30 seconds either side.
- The volumetric flow rate measurements were then calculated and added to the data set (Equation 4.1).
- The shear viscosity estimate was then calculated (Equation 4.7).
- The NIR data that matched the times of the throughput measurements was added to the data set.
- The yield stress data, mass change data and molecular weight data was then added to the data set.

• Data captured from validation experiments (February 2018)

- Labelling the data.
- Applying a -5 bar offset to $P1$ due to drift once processing temperatures were reached. The transducer could not be zeroed at temper-

ature and so the adjustment had to be applied when the data was exported.

- All pressure data was converted from bar to kPa.
- Temperature recordings from $T1$ and $T2$ were treated for values of 0 by replacing with the preceding non-zero value.
- The times at which the throughput measurements were recorded were input manually to match the DAQ system clock.
- These times were then used to identify the rows in the raw data set which matched to the processing experiments so that a subset of the validation data set could be generated. The validation data set was divided into subsets for each processing run per the times recorded for the throughput measurements plus 30 seconds either side.
- The volumetric flow rate measurements were then calculated and added to the data set (Equation 4.1).
- The shear viscosity estimate was then calculated (Equation 4.7).
- The NIR data that matched the times of the throughput measurements was added to the data set.
- The yield stress data, mass change data and molecular weight data was then added to the data set.

6.9 Feature Selection

There were 612 recorded features ($F = 612$) available to build the models including all pressure, temperature, shear viscosity and near-infrared spectral data.

Using all of the features resulted in restrictively slow training of models and significantly increased computational load costs. In addition, a large number of features contained noisy data which are not useful to gain insight regarding the response. A heuristic approach to feature selection was adopted that took these considerations into account.

6.9.1 Feature Selection Methodology

The following methodology was developed to select a subset of features to train the soft sensor models.

- Get the principal components (PCs) of the raw variables.
  - Pressure, temperature, shear viscosity estimate, ΔP_{asd}, ΔP and NIR spectra.
- Create a number of Random Forest (RF) models using 100 % of the training data set.
  - Use an m value equal to $\frac{F}{3}$, this is an accepted heuristic (Breiman, 2001; Kuhn and Johnson, 2013).
  - Vary the number of trees e.g. 10, 20, 40, 100.
- Capture the top 30 PCs using the feature importance scores from each RF model (Section 3.5.3).
- Gather the PCs from the list of top 30 PCs from each model.
- Use these PCs to create a PCA-Random Forest soft sensor model.

6.10 Summary

This chapter has covered all of the perceived concerns, analysis and treatments of the recorded processing data. This has included sampling rates of the hardware, temperature, pressure and NIR spectral data. Additionally, a method has been proposed to reduce the large number of available features to develop and train a soft sensor model.

Chapter 7

Degradation Profile Analysis

7.1 Introduction

This chapter analyses, and presents discussion, for the mass change and molecular weight of the PLA samples at varying times of accelerated degradation (see Section 5.4). PLA has a number of complex degradation mechanisms which are influenced by product properties, processing conditions and the medium in which degradation occurs (Tsuji et al., 2003; Farrar, 2008; Tsuji, 2010). The approach to modelling each of the mass change and molecular weight features is presented in the next section. Unfortunately, the results were not as desired and the rationale for this is also discussed.

7.2 Soft Sensor Model Development

The initial data set, comprising of the data from processing runs 1 to 24 recorded in March 2017, was used as the training data set. The data captured for runs 25

to 30 in February 2018 was the validation data set. The validation set checked the final model against overfitting and also gave an indication of how well the model generalises to data which it had not been trained on.

The training set was randomly split using the caret (version 6.0-77) package in R with a pseudo-random number generator seed of 1010. This seed number generates a sequence of random numbers. Any randomisation that is coded will be repeated every time the code is run which will return the same repeatable results. For example, when generating each new bootstrap data set for each tree in the Random Forest model, each newly generated data set is randomly resampled with replacement from the original data set. Without the random seed the results from the model could not be replicated as every time the code is run a different random resampling takes place which will impact on the result of the model.

The soft sensor was modelled using R (version 3.5.0) software (R Core Team, 2018) as a back end and RStudio (version 1.1.447) software (RStudio Team, 2018) as a front end. The model was developed using the training data set and was tested on how well it generalises to unseen data using the validation data set. A varying percentage of the training set was investigated to fit the model. These percentages determined how much of the training set was used to train the model. The percentages investigated were 80 %, 75 %, 70 % and 65 %.

All possible values of m were trialled using custom written routines in R. This resulted in a number equal to m models being trained for each of the four training data set percentages. The training percentage and m value combination with the lowest RMSE value on the validation set was chosen as the best model in each case.

7.3 Mass Change Modelling

The mass change profiles for the samples, from each of the processing runs in Figure 7.1, follow profiles already reported in the literature for PLA under accelerated degradation conditions (Weir et al., 2004b). That is, each point (which represents a processing run) has little variation in mass before mass loss occurs during late stage degradation. The samples are estimated to degrade at ≈27 times their normal rate under the accelerated conditions (Weir et al., 2004b).

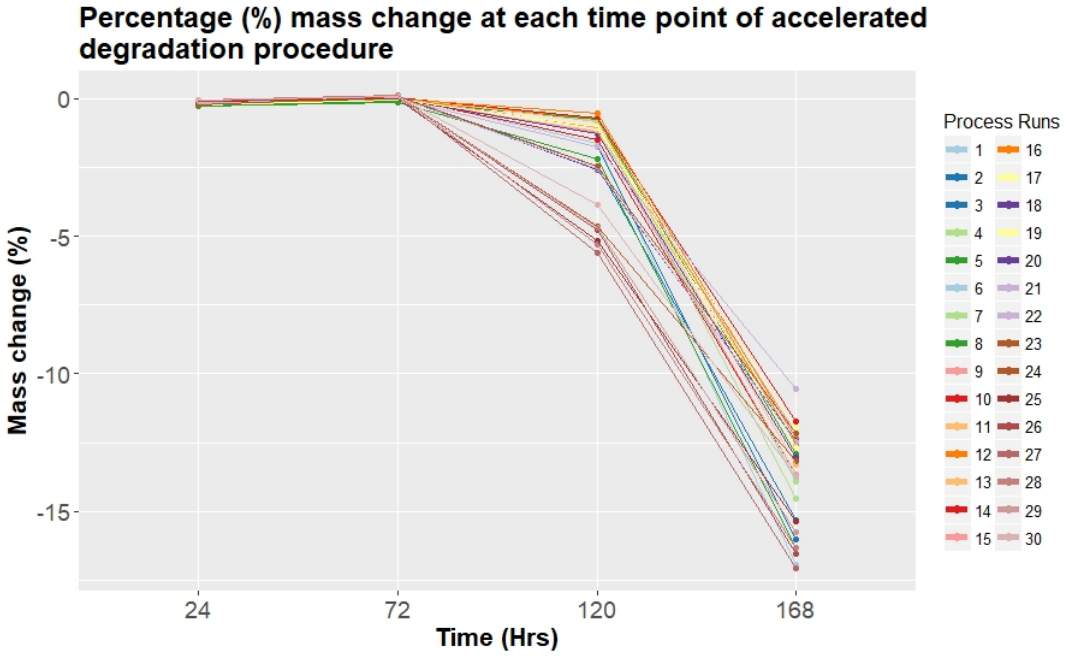

Figure 7.1: The mean % mass change of triplicate samples for all processing runs.

In Figure 7.1, it is clearly visually evident that there is little variation in the mean % mass change for all processing runs at 24 hours and 72 hours. Figures 7.2 - 7.5 highlight that the variation in % mass change within triplicates and

between the triplicate mean values for all processing runs at the degradation time points are not large. The black line in Figures 7.2 - 7.5 represent the variance between the mean values of the triplicates for all processing runs at each degradation point. This implies that the distance from the mean of the observations and the distance between each observation is not large. In some cases the variance within triplicates is significantly greater than the variance between the mean value of all thirty processing runs.

Figures 7.2, 7.4 and 7.5 present processing run 23 as having a greater mass change variance than the other processing runs. At each of the degradation points, there is a mass change measurement, which is significantly larger or smaller than the other two recorded measurements at those time points. The cause of this cannot be determined with certainty but one possibility may be that the processing conditions were not in a steady state and caused variability in the extrudate properties for that processing run. After reviewing the pressure signal for processing run 23 (Figure D.8 (c)), there are fluctuations in the signal that could indicate that the process may not have been in steady state. A number of the other recorded pressure signals are similar to processing run 23 (these can be viewed in Appendix D) and none of those samples have the same mass change variance. Another possibility is that there may have been handling errors during sample preparation or the degradation procedure for that processing run. Although best efforts were made to minimise any risk of this it cannot be ruled out.

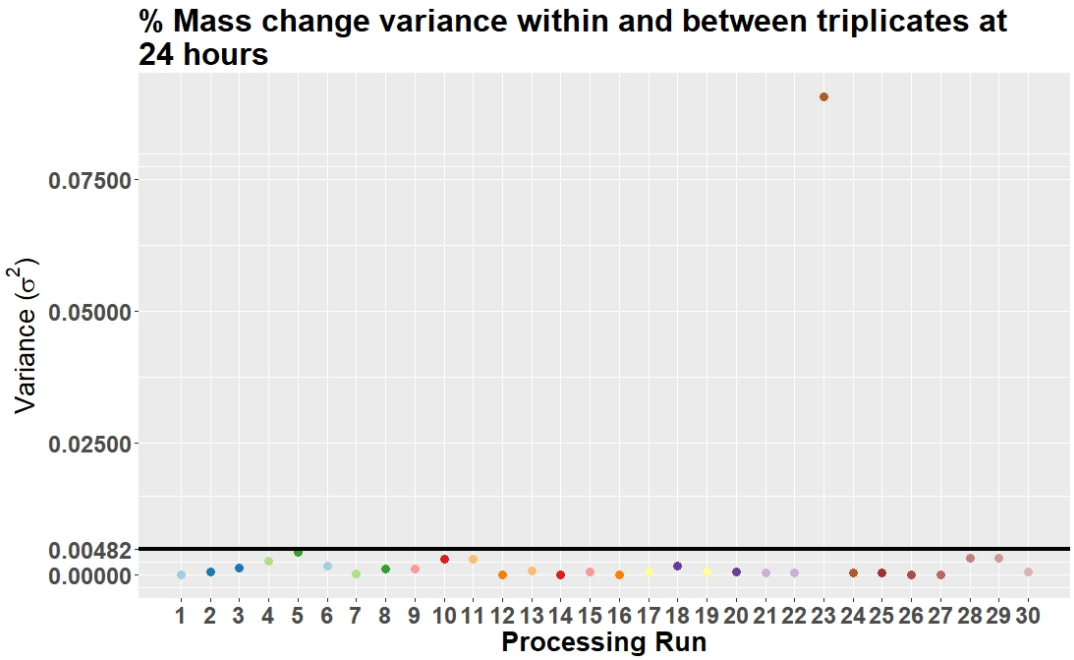

Figure 7.2: The $\%\Delta M$ variance within and between triplicates at 24 hours; the black line represents the variance between the mean values of the triplicates for all 30 processing runs.

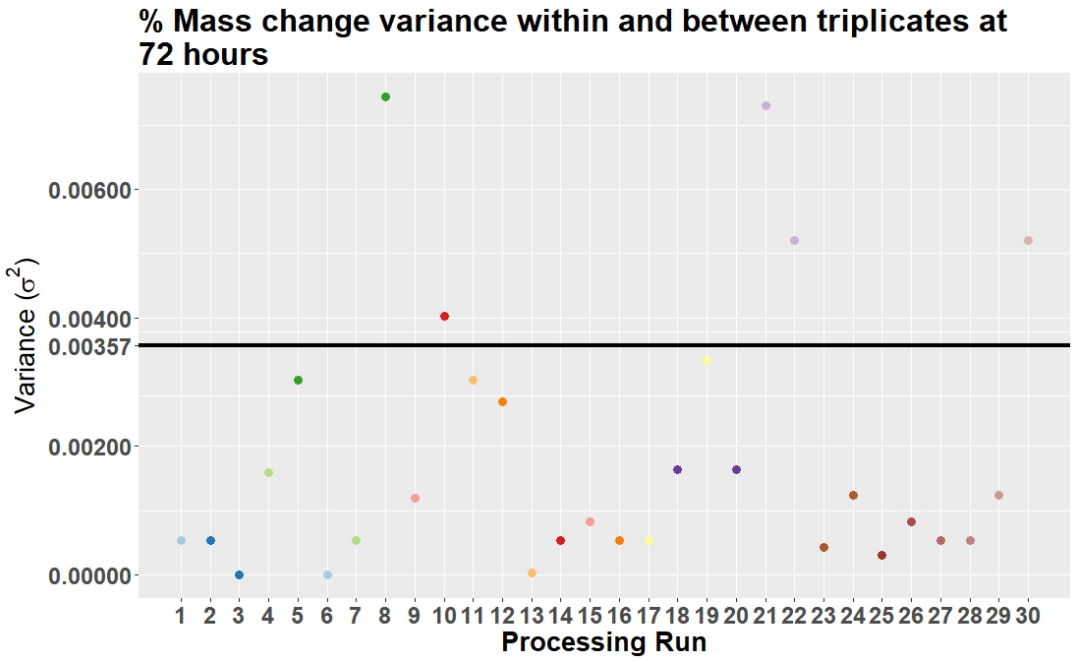

Figure 7.3: The $\%\Delta M$ variance within and between triplicates at 72 hours; the black line represents the variance between the mean values of the triplicates for all 30 processing runs.

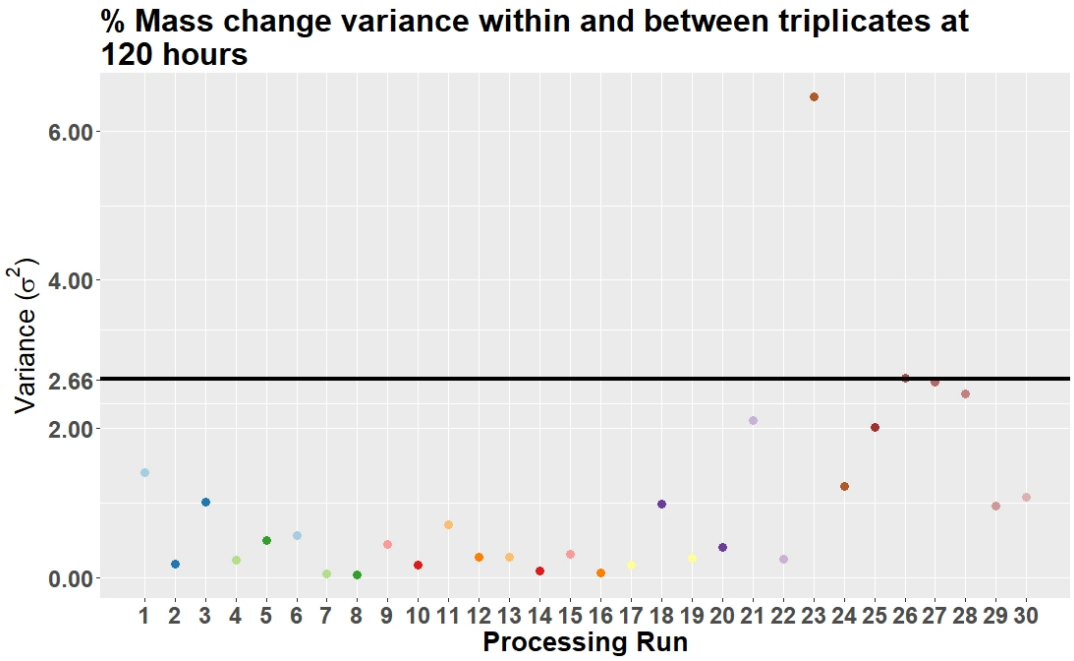

Figure 7.4: The $\%\Delta M$ variance within and between triplicates at 120 hours; the black line represents the variance between the mean values of the triplicates for all 30 processing runs.

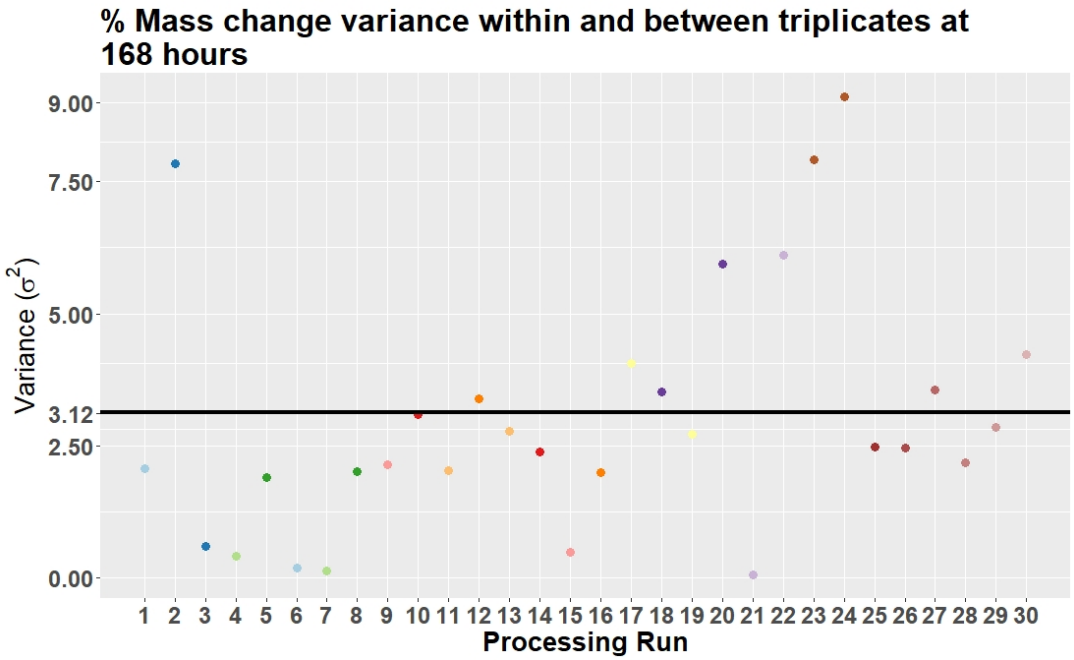

Figure 7.5: The $\%\Delta M$ variance within and between triplicates at 168 hours; the black line represents the variance between the mean values of the triplicates for all 30 processing runs.

7.3.1 Results

The resulting models have not made good predictions, even for samples that had undergone accelerated degradation conditions for 168 hours, which had the greatest variance between runs (see Figure 7.1 and Figure 7.5). A mean value of the triplicate results of the mass change measurements at 168 hours was used when developing the soft sensor model (Figure 7.8). The steps outlined in Section 6.9 were followed, resulting in a subset of 47 principal components being chosen to train the model. This subset of PCs contained a mixture of higher and lower variance PCs. It has been shown previously that using some lower variance PCs can lead to better models for regression than using just the

higher variance PCs (Jolliffe, 1982). Figure 7.6 presents a Principal Component Analysis Random Forest (PCA-RF) out-of-bag (OOB) training error for a soft sensor created to predict the % mass change of samples at 168 hours. This soft sensor had 47 principal components, an m value of 16 and used 65 % of the training data.

Figure 7.7 demonstrates how the model has fit the training data by making predictions using the 35 % of data from the training data set, which was not used to train the model. The model is shown to have a good fit of the training data in Figure 7.7. Unfortunately, when applying the model to the validation data set the predictions are not as accurate. This is evident when viewing Figure 7.8. There is little variation between the predictions for all processing runs and only one predicted mean value is within the observed triplicate values (processing run 30 in Figure 7.8). The distance between the predicted mean and the observed mean for all processing runs in the validation data set is in the range ≈1.5-4 %. As the predicted mean for all processing runs was very similar, it may indicate that the proposed approach is not be suitable as the predictions do not appear to be sensitive to the variation in this response variable. The models for the the other % mass change time points have had similar results and only the best model has been reported here. The models have not generalised to the validation data set.

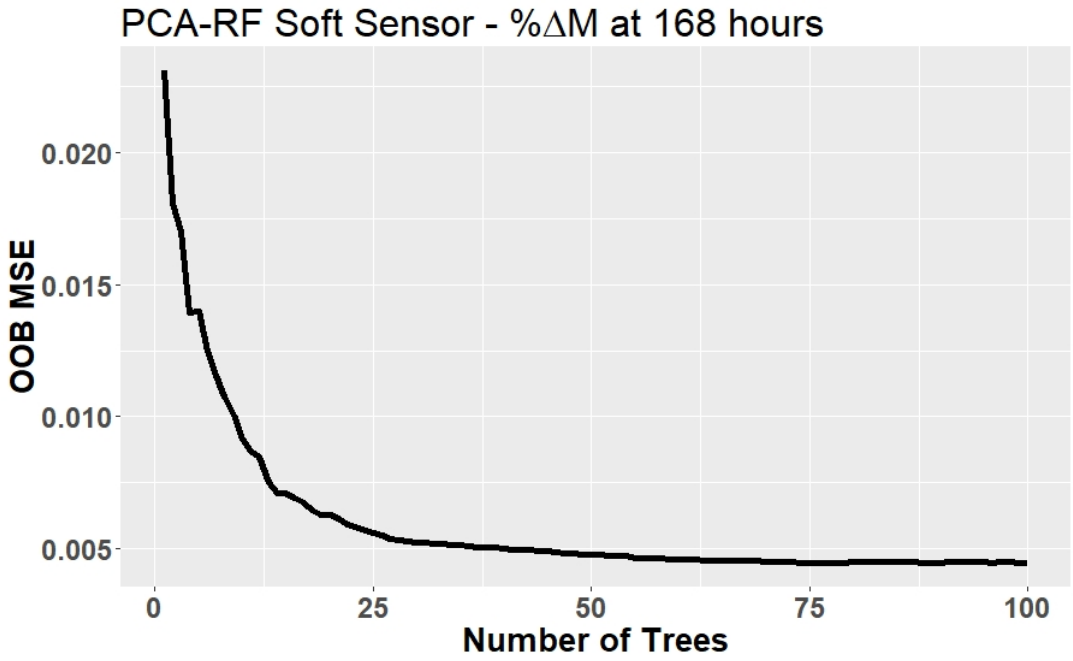

Figure 7.6: The PCA-RF soft sensor model out-of-bag error for % mass change of samples at 168 hours.

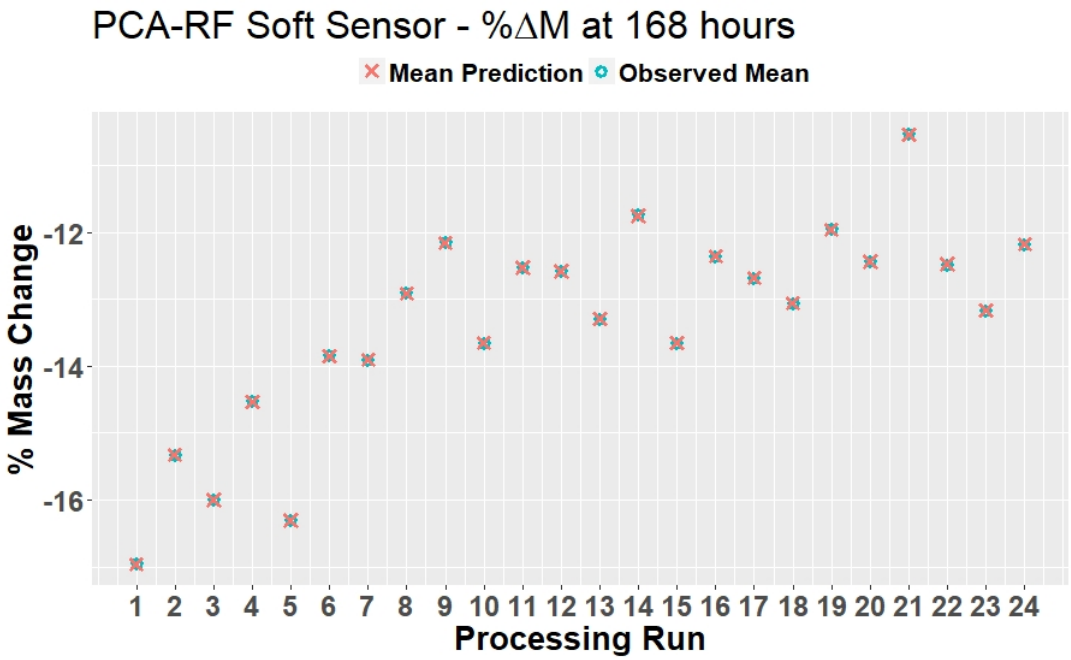

Figure 7.7: The PCA-RF soft sensor model with mean predictions and observed values of the training data samples for % mass change of samples at 168 hours; the predictions are made using the 35 % of data from the training set, which was not used to train the model.

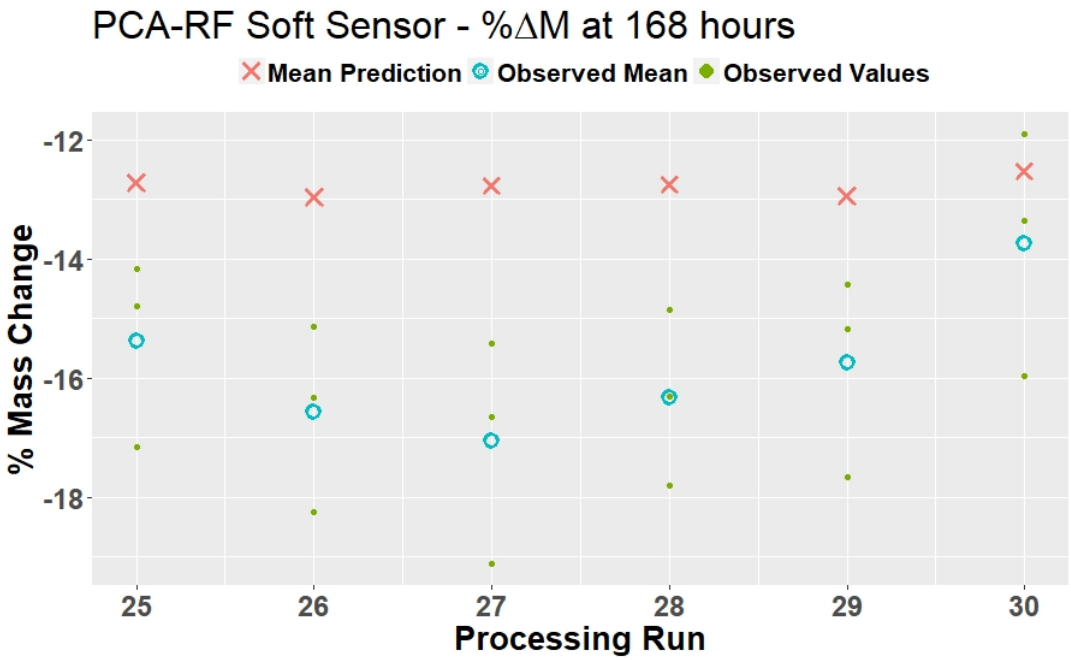

Figure 7.8: The PCA-RF soft sensor model for % mass change with mean predictions and observed values of samples at 168 hours degradation for all processing runs in the validation data set.

7.3.2 Discussion

Farrar (2008) considered the challenges in modelling the complexity of mass loss in bioresorbable polymer products in general. The major point raised by the authors is that the input variables required to create a model for mass loss are monomer content, oligomer content and the number of units in an oligomer and these need to be determined experimentally (Farrar, 2008). There has been no work carried out to capture monomer or oligomer data, which the literature regards as the key metrics to model mass loss. Therefore, it cannot be investigated whether the inline process data which has been recorded may contain information which would allow inference of monomer or oligomer properties, which in

turn could provide useful information for mass loss predictions.

7.4 Molecular Weight Modelling

The molecular weight was tested using a single sample from each processing run at each degradation time point. Triplicate samples were determined for some processing runs for samples that had not undergone degradation, which allow for an estimate in the variability of measurements on samples for the same run (Figures 7.9 and 7.10). The height of the bars in Figure 7.9 represent the mean value of the measured triplicates, while each black dot represents a single measurement for processing runs 1 to 6. Figure 7.10 presents the variance within the measured triplicates for processing runs 1 to 6. The dotted black line (value = 15.9) in the figure represents the variance between the mean values of the triplicates recorded for processing runs 1 to 6. The solid black line (value = 103.1) in the figure represents the variance between the values of the single samples recorded for all 30 processing runs

Due to the expense and time intensive demand associated with characterising large numbers of samples, the molecular weight of single samples from each processing run at each degradation time point was determined and presented in Figures 7.11 - 7.15. All of the results are presented as 'polystyrene equivalent' weight average molecular weights, as the gel permeation chromatography (GPC) system was calibrated with polystyrene standards. The weight average molecular weight (M_w) gives a 'weighted average' which accounts for the mass of each molecule as well as the number of molecules in sample. The trend presented in Figures 7.11 - 7.15 when compared to Figure 7.1, which highlights a

reduction in molecular weight prior to any reduction in mass, is in keeping with the literature (Brown and Farrar, 2008).

Figure 7.9: The triplicate samples for processing runs 1-6 for samples which had not undergone the accelerated degradation procedure.

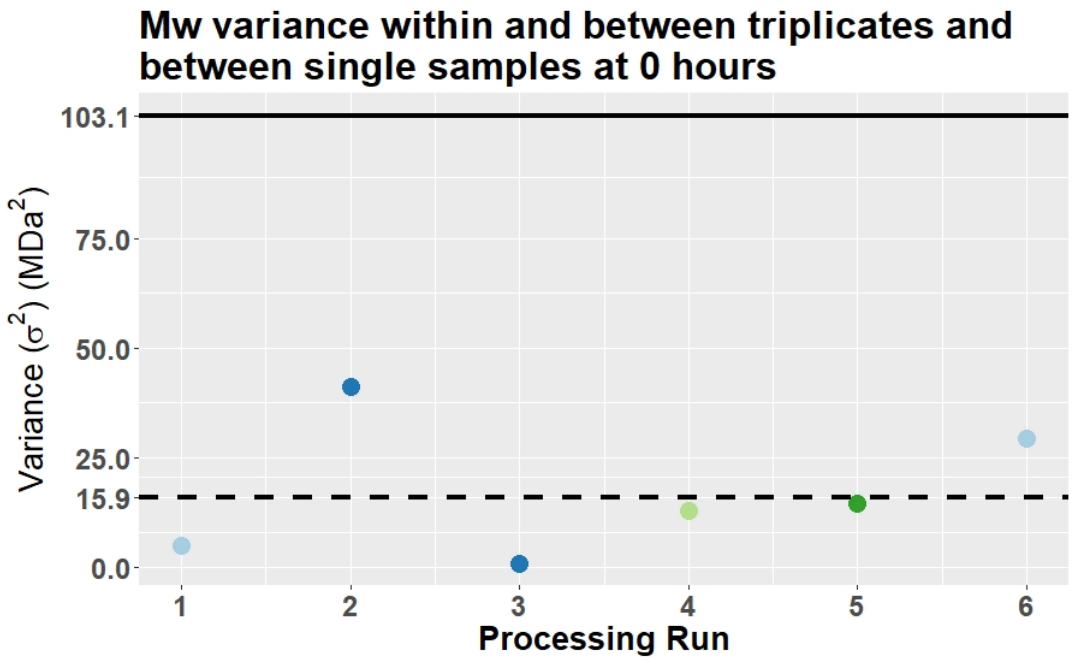

Figure 7.10: The variance within triplicate measurements of molecular weight for processing runs 1 to 6; the dotted black line (15.9) represents the variance between the mean values of the triplicates recorded for processing runs 1 to 6; the solid black line (103.1) represents the variance between the values of the single samples recorded for all 30 processing runs.

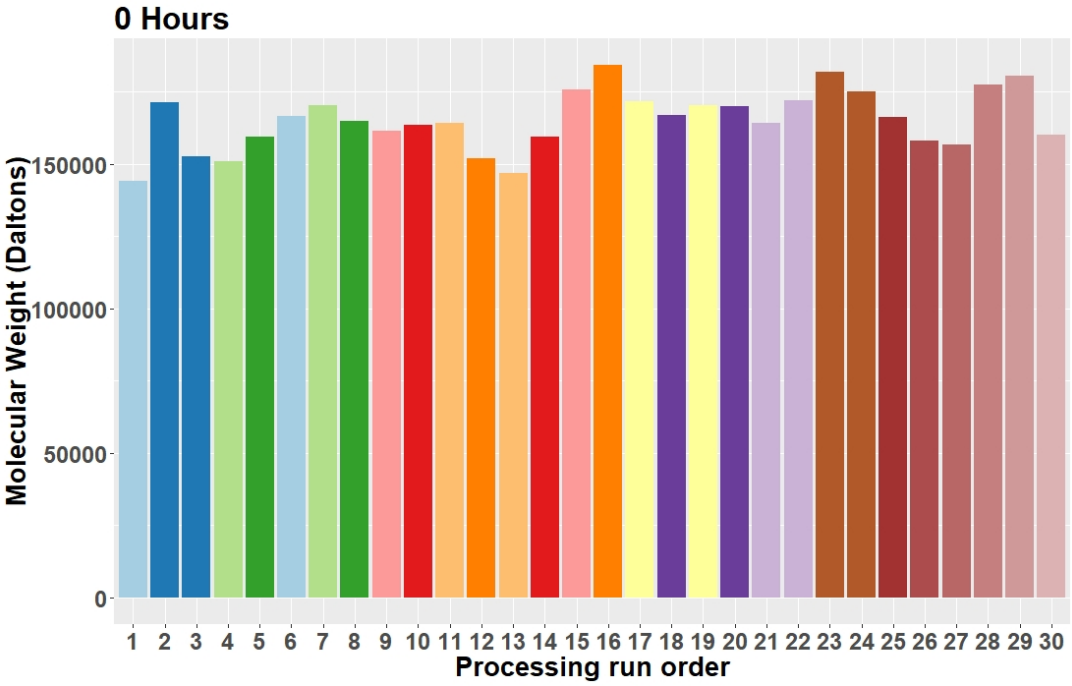

Figure 7.11: The molecular weight of non degraded samples.

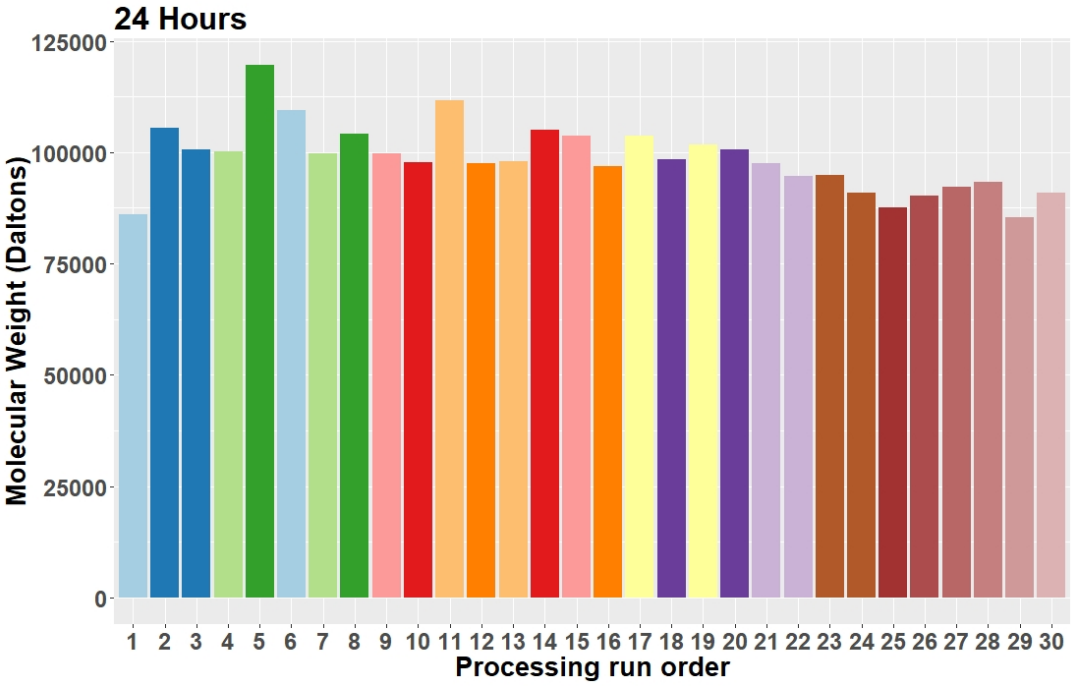

Figure 7.12: The molecular weight of 24 hours degraded samples.

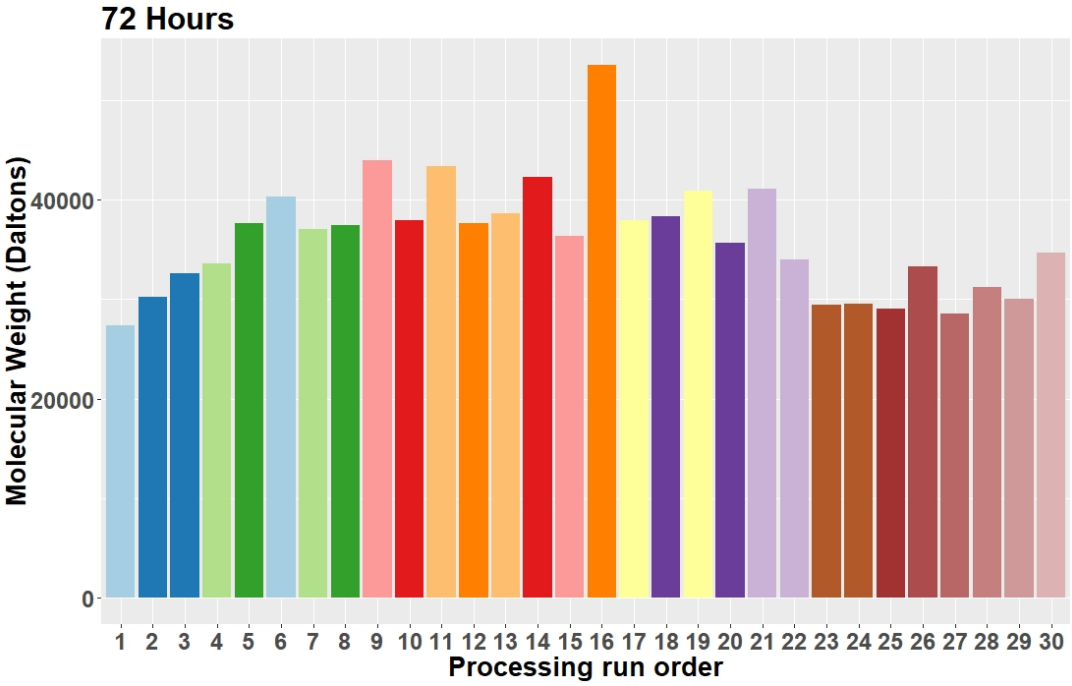

Figure 7.13: The molecular weight of 72 hours degraded samples.

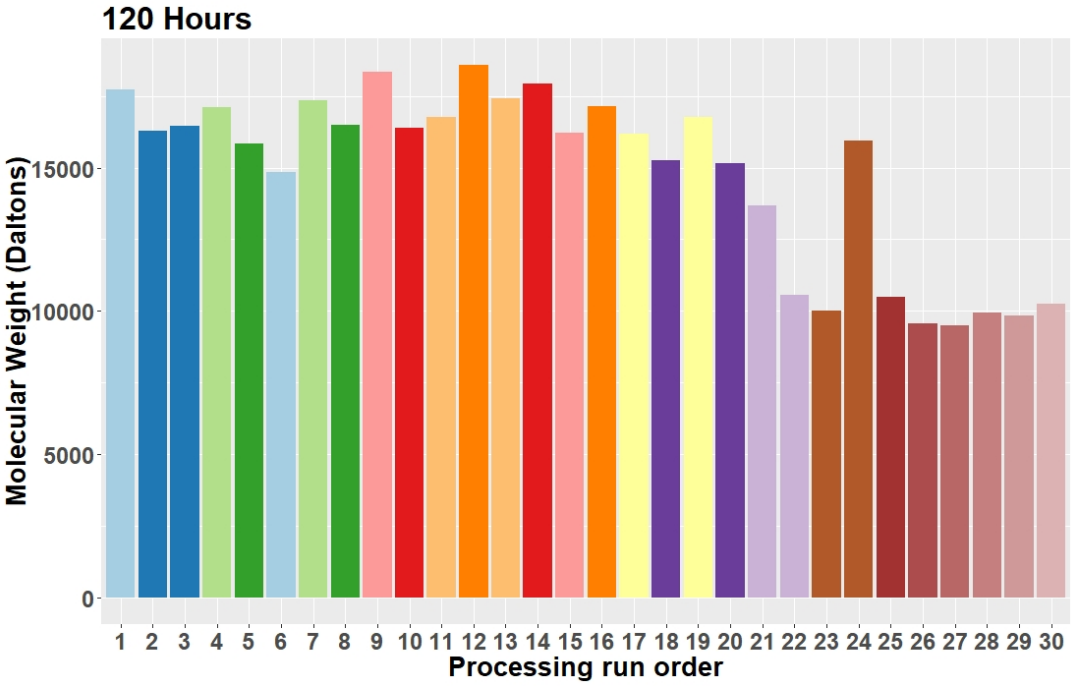

Figure 7.14: The molecular weight of 120 hours degraded samples.

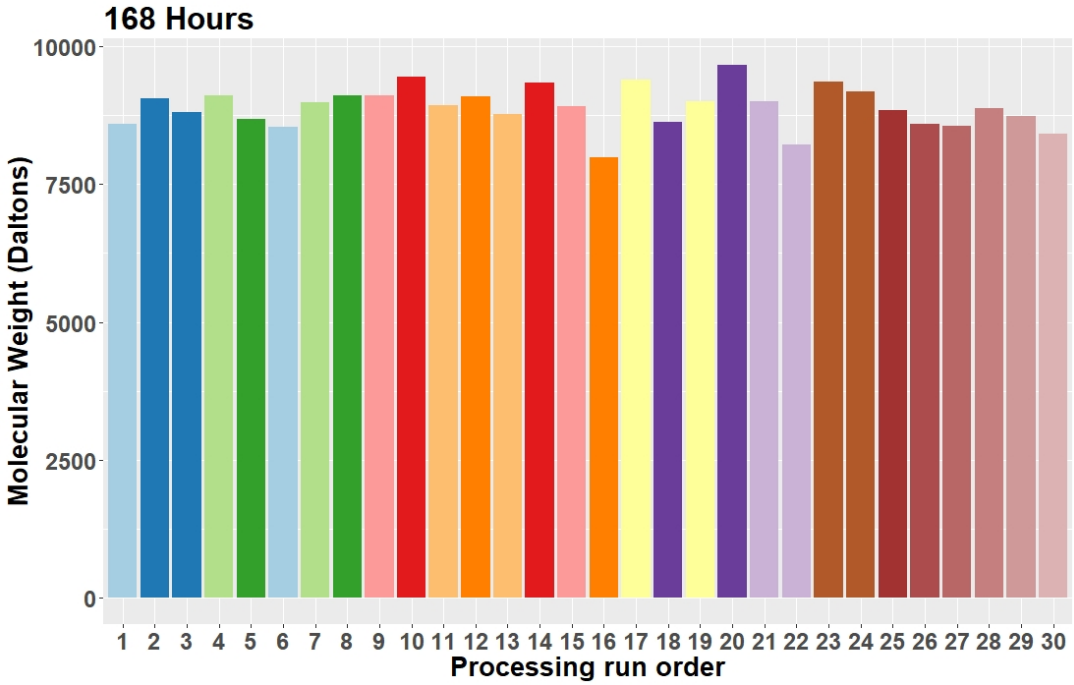

Figure 7.15: The molecular weight of 168 hours degraded samples.

In Figure 7.14, there appears to be an unusual drop in the values recorded for samples after processing run 21. Further investigation into this reveals that these samples were recorded after a power cut, which resulted in a delay of 16 hours before the samples could be evaluated. These results may be accurate or the delay could have resulted in reduced measurements, as the samples were retained in the solvent solution for much longer than other samples tested at the same degradation time point. Regrettably, it was not possible to repeat the tests for the samples from these processing runs.

7.4.1 Results

The methodology developed for the soft sensor, described in Sections 6.9 and 7.2, was applied to model the molecular weight at each of the degradation time

points. These models have not produced useful results. One consideration for the cause of this undesirable outcome is that there is no significant difference between heights of the bars in Figure 7.9 and Figures 7.11 to 7.15. Figure 7.10 presents the variance within and between triplicate measurements for processing runs 1 to 6 as well as between single samples recorded for all processing runs, which have had molecular weight recorded at 0 hours. The variance between the mean triplicate measurements is less than the variance within triplicate measurements for some processing runs. Unfortunately, there are no triplicate measurements at the other degradation points for a similar evaluation. All of these contributing factors result in measurement uncertainty of the absolute values of molecular weight.

The initial and validation experiments were carried out over a range of temperatures which were based on the published literature and offline differential scanning calorimetry (DSC) analysis (Appendix B). These temperatures may have been restricted to too narrow a range to induce enough thermal degradation to create more variable molecular weight responses. While the process data is highly variable between processing runs (see Section 6.4 and Appendix D), the response feature has little variation at each time point.

The model evaluation statistics are presented for samples, which have not been degraded, in Table 7.1. A normalised mean squared error (NMSE, see Equation 7.1), is presented in Table 7.1 (Hanna, 1988). The mean squared error (MSE, see Equation 3.3) is normalised by the product of the model mean predictions ($\bar{y_p}$) and the observed mean response values ($\bar{y_o}$) to give the NMSE. This normalisation attempts to ensure that the NMSE will not be biased towards models which overpredict or underpredict (Hanna, 1988). An NMSE value closer

to zero indicates better model performance.

$$NMSE = \frac{1}{n}\sum_{i=1}^{n}\frac{(y_{oi} - y_{pi})^2}{\bar{y_o} \times \bar{y_p}} \tag{7.1}$$

The PCA-RF molecular weight soft sensor OOB training error, for samples which have not been degraded, is presented in Figure 7.16. This model was trained with 80 % of the training data, 53 principal components and had an m value of 16. A number of data splits of the training data set were tested along with every possible m value combination. The models were tested on the validation data set and the model with lowest RMSE value was determined as the best. The best resulting model has been presented here. The RMSE value is ≈5 % of the mean recorded molecular weight values at 0 hours. The NMSE value here is low. The model is shown to have fit the training data well by making predictions using the 20 % of data from the training data set, which was not used to train the model, in Figure 7.17. Figure 7.18 illustrates an example of the model predictions for samples which have not been degraded using the validation data set. The red crosses represent the model mean predictions for each processing run. The soft sensor model tends to predict a value close to the average of the measured responses in the training data set (Figure 7.18). This indicates that the model has not generalised beyond the training data set.

Table 7.1: Measurement statistics to evaluate the model on samples which have not been degraded; the model was trained with 80 % of the training data set, used 53 principal components as predictors and had an m value of 16.

Error Measurements on Validation Data Set		
MSE (Da^2)	RMSE (Da)	NMSE
77633721	8811	0.003

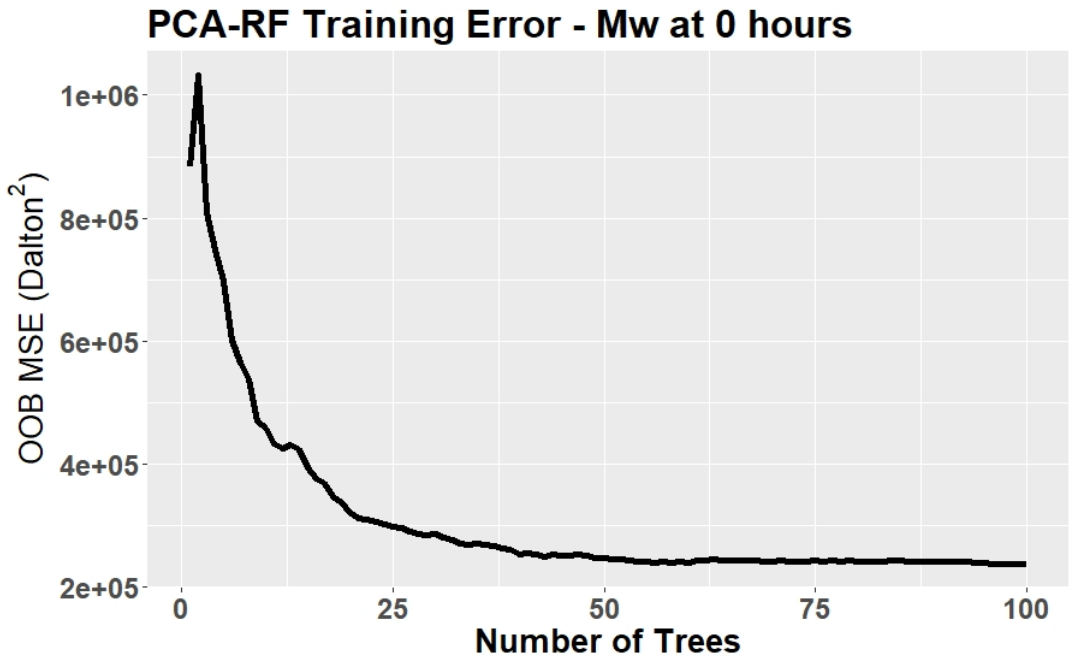

Figure 7.16: The PCA-RF soft sensor model out-of-bag error for molecular weight of nondegraded samples.

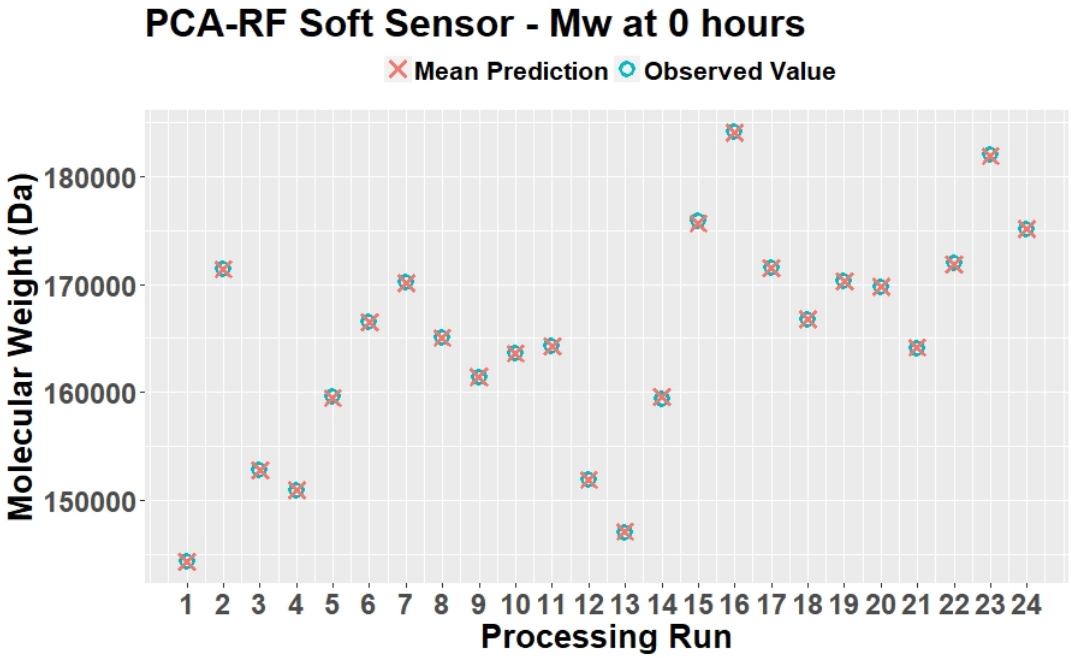

Figure 7.17: The PCA-RF soft sensor model with mean predictions and observed values of the training data samples for molecular weight of nondegraded samples; the predictions are made using the 20 % of data from the training set, which was not used to train the model.

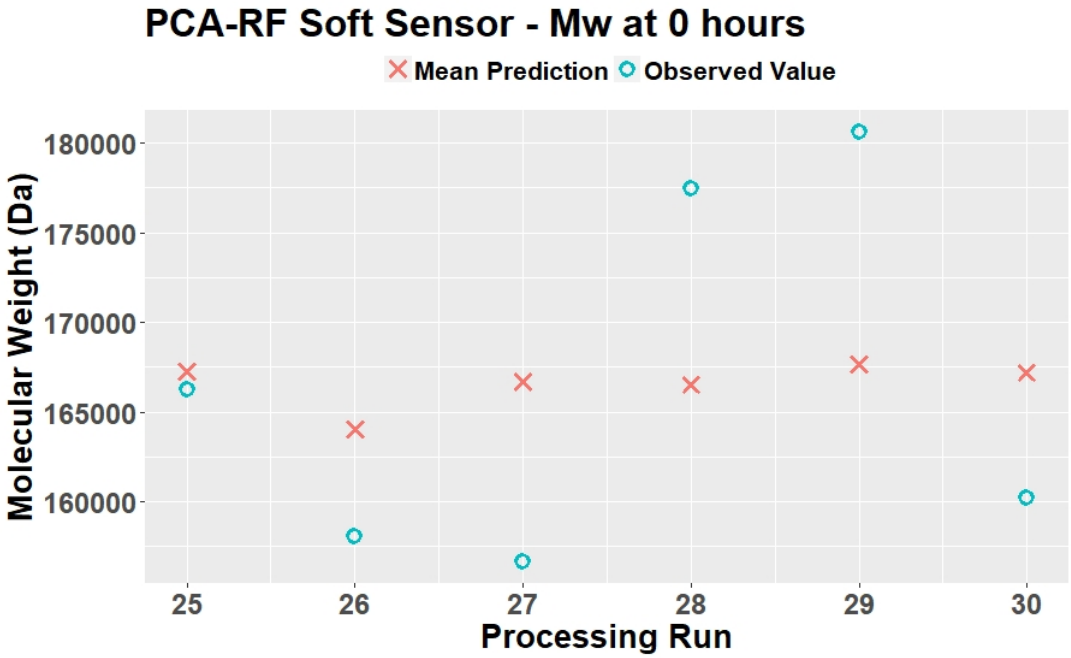

Figure 7.18: The PCA-RF soft sensor model for molecular weight with mean predictions and observed values of samples which have undergone no degradation for all processing runs in the validation data set.

7.4.2 Discussion

The results indicate that the proposed approach may not be suitable for predicting the molecular weight of PLA samples as the model error has not generalised to the validation data set. The results are similar for all models developed at all degradation time points. The presented RMSE and the NMSE values do not indicate poor model performance. However, it is clear when viewing Figure 7.18 that the model has not captured the variability in the validation data set based on the distance between the mean predictions and the observed values. It is not evident whether it is the inline process data, the sensor hardware, the processing conditions or the model or a combination of these which is not suitable to make

good predictions of the molecular weight. Further investigation is required to determine how the approach can be improved upon.

7.5 Summary

The mass change and molecular weight data has been discussed in depth. The models produced from the inline process data, obtained through the experimental trials, have not made useful predictions (see Figure 7.18). The mechanisms surrounding the degradation of PLA are complex and it is possible that the processing conditions in the initial and validation experiments were too narrow to induce enough variability in mass change and molecular weight. The yield stress soft sensor, presented in Chapter 8, has shown that the proposed soft sensor methodology can be successful. Additionally, there are a number of variables which have not been measured or accounted for e.g. moisture content during processing, monomer content of the degraded samples and oligomer content/type of the degraded samples. These variables could be useful in developing models to make accurate mass change and molecular weight predictions.

Chapter 8

Yield Stress Soft Sensor

8.1 Introduction

This chapter presents a novel hybrid Principal Component Analysis Random Forest (PCA-RF) soft sensor model for the prediction of yield stress of PLA. Part of this work has been published in Polymer Testing (Mulrennan et al., 2018). Mechanical properties are key performance metrics when evaluating processed PLA and a number of studies have viewed yield stress (σ_y) as a critical mechanical characteristic when assessing samples (Auras et al., 2003; Weir et al., 2004c; Signori, Coltelli, and Bronco, 2009; Mulrennan et al., 2018). The yield point on the stress-strain curve indicates the limit of elastic behaviour of a sample and the stress at which this occurs is referred to as the yield stress. Currently there are no inline monitoring technologies which can quantify whether a PLA sample's yield stress will be within specification post processing. This work aims to minimise the time between production and receiving feedback about the extruded material's quality. This real-time feedback will allow manufacturers to

state, with a degree of confidence, whether a product will be within specification during processing.

8.2 Exploratory Data Analysis

The yield stress results are plotted in Figure 8.1 for each processing experiment. Processing runs which have the same colour represent replicate runs. The height of each bar represents the mean value of the tested triplicates. Each black dot represents the test result or each individual sample. It can be clearly seen in Figures 8.1, 8.2 and 8.3 that the yield stress values have significant variation within triplicates, between processing runs and between replicates. The runs 25 to 30 are not included in Figure 8.3 as these correspond to the runs from the validation experiments and there are no replicates within these.

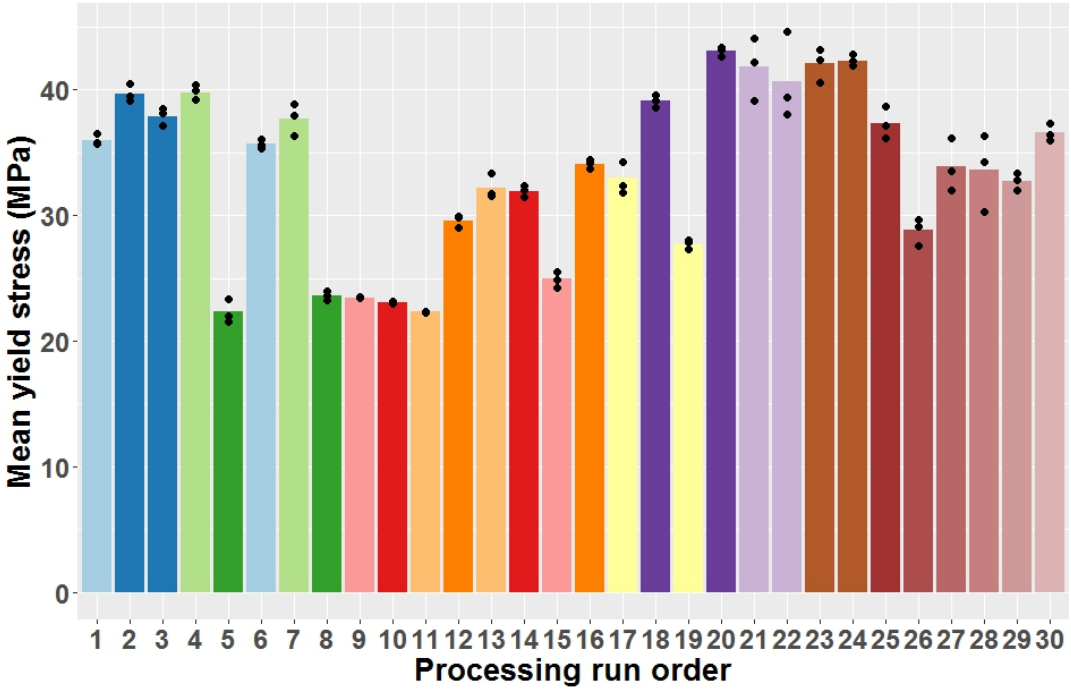

Figure 8.1: The mean yield stress for each processing run is represented by the height of the bars. Each black dot represents a single measurement of yield stress.

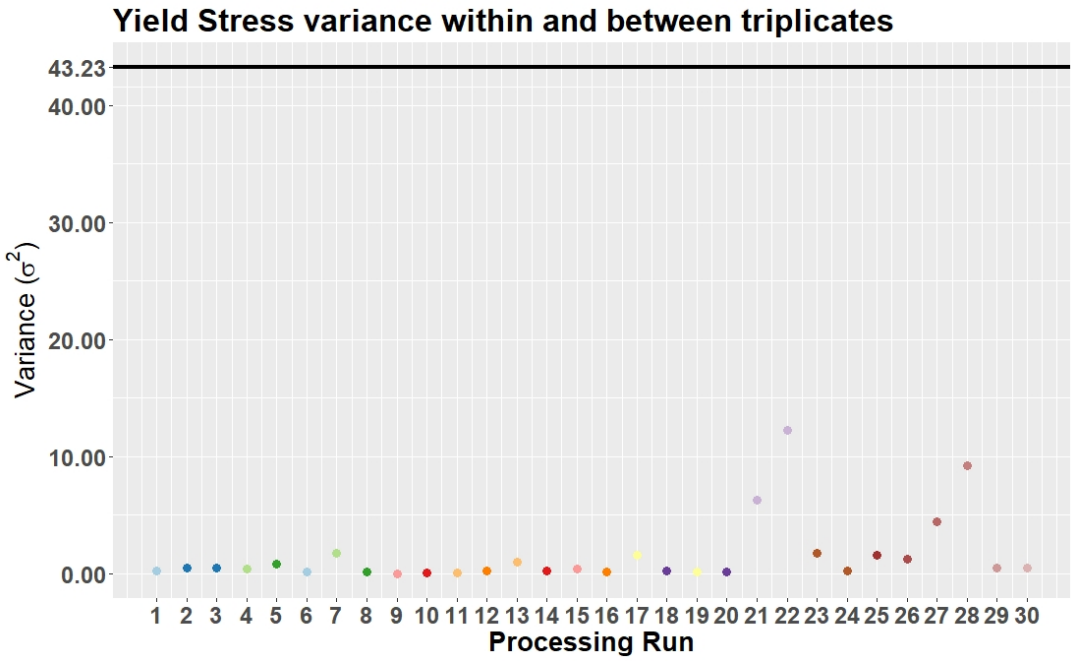

Figure 8.2: The yield stress variance within triplicate measurements; the black line represents the variance between the mean values of the triplicates for all processing runs.

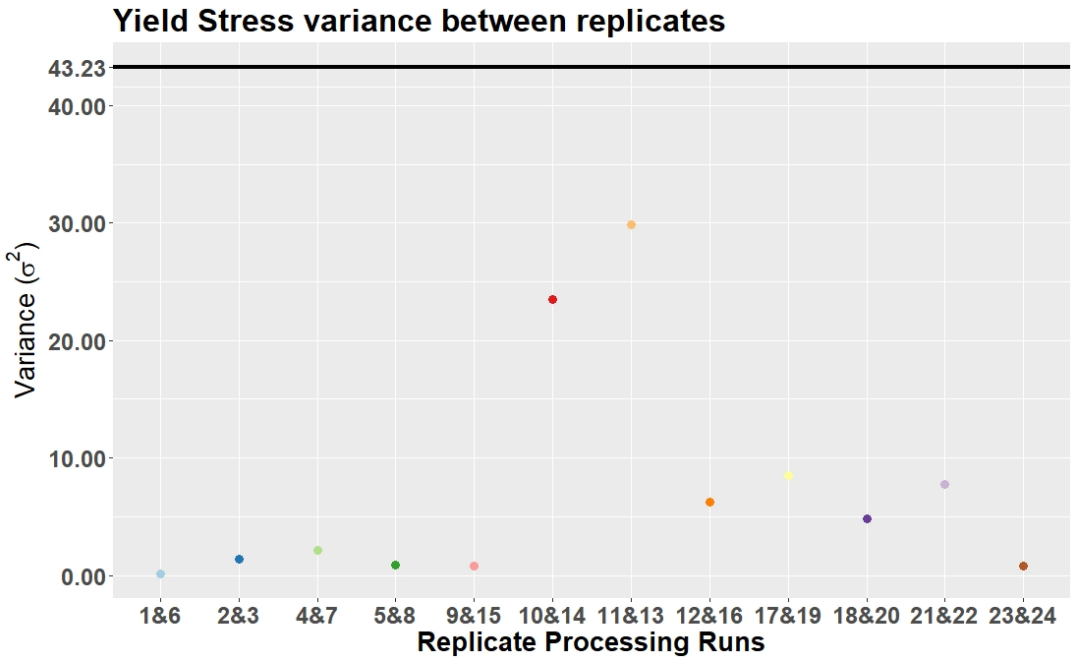

Figure 8.3: The yield stress variance between replicate runs; the black line represents the variance between the mean values of the triplicates for each processing run.

8.3 Initial Soft Sensor

A soft sensor model was initially developed using only the pressure and shear viscosity data to predict the yield stress of samples from the training data set (Mulrennan et al., 2018). This approach was taken to determine whether a soft sensor technology could be developed using much more cost effective hardware, in comparison to a system incorporating a NIR spectrometer and fibre optic probes, to predict the yield stress of PLA. The initial soft sensor was developed using only the training data set as the validation data set was not available at the time. The training data set comprised of data recorded from the initial experiments and relates to processing runs 1 to 24. Further detail on the initial

experiments can be found in Section 4.4.1. The training data was split using 80 % to train the initial soft sensor and 20 % to test the model performance. The 20 % is referred to as the test data set and the performance of the model on the test data set can be viewed in Figure 8.4.

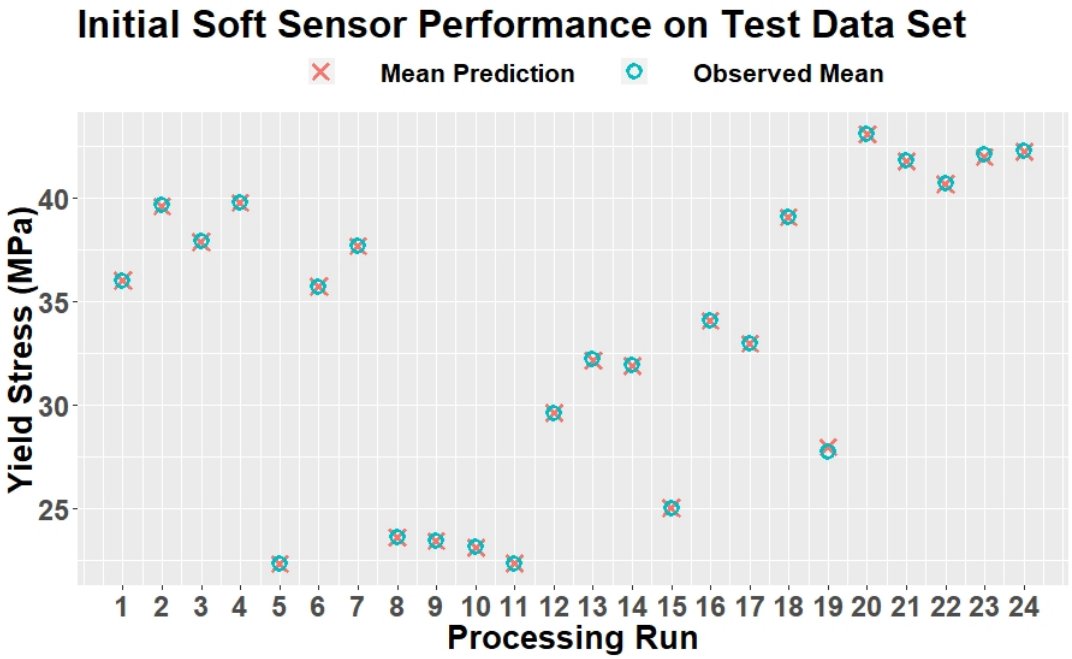

Figure 8.4: The initial PCA-RF soft sensor model developed in the Mulrennan et al. (2018) Polymer Testing publication. The model made predictions using the test data set. The model mean predictions and mean observations for each processing run in the test data set are presented; the observed mean is the target value for the model.

A thorough discussion on the initial soft sensor has been presented in Mulrennan et al. (2018). The model fits the test data set well as presented in Figure 8.4 but this fit does not transfer to the validation data set. The distance between the observed response mean and the predicted mean for the initial soft sensor presented in Figure 8.5 indicates that this model does not generalise well to the validation data set. It will be shown in the next section that the predic-

tion performance of the soft sensor model improves greatly with the addition of temperature and NIR spectral data.

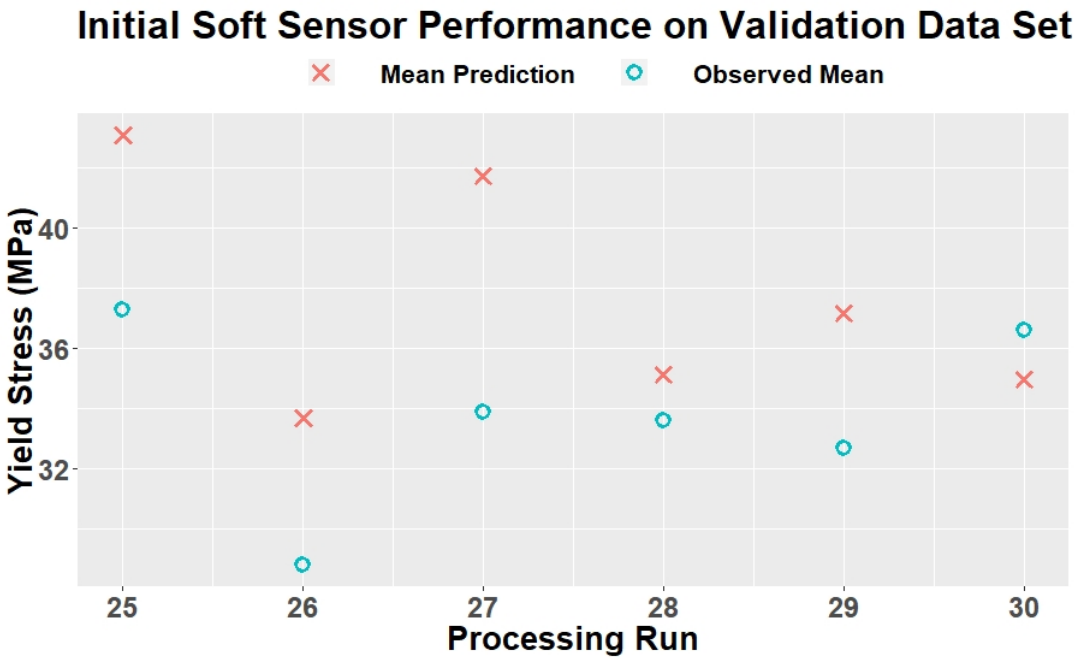

Figure 8.5: The initial PCA-RF soft sensor model developed in the Mulrennan et al. (2018) Polymer Testing publication. The model made predictions using the validation data set. The model mean predictions and mean observations for each processing run in the validation data set are presented; the observed mean is the target value for the model.

8.4 Soft Sensor Results

The soft sensor has been developed following the same approach outlined in Section 7.2. The steps outlined in Section 6.9 were followed, resulting in a subset of 49 principal components being chosen to train each model. This subset of PCs contained a mixture of higher and lower variance PCs.

Models were trained using 80 %, 75 %, 70 % and 65 % of training data, with 100 trees and all values of m. All possible values from 1-49 were trialled using

custom written routines in R. This resulted in 49 models being trained for each of the four training data set percentages. The root mean squared errors (RMSE) on the validation data set, for each of the developed models, are presented in Figure 8.6. The training percentage and m value combination with the lowest RMSE value on the validation set is represented as the black dot in Figure 8.6. The best of the 196 models is presented in Section 8.4.1.

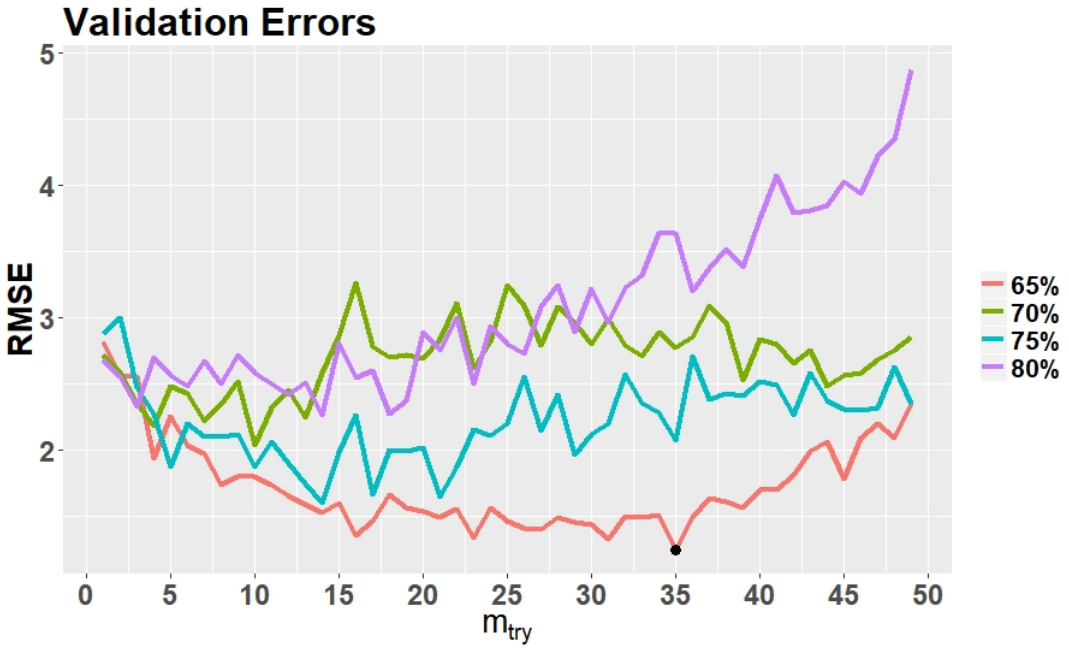

Figure 8.6: The validation error of every model tested on the validation data set which consists of processing runs 25-30; the percentages represent how much of the training data set was used to train each of the models; every possible m value was tested for each percentage of training data.

8.4.1 Final Model

The final PCA-Random Forest model had used 65 % of the data in the training set to train the model. The model had an m value of 35. The final training error (MSE) for the model is 0.14 MPa^2 while the RMSE value for the model

is 0.37 MPa. The predictions made by the model on the 35% of data from the training set which was not used to train the model are presented in Figure 8.7. There is minimal distance between the average predictions and the mean values of yield stress in the training set, which demonstrates that the model has fit the training data accurately.

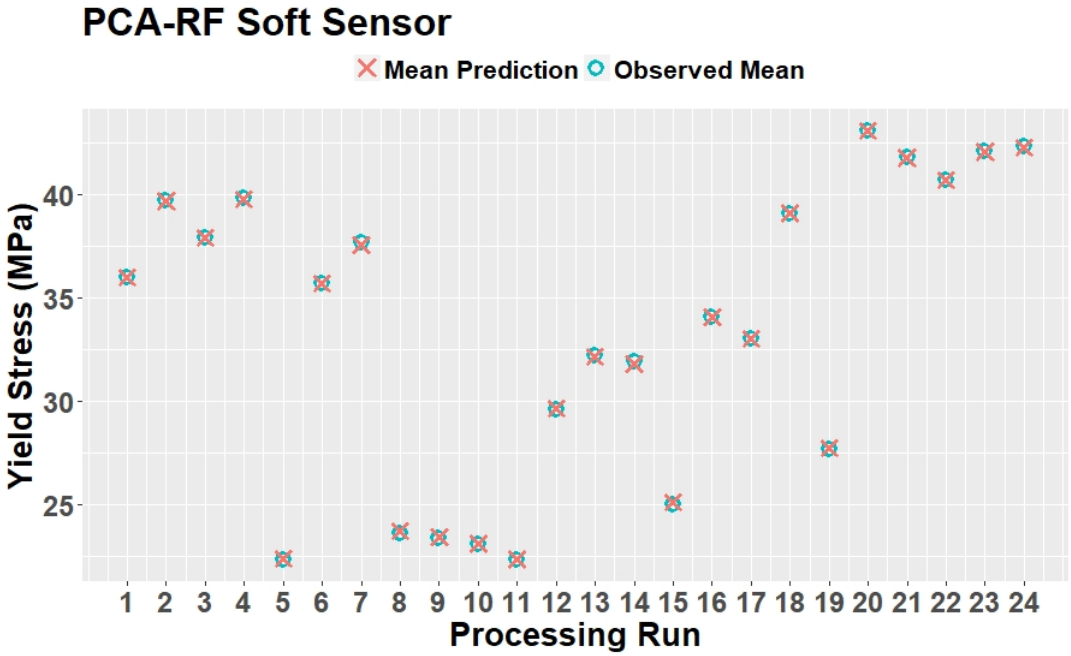

Figure 8.7: The PCA-RF soft sensor model predictions on the 35% of data from training data which was not used to train the model.

This model was then used to make predictions on the validation data set and had a RMSE value of 1.24 MPa on that data. The mean predictions by the soft sensor model for each of the processing runs in the validation data set are presented in Figure 8.8. The red crosses in Figure 8.8 represent the mean values of all of the predictions for each processing run and the bars either side each red crosses represent the 95 % prediction intervals. A mean value is used to represent the model predictions as the model makes a prediction for every

observation in the validation data set. In practice the user would not use the prediction made at a rate of ≈7-10 Hz (see Section 6.3) as these would include predictions made from noisy data. By averaging the predictions the signal to noise ratio is increased. The mean value of the observed yield stress (σ_y) of the triplicates tested for each processing run are represented by the blue circles in Figure 8.8.

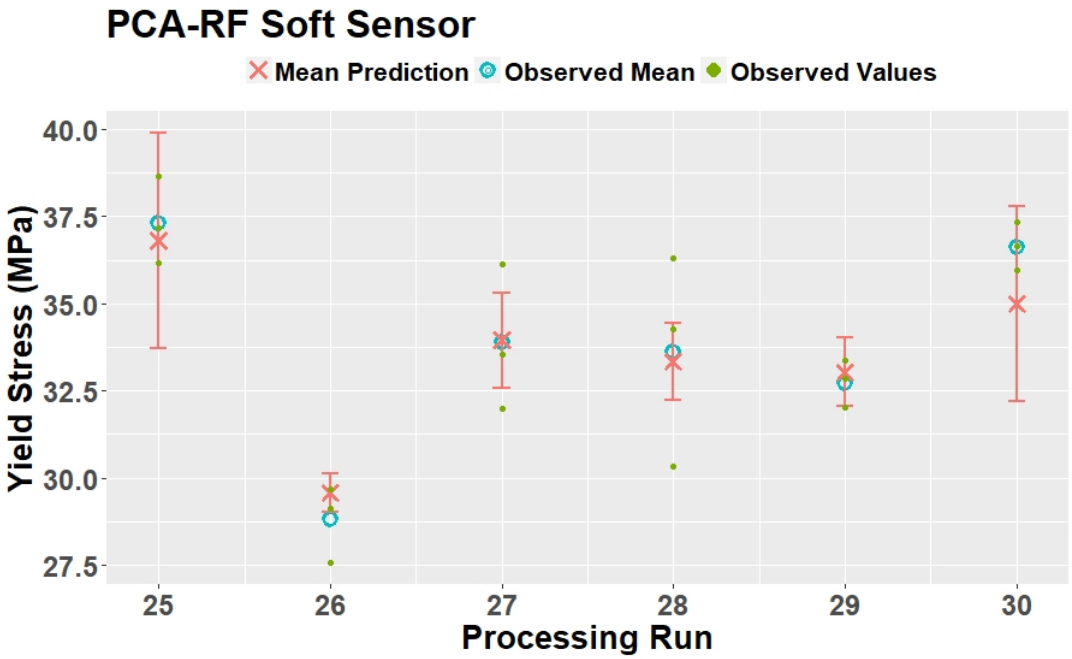

Figure 8.8: The PCA-RF soft sensor model mean predictions with 95 % prediction intervals and observed values for each processing run in the validation data set; the observed mean is the target value for the model.

This image clearly highlights the potential of the yield stress soft sensor. It is visually evident in most cases that the distance between the mean prediction values and the mean observed values could be argued to be acceptable. Measurement statistics to evaluate the final model's performance on the validation data set are presented in Table 8.1.

Table 8.1: Measurement statistics to evaluate the final model which was trained with 65 % of the training data set and had an m value of 35.

Error Measurements on Validation Data Set		
MSE (MPa^2)	RMSE (MPa)	NMSE
1.54	1.24	0.001

8.5 Discussion

There is significant variance between some of the yield stress (σ_y) triplicate measurements and between replicate runs. The pressure measurement statistics (Section 6.4 and Appendix D) have been investigated for relationships between pressure fluctuations during processing and increased variance in the yield stress triplicates. There is no apparent pattern which relates the pressure processing measurements to the variability between triplicates and replicate runs. A detailed investigation of the collected processing data has yielded no insight as to why this might be. The literature points to a number of possible causes, of which moisture content of the processed material and the atmosphere in which processing takes place are two, which are most likely. Although aware of these prior to carrying out the experiments, the facilities to enable better control of both were not available.

It is well known that moisture promotes hydrolytic degradation of PLA during processing (Wang et al., 2008; Speranza, De Meo, and Pantani, 2014) and that oxygen promotes thermo-oxidative degradation of PLA at high temperatures (Gupta and Deshmukh, 1982). Best efforts were made to minimise the moisture content of the material by oven drying the raw resin prior to processing.

Unfortunately, PLA is very hygroscopic and spent time in ambient conditions in the feed hopper. As such, it is likely that the material absorbed moisture from the atmosphere and the longer the material was in the feed hopper, the greater the level of moisture content. A further limitation was that the process did not have an inert gas such as nitrogen to conduct the experiments, as was the approach in a number of studies (Weir et al., 2004c; Signori, Coltelli, and Bronco, 2009; Paakinaho et al., 2009; Ellä, Nikkola, and Kellomäki, 2010; Speranza, De Meo, and Pantani, 2014). A nitrogen atmosphere located where the material is fed into the barrel would have minimised the level of thermo-oxidative degradation. An additional nitrogen atmosphere in the feed hopper could have reduced any moisture absorption by the material. Signori, Coltelli, and Bronco (2009) found that processing with a nitrogen atmosphere had a greater reduction in the level of process induced degradation than moisture removal prior to processing.

These trials were carried out over a range of processing conditions which were based on the published literature and offline differential scanning calorimetry (DSC) analysis (Appendix B). These conditions may not be representative of industrial practice. To implement a real-time soft sensor in industry, trials would need to be carried out under industrial conditions to further develop the model.

A mean value of yield stress of triplicate samples has been used to develop the model and considering the variation between some triplicates, a large number of samples would need to be tested to ensure confidence in the measurements. As previously considered, more controlled processing conditions may reduce the variability between samples and replicate runs.

As discussed in Section 4.4.2, none of the processing runs in the validation data set had the same experimental conditions as those in the training data set.

The model has shown the capacity to make accurate predictions beyond the identical processing conditions in which it has been trained on. This soft sensor model has the ability to learn from experience over time. This is achieved by updating the model with new observations taken from subsequent production runs. This can lead to robust predictions as the soft sensor model can adapt to changing environmental conditions (e.g. ambient temperature, humidity levels), the change of a batch of material or wear on process hardware. Therefore, it is hoped that this soft sensor model's performance will improve with additional data and that prediction errors will be further minimised.

Section 8.3 presents the initial development work for an inline yield stress soft sensor. The initial work developed a model only using the inline pressure measurements and the shear viscosity estimate (Mulrennan et al., 2018). This model fit the initial data set well (Figure 8.4) but did not generalise to the validation data set as well as the model developed using the pressure, temperature, shear viscosity and NIR measurements (compare Figure 8.5 and Figure 8.8). It can be determined that the NIR data has improved the performance of the model to predict the yield stress.

A drawback with the model is that it cannot extrapolate beyond the conditions it was trained on i.e. the process measurements or the discrete response feature values used in training are limiting factors. This means that any predictions from the model based on process data outside the range which it has been trained on cannot be considered reliable. Additionally, the model will not be able to predict values of yield stress which are beyond the discrete range of values which it has been trained on.

The model has no feedback mechanism built into it, which means its pre-

dictions cannot be verified until laboratory assessment is complete. Therefore, if data is recorded that is beyond the range of values used to train the model, samples that may be out of specification could possibly not be identified until laboratory assessment is completed.

It is unlikely that the model can be transferred for use with other extruders, unless they are of similar configuration and size, as there can be large variation between screws, heating systems and mechanical shear. All of these will have an impact on the inline process data. Further model development would be required to extend the model for use with other extruders. Further investigation is required to evaluate whether the model can be transferred to other PLA material grades.

8.6 Conclusions

The yield stress soft sensor described here can be implemented by incorporating an instrumented slit or possibly capillary die to existing extrusion lines with minimal disruption. By using a combination of inline pressure measurements from the die (which allow for the shear viscosity of PLA to be estimated), thermocouple temperature measurements and NIR spectral data, a soft sensor model has been developed, which has successfully predicted the yield stress of extruded PLA sheet.

The data obtained from the sensors embedded in the slit die, along with the model, can give a real-time estimate of what the yield stress of the extruded PLA will be during processing. The soft sensor essentially will provide process engineers with a significant real-time Quality Assurance (QA) tool. The R

software used to create the models is open source which means it is readily available and the resulting model can be implemented alongside existing data acquisition (DAQ) systems.

The soft sensor can provide immediate system feedback about PLA properties, which can alert system operators to processing issues in real-time rather than having to wait for the offline laboratory analysis. By implementing the soft sensor model in a production line, a manufacturer could save time and raw material if the soft sensor indicates that the products are going out of specification. This can allow the early stopping or the adjustment of processing parameters. This would lead to reduced scrap rates and in turn reduced manufacturing costs.

The soft sensor described here has excellent performance, as can be viewed in Figure 8.8 and highlights the potential for use in industry. It has been demonstrated that the model has accurately predicted the yield stress of PLA from random subsets of recorded inline data. The feedback system from the soft sensor can advance plant efficiency as it represents improved data acquisition, analysis and modelling.

Chapter 9

Conclusions and Future Work

This chapter reports the conclusions of this thesis and the recommendations for future research.

9.1 Conclusions

The aim of this project was to investigate whether soft sensors could be developed using inline process data collected from a twin screw extrusion process. The objectives included searching for correlations between inline process data and end material properties of PLA. Additionally it was of interest to explore whether soft sensors could predict the final material properties of extruded PLA. The following sections report the conclusions of the investigation.

9.1.1 Degradation Properties

The methodology proposed in this thesis for the development of soft sensors has not resulted in similar success for the prediction of molecular weight or mass

change. Both properties were investigated at a number of degradation time points using an accelerated procedure. The degradation profile evidenced by both properties follows what has already been published in a number of articles (Weir et al., 2004b; Brown and Farrar, 2008). Although the methods have not resulted in robust predictions on the validation data set, that should not result in the abandonment of the technique. The processing conditions investigated may not be an accurate representation of extremes that could be faced in industry. The methodology has been shown to be successful with the development of the yield stress soft sensor. As such, the conclusion is the proposed methodology does not appropriately model any relationship between inline process data and the degradation properties considered, within the range of processing conditions investigated.

Variance Discussion

It is possible that the approach may be more suitable for response variables which have higher variation in their measurements. This theory was investigated by normalising (μ=0, σ=1) the recorded variance within triplicates and between processing runs for the mass change at 168 hours, the molecular weight at 0 hours and the yield stress. These all correspond to the measurements used for the models presented in Chapters 7 and 8. By normalising these values, it allows for the variances to be compared by using the same scale for each response variable. These results are presented in Figures 9.1, 9.2 and 9.3. The variance between processing runs is represented by the black line in each figure while each dot represents the variance within triplicates. It is evident in these figures that the distance between the triplicate variances and the processing runs variance is

significantly greater in Figure 9.3 when compared to the other two figures. This may explain why the approach has had more success predicting the yield stress.

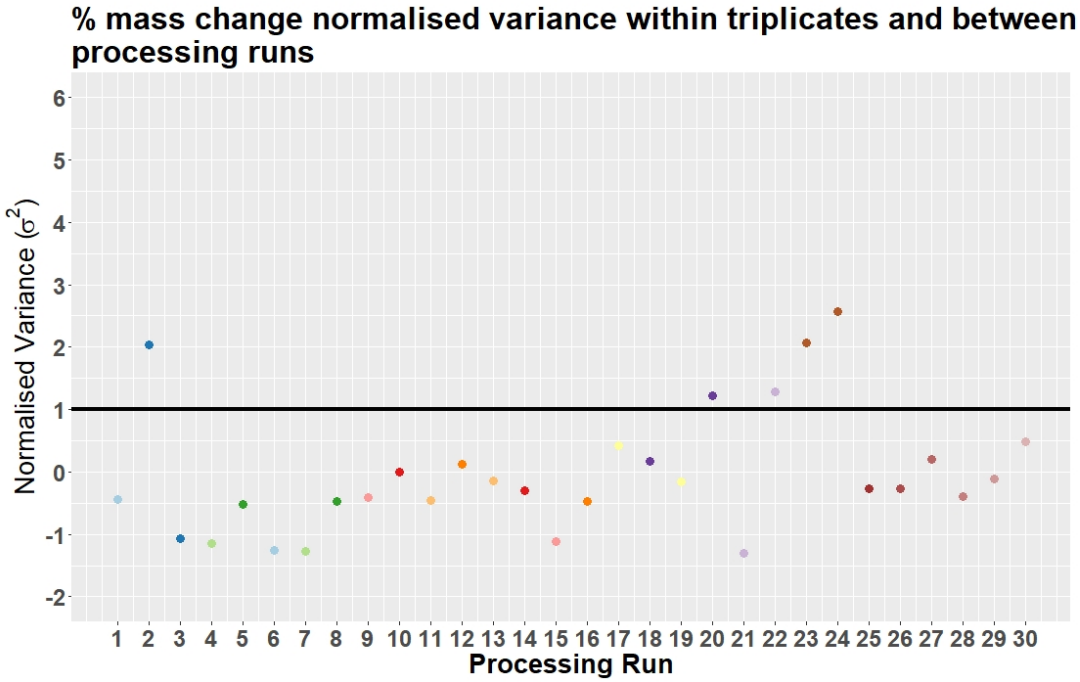

Figure 9.1: The normalised variance measurements of mass change data at 168 hours; the black line represents the normalised variance between the mean values of the triplicates for each processing run.

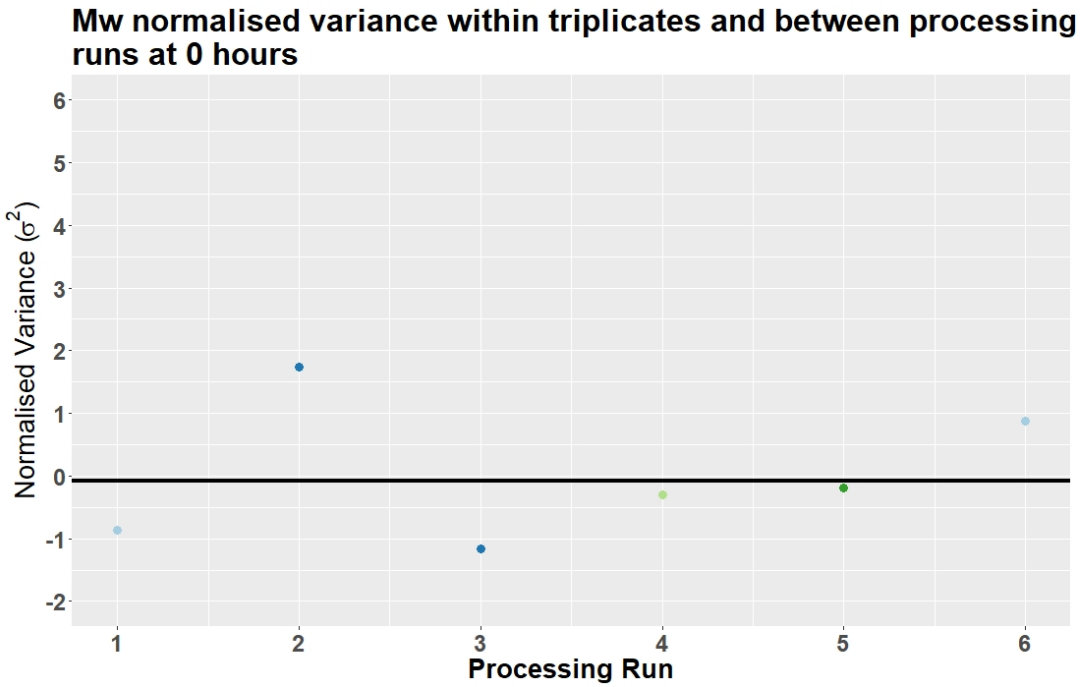

Figure 9.2: The normalised variance measurements of molecular weight data at 0 hours; the black line represents the normalised variance between the mean values of the triplicates for each processing run.

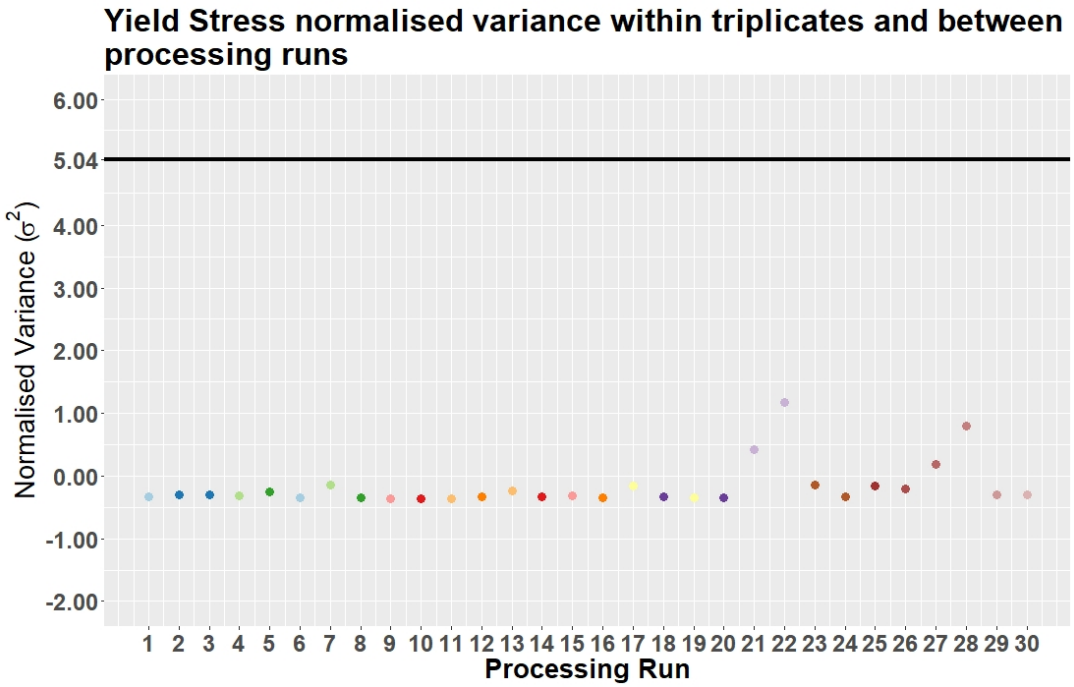

Figure 9.3: The normalised variance measurements of yield stress data; the black line represents the normalised variance between the mean values of the triplicates for each processing run.

9.1.2 Yield Stress Soft Sensor

The yield stress soft sensor described in Chapter 8 has shown that the recorded inline process data is correlated with the yield stress of the extruded PLA sheet. This is evidenced by the success of the model in predicting the average yield stress of the samples tested from the validation experimental runs. The model was not trained with any data from the validation experiments. The soft sensor made excellent predictions of the yield stress arising from the validation experiments.

The instrumented slit die, designed and implemented in this study, has resulted in additional residence times in the range of ≈3.2-5.4 seconds (see Section

4.3.2) for all processing runs. The additional residence time should not be prohibitive to industry, especially when considering the benefits associated with accurate inline predictions of the materials properties. The soft sensor essentially will provide a significant real-time Quality Assurance (QA) tool. This will provide immediate system feedback about the yield stress of PLA rather than having to wait for the offline laboratory analysis. Once laboratory results can be reliably predicted using the soft sensor, the need for offline testing can be greatly reduced.

A possible barrier to adoption of this technology to industry, especially for a small to medium enterprise (SME), is that the NIR spectroscopy system may be considered cost prohibitive. The NIR system used for the experimental work in this thesis cost ≈€90,000, which is a significant investment for companies. The results of initial modelling work using only pressure data from the slit die is presented in Mulrennan et al. (2018). The model returned satisfactory training results using the initial experimental data set (Mulrennan et al., 2018). However, it did not generalise well to the validation data set when that model was applied to it as discussed in Section 8.3. Therefore, it can be determined that the NIR data is necessary for the success of the yield stress soft sensor.

Figure 8.8 demonstrates the success of the yield stress soft sensor and exhibits its potential for use in industry. The yield stress soft sensor results suggest that recorded inline process data can be used to make accurate predictions of the material properties for extruded PLA sheet.

9.2 Future Work

9.2.1 Publications

The feature selection methodology (Section 6.9) and the resulting yield stress soft sensor (Chapter 8) will be published. The accompanying experimental details will also be included. This publication will differ from Mulrennan et al. (2018) in the following areas:

- The feature selection methodology.
- The use of the NIR spectral data.
- The soft sensor has been validated using new experimental data.

The results from the investigation of modelling the degradation characteristics from inline process data will also be published (see Chapter 7). Although the results could possibly be considered as negative, it is important that they are shared. This will prevent other researchers with interest in the field from repeating the work and also give guidelines for improving upon what has already been done.

9.2.2 Molecular Weight and Degradation Soft Sensor

Further experimental work should be carried out to investigate the viability of developing a molecular weight or degradation profile soft sensor using the inline process data. It would be beneficial to source and have input from an industrial partner prior to designing any further experiments. Any new experimental

design of the process conditions should extend the range of investigated temperatures and feed rates. This is necessary to assess whether the variance of molecular weight for non degraded samples will increase because of increased temperatures and residence times. The next implementation of the degradation study should incorporate offline measurements of monomer content and oligomer content/type. This needs to be followed by an investigation into whether these properties can be modelled from the inline process data. If so, can those predictions be used to model other degradation properties, e.g. molecular weight or mass change, at varying points of time.

9.2.3 Development of the Yield Stress Soft Sensor

It is evident that the performance of the yield stress soft sensor has been demonstrated within the limits of the experimental conditions tested. A real-time implementation of the soft sensor model should be developed through industrial collaboration under manufacturing conditions.

There are a number of considerations when examining the processing conditions of the initial and validation experiments. Attempts were made to minimise the moisture content of the material. This involved drying the PLA resin prior to processing. Due to the hygroscopic nature of the material it is possible that the resin absorbed atmospheric moisture while located in the feed hopper. Increased moisture content results in increased hydrolytic degradation during processing at high temperatures. For future experiments, it would be beneficial to have an inert nitrogen gas atmosphere in the feed hopper to prevent the material from absorbing atmospheric moisture.

The feeding zone of the extruder, were the material is fed in from the feed hopper, also creates an additional concern with regard to thermo-oxidative degradation. PLA undergoes increased levels of thermal degradation in oxygen atmospheres. By introducing a nitrogen gas atmosphere at the feeding zone, the material's exposure to oxygen will be minimised in the barrel and at the entrance to the barrel. This will reduce any possible thermo-oxidative degradation taking place.

There was no industrial partner involved in the design of experiments. To bring the development of the soft sensor to the next stage, an industrial partner should be approached and experimental work should be determined with their input. The processing conditions were examined under a limited set of conditions and it is unknown how reflective these are of industrial practice. Further experimental runs should widen the scope of what has already been trialled.

As discussed in Chapter 8, there is considerable variation within triplicates for some processing runs and also between replicate runs. The full extent of this variation should be investigated by completing more offline tensile tests for each processing run in future experiments. This will allow the variability within and between processing runs to be fully captured. By carrying out more tensile tests, a more accurate measurement of the mean and variance statistics for each processing run can be made. These measurements will be very useful in assessing how variable the process is and also provide a confidence level for the response.

Bibliography

Abeykoon, Chamil (2014). "A Novel Soft Sensor for Real-Time Monitoring of the Die Melt Temperature Profile in Polymer Extrusion". In: *IEEE Transactions on Industrial Electronics* 61.12, pp. 7113–7123. DOI: 10.1109/TIE.2014.2321345.

Abeykoon, Chamil, Adrian L. Kelly, Elaine C. Brown, Javier Vera-Sorroche, Phil D. Coates, Eileen Harkin-Jones, Ken B. Howell, Jing Deng, Kang Li, and Mark Price (2014a). "Investigation of the process energy demand in polymer extrusion: A brief review and an experimental study". In: *Applied Energy* 136, pp. 726–737. DOI: 10.1016/j.apenergy.2014.09.024.

Abeykoon, Chamil, Adrian L. Kelly, Javier Vera-Sorroche, Elaine C. Brown, Phil D. Coates, Jing Deng, Kang Li, Eileen Harkin-Jones, and Mark Price (2014b). "Process efficiency in polymer extrusion: Correlation between the energy demand and melt thermal stability". In: *Applied Energy* 135, pp. 560–571. DOI: 10.1016/j.apenergy.2014.08.086.

Abeykoon, Chamil, Kang Li, Marion McAfee, Peter J Martin, Qun Niu, Adrian Kelly, and Jing Deng (2011). "A new model based approach for the prediction and optimisation of thermal homogeneity in single screw extrusion". In:

Control Engineering Practice 19.8, pp. 862–874. DOI: 10.1016/j.conengprac.2011.04.015.

Abeykoon, Chamil, Peter J. Martin, Adrian L. Kelly, and Elaine C. Brown (2012). "A review and evaluation of melt temperature sensors for polymer extrusion". In: *Sensors and Actuators A: Physical* 182, pp. 16–27. DOI: 10.1016/j.sna.2012.04.026.

Abu-Zahra, Nidal (2004). "Real-time viscosity and density measurements of polymer melts using dielectric and ultrasound sensors fusion". In: *Mechatronics* 14.7, pp. 789–803. DOI: 10.1016/j.mechatronics.2003.11.001.

Aho, Johanna and Seppo Syrjälä (2011). "Shear viscosity measurements of polymer melts using injection molding machine with adjustable slit die". In: *Polymer Testing* 30.6, pp. 595–601. DOI: 10.1016/j.polymertesting.2011.04.014.

Alig, Ingo, Bernd Steinhoff, and Dirk Lellinger (2010). "Monitoring of polymer melt processing". In: *Measurement Science and Technology* 21.6, p. 062001. DOI: 10.1088/0957-0233/21/6/062001.

Allaire, JJ, Yihui Xie, Jonathan McPherson, Javier Luraschi, Kevin Ushey, Aron Atkins, Hadley Wickham, Joe Cheng, and Winston Chang (2017). *rmarkdown: Dynamic Documents for R*. R package version 1.7. URL: https://CRAN.R-project.org/package=rmarkdown.

Auras, Rafael, Bruce Harte, and Susan Selke (2004). "An overview of polylactides as packaging materials." In: *Macromolecular bioscience* 4.9, pp. 835–64. DOI: 10.1002/mabi.200400043.

Auras, Rafael, Bruce Harte, Susan Selke, and Ruben Hernandez (2003). "Mechanical, Physical, and Barrier Properties of Poly(Lactide) Films". In: *Jour-*

nal of Plastic Film and Sheeting 19.2, pp. 123–135. DOI: 10.1177/8756087903039702.

Auras, Rafael, Loong-Tak Lim, Susan Selke, and Hideto Tsuji, eds. (2010). *Poly(lactic acid) - Synthesis, Structures, Properties, Processing and Application*. Hoboken, NJ, USA: Wiley-Blackwell. DOI: 10.1002/9780470649848.

Barber, Alan, Burton Elrod, David McGuire, and Lonnie Paulos (2000). "Bio-screw fixation of patellar tendon autografts". In: *Biomaterials* 21.24, pp. 2623–2629. DOI: 10.1016/S0142-9612(00)00130-7.

Barbieri, Davide, Joost de Bruijn, Xiaoman Luo, Silvia Farè, Dirk Grijpma, and Huipin Yuan (2013). "Controlling dynamic mechanical properties and degradation of composites for bone regeneration by means of filler content." In: *Journal of the mechanical behavior of biomedical materials* 20, pp. 162–72. DOI: 10.1016/j.jmbbm.2013.01.012.

Barbour, Andrew and Robert Parker (2014). "psd: Adaptive, sine multitaper power spectral density estimation for R". In: *Computers & Geosciences* 63, pp. 1–8. DOI: 10.1016/j.cageo.2013.09.015.

Barnes, S.E., M.G. Sibley, H.G.M Edwards, and P.D. Coates (2007). "Process monitoring of polymer melts using in-line spectroscopy". In: *Transactions of the Institute of Measurement and Control* 29.5, pp. 453–465. DOI: 10.1177/0142331207084336.

Beleites, Claudia and Valter Sergo (2017). *hyperSpec: a package to handle hyperspectral data sets in R*. R package version 0.99-20171005. URL: http://hyperspec.r-forge.r-project.org.

Bell, Stephanie (1999). "A Beginner's Guide to Uncertainty of Measurement". In: *Measurement Good Practice Guide* 11.2, p. 41.

Bendada, A and M Lamontagne (2004). "A new infrared pyrometer for polymer temperature measurement during extrusion moulding". In: *Infrared Physics & Technology* 46.1-2, pp. 11–15. DOI: 10.1016/j.infrared.2004.03.002.

Bergmann, Björn, Wolfgang Becker, Jan Diemert, and Peter Elsner (2013). "On-Line Monitoring of Molecular Weight Using NIR Spectroscopy in Reactive Extrusion Process". In: *Macromolecular Symposia* 333.1, pp. 138–141. DOI: 10.1002/masy.201300043.

Bergström, Jörgen S. and Danika Hayman (2016). "An Overview of Mechanical Properties and Material Modeling of Polylactide (PLA) for Medical Applications". In: *Annals of Biomedical Engineering* 44.2, pp. 330–340. DOI: 10.1007/s10439-015-1455-8.

Biau, Gérard (2012). "Analysis of a Random Forests Model". In: *Journal of Machine Learning Research* 13, pp. 1063–1095. arXiv: 1005.0208.

Bishop, Christopher (2006). *Pattern Recognition and Machine Learning*. 1st ed. Springer-Verlag New York, p. 738.

Blum, Avrim and Pat Langley (1997). "Selection of relevant features and examples in machine learning". In: *Artificial Intelligence* 97.1-2, pp. 245–271. DOI: 10.1016/S0004-3702(97)00063-5.

Breiman, Leo (1996a). "Bagging predictors". In: *Machine Learning* 24.2, pp. 123–140. DOI: 10.1007/BF00058655.

— (1996b). *Out-of-bag estimation*. URL: https://www.stat.berkeley.edu/users/breiman/OOBestimation.pdf (visited on July 11, 2016).

— (2001). "Random Forests". In: *Machine Learning* 45.1, pp. 5–32. DOI: 10.1023/A:1010933404324.

Breiman, Leo, Jerome Friedman, Charles Stone, and R Olshen (1984). *Classification and Regression Trees*. Chapman and Hall/CRC, p. 368.

Brown, E. C., A. L. Kelly, and P. D. Coates (2004). "Melt temperature field measurement in single screw extrusion using thermocouple meshes". In: *Review of Scientific Instruments* 75.11, p. 4742. DOI: 10.1063/1.1808895.

Brown, Malcolm and David Farrar (2008). "Development of bioresorbable polymers in orthopaedics". In: *Plastics, Rubber and Composites* 37.2-4, pp. 46–49. DOI: 10.1179/174328908X283339.

Bur, Anthony, Steven Roth, Mark Spalding, Daniel Baugh, Kurt Koppi, and Walter Buzanowski (2004). "Temperature gradients in the channels of a single-screw extruder". In: *Polymer Engineering and Science* 44.11, pp. 2148–2157. DOI: 10.1002/pen.20221.

Bur, Anthony, Mark Vangel, and Steven Roth (2001). "Fluorescence based temperature measurements and applications to real-time polymer processing". In: *Polymer Engineering & Science* 41.8, pp. 1380–1389. DOI: 10.1002/pen.10838.

Carrasco, F, P Pagès, J Gámez-Pérez, O.O. Santana, and M.L. Maspoch (2010). "Processing of poly(lactic acid): Characterization of chemical structure, thermal stability and mechanical properties". In: *Polymer Degradation and Stability* 95.2, pp. 116–125. DOI: 10.1016/j.polymdegradstab.2009.11.045.

Castro-Aguirre, E., F. Iñiguez-Franco, H. Samsudin, X. Fang, and R. Auras (2016). "Poly(lactic acid)—Mass production, processing, industrial applications, and end of life". In: *Advanced Drug Delivery Reviews* 107, pp. 333–366. DOI: 10.1016/j.addr.2016.03.010.

Chen, Xi, Furong Gao, and Guohua Chen (2004). "A soft-sensor development for melt-flow-length measurement during injection mold filling". In: *Materials Science and Engineering: A* 384.1-2, pp. 245–254. DOI: 10.1016/j.msea.2004.06.039.

Chen, Z.-L., P.-Y. Chao, and S.-H. Chiu (2003). "Proposal of an empirical viscosity model for quality control in the polymer extrusion process". In: *Polymer Testing* 22.5, pp. 601–607. DOI: 10.1016/S0142-9418(02)00163-0.

Cherfi, A, G Fevotte, and C Novat (2002). "Robust on-line measurement of conversion and molecular weight using NIR spectroscopy during solution polymerization". In: *Journal of Applied Polymer Science* 85.12, pp. 2510–2520. DOI: 10.1002/app.10727.

Chiu, Shih-Hsuan, Hsuan-Chi Yiu, and Sheng-Hong Pong (1997). "Development of an in-line viscometer in an extrusion molding process". In: *Journal of Applied Polymer Science* 63.7, pp. 919–924. DOI: 10.1002/(SICI)1097-4628(19970214)63:7<919::AID-APP12>3.0.CO;2-M.

Coates, P.D., S.E. Barnes, M.G. Sibley, E.C. Brown, H.G.M. Edwards, and I.J. Scowen (2003). "In-process vibrational spectroscopy and ultrasound measurements in polymer melt extrusion". In: *Polymer* 44.19, pp. 5937–5949. DOI: 10.1016/S0032-3861(03)00544-5.

Cox, W. P. and E. H. Merz (1958). "Correlation of dynamic and steady flow viscosities". In: *Journal of Polymer Science* 28.118, pp. 619–622. DOI: 10.1002/pol.1958.1202811812.

Cutright, Duane and Ervin Hunsuck (1971). "Tissue reaction to the biodegradable polylactic acid suture". In: *Oral Surgery, Oral Medicine, Oral Pathology* 31.1, pp. 134–139. DOI: 10.1016/0030-4220(71)90044-2.

Cutright, Duane, Ervin Hunsuck, and Joe Beasley (1971). "Fracture reduction using a biodegradable material, polylactic acid." In: *Journal of oral surgery (American Dental Association : 1965)* 29.6, pp. 393–7.

Dealy, John (1982). *Rheometers for molten plastics: a practical guide to testing and property measurement*. Van Nostrand Reinhold, p. 302.

Dealy, John and Taras Broadhead (1993). "Process rheometers for molten plastics: A survey of existing technology". In: *Polymer Engineering and Science* 33.23, pp. 1513–1523. DOI: 10.1002/pen.760332302.

Dealy, John and Alejandro Rey (1996). "Effect of Taylor diffusion on the dynamic response of an on-line capillary viscometer". In: *Journal of Non-Newtonian Fluid Mechanics* 62.2-3, pp. 225–234. DOI: 10.1016/0377-0257(95)01403-9.

Dealy, John and Kurt Wissbrun (1990). *Melt Rheology and Its Role in Plastics Processing*. Dordrecht: Springer Netherlands. DOI: 10.1007/978-94-009-2163-4.

Deng, J., K. Li, E. Harkin-Jones, M. Price, M. Fei, A. Kelly, J. Vera-Sorroche, P. Coates, and E. Brown (2013). "Low-cost process monitoring for polymer extrusion". In: *Transactions of the Institute of Measurement and Control* 36.3, pp. 382–390. DOI: 10.1177/0142331213502696.

Deng, Jing, Kang Li, Eileen Harkin-Jones, Mark Price, Nayeem Karnachi, Adrian Kelly, Javier Vera-Sorroche, Phil Coates, Elaine Brown, and Minrui Fei (2014). "Energy monitoring and quality control of a single screw extruder". In: *Applied Energy* 113, pp. 1775–1785. DOI: 10.1016/j.apenergy.2013.08.084.

Dote, Yasuhiko and Seppo Ovaska (2001). "Industrial applications of soft computing: A review". In: *Proceedings of the IEEE* 89.9, pp. 1243–1264. DOI: 10.1109/5.949483.

Drexler, Leonard and Chang Dae Han (1973). "Studies of converging flows of viscoelastic polymeric melts. II. Velocity measurements in the entrance region of a sharp-edged slit die". In: *Journal of Applied Polymer Science* 17.8, pp. 2355–2368. DOI: 10.1002/app.1973.070170804.

Ellä, Ville, Tuija Annala, Satu Länsman, Manu Nurminen, and Minna Kellomäki (2011). "Knitted polylactide 96/4 L/D structures and scaffolds for tissue engineering: shelf life, in vitro and in vivo studies." In: *Biomatter* 1.1, pp. 102–13. DOI: 10.4161/biom.1.1.17447.

Ellä, Ville, Lila Nikkola, and Minna Kellomäki (2010). "Process-induced monomer on a medical-grade polymer and its effect on short-term hydrolytic degradation". In: *Journal of Applied Polymer Science* 119.5, pp. 2996–3003. DOI: 10.1002/app.33027.

Fambri, Luca and Claudio Migliaresi (2010). "Crystallization and thermal properties". In: *Poly(lactic acid) - Synthesis, Structures, Properties, Processing and Application*. Ed. by Rafael Auras, Loong-Tak Lim, Susan Selke, and Hideto Tsuji. Hoboken, NJ, USA: Wiley-Blackwell. Chap. 9, pp. 113–124. DOI: 10.1002/9780470649848.ch9.

Farrar, David (2008). "Modelling of the degradation process for bioresorbable polymers". In: *Degradation Rate of Bioresorbable Materials*. Ed. by Fraser J. Buchanan. Elsevier. Chap. 9, pp. 183–206. DOI: 10.1533/9781845695033.3.183.

Fischer, Dieter, Jan Müller, Sven Kummer, and Bernd Kretzschmar (2011). "Real Time Monitoring of Morphologic and Mechanical Properties of Polymer Nanocomposites During Extrusion by near Infrared and Ultrasonic Spectroscopy". In: *Macromolecular Symposia* 305.1, pp. 10–17. DOI: 10.1002/masy.201000113.

Fontoura, J. and A. F Santos (2003). "Monitoring and control of styrene solution polymerization using NIR spectroscopy". In: *Journal of Applied Polymer Science* 90, pp. 1273–1289. DOI: 10.1002/app.12746/full.

Fortuna, Luigi, Salvatore Graziani, Alessandro Rizzo, and Maria Xibilia (2007). *Soft Sensors for Monitoring and Control of Industrial Processes*. Advances in Industrial Control. London: Springer London, p. 267. DOI: 10.1007/978-1-84628-480-9.

Gao, Jun, Gregory Walsh, David Bigio, Robert Briber, and Mark Wetzel (2000). "Mean residence time analysis for twin screw extruders". In: *Polymer Engineering & Science* 40.1, pp. 227–237. DOI: 10.1002/pen.11155.

Garlotta, Donald (2002). "A Literature Review of Poly (Lactic Acid)". In: *Journal of Polymers and the Environment* 9.2, pp. 63–84. DOI: 10.1023/A:1020200822435.

Ghosh, S, J.C. Viana, R.L. Reis, and J.F. Mano (2007). "Effect of processing conditions on morphology and mechanical properties of injection-molded poly(l-lactic acid)". In: *Polymer Engineering & Science* 47.7, pp. 1141–1147. DOI: 10.1002/pen.20799.

Giese, Erhard (1988). "Fiber optical pressure transducer". EP Patent App. EP19870106895. URL: https://www.google.com/patents/EP0290646A1?cl=en.

Gonzalez, G.D. (1999). "Soft sensors for processing plants". In: *Proceedings of the Second International Conference on Intelligent Processing and Manufacturing of Materials. IPMM'99 (Cat. No.99EX296)* 1, pp. 59–69. DOI: 10.1109/IPMM.1999.792454.

Goodfellow, Ian, David Warde-Farley, Mehdi Mirza, Aaron Courville, and Yoshua Bengio (2013). "Maxout Networks". In: *Proceedings of the 30th International Conference on Machine Learning*. Ed. by Sanjoy Dasgupta and David McAllester. Vol. 28. Proceedings of Machine Learning Research 3. PMLR, pp. 1319–1327.

Gorrasi, Giuliana and Roberto Pantani (2013). "Effect of PLA grades and morphologies on hydrolytic degradation at composting temperature: Assessment of structural modification and kinetic parameters". In: *Polymer Degradation and Stability* 98.5, pp. 1006–1014. DOI: 10.1016/j.polymdegradstab.2013.02.005.

Groot, Wim and Tobias Borén (2010). "Life cycle assessment of the manufacture of lactide and PLA biopolymers from sugarcane in Thailand". In: *The International Journal of Life Cycle Assessment* 15.9, pp. 970–984. DOI: 10.1007/s11367-010-0225-y.

Gu, Shu-ying, Cun-yang Zou, Kai Zhou, and Jie Ren (2009). "Structure-rheology responses of polylactide/calcium carbonate composites". In: *Journal of Applied Polymer Science* 114.3, pp. 1648–1655. DOI: 10.1002/app.30768.

Gupta, M C and V G Deshmukh (1982). "Thermal oxidative degradation of poly-lactic acid". In: *Colloid & Polymer Science* 260.5, pp. 514–517. DOI: 10.1007/BF01452999.

Guyon, Isabelle and André Elisseeff (2003). "An Introduction to Variable and Feature Selection". In: *Journal of Machine Learning Research (JMLR)* 3.3, pp. 1157–1182. DOI: 10.1016/j.aca.2011.07.027.

Hakkarainen, M. (2000). "Rapid (bio)degradation of polylactide by mixed culture of compost microorganisms—low molecular weight products and matrix changes". In: *Polymer* 41.7, pp. 2331–2338. DOI: 10.1016/S0032-3861(99)00393-6.

Han, Chang Dae and Marvin Charles (1970). "A criterion for fully developed flow of polymer melts in a circular tube". In: *AIChE Journal* 16.3, pp. 499–501. DOI: 10.1002/aic.690160334.

Hanna, Steven R. (1988). "Air quality model evaluation and uncertainty". In: *Journal of the Air Pollution Control Association* 38.4, pp. 406–412. DOI: 10.1080/08940630.1988.10466390.

Hastie, Trevor, Robert Tibshirani, and Jerome Friedman (2009). *The Elements of Statistical Learning*. 2nd ed. Springer Series in Statistics. New York, NY: Springer New York. DOI: 10.1007/978-0-387-84858-7.

Hyon, S.-H., K Jamshidi, and Y Ikada (1998). "Effects of residual monomer on the degradation of DL-lactide polymer". In: *Polymer International* 46.3, pp. 196–202. DOI: 10.1002/(SICI)1097-0126(199807)46:3<196::AID-PI914>3.0.CO;2-Y.

Al-Itry, Racha, Khalid Lamnawar, and Abderrahim Maazouz (2012). "Improvement of thermal stability, rheological and mechanical properties of PLA, PBAT and their blends by reactive extrusion with functionalized epoxy". In: *Polymer Degradation and Stability* 97.10, pp. 1898–1914. DOI: 10.1016/j.polymdegradstab.2012.06.028.

James, Gareth, Daniela Witten, Trevor Hastie, and Robert Tibshirani (2013). *An Introduction to Statistical Learning*. Vol. 103. Springer Texts in Statistics. New York, NY: Springer New York, p. 426. DOI: 10.1007/978-1-4614-7138-7.

Jamshidian, Majid, Elmira Arab Tehrany, Muhammad Imran, Muriel Jacquot, and Stéphane Desobry (2010). "Poly-Lactic Acid: Production, Applications, Nanocomposites, and Release Studies". In: *Comprehensive Reviews in Food Science and Food Safety* 9.5, pp. 552–571. DOI: 10.1111/j.1541-4337.2010.00126.x.

Jolliffe, Ian (1982). "A Note on the Use of Principal Components in Regression". In: *Applied Statistics* 31.3, pp. 300–303. DOI: 10.2307/2348005.

— (2002). *Principal Component Analysis*. 2nd ed. Springer Series in Statistics. New York: Springer-Verlag, p. 488. DOI: 10.1007/b98835.

Kadlec, Petr, Bogdan Gabrys, and Sibylle Strandt (2009). "Data-driven Soft Sensors in the process industry". In: *Computers & Chemical Engineering* 33.4, pp. 795–814. DOI: 10.1016/j.compchemeng.2008.12.012.

Kadlec, Petr, Ratko Grbić, and Bogdan Gabrys (2011). "Review of adaptation mechanisms for data-driven soft sensors". In: *Computers & Chemical Engineering* 35.1, pp. 1–24. DOI: 10.1016/j.compchemeng.2010.07.034.

Karamanlioglu, Mehlika and Geoffrey Robson (2013). "The influence of biotic and abiotic factors on the rate of degradation of poly(lactic) acid (PLA) coupons buried in compost and soil". In: *Polymer Degradation and Stability* 98.10, pp. 2063–2071. DOI: 10.1016/j.polymdegradstab.2013.07.004.

Kelly, A. L., E. C. Brown, K. Howell, and P. D. Coates (2008). "Melt temperature field measurements in extrusion using thermocouple meshes". In: *Plastics,*

Rubber and Composites 37.2-4, pp. 151–157. DOI: 10.1179/174328908X283393.

Kopinke, F.-D. and K. Mackenzie (1997). "Mechanistic aspects of the thermal degradation of poly(lactic acid) and poly(β-hydroxybutyric acid)". In: *Journal of Analytical and Applied Pyrolysis* 40-41, pp. 43–53. DOI: 10.1016/S0165-2370(97)00022-3.

Kopinke, F.-D., M Remmler, K Mackenzie, M. Möder, and O. Wachsen (1996). "Thermal decomposition of biodegradable polyesters—II. Poly(lactic acid)". In: *Polymer Degradation and Stability* 53.3, pp. 329–342. DOI: 10.1016/0141-3910(96)00102-4.

Kroll, Andreas (2007). *Grey-box models: Concepts and application*. 1st ed. Vol. 57. Frontiers in artificial intelligence and applications. IOS Press, pp. 42–51.

Kubat, Miroslav (2015). *An Introduction to Machine Learning*. Cham: Springer International Publishing, p. 291. DOI: 10.1007/978-3-319-20010-1.

Kuhn, Max and Kjell Johnson (2013). *Applied Predictive Modeling*. New York, NY: Springer New York, p. 620. DOI: 10.1007/978-1-4614-6849-3.

Kulkarni, R. K., K. C Pani, C. Neuman, and F. Leonard (1967). "Polylactic acid for surgical implants". In: *Plastic and Reconstructive Surgery* 39.4, p. 430. DOI: 10.1097/00006534-196704000-00026.

Lane, S., E. B. Martin, A. J. Morris, and P. Gower (2003). "Application of exponentially weighted principal component analysis for the monitoring of a polymer film manufacturing process". In: *Transactions of the Institute of Measurement and Control* 25.1, pp. 17–35. DOI: 10.1191/0142331203tm071oa.

Leroy, Adrien, Sofia Ribeiro, Carole Grossiord, Antoine Alves, Robert Vestberg, Vincent Salles, Céline Brunon, Kerstin Gritsch, Brigitte Grosgogeat, and Yves Bayon (2017). "FTIR microscopy contribution for comprehension of degradation mechanisms in PLA-based implantable medical devices". In: *Journal of Materials Science: Materials in Medicine* 28.6, p. 87. DOI: 10.1007/s10856-017-5894-7.

Li, P. X., O. H. Campanella, and A. K. Hardacre (2004). "Using an In-Line Slit-Die Viscometer to Study the Effects of Extrusion Parameters on Corn Melt Rheology". In: *Cereal Chemistry* 81.1, pp. 70–76. DOI: 10.1094/CCHEM.2004.81.1.70.

Liu, Hongzhi and Jinwen Zhang (2011). "Research progress in toughening modification of poly(lactic acid)". In: *Journal of Polymer Science Part B: Polymer Physics* 49.15, pp. 1051–1083. DOI: 10.1002/polb.22283.

Liu, Xueqin, Kang Li, Marion McAfee, and Jing Deng (2012a). "Application of nonlinear PCA for fault detection in polymer extrusion processes". In: *Neural Computing and Applications* 21.6, pp. 1141–1148. DOI: 10.1007/s00521-011-0581-y.

— (2012b). "Polymer Extrusion Process Monitoring Using Nonlinear Dynamic Model-based PCA". In: *UKACC*, pp. 7–12.

Liu, Xueqin, Kang Li, Marion McAfee, Bao Kha Nguyen, and Gerard McNally (2012c). "Dynamic gray-box modeling for on-line monitoring of polymer extrusion viscosity". In: *Polymer Engineering & Science* 52.6, pp. 1332–1341. DOI: 10.1002/pen.23080.

Maddock, B. H. (1959). "A visual analysis of flow and mixing in extruder screws". In: *SPE Journal*, pp. 383–389.

Maddock, B. H. (1964). "Measurement and analysis of extruder stability". In: *SPE Journal* 20, pp. 1277–1283.

Maier, Christian (1996). "Infrared temperature measurement of polymers". In: *Polymer Engineering & Science* 36.11, pp. 1502–1512. DOI: 10.1002/pen.10545.

Mandenius, Carl and Robert Gustavsson (2015). "Mini-review: Soft sensors as means for PAT in the manufacture of bio-therapeutics". In: *Journal of Chemical Technology and Biotechnology* 90.2, pp. 215–227. DOI: 10.1002/jctb.4477.

Massart, D.L., B.G.M. Vandeginste, S.N. Deming, Y. Michotte, and L. Kaufman, eds. (2003). *Chemometrics: a textbook*. Vol. 2. Elsevier, pp. 1–488.

Matloff, Norman (2017). *Statistical Regression and Classification: From Linear Models to Machine Learning*. Chapman and Hall/CRC.

Maurus, Peter and Christopher Kaeding (2004). "Bioabsorbable implant material review". In: *Operative Techniques in Sports Medicine* 12.3, pp. 158–160. DOI: 10.1053/j.otsm.2004.07.015.

McAfee, Marion and G McNally (2006). "Real-time measurement of melt viscosity in single-screw extrusion". In: *Transactions of the Institute of Measurement and Control* 28.5, pp. 481–497. DOI: 10.1177/0142331206069478.

McAfee, Marion and S Thompson (2007a). "A novel approach to dynamic modelling of polymer extrusion for improved process control". In: *Proceedings of the Institution of Mechanical Engineers, Part I: Journal of Systems and Control Engineering* 221.4, pp. 617–628. DOI: 10.1243/09596518JSCE357.

McAfee, Marion and Stephen Thompson (2007b). "A Soft Sensor for Viscosity Control of Polymer Extrusion". In: *Control Conference (ECC)*. Vol. 44. 0, pp. 5671–5678.

McKay, B, Barry Lennox, Mark Willis, Geoffrey W Barton, and Gary Montague (1996). "Extruder modelling: a comparison of two paradigms". In: *UKACC International Conference on Control. Control '96*. Vol. 427. IEEE, pp. 734–739. DOI: 10.1049/cp:19960643.

McLauchlin, Andrew R., Oana Ghita, and Ali Gahkani (2014). "Quantification of PLA contamination in PET during injection moulding by in-line NIR spectroscopy". In: *Polymer Testing* 38, pp. 46–52. DOI: 10.1016/j.polymertesting.2014.06.007.

Mevik, Bjørn-Helge, Ron Wehrens, and Kristian Hovde Liland (2016). *pls: Partial Least Squares and Principal Component Regression*. R package version 2.6-0. URL: https://CRAN.R-project.org/package=pls.

Michalski, Ryszard, Jaime Carbonell, and Tom Mitchell, eds. (1983). *Machine Learning: An Artificial Intelligence Approach*. Berlin, Heidelberg: Springer Berlin Heidelberg. DOI: 10.1007/978-3-662-12405-5.

Middleton, John and Arthur Tipton (2000). "Synthetic biodegradable polymers as orthopedic devices". In: *Biomaterials* 21.23, pp. 2335–2346. DOI: 10.1016/S0142-9612(00)00101-0.

Migler, Kalman and Anthony Bur (1998). "Fluorescence based measurement of temperature profiles during polymer processing". In: *Polymer Engineering & Science* 38.1, pp. 213–221. DOI: 10.1002/pen.10182.

Milborrow, Stephen (2017). *rpart.plot: Plot 'rpart' Models: An Enhanced Version of 'plot.rpart'*. R package version 2.1.2. URL: https://CRAN.R-project.org/package=rpart.plot.

Mitchell, Tom (1997). *Machine learning*. McGraw-Hill, p. 432.

Montano-Herrera, Liliana, Steven Pratt, Monica Arcos-Hernandez, Peter Halley, Paul Lant, Alan Werker, and Bronwyn Laycock (2014). "In-line monitoring of thermal degradation of PHA during melt-processing by Near-Infrared spectroscopy." In: *New biotechnology* 31.4, pp. 357–63. DOI: 10.1016/j.nbt.2013.10.005.

Mulrennan, Konrad, John Donovan, Leo Creedon, Ian Rogers, John G. Lyons, and Marion McAfee (2018). "A soft sensor for prediction of mechanical properties of extruded PLA sheet using an instrumented slit die and machine learning algorithms". In: *Polymer Testing* 69, pp. 462–469. DOI: 10.1016/j.polymertesting.2018.06.002.

Mulrennan, Konrad, Marion McAfee, John Donovan, Leo Creedon, Fraser Buchanan, and Mark Billham (2017a). "Developing a soft sensor Random Forest model for the inline product characterization of Polylactide (PLA) in a twin screw melt extrusion process". In: *ANTEC 17*. Anaheim, pp. 1024–1031.

— (2017b). "Using machine learning as a Quality Assurance tool for a polymer extrusion process". In: *International Manufacturing Conference 34*. Sligo.

Mulrennan, Konrad, Marion McAfee, John Donovan, Leo Creedon, Thomas Smyth, Fraser Buchanan, and Mark Billham (2017c). "Degradation Profiles of Polylactide - A Comparative Study of Machine Learning Soft Sensors used for Inline Prediction". In: *Polymer Processing Society (PPS) 33*. Cancun.

Muroga, Shun, Yuta Hikima, and Masahiro Ohshima (2018). "Visualization of hydrolysis in polylactide using near-infrared hyperspectral imaging and chemometrics". In: *Journal of Applied Polymer Science* 135.8, pp. 1–10. DOI: 10.1002/app.45898.

Nair, Lakshmi and Cato Laurencin (2007). "Biodegradable polymers as biomaterials". In: *Progress in Polymer Science* 32.8-9, pp. 762–798. DOI: 10.1016/j.progpolymsci.2007.05.017.

Navarro-Baena, Iván, Valentina Sessini, Franco Dominici, Luigi Torre, Jose M Kenny, and Laura Peponi (2016). "Design of biodegradable blends based on PLA and PCL: From morphological, thermal and mechanical studies to shape memory behavior". In: *Polymer Degradation and Stability* 132, pp. 97–108. DOI: 10.1016/j.polymdegradstab.2016.03.037.

Nekhamanurak, B, P Patanathabutr, and N Hongsriphan (2012). "Mechanical Properties of Hydrophilicity Modified CaCO3-Poly (Lactic Acid) Nanocomposite". In: *International Journal of Applied Physics and Mathematics* 2.2, pp. 98–103. DOI: 10.7763/IJAPM.2012.V2.62.

Nguyen, Bao Kha, Gerard McNally, and Alan Clarke (2014). "Real time measurement and control of viscosity for extrusion processes using recycled materials". In: *Polymer Degradation and Stability* 102.1, pp. 212–221. DOI: 10.1016/j.polymdegradstab.2013.12.036.

Nishida, Haruo (2010). "Thermal degradation". In: *Poly(lactic acid) - Synthesis, Structures, Properties, Processing and Application*. Ed. by Rafael Auras, Loong-Tak Lim, Susan Selke, and Hideto Tsuji. Hoboken, NJ, USA: Wiley-Blackwell. Chap. 23, pp. 401–412. DOI: 10.1002/9780470649848.ch23.

Nogueira, Evandro, Cristiano Borges, and José Pinto (2005). "In-line monitoring and control of conversion and weight-average molecular weight of polyurethanes in solution step-growth polymerization based on near infrared spectroscopy and torquemetry". In: *Macromolecular Materials and Engineering* 290.4, pp. 272–282. DOI: 10.1002/mame.200400308.

Noreiga, Maria and Chris Rauwendaal (2010). *Troubleshooting the Extrusion Process*. Second. Hanser Publications, p. 194.

Nuutinen, Juha-pekka, Claude Clerc, and Pertti Törmälä (2003). "Mechanical properties and in vitro degradation of self-reinforced radiopaque bioresorbable polylactide fibres". In: *Journal of Biomaterials Science, Polymer Edition* 14.7, pp. 665–676. DOI: 10.1163/156856203322274923.

Ohkita, Tsutomu and Seung-Hwan Lee (2006). "Thermal degradation and biodegradability of poly (lactic acid)/corn starch biocomposites". In: *Journal of Applied Polymer Science* 100.4, pp. 3009–3017. DOI: 10.1002/app.23425.

OSC (2015). "Estimating the reproducibility of psychological science". In: *Science* 349.6251, aac4716. DOI: 10.1126/science.aac4716.

Othman, Nida Sheibat, Gilles Févotte, Dominique Peycelon, Jean-bernard Egraz, and Jean-marc Suau (2004). "Control of polymer molecular weight using near infrared spectroscopy". In: *AIChE Journal* 50.3, pp. 654–664. DOI: 10.1002/aic.10059.

Paakinaho, K., V. Ellä, S. Syrjälä, and M. Kellomäki (2009). "Melt spinning of poly(l/d)lactide 96/4: Effects of molecular weight and melt processing on hydrolytic degradation". In: *Polymer Degradation and Stability* 94.3, pp. 438–442. DOI: 10.1016/j.polymdegradstab.2008.11.010.

Paakinaho, K, H Heino, J Väisänen, P Törmälä, and M Kellomäki (2011). "Effects of lactide monomer on the hydrolytic degradation of poly(lactide-co-glycolide) 85L/15G". In: *Journal of the mechanical behavior of biomedical materials* 4.7, pp. 1283–90. DOI: 10.1016/j.jmbbm.2011.04.015.

Peng, Roger (2016). "Report Writing for Data Science in R". In: p. 114. URL: https://leanpub.com/reportwriting.

Peng, Roger and Elizabeth Matsui (2017). *The Art of Data Science: A Guide for Anyone Who Works with Data*, p. 159. URL: http://leanpub.com/artofdatascience.

R Core Team (2018). *R: A Language and Environment for Statistical Computing*. R Foundation for Statistical Computing. Vienna, Austria. URL: http://www.R-project.org/.

Ramot, Yuval, Moran Haim Zada, Abraham Domb, and Abraham Nyska (2016). "Biocompatibility and safety of PLA and its copolymers". In: *Advanced Drug Delivery Reviews*. DOI: 10.1016/j.addr.2016.03.012.

Raschka, Sebastian and Mirjalili Vahid (2017). *Python Machine Learning*. 2nd ed. Packt, p. 850.

Rauwendaal, Chris (2014). *Polymer Extrusion 5E*. 5th. Hanser Publications.

Rauwendaal, Chris and Franco Fernandez (1985). "Experimental study and analysis of a slit die viscometer". In: *Polymer Engineering and Science* 25.12, pp. 765–771. DOI: 10.1002/pen.760251207.

Renouf-Glauser, Annette, John Rose, David Farrar, and Ruth Elizabeth Cameron (2005). "The effect of crystallinity on the deformation mechanism and bulk mechanical properties of PLLA." In: *Biomaterials* 26.29, pp. 5771–82. DOI: 10.1016/j.biomaterials.2005.03.002.

Revesz, H and H Hubeny (1977). "Continuous measurement and control of viscosity throughout the extrusion process". In: *3rd International IFAC conference on instrumentation and automation in the paper, rubber and plastics industries*, pp. 69–76.

Rezazadeh, Ghader, Mina Ghanbari, Iraj Mirzaee, and Aliasghar Keyvani (2010). "On the modeling of a piezoelectrically actuated microsensor for simultaneous measurement of fluids viscosity and density". In: *Measurement* 43.10, pp. 1516–1524. DOI: 10.1016/j.measurement.2010.08.022.

Riesch, C, E Reichel, A Jachimowicz, J Schalko, P Hudek, B Jakoby, and F Keplinger (2009). "A suspended plate viscosity sensor featuring in-plane vibration and piezoresistive readout". In: *Journal of Micromechanics and Microengineering* 19.7, p. 075010. DOI: 10.1088/0960-1317/19/7/075010.

Robin, Frédéric, Nicolas Bovet, Nicolas Pineau, Heike Schuchmann, and Stefan Palzer (2011). "Online shear viscosity measurement of starchy melts enriched in wheat bran". In: *Journal of food science* 76.5, E405–12. DOI: 10.1111/j.1750-3841.2011.02193.x.

RStudio Team (2018). *RStudio: Integrated Development Environment for R*. RStudio, Inc. Boston, MA. URL: http://www.rstudio.com/.

Rumelhart, David, Geoffrey Hinton, and Ronald Williams (1986). "Learning representations by back-propagating errors". In: *Nature* 323.6088, pp. 533–536. DOI: 10.1038/323533a0.

Sabota, K.D., D.R. Lawson, and J.S. Huizinga (1995). "Advanced Temperature Measurements in Polymer Extrusion". In: *ANTEC 95*. Boston, pp. 2832–2842.

Sabzi, Mohammad, Long Jiang, Mohammad Atai, and Ismail Ghasemi (2013). "PLA/sepiolite and PLA/calcium carbonate nanocomposites: A comparison study". In: *Journal of Applied Polymer Science* 129.4, pp. 1734–1744. DOI: 10.1002/app.38866.

Saerens, Lien, Lien Dierickx, Thomas Quinten, Peter Adriaensens, Robert Carleer, Chris Vervaet, Jean Paul Remon, and Thomas De Beer (2012). "In-line NIR spectroscopy for the understanding of polymer-drug interaction during pharmaceutical hot-melt extrusion". In: *European journal of pharmaceutics and biopharmaceutics : official journal of Arbeitsgemeinschaft für Pharmazeutische Verfahrenstechnik e.V* 81.1, pp. 230–7. DOI: 10.1016/j.ejpb.2012.01.001.

Saerens, Lien, Chris Vervaet, Jean Paul Remon, and Thomas De Beer (2014). "Process monitoring and visualization solutions for hot-melt extrusion: a review." In: *The Journal of pharmacy and pharmacology* 66.2, pp. 180–203. DOI: 10.1111/jphp.12123.

Segal, Mark (2004). *Machine Learning Benchmarks and Random Forest Regression*. URL: https://escholarship.org/uc/item/35x3v9t4 (visited on November 11, 2017).

Shaw, Montgomery (2012). *Introduction to Polymer Rheology*. Hoboken, NJ, USA: John Wiley & Sons, Inc. DOI: 10.1002/9781118170229.

Shen, X, R Malloy, and J Pacini (1992). "An experimental evaluation of melt temperature sensors for thermoplastic extrusion". In: *ANTEC 92*. Detroit, pp. 918–926.

Signori, Francesca, Maria-Beatrice Coltelli, and Simona Bronco (2009). "Thermal degradation of poly(lactic acid) (PLA) and poly(butylene adipate-co-

terephthalate) (PBAT) and their blends upon melt processing". In: *Polymer Degradation and Stability* 94.1, pp. 74–82. DOI: 10.1016/j.polymdegradstab.2008.10.004.

Sikorska, Wanda, Piotr Dacko, Michał Sobota, Joanna Rydz, Marta Musioł, and Marek Kowalczuk (2008). "Degradation Study of Polymers from Renewable Resources and their Compositions in Industrial Composting Pile". In: *Macromolecular Symposia* 272.1, pp. 132–135. DOI: 10.1002/masy.200851219.

Silva, Wandeklebio, Dennis Chicoma, and Reinaldo Giudici (2011). "In-situ real-time monitoring of particle size, polymer, and monomer contents in emulsion polymerization of methyl methacrylate by near infrared spectroscopy". In: *Polymer Engineering & Science* 51.10, pp. 2024–2034. DOI: 10.1002/pen.22100.

Smith, Steven (2003). "Applications of the DFT". In: *Digital Signal Processing*. Elsevier. Chap. 9, pp. 169–184. DOI: 10.1016/B978-0-7506-7444-7/50046-7.

Son, Younggon (2007). "Determination of shear viscosity and shear rate from pressure drop and flow rate relationship in a rectangular channel". In: *Polymer* 48.2, pp. 632–637. DOI: 10.1016/j.polymer.2006.11.048.

Song, Le, Fengzhou Fang, and Jibo Zhao (2013). "Study on viscosity measurement using fiber Bragg grating micro-vibration". In: *Measurement Science and Technology* 24.1, p. 015301. DOI: 10.1088/0957-0233/24/1/015301.

Speranza, V., A. De Meo, and R. Pantani (2014). "Thermal and hydrolytic degradation kinetics of PLA in the molten state". In: *Polymer Degradation and Stability* 100, pp. 37–41. DOI: 10.1016/j.polymdegradstab.2013.12.031.

Srivastava, Nitish, Geoffrey Hinton, Alex Krizhevsky, Ilya Sutskever, and Ruslan Salakhutdinov (2014). "Dropout: A Simple Way to Prevent Neural Networks from Overfitting". In: *Journal of Machine Learning Research* 15, pp. 1929–1958. URL: http://jmlr.org/papers/v15/srivastava14a.html.

Stoica, Petre and Randolph Moses (2005). New Jersey: Prentice Hall, p. 447.

The University of Akron (2019). *Extrusion Process*. URL: https://uakron.edu/cpspe/agpa-k12outreach/images/toy_extrusionprocess.png (visited on March 5, 2019).

Therneau, Terry, Beth Atkinson, and Brian Ripley (2015). *rpart: Recursive Partitioning and Regression Trees*. R package version 4.1-10. URL: https://CRAN.R-project.org/package=rpart.

Tsuji, Hideto (2010). "Hydrolytic degradation". In: *Poly(lactic acid) - Synthesis, Structures, Properties, Processing and Application*. Ed. by Rafael Auras, Loong-Tak Lim, Susan Selke, and Hideto Tsuji. Hoboken, NJ, USA: Wiley-Blackwell. Chap. 21, pp. 345–381. DOI: 10.1002/9780470649848.ch21.

Tsuji, Hideto, Ippei Fukui, Hiroyuki Daimon, and Koichi Fujie (2003). "Poly(l-lactide) XI. Lactide formation by thermal depolymerisation of poly(l-lactide) in a closed system". In: *Polymer Degradation and Stability* 81.3, pp. 501–509. DOI: 10.1016/S0141-3910(03)00150-2.

Tsuji, Hideto, Takashi Saeki, Takayuki Tsukegi, Hiroyuki Daimon, and Koichi Fujie (2008). "Comparative study on hydrolytic degradation and monomer recovery of poly(l-lactic acid) in the solid and in the melt". In: *Polymer Degradation and Stability* 93.10, pp. 1956–1963. DOI: 10.1016/j.polymdegradstab.2008.06.009.

Urbanek, Simon and Jeffrey Horner (2015). *Cairo: R graphics device using cairo graphics library for creating high-quality bitmap (PNG, JPEG, TIFF), vector (PDF, SVG, PostScript) and display (X11 and Win32) output*. R package version 1.5-9. URL: https://CRAN.R-project.org/package=Cairo.

Vera-Sorroche, Javier, Elaine Brown, Adrian Kelly, and Phil Coates (2012). "Monitoring of Thermal Homogeneity in Single Screw Extrusion using Infrared Temperature Sensors". In: *ANTEC 12*. Orlando, pp. 2172–2179.

Vera-Sorroche, Javier, Adrian L. Kelly, Elaine C. Brown, Tim Gough, Chamil Abeykoon, Phil D. Coates, Jing Deng, Kang Li, Eileen Harkin-Jones, and Mark Price (2014). "The effect of melt viscosity on thermal efficiency for single screw extrusion of HDPE". In: *Chemical Engineering Research and Design* 92.11, pp. 2404–2412. DOI: 10.1016/j.cherd.2013.12.025.

Vera-Sorroche, Javier, Adrian Kelly, Elaine Brown, Phil Coates, Nayeem Karnachi, Eileen Harkin-Jones, Kang Li, and Jing Deng (2013). "Thermal optimisation of polymer extrusion using in-process monitoring techniques". In: *Applied Thermal Engineering* 53.2, pp. 405–413. DOI: 10.1016/j.applthermaleng.2012.04.013.

Vergnes, B., G. Della Valle, and J. Tayeb (1993). "A specific slit die rheometer for extruded starchy products. Design, validation and application to maize starch". In: *Rheologica Acta* 32.5, pp. 465–476. DOI: 10.1007/BF00396177.

Vink, Erwin and Steve Davies (2015). "Life Cycle Inventory and Impact Assessment Data for 2014 Ingeo^{TM} Polylactide Production". In: *Industrial Biotechnology* 11.3, pp. 167–180. DOI: 10.1089/ind.2015.0003.

Vink, Erwin, Karl Rábago, David Glassner, Bob Springs, Ryan P O'Connor, Jeff Kolstad, and Patrick Gruber (2004). "The sustainability of NatureWorks

polylactide polymers and Ingeo polylactide fibers: an update of the future." In: *Macromolecular bioscience* 4.6, pp. 551–64. DOI: 10.1002/mabi.200400023.

Wachsen, O, K Platkowski, and K.-H. Reichert (1997). "Thermal degradation of poly-l-lactide—studies on kinetics, modelling and melt stabilisation". In: *Polymer Degradation and Stability* 57.1, pp. 87–94. DOI: 10.1016/S0141-3910(96)00226-1.

Wagner, M G, G A Montague, and M T Tham (1997). "Neural networks for steady state modelling of an extruder". In: *Artificial Intelligence in Engineering* 11, pp. 375–382. DOI: https://doi.org/10.1016/S0954-1810(96)00056-8.

Wang, Yaming, Bernd Steinhoff, Christoph Brinkmann, and Ingo Alig (2008). "In-line monitoring of the thermal degradation of poly(l-lactic acid) during melt extrusion by UV–vis spectroscopy". In: *Polymer* 49.5, pp. 1257–1265. DOI: 10.1016/j.polymer.2008.01.010.

Ward, L and P Greenwood (2007). "1/f noise". In: *Scholarpedia* 2.12. revision #90924, p. 1537. DOI: 10.4249/scholarpedia.1537.

Weiler, Walter and Sylwester Gogolewski (1996). "Enhancement of the mechanical properties of polylactides by solid-state extrusion. I. Poly(D-lactide)." In: *Biomaterials* 17.5, pp. 529–35. DOI: 10.1016/0142-9612(96)82728-1.

Weir, N A, F J Buchanan, J F Orr, and G R Dickson (2004a). "Degradation of poly-L-lactide. Part 1: in vitro and in vivo physiological temperature degradation." In: *Proceedings of the Institution of Mechanical Engineers. Part H, Journal of engineering in medicine* 218.5, pp. 307–319. DOI: 10.1243/0954411041932782.

Weir, N A, F J Buchanan, J F Orr, D F Farrar, and G R Dickson (2004b). "Degradation of poly-L-lactide. Part 2: increased temperature accelerated degradation". In: *Proceedings of the Institution of Mechanical Engineers. Part H, Journal of engineering in medicine* 218.5, pp. 321–330. DOI: 10.1243/0954411041932809.

Weir, N A, F J Buchanan, J F Orr, D F Farrar, and A Boyd (2004c). "Processing, annealing and sterilisation of poly-l-lactide". In: *Biomaterials* 25.18, pp. 3939–3949. DOI: 10.1016/j.biomaterials.2003.10.076.

Whitaker, Darren A., Fraser Buchanan, Mark Billham, and Marion McAfee (2018). "A UV-Vis spectroscopic method for monitoring of additive particle properties during polymer compounding". In: *Polymer Testing* 67, pp. 392–398. DOI: 10.1016/j.polymertesting.2018.03.030.

Whitaker, Darren, Konrad Mulrennan, Inari Lyyra, Elina Talvitie, Minna Kellomäki, and Marion McAfee (2015). "In-situ monitoring of thermal degradation during melt processing of PLA". In: *The 8th European Symposium on Biopolymers*. Rome.

Wickham, Hadley (2017). *tidyverse: Easily Install and Load the 'Tidyverse'*. R package version 1.2.0. URL: https://CRAN.R-project.org/package=tidyverse.

Wickham, Hadley and Garrett Grolemund (2016). *R for Data Science*. O'Reilly Media, p. 522. URL: http://r4ds.had.co.nz/.

Williams, Graham (2017). *rattle: Graphical User Interface for Data Science in R*. R package version 5.1.0. URL: https://CRAN.R-project.org/package=rattle.

Workman, Jerry and Lois Weyer (2007). *Practical Guide to Interpretive Near-Infrared Spectroscopy*. 1st ed. CRC Press Taylor & Francis Group, p. 344.

Xie, Yihui (2017). *knitr: A General-Purpose Package for Dynamic Report Generation in R*. R package version 1.17. URL: https://CRAN.R-project.org/package=knitr.

Yuzay, Isinay, Rafael Auras, and Susan Selke (2010). "Poly(lactic acid) and zeolite composites prepared by melt processing: Morphological and physical-mechanical properties". In: *Journal of Applied Polymer Science* 115.4, pp. 2262–2270. DOI: 10.1002/app.31322.

Appendix A

Polymer Processing Society 33 - Summary

Introduction

This section summarises the experimental conditions and models that were disseminated at the Polymer Processing Society Conference 33 in Cancun, Mexico in December 2017 (Mulrennan et al., 2017c).

Experimental Set Up

The PLA grade used in this study was Ingeo™ Biopolymer 2003D and was obtained from NatureWorks LLC. This is a general purpose extrusion grade which is suitable for sheet production and can be processed on conventional extrusion equipment. The PLA was processed in a Haake Rheomex OS laboratory scale twin screw extruder. The extruder has 16 mm co-rotating screws in a length

to diameter ratio of 25:1. The material was fed from a volumetric feeder at a constant rate (20 %) for all extrusion runs. The PLA resin was prepared for extrusion by undergoing cryogenic grinding into a powder form. Prior to processing the PLA was dried overnight at 65 °C to remove any residual moisture. There were twelve processing runs in total with varying process settings for the temperature profile of the barrel zones, adapter zone and die zone and the screw speed was varied also. The temperature in the barrel zones 1-3 remained constant for all processing runs. The temperature in barrel zones 4-5, the adapter and the die was varied in the range from 200-240 °C and the screw speed ranged from 200-400 RPM. See Table A.1 and Table A.2 for more detail on each of the experimental levels.

Table A.1: Factor levels for the temperature profile.

Factor Level	Temperature Profile (°C)						
	Zone 1	Zone 2	Zone 3	Zone 4	Zone 5	Adaptor	Die
Low	210	200	200	200	200	200	200
Mid	210	200	200	210	220	220	220
High	210	200	200	230	240	240	240

Table A.2: Factor levels for the screw speed.

Factor Level	Screw Speed (RPM)
Low	200
Mid	300
High	400

The PLA was extruded as a sheet through a slit die with a 130 mm slit length, 2 mm slit height and 39.25 mm slit width (see Figures A.1 and A.2). The slit die had two pressure transducers at a distance of 35 mm apart along the length of the die. A slit die was used so that an inline estimate of the shear viscosity (η) could be developed. This approach was taken to investigate whether the η estimate would make a good predictor variable for the models by exploiting the relationship between η and the polymer's molecular weight (i.e. a change in molecular weight will result in a change in η). Mulrennan et al. (2017a) gives a detailed discussion on the slit die used in the study and the shear viscosity model. Post extrusion, the PLA underwent an accelerated degradation procedure (see Section 5.4 for more details) and characterisation tests were carried out. The samples were tested at 0, 24, 72, 120 and 168 hours during the PLA accelerated degradation cycle. The accelerated degradation procedure degrades the PLA at approximately 27 times the normal rate. The samples were tested for flexural strength, the percentage mass change and the molecular weight at each of the time points. Mulrennan et al. (2017a) gives a detailed discussion on the mechanical and mass change post-processing characterisation of the PLA samples. Mulrennan et al. (2017c) focuses on modelling the molecular weight degradation profile. It can be noted that the models for the flexural strength and percentage mass change show similar performance.

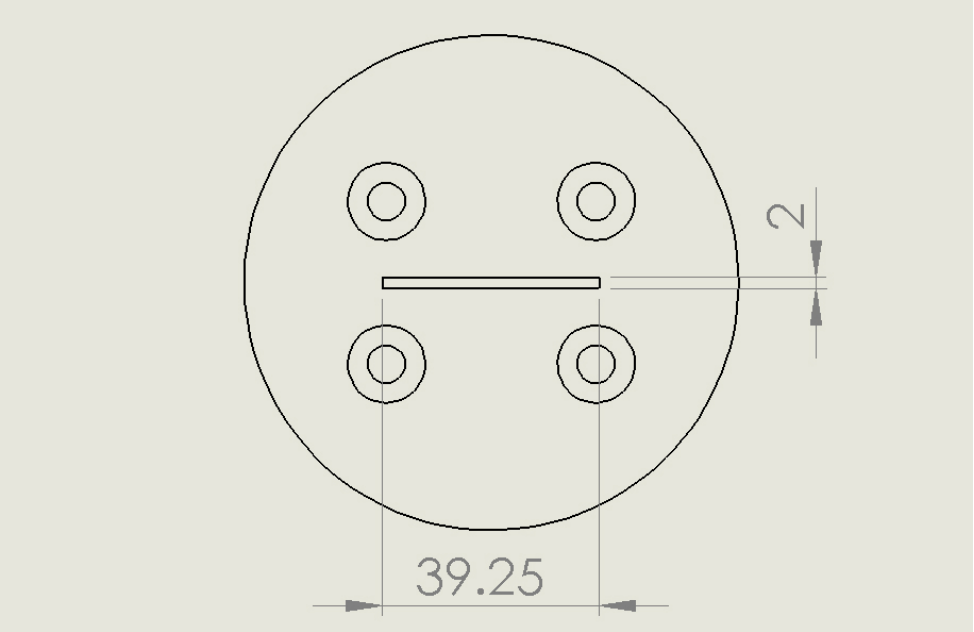

Figure A.1: The slit die front view as discussed in Mulrennan et al. (2017a) and Mulrennan et al. (2017c) (measurements are in mm).

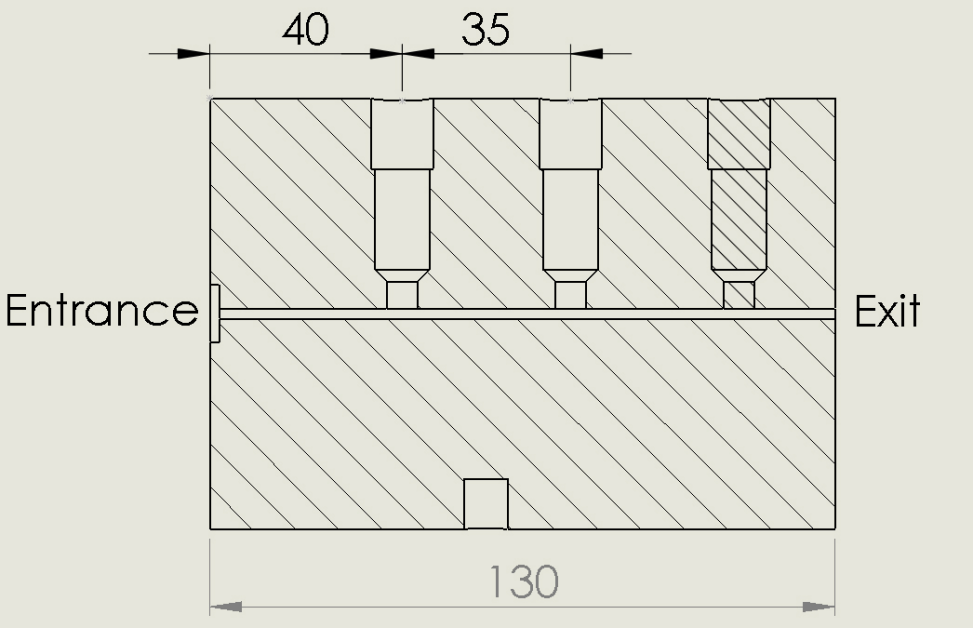

Figure A.2: The slit die cross sectional view as discussed in Mulrennan et al. (2017a) and Mulrennan et al. (2017c) (measurements are in mm).

Machine Learning Soft Sensors

All of the models were developed using R (version 3.3.3) software as a back end and RStudio (version 1.0.143) as a front end. The Bagging and Random Forest models were built using the randomForest package (version 4.6-12). A detailed description of Bagging models and also Random Forest models can be found in Chapter 3. The Neural Network models were built using the h2o package (version 3.10.5.3) in RStudio. The h2o package required the installation of the Java development kit (version JDK 8u144) and the Java run time environment (version JRE 8u144).

The data set was split into a training set and a test set for the Bagging and Random Forest models. The split for the Bagging and Random Forest models was 80 % training data and 20 % test set. The Neural Network requires the original data set be split into training, validation and test sets. The split for the Neural Network models was 50 % training data, 25 % validation data and 25 % test data. The test set in all cases contains data which the models did not see during the training or validation phases.

The Neural Networks were constructed using a feed forward architecture with multiple hidden layers. The networks were trained using backpropagation (Rumelhart, Hinton, and Williams, 1986) along with the dropout technique (Srivastava et al., 2014) and maxout activation units (Goodfellow et al., 2013). The dropout technique trains a number of models by randomly dropping out input variables, hidden activation units and their connections. The final prediction was made by averaging the predictions from the ensemble of models trained. It should be noted that all of the models trained using the dropout technique share

the same weights. The maxout activation unit is a piece-wise linear approximation function. The term maxout relates to choosing the maximum output from a number of linear feature extractors (each performs linear regression) as the input to the next layer. The output layer uses a linear activation function.

Appendix B

Differential Scanning Calorimetry (DSC)

Differential scanning calorimetry (DSC) was performed to thermally characterise the raw material resin in order to aid in identifying a suitable processing window. Prior to testing, the raw material was dried at 65 °C for four hours to remove any residual moisture. DSC profiles were created on a Perkin Elmer Model DSC 6 in the range 30 °C - 200 °C at a heating rate of 10 °C/min, in triplicate. The sample masses were measured as 5.1 mg, 5.6 mg and 4.9 mg using an analytical balance. Each sample was placed in an aluminium pan in the furnace alongside an empty pan as reference. An inert atmosphere was maintained at a constant pressure by a controlled flow of nitrogen gas through the furnace at a rate of 20 ml/min. The glass transition temperature (T_g) was found to be 59.5 °C and the melting temperature (T_m) was 150 °C. As a general rule of thumb, processing temperatures are usually at a minimum of 50 °C above the melting temperature to ensure melting of all of the crystallites (Rauwendaal, 2014).

Appendix C

Parallel Plate Rheology

Knowledge of a polymer's melt flow properties is required in order to understand the best operating conditions for the extrusion process (Shaw, 2012; Rauwendaal, 2014). A secondary interest in this rheological investigation was to evaluate the PLA's rheological properties to enable an estimate of the shear viscosity (η) be computed inline using a slit die (Section 2.3.1). This was desirable to evaluate whether the η estimate would make a good predictor variable for any models developed. The aim was to exploit the relationship between η and the polymer's molecular weight when developing soft sensors i.e. a change in molecular weight will result in a change in η.

A TA Instruments Discovery HR parallel plate rheometer, with an environmental test chamber, was used for these tests in two different laboratories. As the project developed, access to the facilities changed. Initially, samples were tested in triplicate over a range of temperatures, from 180 °C to 230 °C in steps of 10 °C. Prior to any testing, the raw material was dried for four hours at 65 °C. The raw material was cut from compression moulded sheets into 25 mm diame-

ter discs which had a thickness of 1 mm. Tests were performed in the rotational mode of the instrument which is limited to a maximum shear rate ($\dot{\gamma}$) of 10 s^{-1}. Five tests were conducted at each temperature. An inert atmosphere of two bar was maintained by a controlled flow of nitrogen gas through the environmental chamber.

The estimated $\dot{\gamma}$ of the PLA in the slit was found to be in the range 37-58 s^{-1}, (Equation 4.5), which exceeds the upper limit of the rheometer in the rotational mode. By operating the rheometer in an oscillatory mode, it allows for a range of $\dot{\gamma}$ up to ≈630 s^{-1} to be investigated. The Cox-Merz rule (Equation C.1) states that the apparent viscosity (η) at a given shear rate ($\dot{\gamma}$) is approximately equal to the dynamic viscosity ($\overset{*}{\eta}$) at a given frequency (ω) (Cox and Merz, 1958).

$$\eta(\dot{\gamma}) = \overset{*}{\eta}(\omega) \tag{C.1}$$

The tests that were run in the oscillatory mode were performed in a different facility. Prior to testing, the raw material was dried for four hours at 65 °C. In this instance the raw material resin was fed onto the fixed lower plate, the upper plate was moved into position and any excess polymer was cleaned from the edges. The PLA was tested in the oscillatory mode over a range of temperatures, from 200 °C to 230 °C in steps of 10 °C, which covers the range of temperatures the material was exposed to during processing. The test chamber had an oxygen atmosphere and each temperature was tested six times. It was originally planned to use an Arrhenius viscosity model to model the changes to η caused by shifting temperatures. Closer inspection of the measured η at temperature in the oscillatory mode revealed that this approach cannot be achieved using

the data collected from the rheometer. The results from both the rotational and oscillatory methods are plotted in Figure C.1.

Figure C.1 (b), (d) and (f) highlight the variation between runs which were recorded at the same temperature with the same process conditions. The colours of the curves in each figure represent an individual process run at a distinct temperature using a specific mode of the rheometer. The curves presented in each figure within Figure C.1 should overlay on top of each other. The results presented in Figure C.1 indicate that the Rabinowitsch correction factor cannot be calculated with confidence from the data captured in the oscillatory mode of the rheometer. The Rabinowitsch correction factor, also known as the polymer's shear thinning index, is used to account for η decreasing as $\dot{\gamma}$ increases.

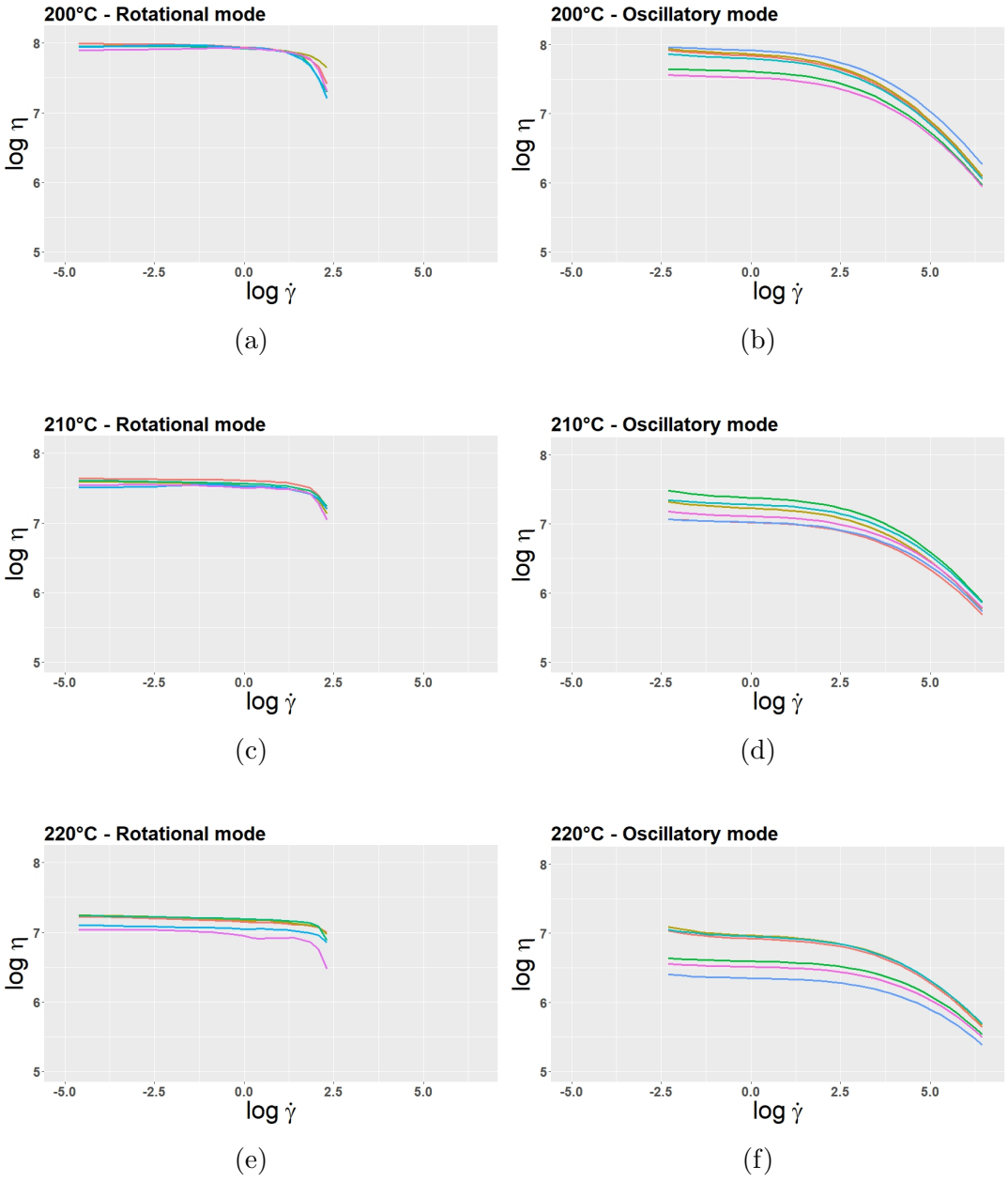

(a) (b) (c) (d) (e) (f)

Figure C.1: The η versus $\dot{\gamma}$ curves; the colours of lines represent a single process run at temperature.

It can be clearly seen in Figure C.1 (b), (d) and (f) that there is large variation between the measured η at each of the investigated temperatures in the oscillatory mode. A possible reason for this is the set up of the rheometer. Rather than having an inert nitrogen atmosphere to minimise degradation, the gas that was pumped through the environmental chamber in oscillatory mode was oxygen. PLA has been shown to undergo thermally activated oxidation (Gupta and Deshmukh, 1982). It is evident when viewing Figure C.1 (a), (c) and (e) that the rotational mode which had the nitrogen atmosphere, has much more repeatable results than the oscillatory mode which had an oxygen atmosphere. The differences in the material loading for each of the rheometers may also have resulted in varying residence times between the tests carried out in each rheometer. There was no access to a compression moulder to prepare sheets for cutting samples to test in the oscillatory mode. Although best efforts were taken to minimise residence times in each instance there were unavoidable differences between the methods. Access to equipment and changes to the set up were beyond the control of the author when using the rheometer in the oscillatory mode. It is reasonable to assume that the level of degradation which occurs is variable under these test conditions.

Appendix D

Pressure Measurement Statistics

The Tables D.1, D.2, D.3, D.4, D.5, D.6, D.7, D.8, D.9, D.10, D.11 and D.12 present statistical measurements of the recorded pressure signals. The statistical assessment of the measurements obtained from transducer $P3$ have been presented in Section 6.4. The transducers $P1$ and $P2$ and the pressure drop measurements between $P1$ and $P2$ (ΔP_{asd}) as well $P2$ and $P3$ (ΔP) are presented here. The recorded pressure signals from transducer $P1$ and their power spectrums are plotted in Section D.1.

Table D.1: Measurement statistics for pressure transducer P1 for processing runs 1-10; SD = standard deviation.

Processing Run	**1**	**2**	**3**	**4**	**5**	**6**	**7**	**8**	**9**	**10**
Max (kPa)	1712	1931	1935	2210	2370	1734	2435	2526	1968	1812
Min (kPa)	1308	1340	1262	1693	1968	1254	2032	1931	1515	1377
Mean (kPa)	1546	1678	1600	2012	2201	1571	2295	2277	1787	1636
SD (kPa)	70	110	113	74	84	77	69	93	90	63
Variance (kPa^2)	4940	12171	12763	5475	7058	5939	4819	8616	8082	4006

Table D.2: Measurement statistics for pressure transducer P1 for processing runs 11-20; SD = standard deviation.

Processing Run	**11**	**12**	**13**	**14**	**15**	**16**	**17**	**18**	**19**	**20**
Max (kPa)	1368	1381	1386	1881	1972	1459	2489	3084	2499	3081
Min (kPa)	988	973	942	1423	1537	1057	2032	2664	1981	2513
Mean (kPa)	1192	1216	1187	1704	1780	1258	2289	2926	2280	2893
SD (kPa)	82	71	85	62	86	73	99	58	97	79
Variance (kPa^2)	6663	5044	7284	3871	7351	5369	9781	3409	9417	6258

Table D.3: Measurement statistics for pressure transducer P1 for processing runs 21-30; SD = standard deviation.

Processing Run	**21**	**22**	**23**	**24**	**25**	**26**	**27**	**28**	**29**	**30**
Max (kPa)	3203	3278	2398	2301	4071	1972	2856	2734	2268	2710
Min (kPa)	2752	2692	1963	1875	3563	1457	2578	2445	1868	2223
Mean (kPa)	2972	3017	2210	2148	3862	1702	2717	2596	2060	2470
SD (kPa)	89	117	91	82	75	120	63	64	84	116
Variance (kPa^2)	7958	13633	8233	6667	5625	14314	4008	4109	7116	13329

Table D.4: Measurement statistics for pressure transducer P2 for processing runs 1-10; SD = standard deviation.

Processing Run	**1**	**2**	**3**	**4**	**5**	**6**	**7**	**8**	**9**	**10**
Max (kPa)	1272	1438	1405	1608	1718	1265	1778	1795	1168	1023
Min (kPa)	913	790	778	1158	1290	735	1418	1358	735	518
Mean (kPa)	1133	1229	1165	1458	1566	1120	1641	1612	972	853
SD (kPa)	60	94	94	61	77	63	61	80	78	55
Variance (kPa^2)	3593	8764	8764	3754	5972	3950	3709	6459	6080	3035

Table D.5: Measurement statistics for pressure transducer P2 for processing runs 11-20; SD = standard deviation.

Processing Run	**11**	**12**	**13**	**14**	**15**	**16**	**17**	**18**	**19**	**20**
Max (kPa)	670	663	658	1023	1103	725	2070	2435	2088	2478
Min (kPa)	268	303	280	675	620	335	1625	2088	1638	2078
Mean (kPa)	506	492	477	888	917	546	1896	2324	1898	2335
SD (kPa)	70	65	73	52	76	66	84	48	85	62
Variance (kPa^2)	4853	4218	5371	2696	5806	4399	7000	2267	7191	3821

Table D.6: Measurement statistics for pressure transducer P2 for processing runs 21-30; SD = standard deviation.

Processing Run	**21**	**22**	**23**	**24**	**25**	**26**	**27**	**28**	**29**	**30**
Max (kPa)	2558	2618	2015	1925	3240	1290	2240	2045	1790	2240
Min (kPa)	2155	2113	1503	1515	2833	833	2010	1803	1503	1820
Mean (kPa)	2358	2405	1840	1779	3064	1048	2133	1928	1640	2042
SD (kPa)	76	95	74	68	57	107	52	52	67	102
Variance (kPa^2)	5800	8984	5509	4568	3291	11390	2663	2675	4444	10346

Table D.7: Measurement statistics for the pressure drop between the transducers in the slit die (ΔP) for processing runs 1-10; SD = standard deviation.

Processing Run	**1**	**2**	**3**	**4**	**5**	**6**	**7**	**8**	**9**	**10**
Max (kPa)	1070	1210	1190	1380	1458	1055	1508	1530	1003	870
Min (kPa)	735	638	618	973	1080	563	1185	1125	613	403
Mean (kPa)	939	1024	967	1244	1328	919	1390	1350	828	709
SD (kPa)	54	85	84	56	69	57	53	73	69	49
Variance (kPa^2)	2883	7146	7089	3156	4716	3227	2849	5317	4711	2352

Table D.8: Measurement statistics for the pressure drop between the transducers in the slit die (ΔP) for processing runs 11-20; SD = standard deviation.

Processing Run	**11**	**12**	**13**	**14**	**15**	**16**	**17**	**18**	**19**	**20**
Max (kPa)	548	523	493	775	850	480	1318	1683	1360	1700
Min (kPa)	183	193	150	465	410	125	935	1365	953	1343
Mean (kPa)	392	361	329	660	680	313	1171	1572	1193	1568
SD (kPa)	64	58	64	46	69	60	75	43	76	55
Variance (kPa^2)	4059	3371	4147	2149	4704	3579	5551	1834	5721	3031

Table D.9: Measurement statistics for the pressure drop between the transducers in the slit die (ΔP) for processing runs 21-30; SD = standard deviation.

Processing Run	**21**	**22**	**23**	**24**	**25**	**26**	**27**	**28**	**29**	**30**
Max (kPa)	1768	1828	1258	1178	2858	1180	1853	1825	1435	1823
Min (kPa)	1403	1360	800	805	2475	780	1640	1605	1165	1458
Mean (kPa)	1586	1626	1099	1044	2691	972	1752	1719	1299	1648
SD (kPa)	68	85	67	60	52	95	46	46	60	90
Variance (kPa^2)	4642	7251	4471	3619	2746	9015	2092	2153	3535	8087

Table D.10: Measurement statistics for the pressure drop between the transducers in the adaptor and the entrance of the slit die (ΔP_{asd}) for processing runs 1-10; SD = standard deviation.

Processing Run	**1**	**2**	**3**	**4**	**5**	**6**	**7**	**8**	**9**	**10**
Max (kPa)	616	721	667	855	903	842	953	952	1038	1075
Min (kPa)	153	33	114	282	372	129	418	354	543	454
Mean (kPa)	413	449	435	555	635	451	654	665	815	783
SD (kPa)	48	90	86	53	83	51	48	86	79	46
Variance (kPa^2)	2276	8154	7366	2846	6879	2612	2298	7450	6262	2148

Table D.11: Measurement statistics for the pressure drop between the transducers in the adaptor and the entrance of the slit die (ΔP_{asd}) for processing runs 11-20; SD = standard deviation.

Processing Run	**11**	**12**	**13**	**14**	**15**	**16**	**17**	**18**	**19**	**20**
Max (kPa)	909	885	890	1017	1060	933	575	734	646	705
Min (kPa)	409	358	536	598	669	570	181	437	68	371
Mean (kPa)	687	724	710	816	863	712	393	602	382	558
SD (kPa)	53	60	51	43	77	59	88	40	88	46
Variance (kPa^2)	2791	3542	2605	1840	5865	3481	7663	1581	7737	2095

Table D.12: Measurement statistics for the pressure drop between the transducers in the adaptor and the entrance of the slit die (ΔP_{asd}) for processing runs 21-30; SD = standard deviation.

Processing Run	**21**	**22**	**23**	**24**	**25**	**26**	**27**	**28**	**29**	**30**
Max (kPa)	764	772	601	542	945	886	704	757	527	629
Min (kPa)	440	419	101	43	686	448	443	554	253	200
Mean (kPa)	613	612	370	369	799	654	585	668	420	428
SD (kPa)	70	73	59	55	36	100	39	40	52	100
Variance (kPa^2)	4890	5376	3458	3048	1321	9906	1540	1581	2668	9920

D.1 Pressure Transducer (P1) and PSD Plots

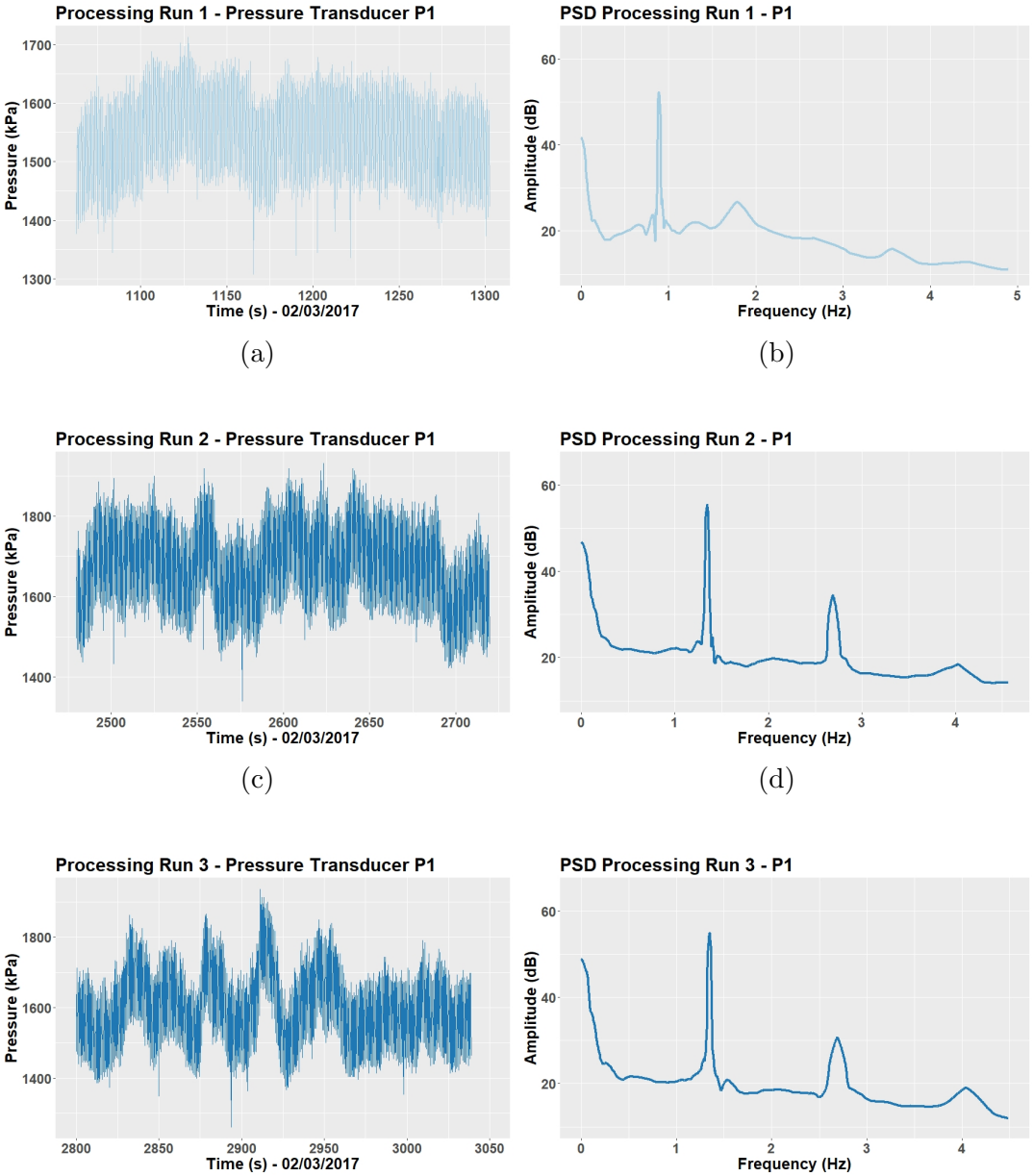

Figure D.1: The pressure signals from the *P1* transducer for processing runs 1-3 along with the power spectrum density plot for each recorded signal.

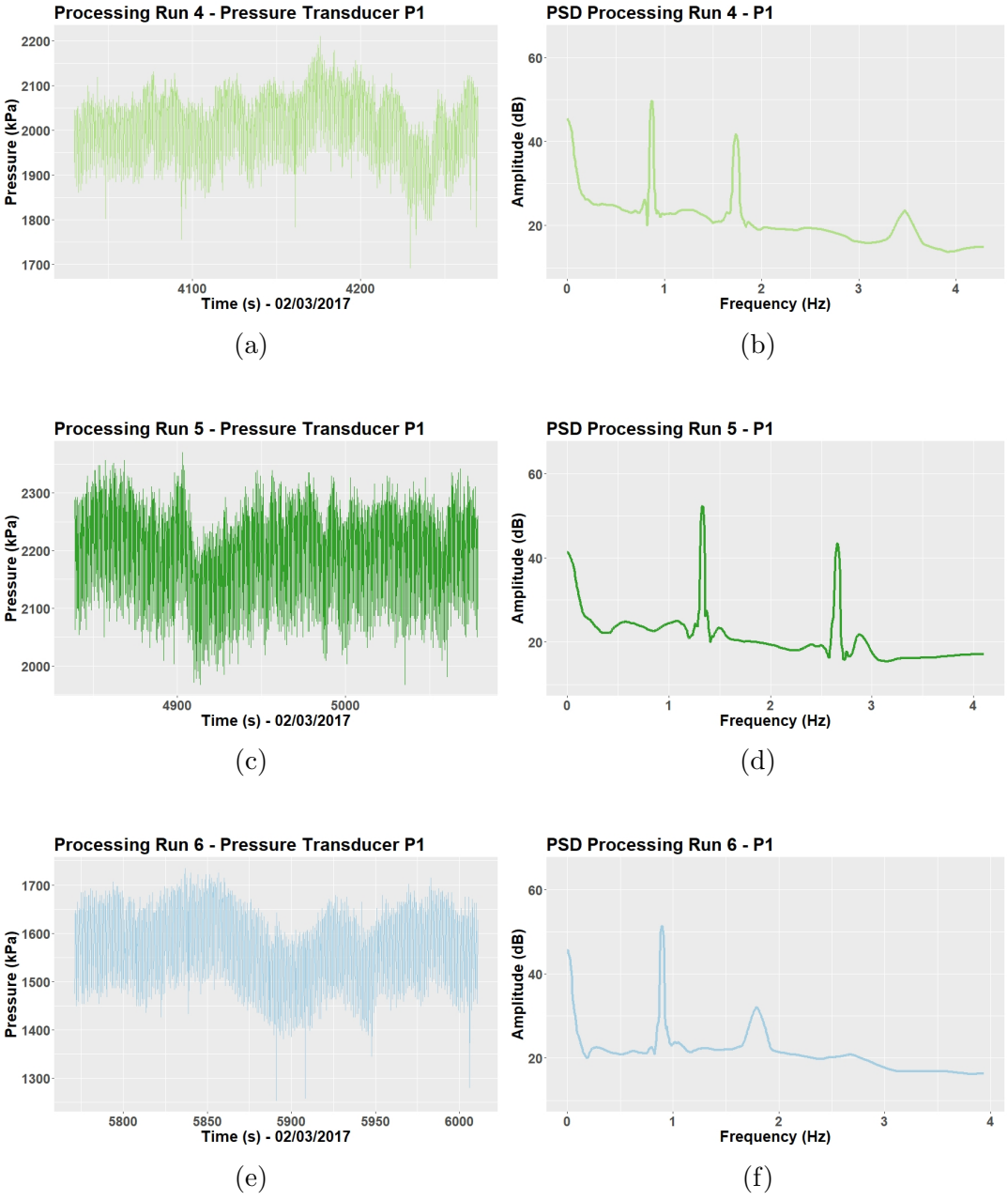

Figure D.2: The pressure signals from the *P1* transducer for processing runs 4-6 along with the power spectrum density plot for each recorded signal.

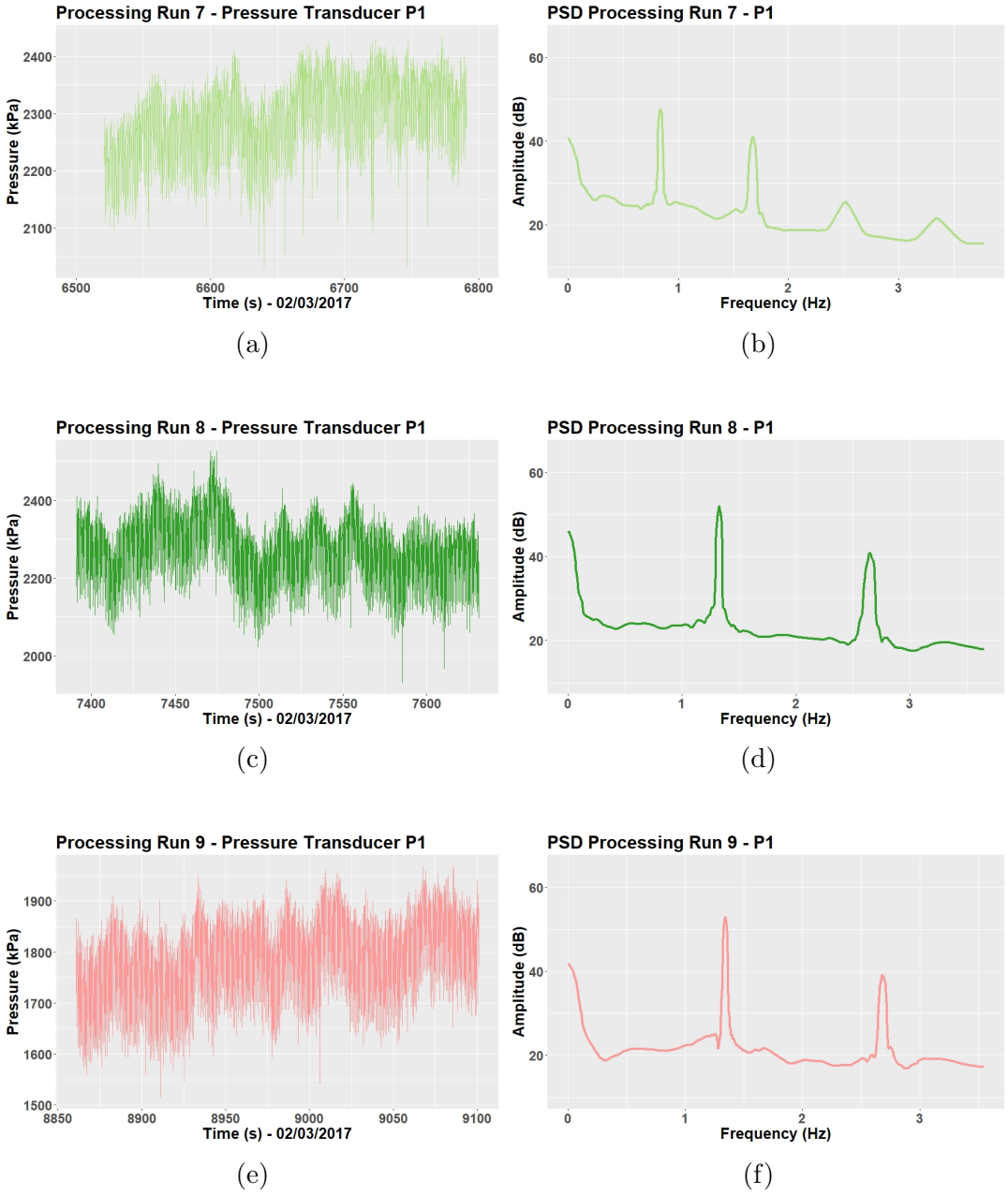

Figure D.3: The pressure signals from the *P1* transducer for processing runs 7-9 along with the power spectrum density plot for each recorded signal.

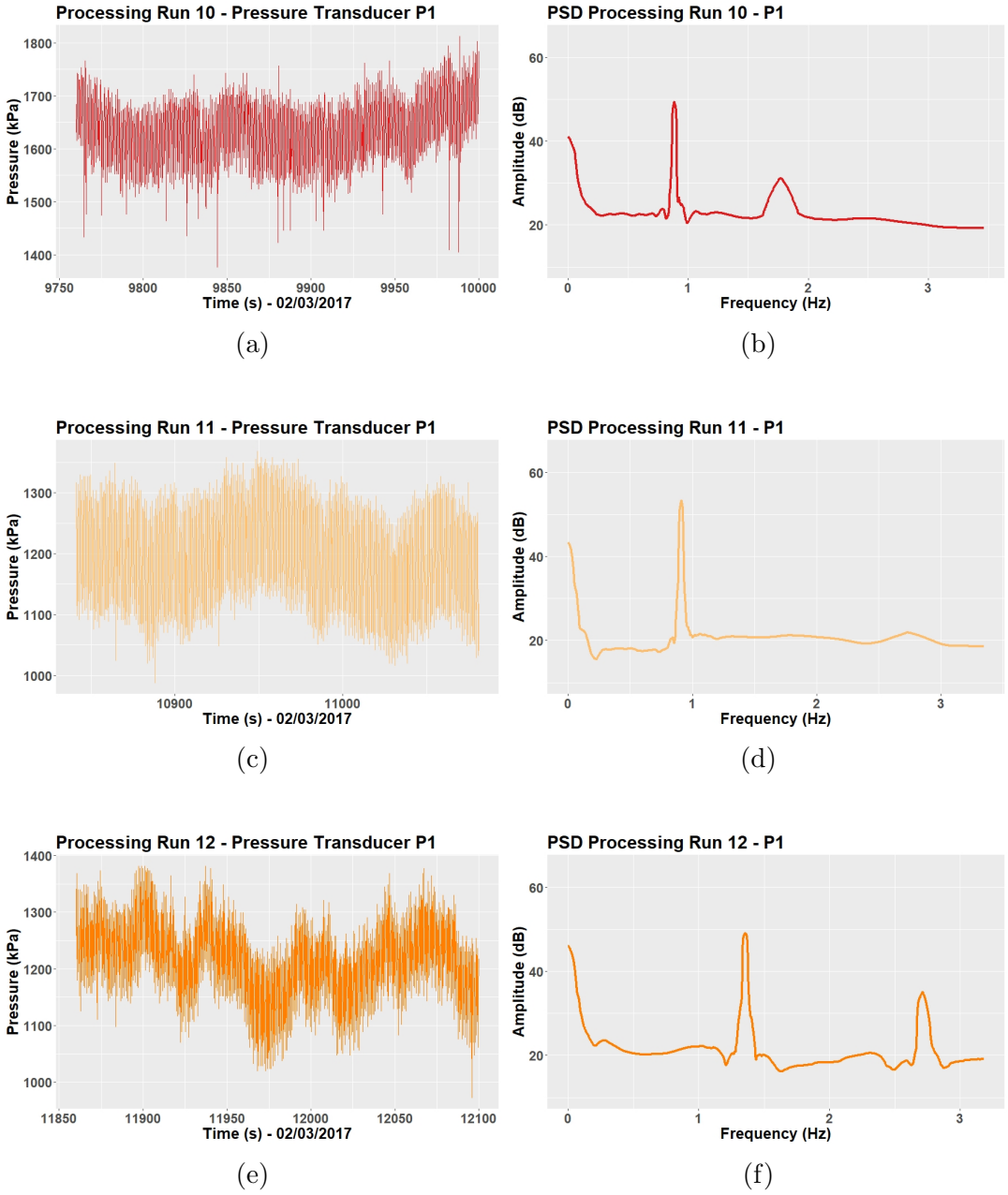

Figure D.4: The pressure signals from the *P1* transducer for processing runs 10-12 along with the power spectrum density plot for each recorded signal.

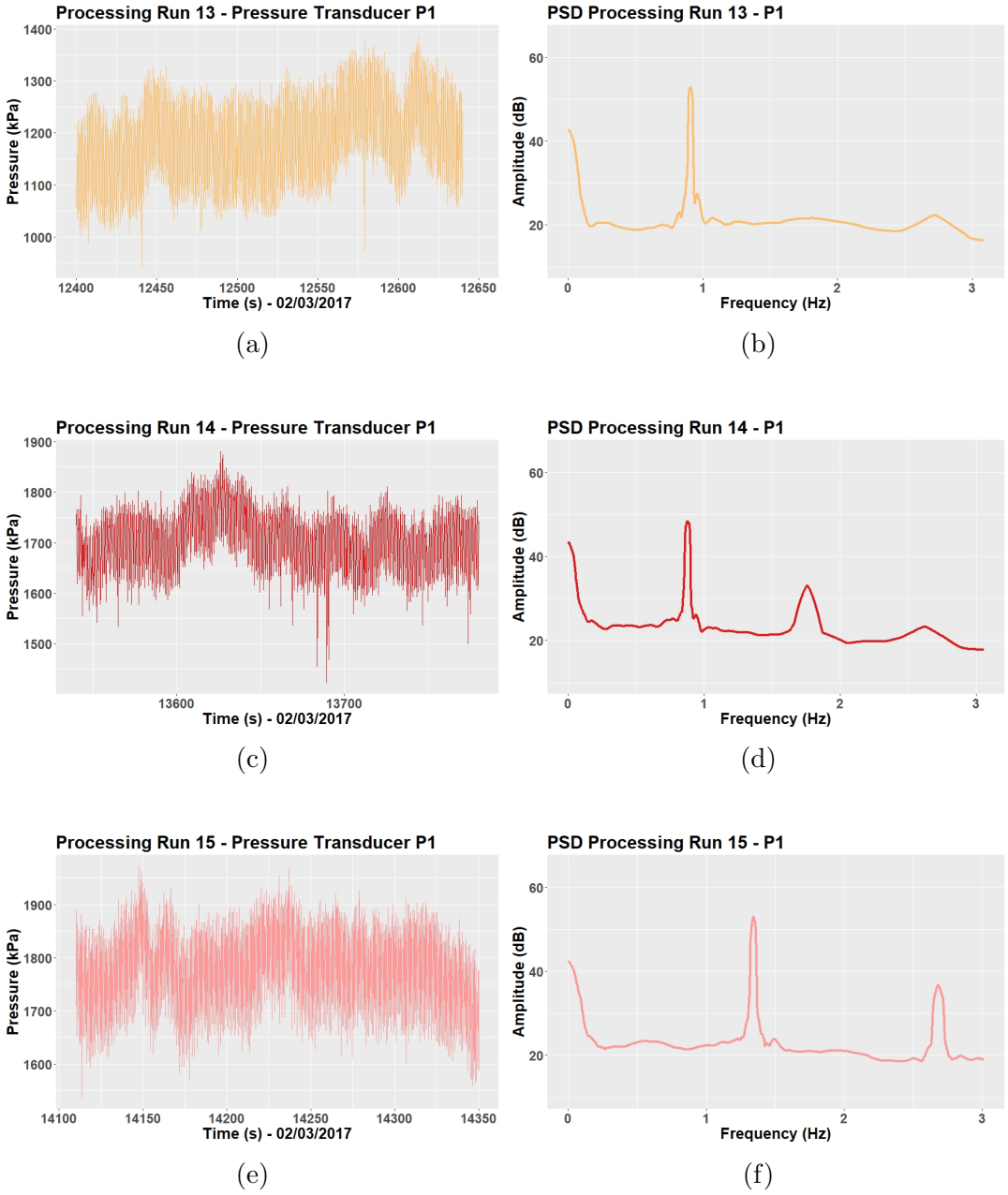

Figure D.5: The pressure signals from the *P1* transducer for processing runs 13-15 along with the power spectrum density plot for each recorded signal.

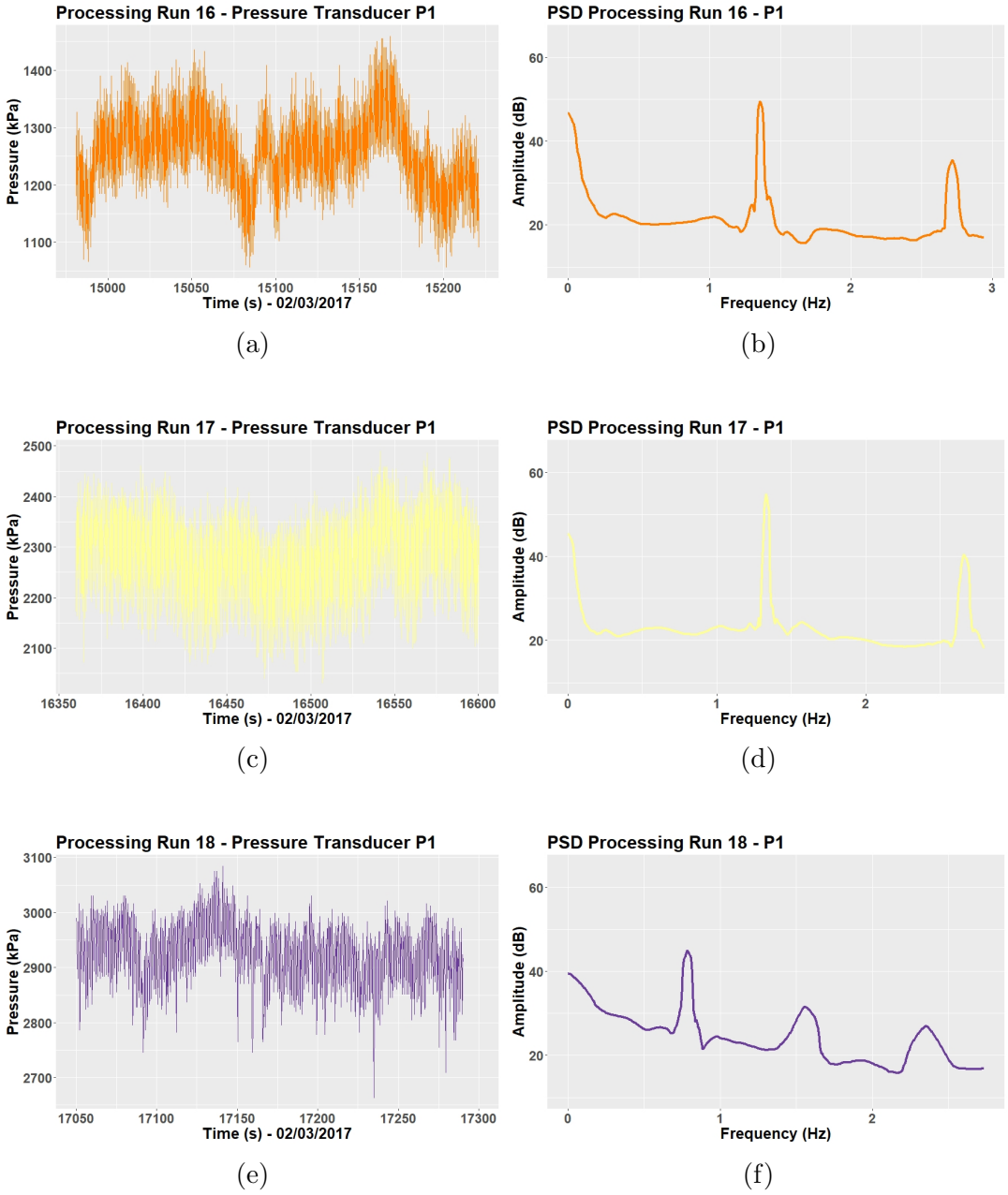

Figure D.6: The pressure signals from the *P1* transducer for processing runs 16-18 along with the power spectrum density plot for each recorded signal.

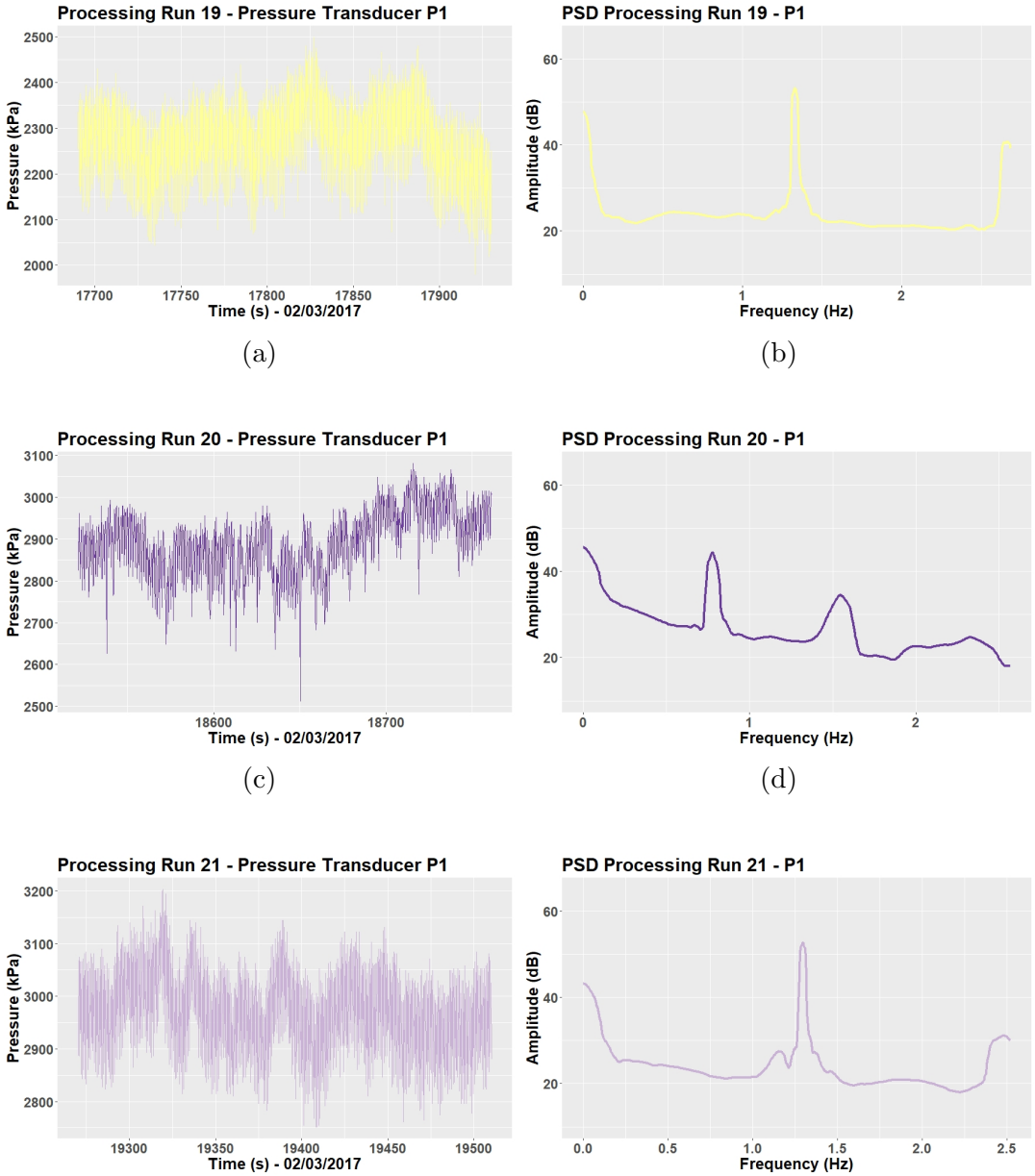

Figure D.7: The pressure signals from the *P1* transducer for processing runs 19-21 along with the power spectrum density plot for each recorded signal.

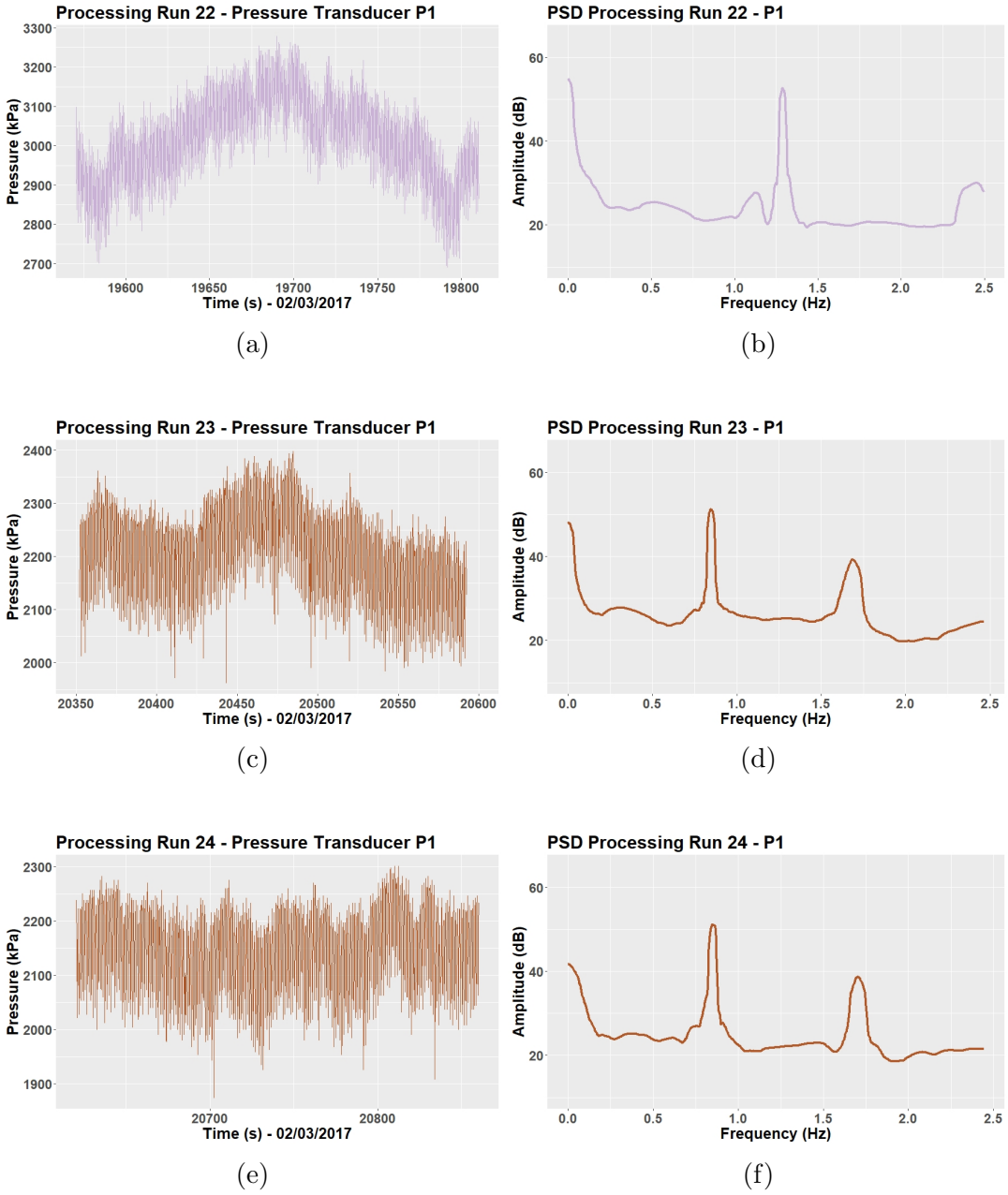

Figure D.8: The pressure signals from the *P1* transducer for processing runs 22-24 along with the power spectrum density plot for each recorded signal.

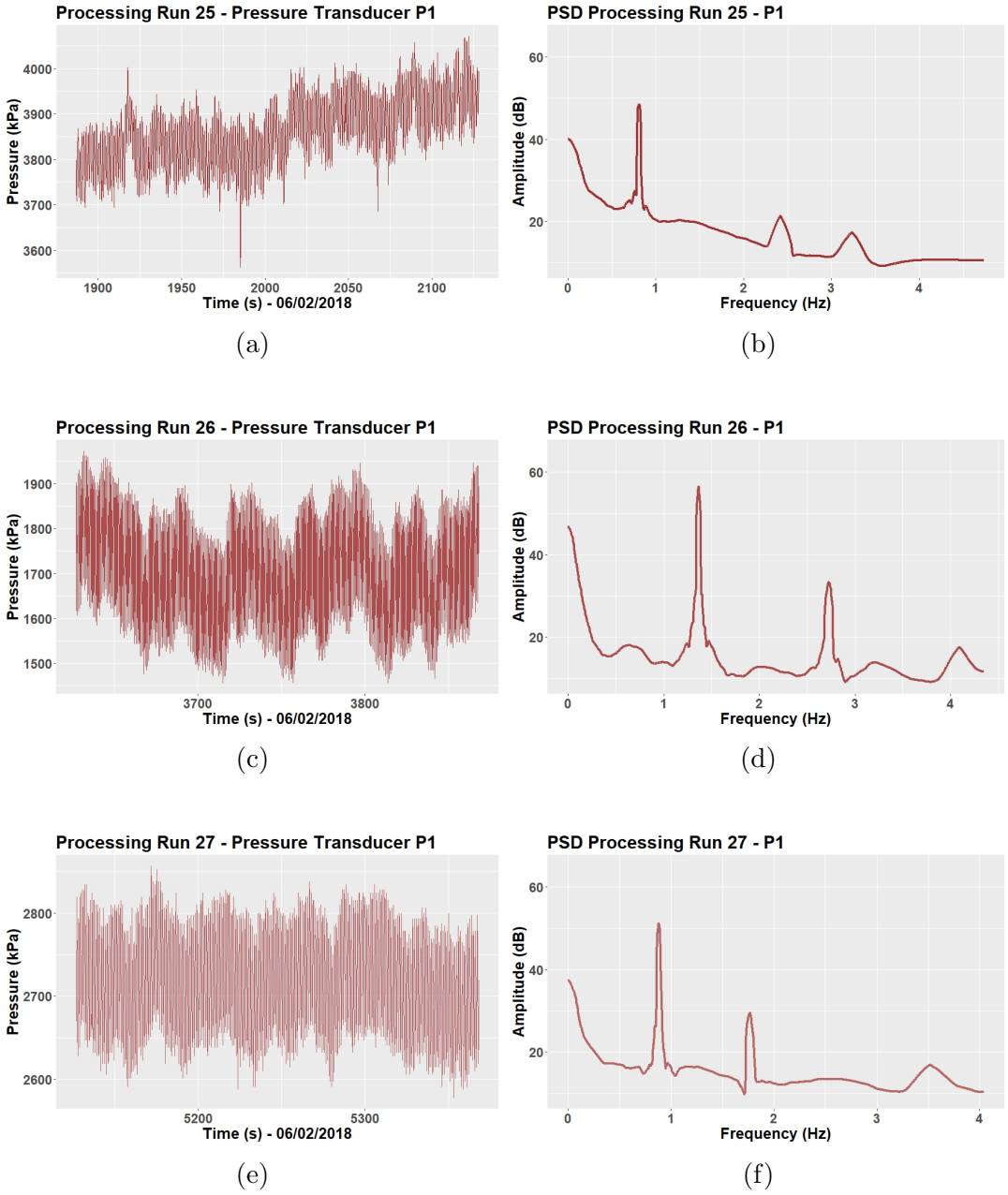

Figure D.9: The pressure signals from the *P1* transducer for processing runs 25-27 along with the power spectrum density plot for each recorded signal.

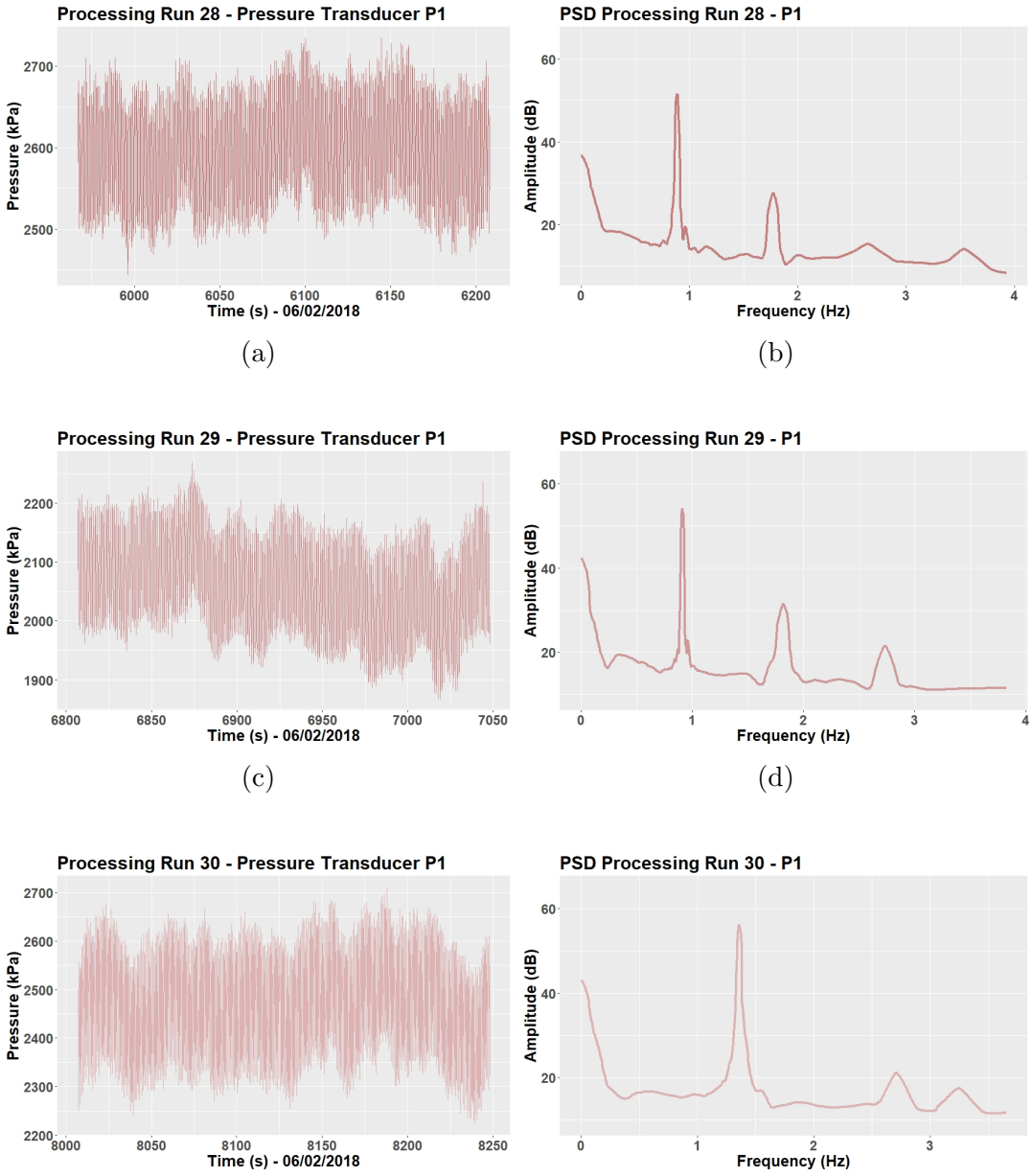

Figure D.10: The pressure signals from the *P1* transducer for processing runs 28-30 along with the power spectrum density plot for each recorded signal.

Appendix E

Temperature Data Plots

Figures E.1 - E.5 present the temperature data captured by each thermocouple for each of the processing runs.

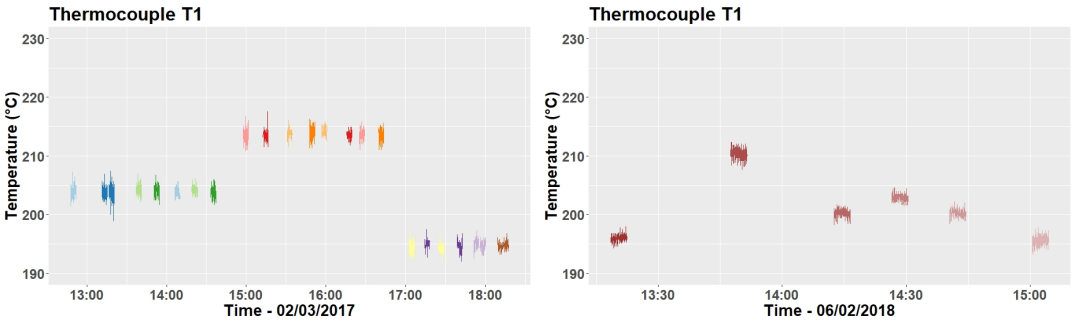

(a) (b)

Figure E.1: The thermocouple signal from the initial experiments (a) and the validation experiments (b) from transducer T1.

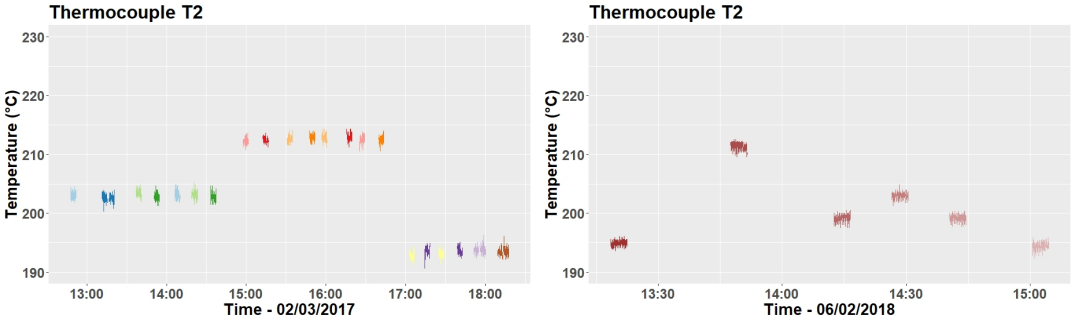

(a) (b)

Figure E.2: The thermocouple signal from the initial experiments (a) and the validation experiments (b) from transducer T2.

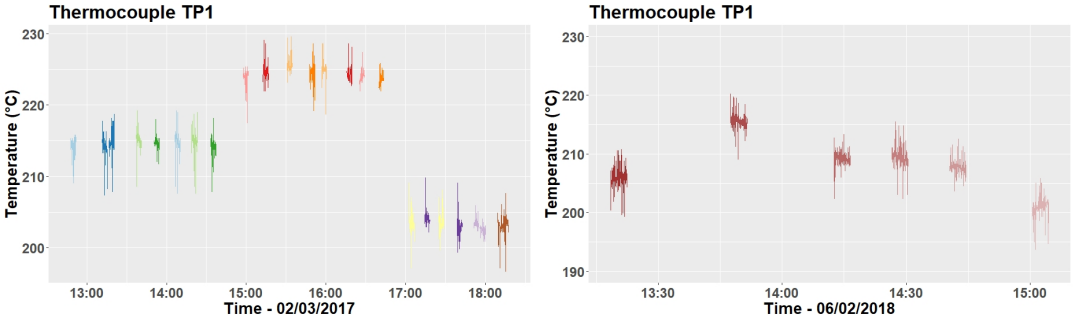

(a) (b)

Figure E.3: The thermocouple signal from the initial experiments (a) and the validation experiments (b) from transducer TP1.

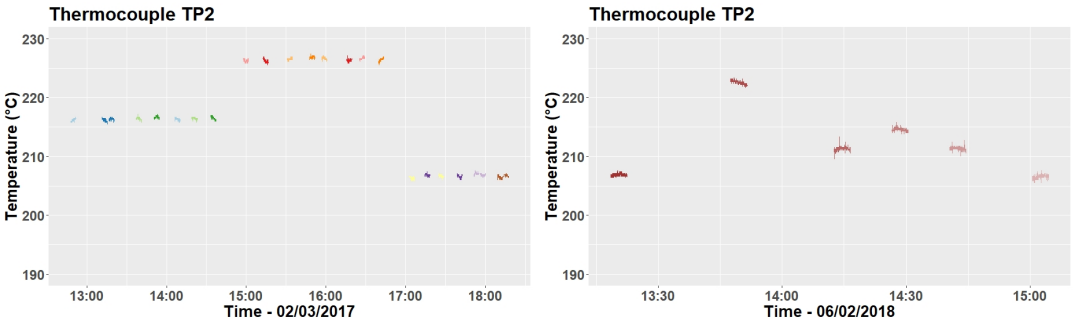

(a) (b)

Figure E.4: The thermocouple signal from the initial experiments (a) and the validation experiments (b) from transducer TP2.

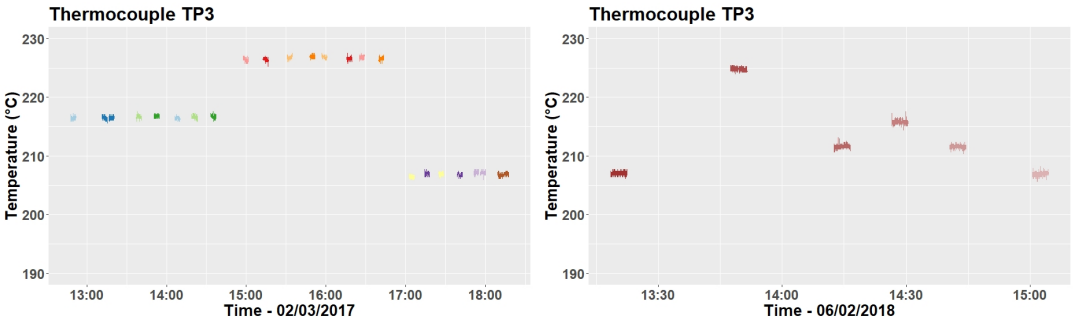

(a) (b)

Figure E.5: The thermocouple signal from the initial experiments (a) and the validation experiments (b) from transducer TP3.